THESE DE DOCTORAT DE L'UNIVERSITE PIERRE ET MARIE CURIE

Spécialité :
Astrophysique des hautes énergies
Ecole Doctorale : Particles, Noyaux et Cosmos

Presentée par
Boutayeb BOUHOU

Pour obtenir le grade de
DOCTEUR de L'UNIVERSITÉ PIERRE ET MARIE CURIE

Sujet de thèse:

Recherche conjointe d'ondes gravitationnelles et de neutrinos cosmiques de haute énergie avec les détecteurs VIRGO-LIGO et ANTARES

soutenue le 19 décembre 2012

devant le jury composé de:

M. E. Chassande-Mottin	Co-directeur de thèse
M. A. Kouchner	Directeur de thèse
Mme. A. Margiotta	Rapporteur
Mme. F. Marion	Rapporteur
M. A. Meregaglia	Examinateur
M. J.P. Tavernet	Président du jury

CONTENTS

INTRODUCTION

High-energy multimessenger astronomy has entered an exciting era with the development and operation of new detectors offering unprecedented opportunities to observe the universe through all kind of cosmic radiations. These includes high-energy ($\gg$ GeV) neutrinos (HENs) and gravitational waves (GWs) which are on the waiting list for a first detection (see e.g. [1, 2] for recent reviews on these subjects). Contrary to high-energy photons (which are absorbed through interactions in the source and by intervening photon backgrounds) and charged cosmic rays (which are deflected by ambient magnetic fields), both HENs and GWs can escape from the sources and travel at the speed of light through magnetic fields and matter without being altered. They are therefore expected to provide important information about the processes taking place in the core of the production sites and they could even reveal the existence of sources opaque to hadrons and photons, that would have remained undetected so far.

No GW nor cosmic HEN have been individually detected so far. The detection of coincident GW and HEN events would hence be a landmark observation confirming the astrophysical origin of both signals. Coincident searches are also a way to enhance the sensitivity of each individual channel by correlating the HEN and GW significances, considering that the two types of detectors have uncorrelated backgrounds.

In this thesis, we investigate the potentials of combining GW and HEN observations. We

implement and conduct two such analyses using the data of the neutrino telescope ANTARES and the GW interferometric detectors Virgo and LIGO.

The multimessenger approach followed here could improve our understanding of the properties of the astrophysical processes at the origin of both emissions. While GW emission requires relativistic bulk motion of massive objects such as gravitational collapse or merger of compact objects, the production of HEN arises from the interaction of hadrons in relativistic jets. A joint detection would then sign the presence of accelerated hadrons in the source and constrain the progenitor nature thanks to the GW detection.

The results presented in this thesis is the outcome of a collaborative work. We stress our main contributions in the following list below.

First joint search for gravitational wave and high-energy neutrinos using 2007 data

Late 2007, LIGO and Virgo completed a first joint data taking period. During this period, ANTARES was operating in an incomplete configuration with five active detection strings. We report in Chapter 4 on the analysis of this first concomitant data set.

To allow for a short analysis cycle and the rapid obtaining of results, available tools and methods were re-used. The selection of the neutrino candidates relied on the developments done for a point-source search. The HEN candidates were followed-up in the GW observations with the pipeline originally conceived for GW search triggered by gamma-ray bursts. The outcome of this first search has been submitted for publication and has led to several public presentations.

Methodological developments and application to the second search using 2009-2010 data

LIGO and Virgo completed a second joint data taking period during 2009-2010. During this

period, ANTARES was operating in its complete configuration with twelve detection strings. We report in Chapter 5 on the analysis of this second concomitant data set.

A new and more sophisticated neutrino reconstruction algorithm could be used to analyze this data set, providing reduced error boxes and allowing for more neutrinos candidates. We also developed a new GW search algorithm based on an already existing pipeline (coherent WaveBurst) used for the all-sky burst search. This pipeline searches for the GW signal within the neutrino uncertainty and enables a search in the case of availability of only two GW detectors. This pipeline is much faster than the one used in the first search and includes more sources by extending the search up to 2kHz.

Optimization of the joint search sensitivity

The selection of neutrino candidates used in the first search was not fully satisfactory since it was performed regardless of the combined sensitivity. This lead to a suboptimal search. We proposed and applied a novel optimization procedure for the selection of neutrino candidates taking into account parameters from both GW and HEN data. This optimization, by maximizing the number of detectable sources, is one of the major contributions of this dissertation.

Selection and characterization of the neutrino candidates

We analysed the ANTARES data and selected a set of neutrino candidates using the optimized cuts. This resulted in a list of 1986 neutrino candidates which we fully characterized in terms of pointing precision and background compatibility. The GW data associated to these neutrino candidates are currently being analyzed.

This thesis is divided into five chapters, structure that reflects the above mentioned contributions. Chapters 1 introduces the main physical concepts associated with GW and HEN along with a description of their joint sources. In Chapters 2 and 3, we give an overview of the experiments and review the data analysis tools. The aim of these three chapters is to bring the

reader to the forefront present-day research, theoretical and experimental, in the field of both GW and HEN physics. Finally, in Chapters 4 and 5 we give a detailed presentation of the first and second searches respectively.

REFERENCES

[1] J. K. Becker, Phys. Rept., 458, 173-246 (2008).

[2] K. Riles, To appear in Progress in Particle and Nuclear Physics (2012).

CHAPTER 1

MULTIMESSENGER ASTRONOMY

1.1 High-energy neutrino astronomy

1.1.1 First steps

Neutrinos are among the most intriguing known elementary particles. Their story started on December 4, 1930, when Wolfgang Pauli postulated the existence of an elusive particle in order to explain the missing amount of energy (and momentum) observed in certain nuclear reactions such as β decays. In mid-1930s papers [1], Enrico Fermi took over Pauli and developed a theory incorporating a neutrino to explain the phenomenology of beta decays. This theory became later the basis of weak interaction physics, but it was only in 1956 that Cowan and Reines directly observed the first neutrinos [2]. Their experiment aimed at detecting the interaction of anti-neutrinos, initially produced in a nuclear reactor, with target protons, according to:

$$\overline{\nu}_e + p \longrightarrow n + e^+ \tag{1.1}$$

This led to the discovery of electron neutrinos (ν_e), more than 25 years after Pauli's proposal. It took even longer to discover the muon neutrinos (ν_μ), which are of most interest in the scope of this dissertation. This second step was achieved in 1962 in Brookhaven by Schwartz and his collaborators [3]. It was known at that time that pions π and kaons K produced in atmospheric showers could decay into a muon μ and a neutrino, and that this neutrino could differ from the electron neutrino. The idea was thus to study the interactions of a neutrino beam created by the disintegrations of pions produced via the interactions of 15 GeV protons on a Beryllium target. Only the neutrinos could pass through the 13 m thick steel shield placed after the target. The interaction of the produced neutrinos could then be studied with a spark chamber. Muons could then be identified in the product of the interactions but no electrons. This was the signature of a new species of neutrino: the muon neutrino.

The existence of a third species of neutrino was anticipated in 1975 after the discovery of tau (τ) leptons in Stanford [4]. But 25 more years were needed to directly observe these ν_τ neutrinos. This was done by the DONUT collaboration [5]. The used neutrino beam was obtained by the interaction of 800 GeV protons onto a Tungsten target, producing charmed mesons, which in turn decayed into ν_τ neutrinos. The identification of tau leptons in the subsequent neutrino interactions was obtained with the scanning of nuclear emulsions, looking for the specific signature of tau decays.

In parallel to the efforts made towards the direct detection of neutrinos produced on Earth, a first step towards a possible neutrino astronomy was made in the 60's with the detection of MeV neutrinos originating from the Sun [6]. The first observation, by the Homestake experiment, was followed by several others using different complementary techniques which enabled to confirm the solar origin of the observed events. At the same time, these observations gave rise to the famous "solar neutrino anomaly", which is now explained by the theory of neutrino oscillations. This extends beyond the scope of the present dissertation, but an overview of the solar neutrino history can be found in [7]. In the same energy range to that of solar neutrinos, or slightly above, the detection on February 23, 1987, of 25 events arriving within 12 seconds from the Supernova 1987A, was another landmark for neutrino astronomy [8].

Both observations have encouraged the development of large neutrino telescopes as we will see in chapter 2 for the detection of the astrophysical neutrinos, and were rewarded by the Nobel Prize in Physics in 2002. But the extremely low cross section of weak interactions (of order $6 \times 10^{-44} cm^2$ for an MeV energy experiment) and the poor angular resolution at nuclear energies represent major obstacles in extending stellar neutrino astronomy much beyond targets like the Sun and a few nearby supernovae. Without denying the important role of the various effects due to neutrino itself, the primary goal of present (experimental and theoretical) investigations remains the astrophysical sources of neutrinos. At present, their detection is currently being challenged by large neutrino telescopes with best sensitivity in the TeV-PeV range.

Keeping these considerations in mind, we begin this chapter with the puzzling question of the origin of the observed cosmic rays (section 1.1.2). We then focus on the possible sources of high-energy neutrinos (HEN).

1.1.2 Cosmic rays and neutrinos

One of the main motivations for a neutrino astronomy is to better understand the physics of the observed cosmic rays (CR). In particular, there is a hope that the observation of cosmic neutrinos could unveil the origin of the high-energy cosmic rays observed on Earth. In this section, we briefly describe the current knowledge about cosmic rays. We also describe how

neutrinos could be produced as by-product of the interactions of CR, in the specific cases of atmospheric and cosmogenic neutrinos. The connection in the production mechanism between cosmic rays and astrophysical neutrinos is described in more details in section 1.1.3.

Cosmic rays

Cosmic rays are nuclei and elementary particles originating in the cosmos and reaching the Earth's atmosphere at a rough rate of 10^4 per square meter and per second. Where penetrating the atmosphere, these CR collides the N and O nuclei and produce showers of secondary particles (referred to as atmospheric particles), which can be detected at ground level and even underground. The story of CR began in 1912 when the Austrian physicist Victor Francis Hess published results concluding that there was radiation penetrating the atmosphere from outer space. Later in 1925, Robert Millikan confirmed these observations and termed them "cosmic rays". The relative abundances of the different nuclei is shown in Figure 1.2 while the overall

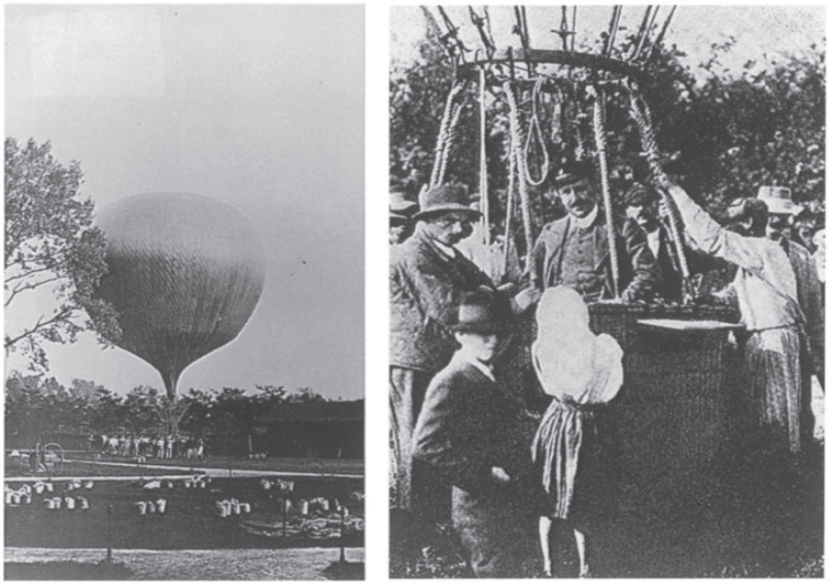

Figure 1.1 – In 1912 (1913), Hess (Klhorster) started his balloon experiments in which he measured the ionisation of the atmosphere with increasing altitude. Left: Preparation of one of his flights. Right: Hess team after one of the successful balloon flights, Especially the flight of August 7, 1912 when V. Hess reached an altitude of 5 km.

spectrum can be seen in Figure 1.3 [9]. The spectrum of cosmic rays varies slightly with the nucleon species, but at the higher energies the chemical composition shows an enrichment with heavier nuclei from the Iron group, as shown in Figure 1.2. Cosmic rays are divided into two classes:

- Primary cosmic rays: are those particles accelerated at astrophysical sources. This in-

cludes electrons, protons, helium, carbon, oxygen and iron.

- Secondary cosmic rays: are those particles produced in interaction of the primaries with interstellar gas. This includes lithium, beryllium, boron, and (part of) antiprotons and positrons.

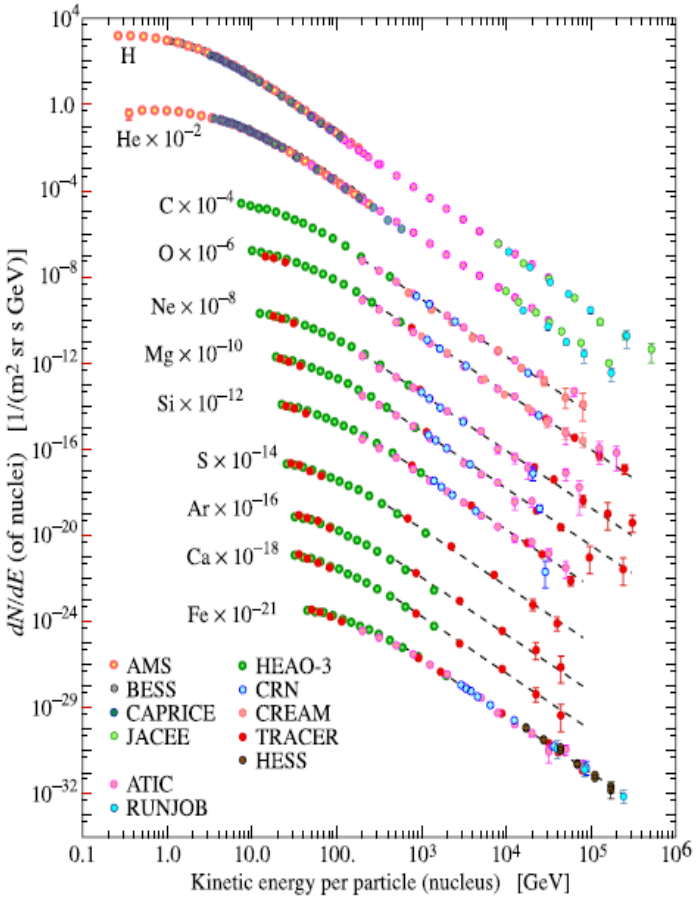

Figure 1.2 – Composition of cosmic rays at different energies. The curves are shown as fluxes of nuclei against energy-per-nucleus. (Source [10])

Perhaps, the most important characteristic of CR is that the observed energy spectra can be well represented by power-law energy distributions. In the first range of these spectra, extending from GeV.nucleon^{-1} to PeV.nucleon^{-1} the spectrum is an isotropic power law in $E^{-\gamma}$, where $\gamma = 2.7$, usually explained as resulting from *galactic* sources such as supernovae. The second energy interval ranging from PeV.nucleon^{-1} to 10 EeV.nucleon^{-1} is also an isotropic power law spectrum with an index $\gamma = 3.1$, possibly originating from *extragalactic* sources, such as active galactic nuclei (AGNs) or sources of gamma-ray bursts (GRBs). Both types of sources

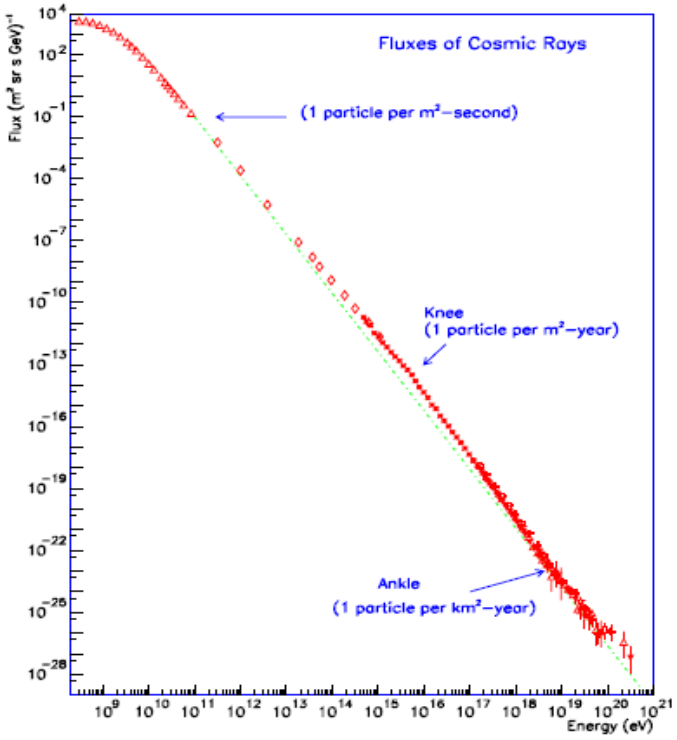

Figure 1.3 – The differential cosmic ray flux vesus energy.

are further discussed in section 1.1.4. The region in between these two energy domains (around $\sim 10^{15-16}$eV) is known as *the knee*, which is poorly understood. Some attempts explain this break as the result of changing propagation characteristics within the galaxy, other as the result of the different production sites.

Beyond 10^{19} eV, where one usually calls the particles "Ultra-High Energy Cosmic Rays" (UHECRs), the spectrum flattens to a slope $\gamma = 2.7$. Particles are also thought to be from extragalactic origin since, at these energies, they cannot be confined magnetically in the Galaxy. The recorded arrival directions are as well nearly isotropic on the sky. The break at $\sim 10^{18-19}$ eV is referred to as the *ankle*. Beyond the ankle, the observed flux seems to vanish. This is compatible with the so called GZK (Greisen-Zatsepin-Kuz'min) effect [11, 12] which predicts a suppression in the spectrum of cosmic rays because of their interaction with diffuse (mainly infrared and microwave) radiations, relics of different stages of the formation of the Universe. As an example, extragalactic protons with energy above the pion production threshold (5×10^{19} eV) lose most of their energy over a distance of about 100 Mpc, small compared to the dimension of the Universe. This implies that cosmic rays can not reach us with an energy of 10^{20} eV unless they originate from a nearby source. This hypothesis remains possible even though there are few sources powerful enough to accelerate particles to such energies at this distance from the

Earth.

The determination of the origin of cosmic rays is also difficult because the arrival directions measured on Earth do not indicate the sources of production. Since they are electrically charged, CR are deflected by interstellar and intergalactic magnetic fields, as opposed to neutrinos. Even at ultra high energy the expected difference between the direction of the source and direction of the particle can reach several degrees. These differences naturally depend on the electric charge carried by cosmic rays, i.e. their composition. This question in the highest energy range remains open. Many experts still favor the hypothesis that highest energy CR are protons, although recent results from the Auger collaboration suggest a transition at around 10^{19} eV, to heavier elements (iron nuclei) [13].

The constraints imposed by the existence of UHECR are related to the size of the potential sources and magnetic field strength prevailing there, which confines charged particles. To acquire a great energy, particles must indeed be confined for some time in the area of acceleration. But the more energetic the particle, the more difficult for magnetic fields (B) to confine it. An upper bound to the maximum energy that can be reached in an acceleration site can be inferred by requiring the Larmor radius ($r_L = E/qBc$) to be smaller than the dimensions of the site, R. The quantities B and R are obtained by the equation:

$$E_{\max} = ZecBR \tag{1.2}$$

As a result of this relationship, only certain types of sources are eligible for particle acceleration beyond 10^{20} eV. They are shown in Figure 1.4. A number of these sources are described in more detail in section 1.1.4, as they are all candidates to neutrino production.

Atmospheric muons and neutrinos

The atmosphere is very rich in particles produced by the interaction of cosmic rays in the air. The vertical flux for different components is shown in Figure 1.5. The most relevant particles for Neutrino Telescopes are atmospheric muons and neutrinos, since they constitute the main physical source of background. The main process responsible for their production is :

$$\begin{aligned} p^+ + p^+ &\longrightarrow \pi^+ + p^+ + n, \\ p^+ + n &\longrightarrow \pi^+ + n + n, \end{aligned} \tag{1.3}$$

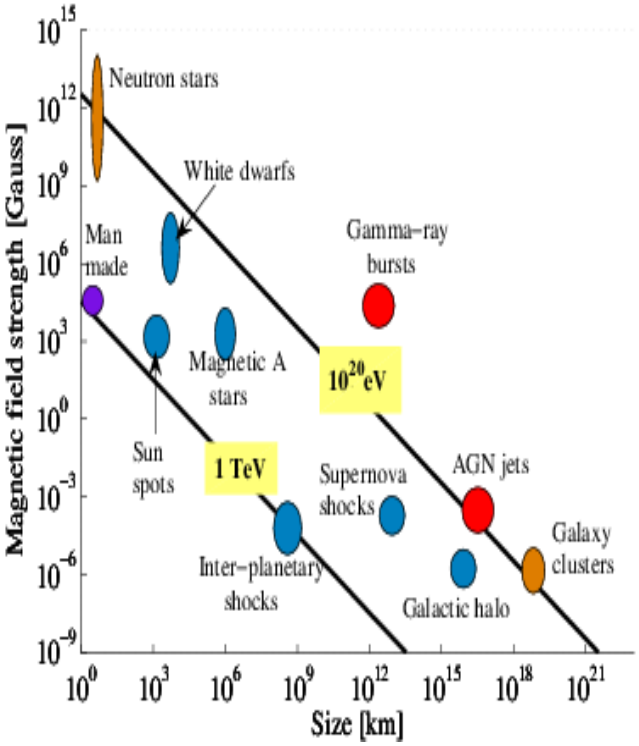

Figure 1.4 – *Hillas diagram (from ([14]) representing the type of sites likely to accelerate cosmic rays to extreme energies. The figure shows the size of the potential sources depending on the intensity of magnetic fields estimated in Gauss units (Earth's magnetic field is of the order of Gauss). To accelerate protons to energies of* $1\,TeV$ *(*$10^{20}\,eV$*), the sources must lie above the corresponding line. This condition, which is necessary, is not necessarily sufficient: accelerating protons* $10^{20}\,eV$ *in clusters of galaxies, for example, requires an acceleration time larger than the age of the universe. As for neutron stars, they are unlikely candidates because of high energy losses associated with the presence of strong magnetic field.*

followed by

$$\begin{aligned} \pi^+ &\longrightarrow \mu^+ + \nu_\mu, \\ \mu^+ &\longrightarrow e^+ + \nu_e + \overline{\nu}_\mu \end{aligned} \tag{1.4}$$

Resulting in both muon- and electron-neutrinos. These neutrinos span energies from few MeV to the highest-energy cosmic rays and they are much more abundant at lower energies. Muons are the most numerous charged particles at sea level. They are the remaining of the secondary cosmic rays in the high atmosphere (typically 15 km) and lose about 2 GeV to ionization before reaching the ground. Their energy and angular distributions reflect the convolution of production spectrum, energy loss in the atmosphere and decay [10]. Further discussions on these atmospheric muons and neutrinos follow in section 2.5.

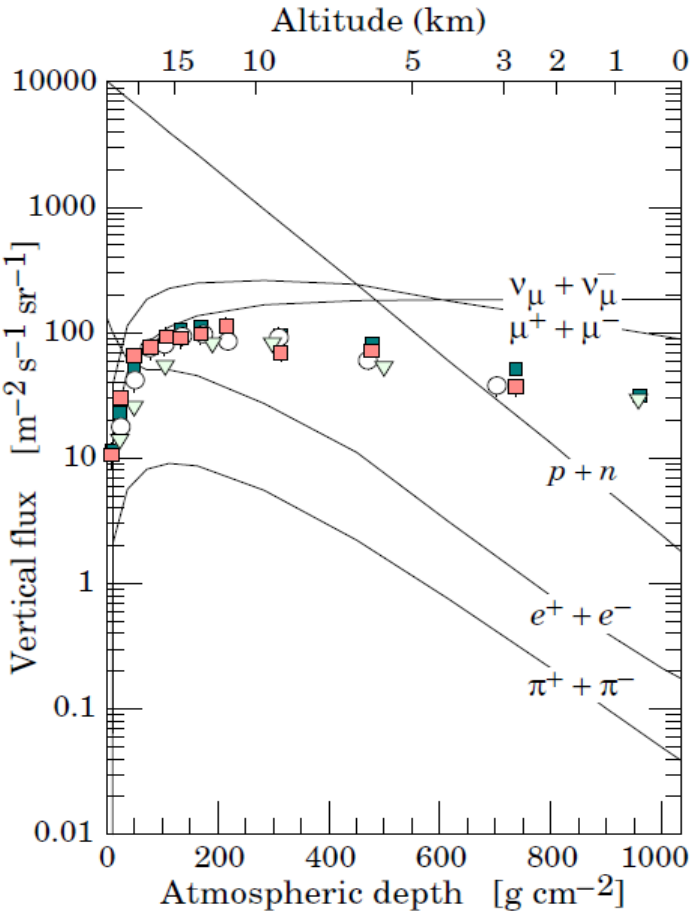

Figure 1.5 – Components of the cosmic rays in the atmosphere with E> 1GeV. The points show measurements of negative muons with energy above 1 GeV. (Source [10])

Cosmogenic neutrinos

As previously stated, as they propagate over cosmological distances, UHECRs may interact with the relic photons fields (GZK effect), These interactions generate pions and neutrons, which decay to produce neutrinos of energy greater than $10^{17} eV$. The accumulation of these neutrinos over cosmological time is known as the cosmogenic neutrino flux [15, 16]. Although guaranteed sources, the predicted fluxes of cosmogenic neutrinos are low compared with the sensitivity of current neutrino telescopes. Estimates of these fluxes depend mainly on the properties of the primary cosmic ray flux, particularly in terms of composition. Another important parameter is the variation of the intensity of injected flux (or density of sources) as a function of redshift. All of these parameters lead to predictions that differ substantially. The detection of such cosmogenic neutrinos would represent an important step for neutrino astronomy. An accurate measurement of flux would further constrain the composition and the variation of the density

of sources of cosmic rays with redshift.

1.1.3 Neutrinos as cosmic probes

Our current knowledge about astrophysical sources largely rely on observations made using photons (electromagnetic radiation), which are the essential messengers of modern astrophysics. The gamma-ray astronomy (in the TeV range) experienced an unprecedented boom with the advent of new Cherenkov telescopes such as WHIPPLE and more recently HESS. These have demonstrated that TeV photons are actually emitted by number of Galactic and extragalactic sources. The study of these sources has put new constraints on models of cosmic ray production. There is indeed a link between the production of charged cosmic rays and that of photons (or neutrinos) at high energy. Photons and neutrinos can be produced in a beam dump scenario, by the interaction of cosmic rays of high energy with the surrounding matter and background radiation (usually produced by synchrotron radiation of charged particles in magnetic fields) as follows:

$$\begin{array}{lccccccc} p/A + p/\gamma \longrightarrow & \pi^0 & + & \pi^+ & + & \pi^- & + \ldots \\ & \downarrow & & \downarrow & & \downarrow & \\ & \gamma + \gamma & & \mu^+ + \nu_\mu & & \mu^- + \overline{\nu}_\mu & \\ & & & \downarrow & & \downarrow & \\ & & & e^+ + \nu_e + \overline{\nu}_\mu & & e^- + \overline{\nu}_e + \nu_\mu & \end{array} \tag{1.5}$$

In this context, the gamma-rays are produced by the decay of neutral pions (π^0). This production is necessarily linked to that of high-energy neutrinos from the decay of charged pions. Similarly, the existence of cosmic rays of high energy necessarily implies the production of HEN. This is known as the "cosmic ray connection". As such, sources of cosmic rays could be revealed by observing gamma-rays or HEN which, due to their electrical neutrality, travel in a straight line indicating the location of their production area. The high-energy photons can also be produced in a purely electromagnetic process without hadron. This is the "Synchrotron Self Compton" scenario where electrons accelerated to high energy generate photons by synchrotron radiation. These photons are further accelerated to TeV energies by collision with the high energy electrons. Therefore photons alone can not readily discern the electromagnetic processes from the hadronic ones. On the contrary, the detection of neutrinos would be an unambiguous signature for hadronic mechanisms.

The other limitation of high energy photons is their absorption by matter or radiation, which prevents them from escaping dense sources. Besides, when they do escape, high-energy photons are absorbed by interaction with the interstellar radiations (similarly to cosmic rays in the GZK

effect). As an example for PeV photons, the mean free path is typically restricted to dimension of our Galaxy. Photons can therefore hardly be used at high energies for astronomical survey over cosmological distances.

Neutrinos do not suffer these limitations: they are neutral and weakly interacting. Therefore, if they can be detected with sufficiently high statistics, they appear to be ideal candidates for high energy astronomy, providing access to cosmological distances and inner regions of astrophysical sources. This makes of the neutrino a singular probe able to open a window of observation on the sky.

In this sense, HEN astronomy can address a number of fundamental questions in astrophysics and cosmology. Among these are the nature of dark matter (see section 1.1.4), the origin of the cosmic rays, and the extreme physics responsible for gravitational energy release in the most luminous objects in the universe. The work presented in this dissertation focuses on the detection of neutrinos in coincidence with gravitational waves, following the advocated lines of a multimessenger approach.

Theoretical upper bounds to the cosmic neutrino flux

If neutrinos of extragalactic origin have not yet been detected, the link (described in the previous paragraph) between cosmic messengers allows to estimate the diffuse neutrino flux produced by the "cosmic accelerators" [17, 18].

The observable spectrum of cosmic rays provides the most restrictive limit. Bahcall and Waxman (WB) have determined a benchmark cosmic neutrino flux, based on the assumption that the observed cosmic rays above 10^{19} eV are protons produced by extragalactic cosmic accelerators. The calculation is based on the production rate (per unit time, volume, and energy) of these ultra high energy protons estimated at:

$$\mathrm{E_p^2}\frac{\mathrm{dN}}{\mathrm{dE_p\,dV\,dt}} \approx 0.65 \times 10^{44}\,\phi(\mathrm{z})\,\mathrm{erg\,Mpc^{-3}\,year^{-1}} \tag{1.6}$$

where $\phi(z)$ (with $\phi(0) = 1$) takes into account the evolution of the production rate as a function of redshift (small since following the GZK effect, the protons lose their energy over relatively small distances). The choice, consistent with the Fermi mechanism, of a E^{-2} differential spectrum is motivated by observations of processes involving shocks (relativistic or not).

The production rate given by equation 1.6 enables to infer an upper limit for the production of HEN from extragalactic sources as AGN or GRBs. The underlying assumption is that the rate of energy injected in the form of neutrinos can not exceed that of the associated protons

even when all are involved in the production of pions (relation 1.5). The resulting limit is:

$$E_\nu^2 \phi_\nu < 2 \times 10^{-8} \xi_z \left[\frac{(E_p^2 \frac{dN}{dE_p\, dV\, dt})_{z=0}}{10^{44}\,\mathrm{erg/Mpc^3\,year}} \right] \quad \mathrm{GeV\,cm^{-2}\,s^{-1}\,sr^{-1}} \tag{1.7}$$

where ξ_z, of the order of unity, indicates the evolution of the injection rate following the redshift. Such a flux is being challenged by current neutrino telescopes which have therefore entered a quite exciting era.

1.1.4 Astrophysical sources of high-energy neutrinos

In this section we present a selected list of astrophysical sources that are candidates for high-energy neutrino emission. These sources can be sorted into 2 types: *galactic* and *extragalactic*. Based on relation (1.5), estimates of the expected neutrino flux can be achieved relying on the recent observations with gamma-rays with, for example, HESS [19] and FERMI [20]. But these estimates can still vary by orders of magnitude depending on the precise model used to infer them. These estimates of neutrino fluxes at Earth must also be corrected to take into account the flavor mixing occurring during propagation. To the first order, neutrinos are produced in a ratio of flavor (see relation (1.5)) ($\nu_e : \nu_\mu : \nu_\tau = 1 : 2 : 0$) but reach the Earth in the proportions ($\nu_e : \nu_\mu : \nu_\tau = 1 : 1 : 1$).

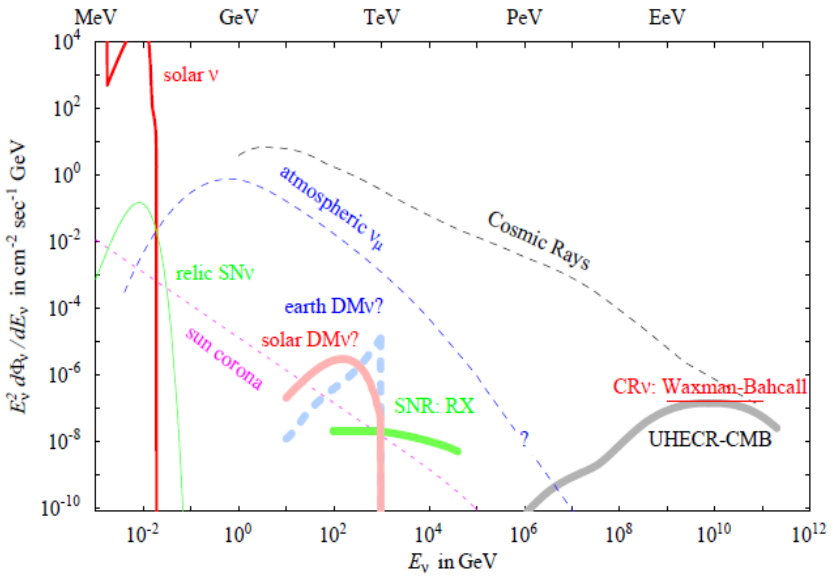

Figure 1.6 – Optimistic astrophysical neutrino fluxes from various sources

Galactic sources

The most promising Galactic sources of neutrinos are briefly reviewed below. Estimates of expected associated neutrino fluxes can be found, for instance, in [21]:

- ***Supernova remnants (SNR)***: They are the prime candidate sources for accelerating the cosmic rays observed up to $\sim 10^{15}$eV thanks to the Fermi mechanism. After the explosion of the star, leading to a supernova, ejected particles can be accelerated to high energies. From the death of the star arises a pulsar with a high magnetic field that contribute to the acceleration of particles. The production of (TeV) neutrinos is expected in the collision of cosmic rays *proton/neutron* with the thermal nucleon in the remnant shell which leads to neutral and charged pions π^+/π^0.
  The observation by HESS of the southern sky with γ rays at the TeV and above revealed two particularly bright SNR. The first one is Vela Junior ($RXJ0852.0-4622$). The flux of γ was observed in a region extending up to $\sim 2°$. The second is $RXJ1713.7-3946$. The observed spectra below 10 TeV look like power laws with hard spectral indices: $\Phi_\gamma = dN_\gamma/dE \propto E^{-\Gamma}$ with $\Gamma \sim 2$, the value suggested by the Fermi acceleration mechanism. Various spectral analyses of these sources seem to favor a hadronic origin for the gamma emissions detected, which could lead to an observable flux for a km-scale neutrino telescope.

  The flux of neutrinos can be calculated from the flux of π^+. First, we get the flux of π from the γ flux, using the π^0 decay and assuming that $\Phi_\pi^+(E) = \Phi_\pi^-(E) = \Phi_\pi^0(E) = \dfrac{-Ed\Phi_\gamma}{2dE}$. Consequently one can deduce the neutrino flux using the $\pi^+ \to \mu^+\nu_\mu$ decay:

$$\Phi_{\nu_\mu}(E) = \int_{E/(1-r)}^{\infty} \frac{d\epsilon \Phi_\pi^+(\epsilon)}{(1-r)\epsilon} = \frac{\Phi_\gamma(E/1-r)}{2(1-r)} \tag{1.8}$$

  where $r = (M_\mu/M_\pi)^2$.

- ***Microquasars***: These objects are binary stellar systems with collimated relativistic jets at radio frequencies. They consist of an accreting compact object, either a black hole or a neutron star, and a companion star. The behavior of these systems resembles, to some extent, that presented by extragalactic quasars, hence the origin of the name. The detection of the microquasar Cygnus X-3 above 100 MeV by both Fermi/LAT and AGILE satellites, together with the short flares from Cygnus X-1 reported by AGILE, confirmed that this class of astrophysical objects are interesting candidates for very high energy gamma-ray observations.

Microquasars could produce HEN according to two models. In the first model, inhomogeneities in the jet could generate internal shocks accelerating electrons and protons arising in a power law energy spectrum. Accelerated protons could interact with X-ray emitted by the accretion disc or synchrotron photons generated in the jet by the accelerated electrons [22]. Both Synchrotron self-Compton (SSC) and strong external X-ray fields can cool extremely relativistic protons through pion production. However, the protons should be accelerated up to very high energies (10^{16} eV) in the inner jet in order to produce a significant flux of multi-TeV neutrinos. It is not established that microquasars can accelerate particles up to such energies at the base of the jets. The high neutrino fluxes predicted by [23] on the basis of this model for different microquasars are in some cases already ruled out by AMANDA II data, and recently by ANTARES [24].

In the second model [25], high-energy gamma-rays and neutrinos could result in matter interactions: accelerated nuclei of the jet could lose neutrons as a result of photo-decay process in collisions with thermal photons from the accretion disk and the massive star. These neutrons propagating toward the disk and the massive star could generate neutrinos by interacting with matter.

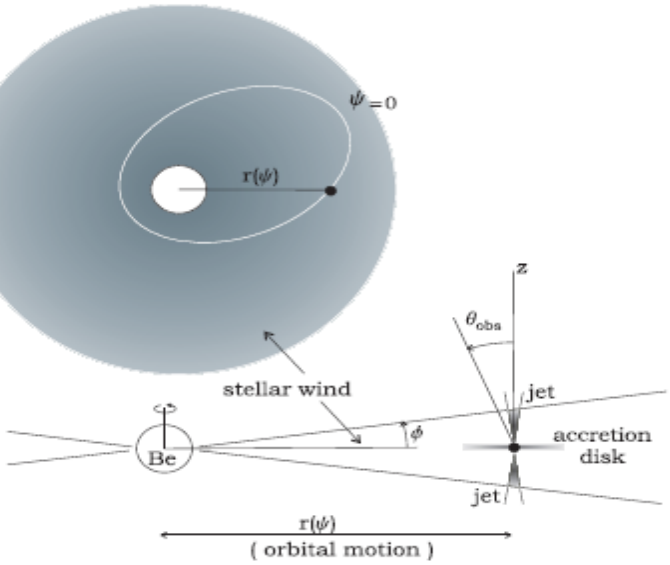

Figure 1.7 – Schematic model of a possible hadronic model of microquasars. (source [26])

- ***Soft gamma-ray repeaters (SGRs)*** They are X-ray pulsars which have quiescent soft (2–10 keV) periodic X-ray emissions with periods ranging from 5 to 10 s. They exhibit repetitive erratic bursting episodes lasting a few hours each and composed of numerous

very short ($\sim$ ms) pulses. Every once in a while they emit a giant flare in which a short (< 0.5 s) spike of harder radiation is observed; such flares can reach peak luminosities of $\sim 10^{47}$ erg/s, in X-rays and γ-rays. A handful of SGR sources are known, most of them in the Milky Way and one in the Large Magellanic Cloud. Three of them have had hard spectrum ($\sim$ MeV energy) giant flares: one with a luminosity of 10^{40} J/s, the two others being two orders of magnitude weaker.

The favoured *magnetar* model for these objects is a neutron star with a huge magnetic field B $\gtrsim 10^{15}$ G, which is subject to star-quakes that are thought to fracture the rigid crust, causing outbursts. The giant flares result from the formation and dissipation of strong localized currents due to magnetic field rearrangements associated with the quakes, and liberate a high flux of X- and γ-rays. Sudden changes in the large magnetic fields would accelerate protons or nuclei that produce neutral and charged pions in interactions with thermal radiation. These hadrons would subsequently decay into TeV or even PeV energies γ-rays and neutrinos, making flares from SGRs potential sources of HEN.
An alternative model involving a large scale rearrangement of the magnetic field has also been proposed by [27], which allows for huge energy releases, and detectable HEN fluxes from Galactic magnetars even for relatively small HEN efficiencies.

- ***The Galactic centre***: Since its observation by the HESS telescope in the TeV domain [28] the centre of our Galaxy has become of particular interest for neutrino astronomy. Indeed, initial observations revealed the presence of two bright sources, one in the direction of Sagitarius A* (HESS J1745-290), the supermassive black hole at the centre of the Galaxy, and another one, close to supernova Sgr A East. After subtraction of these intense sources, a more diffuse emission has been observed. This diffuse emission of photons of energy greater than 100 GeV is strongly correlated with molecular clouds [29], suggesting a hadronic origin of the observed γ-rays. The associated neutrino emission could be observed with the next generation of neutrino telescopes to be built in the Northern hemisphere.

- ***Pulsar wind nebulae (PWNe)***: They are ejecta of shocked relativistic particles produced when a pulsar emits a relativistic wind further interacting with its environment. The best known among these sources is the Crab Nebula that harbors an energetic pulsar[1] whose spin-down power manifests itself as a synchrotron-emitting source of energetic particles. Recent discoveries of very high energy γ-ray emission associated with PWNe have

[1] A rapidly rotating, highly-magnetized neutron star, which generates coherent beams of radiation along its magnetic poles.

opened a new channel for investigations of the structure and evolution of these objects. It is thought that this emission in the TeV band probably originates from inverse-Compton scattering of ambient soft photons with energetic electrons in the nebula [30]. Nevertheless, hadronic models have been considered in which the emission is associated with the decay of neutral pions produced in collisions of energetic ions with ambient hadronic material [31], of particular interest is Vela X.

Extragalactic sources

We discussed in section 1.1.2 that extragalactic sources could be at the origin of the cosmic rays (CR) at the highest energies $E_{CR} > 10^{18}$GeV. In this context, several sources are suggested to produce high energy neutrinos:

- ***Active galactic nuclei (AGNs)***: Active galaxies are galaxies whose center shows increased luminosity with respect to the rest of the galaxy. These galaxies have a concentration of stars, gas and dark matter in the center which make their nucleus active, i.e. gas is being accreted in large quantities and/or stars are being captured, disrupted and swallowed in significant number. AGNs were first observed in 1963 [32] in the radio emission. Some of them are detected in γ-ray range. It has been discovered during the last three decades that these active galaxies have a massive black hole at their center that accretes continuously matter. In the center of the accretion disc, matter is ejected in jet perpendicularly to the accretion disc. Active Galactic nuclei are thought to accelerate electrons in shocks either inside their jets or at the jet termination surface, see Figure 1.8. Certain classes of AGNs (like Blazars) may be capable of accelerating cosmic rays to energies in excess of PeV, which could lead to TeV neutrinos and gamma-rays via photo-meson process. The correlations established by the AUGER collaboration [34] reinforce the hypothesis that AGN could be the source of cosmic rays of ultra high energy, but they are still subject to an intense debate. Searching for neutrinos from known AGN is therefore of particular importance.

  An important factor to take into account when predicting neutrino fluxes associated with the observed high-energy gamma rays, for this type of extragalactic sources, is the absorption by the extragalactic background light (EBL). The spectral index of 2.9 observed by the telescope HESS in the case of the blazar 1ES1101 (z = 0.186) could, for example, correspond to an index in the source, 1.5 [35], which could therefore lead to a neutrino flux significantly more intense than the gamma flux.

  Another feature of blazars is their variability. In the case of PKS2155, an increase of

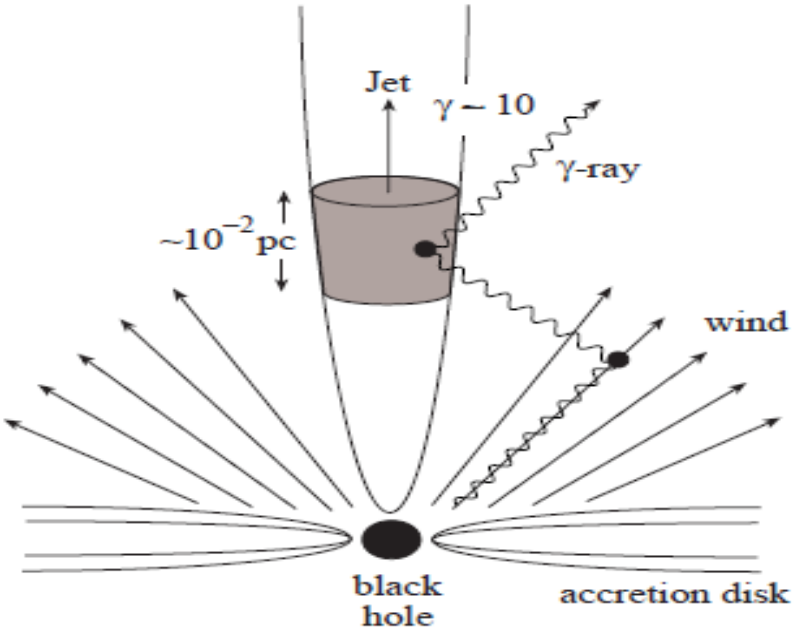

Figure 1.8 – Schematic blazar internal shock scenario. Blazars are a subset of AGNs, that emit high-energy radiation in collimated jets pointing at the Earth. (Source [33])

almost a factor of 100 in the gamma flux has been observed by HESS over a one-hour period [36]. Such a flurry of activity in a short period could allow the detection of neutrinos through the significant reduction of associated background noise. This technique is similar to the one adopted to search for neutrinos from sources of gamma-ray burst (GRB).

- ***Unidentified sources***: Finally, it is interesting to note that a number of sources detected by HESS have no observable counterpart in the electromagnetic spectrum. The origin of this type of source is therefore a theoretical challenge. Observation of high energy neutrinos in the direction of these sources could probably help modeling these objects. The detection of these sources without counterpart underlines once more the possibility of detecting previously unknown sources.

- ***Starburst Galaxies:*** The observation of synchrotron emission in the radio band from some galaxies (where the star formation rate is unsually high) named "starburst galaxies" implies the presence of a few GeV electrons assuming the existence of intense magnetic fields. The presence in these galaxies of many massive stars in formation phase considerably enriches the interstellar medium with matter. So if protons were accelerated together with the electrons (e.g. supernova explosion), this would result in a significant flow of neutrinos by pp interactions (on the order of $\mathrm{dN} = 10^{-7}\mathrm{E}^{-2}\mathrm{GeV}^{-1}\mathrm{cm}^{-2}\mathrm{s}^{-1}\mathrm{sr}^{-1}$),

detectable by the new generation of neutrino telescopes [37].

- ***Gamma-Ray Bursts (GRBs)***: Gamma-ray Bursts (GRBs) (see Figure 1.9) are detected as an intense and short-lived flash of gamma-rays with energies ranging from tens of keVs to tens of GeVs. The morphology of their light curves is highly variable and typically exhibits millisecond variability, suggesting very compact sources and relativistic expansion. GRBs are divided into two classes depending on the duration of their prompt gamma-ray emission, which appears to be correlated with the hardness of their spectra and are believed to arise from different progenitors: short-hard bursts last less than 1–2 seconds while long-soft bursts can last up to dozens of minutes.

  The BATSE detector, launched in 1991 on board the Compton Gamma-Ray Observatory, was the first mission to accumulate observations on more than a thousand GRBs, establishing the isotropy of their sky distribution and characterizing their light curve and broken power-law spectra [38]. The detection of X-ray and optical counterparts pertaining to the afterglow phase of several GRBs, triggered by the first observation of an X-ray transient emission from GRB970228 by the BeppoSAX satellite [39], subsequently confirmed their extragalactic origin by allowing a more accurate localization of the source and a redshift determination. Currently operating GRB missions include *Swift*, hosting a wide-field hard X-ray (15 keV–350 keV) burst alert telescope (BAT) coupled to softer X-ray, ultraviolet and optical telescopes and the GBM on the Fermi Gamma-Ray Space Telescope which focuses on the high-energy (15 keV–300 GeV) emission from GRBs. In the standard picture (see e.g. the review by [40]), the mechanism responsible for the enormous, super-Eddington energy release ($\sim 10^{50} - 10^{52}$ ergs) in the prompt emission and in the afterglow is the dissipation (via internal shocks, magnetic reconnection and external shocks) of bulk kinetic or Poynting flux into highly relativistic particles. The particles are accelerated to a non-thermal energy distribution via the Fermi mechanism in a relativistically expanding fireball ejected by the GRB central engine. The accelerated electrons (and positrons) in the intense magnetic field emit non-thermal photons via synchrotron radiation and inverse Compton scattering.

  The plasma parameters inferred from observations to characterize GRB's baryonic fireballs are such that proton acceleration to energies exceeding 10^{20}eV is likely to be possible in these sources. Moreover, the time averaged energy output of GRBs in photons is comparable to the proton energy production rate required to produce the UHECR flux. Therefore, the canonical baryonic fireball also suggests that GRBs are a prime candidate source for the ultra-high-energy cosmic rays (UHECR), observed at energies

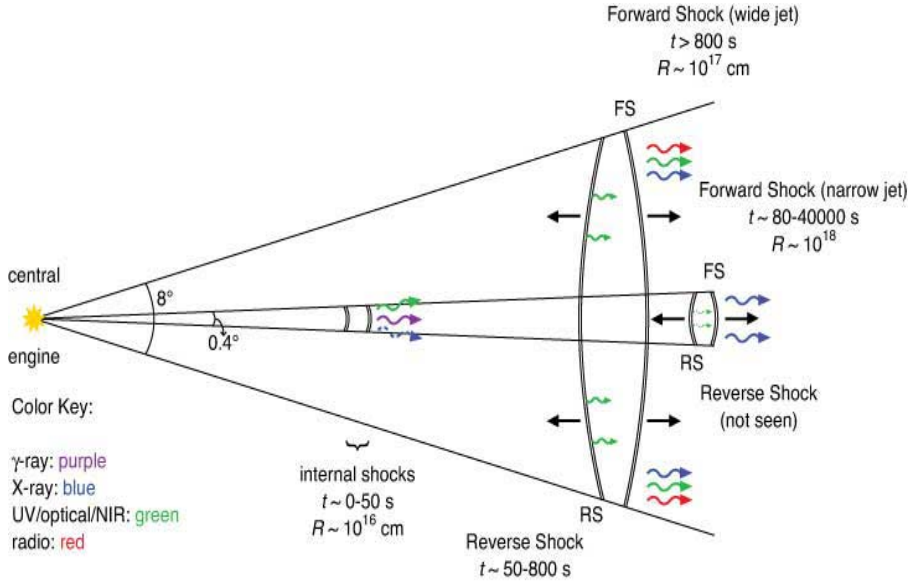

Figure 1.9 – Schematic GRB jet and location of jet photosphere, dissipation (internal shock) and external shock radii.

$E \sim 10^{18} - 10^{20}$ eV. In a baryonic outflow, the internal or external shocks accelerate protons that interact with the gamma-rays and/or other protons inside the fireball producing neutrinos according to the relation 1.5. Such neutrinos are emitted in spatial and temporal coincidence with the GRB prompt electromagnetic signal; their energy is typically in the range $\sim$ TeV to PeV. Neutrinos with higher (up to $\sim 10^{10}$ GeV) energy can also be emitted at the beginning of the afterglow phase, when the outflow is decelerated by external shocks with ambient material and the accelerated protons undergo interactions with the matter outside of the jet [41]. An alternative mechanism for neutrino production in fireballs suggested by [42] involves neutral particles that are picked up by the stream when they acquire a charge, such as a decaying neutron, or, further downstream, a neutral atom that is ionized. Such a particle will be extremely energetic in the jet frame, and immediately attains an energy of a PeV. The associated neutrinos would come within an order of magnitude of that energy ($\sim$ 100 TeV), providing a harder spectrum than the one expected from shock acceleration. The sensitivity achieved by neutrino telescopes is such that their observations will allow in a few years to test and distinguish between GRB models with different physics, and to constrain the physical parameters of such models. The current non-detection of neutrinos by IceCube [43] (see also Chapters 4 and 5) already questions the viability of models in which ultra high energy cosmic rays are the decay products of neutrons that have escaped the fireball with high energy. The

current upper limit is still consistent with the "standard" (i.e., following [44]) predictions of neutrino emission from GRB fireballs.

Gamma-Ray Burst diffuse flux of Waxman-Bahcall

As stated in the previous section, GRBs are considered to be produced from the collapse of stars or the merger of compact objects with the central object being a black hole (or in case of the magnetar model a fast rotating high-mass neutron star which eventually collapses into a black hole). During the collapse the release of high amounts of gravitational energy during a short time in a small volume leads to an explosion or expansion.

Waxman and Bahcall calculated an upper bound for the diffuse flux [45] of muon-neutrinos produced in GRBs. The shape of this flux is the result of relatively general considerations depending on the photon and proton spectra. The observed spectra can be parametrized as following. First one needs to specify the proton spectrum:

$$N_p(E_p) = N_{p,0} E_p^{-2}.exp\left[-\left(\frac{E_p}{\epsilon_{p,max}}\right)\right]; \quad E_p \leq \epsilon_{p,max} \tag{1.9}$$

where $\epsilon_{p,max}$ is a the proton maximum energy. Its value is derived from comparison of acceleration time and synchrotron loss time. $N_{p,0}$ is the normalization of the spectrum. The photon spectrum N_γ(E) is derived from observed GRB photon spectra and is parametrized by the Band function:

$$N_\gamma(E_\gamma) = N_{\gamma,0} \begin{cases} E_\gamma^{-1} & \text{if } \epsilon_{\gamma,min} \leq E_\gamma < \epsilon_{\gamma,b} \\ \epsilon_{\gamma,b} E_\gamma^{-2} & \text{if } \epsilon_{\gamma,b} \leq E_\gamma < \epsilon_{\gamma,max} \\ 0 & \text{else} \end{cases}$$

where $N_{\gamma,0}$ is the normalisation factor. The break energy $\epsilon_{\gamma,b}$ is retrieved from the photon spectrum of a burst. The energy $\epsilon_{\gamma,max}$ is the maximum photon energy, and $\epsilon_{\gamma,min}$ is the lower energy cut-off of the photon spectrum.

Using these spectra Waxman and Bahcall (WB) derived a power-law spectrum of the muon-neutrino at Earth:

$$E_{\nu_\mu}^2 dN_{\nu_\mu}(E_{\nu_\mu})/dE_{\nu_\mu} = N_{\nu_\mu,0} \begin{cases} \epsilon_{\nu_\mu,b}^{-1} E_{\nu_\mu} & \text{if } E_{\nu_\mu} \leq \epsilon_{\nu_\mu,b} \\ 1 & \text{if } \epsilon_{\nu_\mu,b} \leq E_{\nu_\mu} < \epsilon_{\nu_\mu,s} \\ \epsilon_{\nu_\mu,s} E_{\nu_\mu}^{-2} & \text{if } E_{\nu_\mu} \geq \epsilon_{\nu_\mu,s} \end{cases}$$

The first break of the WB spectrum $\epsilon_{\nu_\mu,b} = 10^{14}$eV is connected to the break in the photon spectrum $\epsilon_{\gamma,b}$ via the energetics of the Δ-resonance. It is determined through the minimal

energy necessary to produce a $\Delta(1232)$-resonance in the shock fronts of the bursts.

$$E_\gamma E_p \geq \frac{m_\Delta^2 - m_p^2}{2(1 - cos(\theta_{p\gamma}))} \tag{1.10}$$

where m_Δ and m_p are the rest mass of the Δ-resonance and the proton respectively. We now need an approximation of how much energy is passed from the parent protons to the neutrinos (after pion decay). It is possible to estimate the fraction of energy $f_\pi = 0.2$ passed on from the protons to the pions. In the subsequent decay of the pions about 1/4 of the pion energy is transformed into neutrinos:

$$\begin{aligned} E_{\nu_\mu} &= \frac{1}{4} f_\pi E_p \\ &= \frac{1}{20} . \frac{m_\Delta^2 - m_p^2}{2(1 - cos(\theta_{p\gamma}))E_\gamma} \end{aligned} \tag{1.11}$$

This result then has to be boosted to the observer's frame as well as shifted due to cosmological effects to obtain the observed values:

$$E_{\nu_\mu} = \frac{\Gamma^2}{(1+z)^2} . \frac{1}{20} . \frac{m_\Delta^2 - m_p^2}{2(1 - cos(\theta_{p\gamma}))E_\gamma} \tag{1.12}$$

Using the numerical values given in [46] for the proton mass, $m_p = 0.94$ GeV, and the Δ-mass, $m_\Delta = 1.23$ GeV, leads to:

$$\epsilon_{\nu_\mu,b} = 7.10^5 . \frac{\Gamma^2}{(1+z)^2 \epsilon_{\gamma,b}} \, GeV \tag{1.13}$$

The second energy break of the WB spectrum at $\epsilon_{\nu_\mu,s} = 10^{16}$eV in the neutrino spectrum results from the fact that pions lose energy at very high energy due to synchrotron radiation. It can be obtained by considering synchrotron cooling of the pions. To calculate the energy of this break one has to compare the particle life time τ to the synchrotron loss time t_{syn}.

Some exotic sources

Another hypothetical source of HEN is related to the presence of dark matter in the universe. It was first in 1933 that Zwicky pointed out that a possibly significant amount of mass was missing from observations [47]. The bulk of this dark matter is non-baryonic. One of the candidates is the neutralino, a stable and neutral particle in the minimal standard super-symmetric model. The Galaxy would lie in a halo consisting of these particles, which would, *inter alia*, help explain the anomalous behavior of the distribution of the velocities of visible objects (constant speed

of about 220 km/s regardless of the distance to the center of the Galaxy).

Subject to the Kepler's laws, like any other massive object, these particles revolve with the same average speed. Under the influence of gravity, the neutralinos get trapped at the center of massive bodies, such as the Sun and the Galactic center, where they can annihilate. In this scenario, neutrinos would emerge as by product of the annihilations. The discovery potential of a neutrino telescope like ANTARES for such dark matter particles is discussed, for example, in [48].

1.2 Gravitational waves

Einstein's theory of General Relativity introduces the concept of a dynamical and deformable space-time. The dynamics result from the interaction between space-time and its matter contents. In short, "spacetime tells matter how to move; matter tells spacetime how to curve" [49].

General Relativity describes Gravity as a direct effect of space-time curvature. It predicts that the equations of space-time can give rise to radiative solutions, called *gravitational waves*. Gravitational waves (GW) are ripples in the metric of spacetime that propagate at the speed of light.

Here, we give an introduction to GWs in section 1.2.1 and their phenomenology in section 1.2.2. We present in section 1.2.3 the potential astrophysical sources.

1.2.1 Basics of gravitational-wave theory

In the theory of General Relativity, gravitation is described as a geometrical effect connected to the curvature of space-time. The geometry of space-time is defined by a metric g which determines the distance ds of neighbouring events taking place at space-time coordinates x^α ($\alpha = 0, 1, 2, 3$) and $x^\alpha + dx^\alpha$. We have

$$ds^2 = g_{\mu\nu} dx^\mu dx^\nu \tag{1.14}$$

where Einstein's summation convention in use here implies the summation over indices μ and $\nu = 0, 1, 2, 3$. The metric g used in the above equation through its components $g_{\mu\nu}$ describes how intervals are measured in space-time and hence the properties of the gravitational field.

The curvature of space-time is determined by the energy-matter distribution through the Einstein equations

$$G_{\mu\nu} = R_{\mu\nu} - \frac{1}{2} R = \frac{8\pi G}{c^4} T_{\mu\nu} \tag{1.15}$$

where c is the speed of light, G is the constant of gravitation. The Einstein equations connects the Einstein tensor $G_{\mu\nu}$ which describes the dynamics of space-time geometry and is directly connected to the metric g to the stress-energy tensor $T_{\mu\nu}$ which describes the matter and energy source distribution.

The Einstein equations form a set of 10 non-linear partial differential equations. Finding a solution to those equations is difficult in general. Approximated solutions can be found in the weak field approximation, where the metric results from a small perturbation of the Minkowski metric $\eta_{\mu\nu} = diag(-1, 1, 1, 1)$ of special relativity associated to flat space-time

$$g_{\mu\nu} = \eta_{\mu\nu} + h_{\mu\nu} \tag{1.16}$$

where the term $h_{\mu\nu}$ represents a small (tensor) perturbations with $|h_{\mu\nu}| \ll 1$. In this case, the Einstein equations can be linearized. Applying the Lorentz gauge condition, we get

$$\left(\nabla^2 - \frac{1}{c^2}\frac{\partial^2}{\partial t^2}\right) h_{\mu\nu} = 0 \tag{1.17}$$

This is the wave equation. If the propagation direction be z, the solutions are

$$h_{\mu\nu} = \Re\left\{\varepsilon_{\mu\nu} \exp(\omega t - kz)\right\} \tag{1.18}$$

where $\omega = kc$ and $\varepsilon_{\mu\nu}$ is a 4×4 symmetric matrix of constants.

This implies the existence of oscillatory wave-like solutions to Einstein's equations: *gravitational waves* (GW). They are predicted to propagate at speed of light.

The freedom to choose a coordinate frame allows us to select one where $h_{\mu\nu}$ is transverse traceless (also referred to as "TT gauge"). In this frame, $\varepsilon_{\mu\nu} = h_+\varepsilon^+_{\mu\nu} + h_\times\varepsilon^\times_{\mu\nu}$ can be linearly decomposed into two independent polarization tensors $\varepsilon^+_{\mu\nu}$ and $\varepsilon^\times_{\mu\nu}$ which define the "+" (plus) and "×" (cross) polarizations respectively.

$$\varepsilon^+_{\mu\nu} = \begin{bmatrix} 0 & 0 & 0 & 0 \\ 0 & 1 & 0 & 0 \\ 0 & 0 & -1 & 0 \\ 0 & 0 & 0 & 0 \end{bmatrix} \qquad \varepsilon^\times_{\mu\nu} = \begin{bmatrix} 0 & 0 & 0 & 0 \\ 0 & 0 & 1 & 0 \\ 0 & 1 & 0 & 0 \\ 0 & 0 & 0 & 0 \end{bmatrix}. \tag{1.19}$$

This shows that GW have two independent polarizations.

1.2.2 Phenomenology of gravitational waves

Effect of gravitational waves on matter

Equations (1.18) and (1.19) show that a GW modulates the distance between two nearby objects at the wave frequency ω with opposite sign in the plane *transverse* to the direction of propagation.

This is a *differential strain* effect which is illustrated in Figure 1.10 over a ring of free falling test masses submitted to gravity only. We also see that the effect of the + and × polarization is the same except a rotation of 45° degrees.

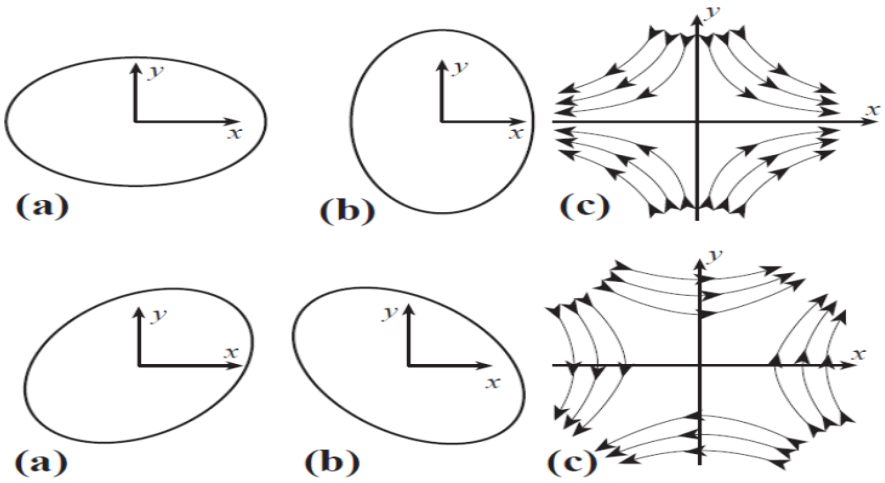

Figure 1.10 – Deformation of a ring of freely falling test masses due to an impinging GW which propagates in the direction normal to the plane of the ring. (a and b top) effect of the "+" polarization. (a and b bottom) effect of the × polarization. (c top) the field lines corresponding to the + polarization (The arrows show the direction of the field). (c bottom), the field lines corresponding to the × polarization.

Production of gravitational waves–Quadrupole formula

Electromagnetic (EM) waves are produced by accelerated charges. Similarly, GW are produced by accelerated masses. The lowest non-vanishing term in the multipole expansion of the source distribution is the quadrupole, since the dipole vanishes due to the conservation of momentum. This is a major difference with respect to EM waves (which are dominated by the dipole). The emission of GW are thus associated to variations of the quadrupolar moment tensor of the mass distribution defined by

$$Q_{ij}(t) = \frac{1}{c^2} \int T_{00}(t,x) x_i x_j d^3x \tag{1.20}$$

where T_{00} is the time component of the stress-energy tensor which is directly connected to the energy density and hence source rest-mass density. Clearly, a spherically symmetric system

cannot emit GW as its quadrupole does not vary. The so-called *quadrupole formula* obtained in the far field and slow motion approximation ($v \ll c$), connects the GW amplitude to the quadrupole moments defined in Equation (1.20). We have

$$h_{ij} = \frac{2}{r}\frac{G}{c^4}\frac{\partial^2}{\partial t^2}Q_{ij}(t - r/c) \tag{1.21}$$

where r is the distance from the observer to the source. This shows that GW are a *radiation* as its amplitude decreases inversely with the distance r to the source.

The leading factor $G/c^4 \approx 8.3 \times 10^{-45}$ s^2/m/kg is extremely small. To generate GW of sufficient amplitude to be detectable, it has to be compensated by very large variations of Q.

These variations have typical magnitude $\ddot{Q} \sim (mv^2)_{\text{nonsph}}$ which is twice the non-spherical part of the kinetic energy inside the source. Let us denote the source characteristic radius R and ϵ the degree of asymmetry of the mass distribution and let us assume that the source evolves over the characteristic time scale T. We then get the estimate $\ddot{Q} \approx \epsilon m R^2/T^2$. Applying this estimate to systems at the human scale, we see that they are unable to reach a sufficient $\ddot{Q}$.

This implies that GW cannot be generated in a laboratory. The sources must involve very massive, dense, relativistic systems and are therefore necessarily high-energy astrophysical processes. To get typical estimates, let us consider a system formed of two compact stars (such as, a neutron-star binary). A detailed discussion of this system as a GW source will be given later in section 1.2.3. For such a source, the above estimate yields $\ddot{Q} \sim m(\Omega R)^2 \sim m^{5/3}\Omega^{2/3}$ using 3rd Kepler's law. For a binary neutron-star system with $m = 1.4M_\odot$ located at $r = 10$ Mpc and orbiting at $\Omega/(2\pi) \sim 100$ Hz, the above estimate gives $h \sim 10^{-21}$. This corresponds to the detectability limits of current GW detectors (as explained in detail in chapter 3).

A consequence of the estimates provided in this section is that GW are produced by the coherent relativistic bulk motion of large mass distributions. This radically differs from EM waves generally produced in Nature by the individual and incoherent motion of charges (atoms or electrons). While EM waves (and neutrino emission) are sensitive to the micro-physics, GW carries information about the global dynamics of the source.

Radiated GW energy

It is interesting to calculate the energy radiated by a GW away from the source. The GW energy flux (per unit time and unit area) is defined by [50]

$$F_{GW} = \frac{c^3}{16\pi G}\langle \dot{h}_+^2(t) + \dot{h}_\times^2(t)\rangle \tag{1.22}$$

where $\dot{x}$ designates the time derivative and where the average $\langle\cdot\rangle$ operates over several periods. This averaging is necessary and arises from the impossibility to define the energy of a gravitational field locally in General Relativity.

For example, the energy flux of a sinusoidal, linearly polarized wave of amplitude H_+ and angular frequency ω is

$$F_{GW} = \frac{c^3}{32\pi G}\omega^2 H_+^2 \tag{1.23}$$

Assuming a frequency of $\omega/(2\pi) = 100$ Hz and amplitude $H_+ = 10^{-21}$, one obtains a flux of 3.3 mW/m^2 (or equivalently 3.3 erg/s/cm^2). This is a considerable energy for astrophysical standard candales. For instance, it is eight orders of magnitude larger than the Crab pulsar luminosity in the ~ 10 keV band.

The GW radiated energy is obtained with

$$E_{GW} = D_L^2 \int d\Omega \int_T F_{GW}(t)dt \tag{1.24}$$

where D_L is the luminosity distance of the source from the detector, Ω is the solid angle and F_{GW} is measured at the detector.

Indirect evidence of existence

In 1993, the physicists Russel Hulse and Joseph Taylor has been awarded the Nobel Prize in Physics for their experimental observations in 1974. These observations consisted in following the evolution of the orbit of the binary pulsar PSR1913+16 as shown in Figure 1.11 [51, 52]. This system is composed of two neutron stars, of which one is a pulsar and the other is dark, bound in an orbit with period $P \sim 7hr45min$.

Hulse and Taylor used their timing measurements of the pulses to infer the details of the orbital motion. The number of pulses received each second increases when the pulsar is moving towards us and is close to its periastron and vice-versa. These observations of the pulse emitted by the pulsar evidenced the orbital decay $dP/dt < 0$ of the binary (about 40 seconds over 30 years). This implies that the system loses energy.

The measured decay is in remarkably close agreement ($\sim 0.2\%$) [52] with the predictions of General Relativity assuming that the system essentially loses energy by radiating GW away. This provided an indirect evidence for the existence of GW.

Since the discovery of PSR1913+16, other binary pulsars have been detected which includes PSR B1534+12 and PSR J0737-3039A/B [53]. All those newly discovered systems exhibit the same orbital decay as PSR1913+16.

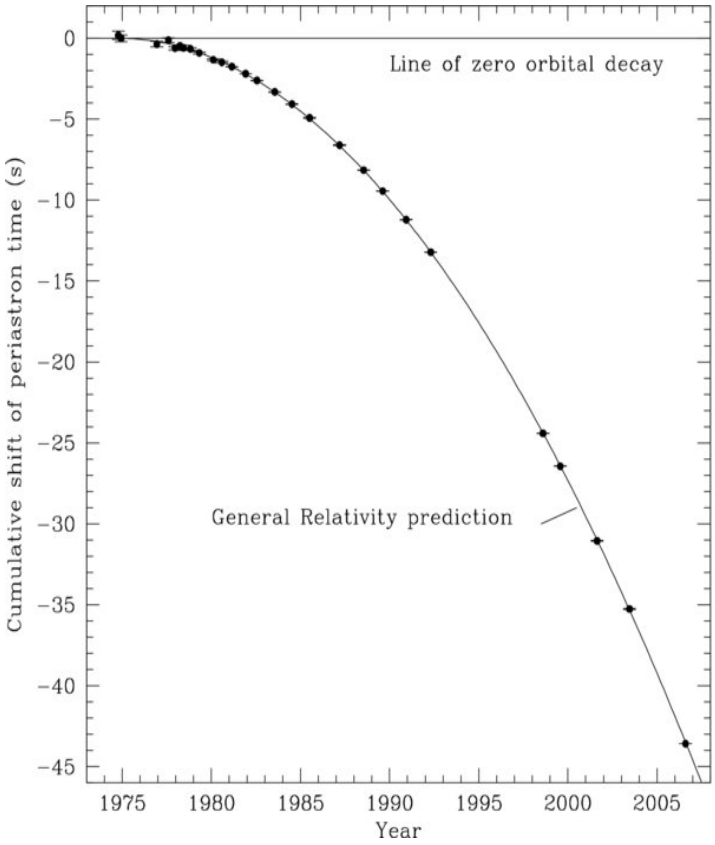

Figure 1.11 – Cumulative shift of the periastron time for PSR 1913+16 from 1975 to 2007. The continuous curve shows the predictions from the General Relativity. The observations are shown with as points with measurement error bars.

1.2.3 Astrophysical sources of gravitational waves

Astrophysical sources of gravitational radiation can be divided into two categories: *permanent* and *transient* sources.

Permanent sources includes *periodic sources* and *stochastic backgrounds*. We refer to periodic sources as sources that emit periodic GW continuously. They are related to isolated rotating neutron stars with some degree of asymmetry (characterized by the ellipticity of the star) that may be due to accretion or pressure from internal magnetic fields for instance. If there is a sufficient degree of asymmetry, such a system is expected to emit a monochromatic GW at twice the rotation period. The wave amplitude is weak (much lower than the noise floor of current detectors). However, since it is permanent, it can be integrated over a long duration. Stochastic GW backgrounds can have an astrophysical or a cosmological origin. Astrophysical backgrounds result from the incoherent superposition of many GW from unresolved faint sources located in the Galaxy or in the nearby Universe. Current cosmological models also predict the existence

of a relic stochastic background from the very early phase of the Universe history. Both types of backgrounds are stochastic GW signals and require at least two detectors in operation to be detected (by the measurement of an excess of correlation).

This thesis focuses on transient sources as they are potentially connected to the emission of high-energy neutrinos. This section discusses into more detail the potential astrophysical sources of transient GW.

Coalescing compact binaries

A large fraction of stars are in binary systems. If both components of the binary end up forming compact bodies (neutron star or black hole) and if their orbit is sufficient tight, the resulting system will eventually coalescence after losing a considerable amount of energy through GW emission. The coalesce of neutron-star and/or black-hole binaries similar to the Hulse-Taylor binary mentioned previously is often considered the most promising source.

During the inspiralling phase where the two bodies are far apart, the dynamics of such a system (and hence the expected GW waveform) can be predicted with great accuracy by using post-Newtonian expansions [54, 55].

The GW signature consists in a *chirp* signal whose frequency sweeps toward high values according to a power law at first order (see Figure 1.12). A substantial amount of energy is radiated in the following phase when the two bodies merge into a black-hole. In this highly relativistic phase, the perturbative treatment of binary dynamics is not valid anymore and one has to resort to numerical simulations. The process is concluded by the ring-down phase during which the resulting distorted black-hole radiates away its asymmetry down to equilibrium.

During the whole coalescence process, a stellar-mass binary with equal masses radiates away of the order of a percent of its rest mass [56]. This corresponds to a GW amplitude of $h \sim 10^{-21}$ observable at Earth for a system located at 10 Mpc as estimated above in section 1.2.2. More precise estimates of the detectability horizon can be obtained: GW detectors can ideally observe those binary systems up to a distance of $\sim$ 30 Mpc and $\sim$ 440 Mpc for initial and advanced detectors respectively.

Although binary systems are fairly common, only a small fraction eventually forms a compact binary that is sufficiently tight to coalesce in less than the Hubble time. A survey of population estimates [57] gives a "realistic" rate of one neutron star–neutron star coalescence[2] per 10,000 year per galaxy equivalent in size to the Milky Way. When converted into a rate of *detectable* coalescences, the above horizons lead to $\sim$ 0.02 events per year with the first generation of (initial) detectors and to $\sim$ 40 events for the second generation (advanced). Large

[2]Similar rates are obtained for the other types of systems mixing neutron-stars and/or black-holes.

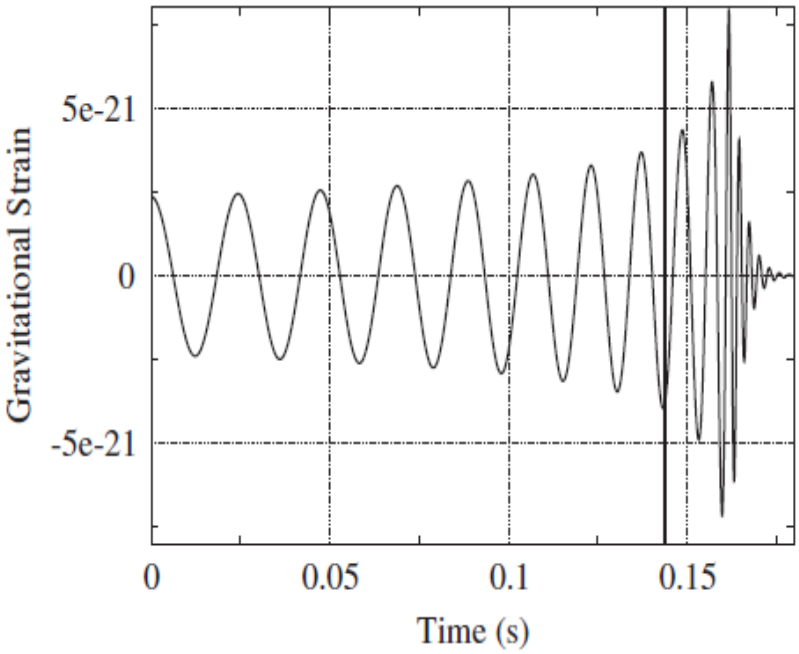

Figure 1.12 – Example of a GW chirp waveform from coalescing compact binaries.

error bars are attached to those estimates reflecting the weakness of the observation constraints we have about those systems. The above stated rates can be 10 times smaller or larger in the "pessimistic" or "optimistic" scenarios respectively.

It is suspected that binary coalescences could be the progenitors of at least a fraction of the short-hard gamma-ray bursts. The "realistic" rates presented above are corroborated by the ones derived from that assumption [57].

Core collapse supernova

Gravitational stellar-core collapse is another potential source of GW if some degree of non-axisymmetry is exhibited during this process. The simulations required to make reliable predictions of the emission levels are very challenging as they have to incorporate many physical ingredients including relativistic magneto-hydrodynamics and a detailed treatment of neutrino transport and nuclear iterations [58]. The current realistic estimate of the amount of radiated GW energy is of order $10^{-7} M_{\odot}$ and corresponds approximately [59] to a distance reach of order $\sim$ 10 kpc with the initial detectors, $\sim$ 100 kpc with the advanced detectors. The detectable sources are therefore located in the Galaxy.

A few mechanisms have been suggested in which GW emission associated with gravitational core-collapses is enhanced. This is connected to the collapse of very massive star associated with high rotation rate possibly due to accretion. In that case, bar or fragmentation instabilities

[60, 61] may lead to the emission of order $10^{-2} M_\odot$ in GW, leading to similar detectability horizons as the coalescing binaries of neutron-stars. This astrophysical scenario may also be at the heart of long-soft GRB.

Star quakes

Several observations indicate that neutron stars may experiment large stress during the course of their life. Although "ordinary" neutron stars are characterized by extremely strong surface magnetic fields ($\sim 10^{12}$ G), many magnetars appear to have fields 100-1000 times stronger, implying enormous pent-up magnetic energy. Soft gamma ray repeaters (SGRs) and anomalous X-ray pulsars (AXPs) are different observational manifestations of the same underlying system with a highly magnetized star which sporadically converts magnetic field energy into radiation [62].

The sudden release of the magnetic energy may also excite to some extent the fundamental or f-modes of the star, which radiate GW with damping times of ~ 200 ms.

Detailed predictions about the GW amplitude are difficult to obtain. An upper-limit of $\sim 10^{49}$ erg on the maximum *total* energy release in an SGR giant flare can be derived from one of the most optimistic models (see [63]), of a giant flare associated with a global reconfiguration of the internal magnetic field. Similarly, [64] estimated a maximum total energy release of $\sim 10^{48}$-10^{49} ergs in a fraction of the parameter space, within the model originally proposed by [63].

1.3 Joint sources of gravitational waves and high-energy neutrinos

In the previous sections, we described models for the single production of GWs or HENs. In this section, we discuss plausible sources of both GW and HEN emissions. We will see that some of the scenarios leading to joint emissions are tighly connected to gamma-ray bursts (GRBs) [65].

GW emission requires relativistic bulk motion of massive objects such as gravitational collapse or merger of compact objects. Production of HEN requires the formation of a fireball and ejection of relativistic particles with some hadronic load. These two requirements restricts the wide range of sources presented so far. The list of plausible sources gives a global and coherent picture of the astrophysical scenarios from both GW and HEN perspectives. When applicable, we will also mention their connection to observations in the electromagnetic spectrum. Note however, that will be especially interested in the sources that are *not* observed electromagnet-

ically. This may due to the source opacity (which often arises in the dense media considered here). This may be also due to observational limitations. For instance, a significant fraction of GRBs are missed by current observatories. Swift/BAT and Fermi/GBM miss about 90 % and 40 % of all GRBs respectively. This is due to the limited fields of view, technical downtime, and orbital passes through the South Atlantic Anomaly.

1.3.1 Core-collapse supernovae with mildly relativistic jet

One of the promising sources are core-collapse supernovae (CCSN) with mildly relativistic jet [66]. There are evidence for the existence of such jets, observed in radio [67].

The HEN emission for this source is somewhat related to the fireball model for (long) GRB presented in section 1.9. In this model, a jet of plasma is ejected at relativitic velocity. Relying on the assumption that protons are accelerated in the jet through Fermi acceleration in internal shocks, pp and $p\gamma$ interactions will produce kaons (K) and pions (π). In these two interactions (non-thermal) neutrinos of TeV energy can be produced through the decay of charged pions and kaons [66, 68]. The charged $\pi^{\pm}$ and $K^{\pm}$ are expected to follow the proton spectrum falling as E^{-2}. About 20% of the proton energy is converted into the produced neutrinos. An ejected mass with a kinetic energy of 3×10^{51} erg and a Lorentz factor of 3 at 10 Mpc would generate ~ 30 neutrino events detected in a km^3 detector [68] which translates to order of few events in ANTARES.

GW emission associated to the gravitational collapse of massive star was already discussed in section 1.2.3. We mentioned that the presence of a high rotation rate (due to accretion for instance) may develop bar-mode instability thus leading to enhanced GW emission. [69] quote upper limits of $P_{max} = 10^{53}$ erg/s at $f = 1$ kHz. If the bar remains coherent for ~ 100 cycles, this conducts to a GW emitted energy of order $10^{-2} M_{\odot}$. Under the (unlikely) assumption of extreme rotation, [70] predicts the formation of fragments ($< 1 M_{\odot}$) leading to the emission of an inspiral-like GW chirp. If we estimate that order of one percent of the rest-mass is emitted during merger, we again get a GW emitted energy of order $10^{-2} M_{\odot}$, this time at frequencies of few hundred Hz.

If core collapse supernovae may lead to significant GW and HEN emission, they may also be faint or undetectable electromagnetically. Mildly relativistic jets might not be powerful enough to break out the star hydrogen envelope [68]. This is usually referred to as the "choked GRB" model. Without an emerging jet, the X-ray, optical, IR, and radio afterglows typical of GRB would also be absent. Also, core collapse of massive star may not lead systematically to SN shock breakout. For instance, some of the nearby GRBs (e.g., GRB060505 or GRB060614) miss a supernova. Even if the process succeeds in yielding a supernova, it may not be observable.

A significant fraction (up to 15 % with 10 Mpc) of supernovae are missed optically in the local Universe because of selection effects and dust extinction.

Choked GRBs may be at the extreme end of a (potentially large) local population of faint long-soft GRBs. A subclass of GRBs with luminosities lower by a few orders of magnitude than typical luminosities has been identified. Less luminous than typical long GRBs, "low-luminosity GRBs", are discovered at much smaller distances (SN 1998bw at redshift $z = 0.0085$, about 40 Mpc away from Earth, SN 2003lw at $z = 0.105$, and SN 2006aj at $z = 0.033$). The event rate per unit volume of those type of events has been estimated to be more than one order of magnitude larger than that of conventional long GRBs.

1.3.2 Other sources

Short–hard GRBs are thought to be driven by NS–NS or NS–BH mergers [71, 72]. As discussed in section 1.2.3, coalescing binaries are expected to emit GWs that are detectable to large distances ([73, 74]), ~ 30 Mpc with the initial versions of LIGO and Virgo. Much less is known about the HEN emission from those systems. If the binary merger is associated to a GRB, this implies the presence of an ultrarelativistic jet. If there is significant baryon loading in the jet, this should eventually conduct to the production of HEN.

Other potential galactic sources of GW+HEN joint emission can be considered in this work. Such sources are Soft Gamma Repeaters (SGRs) which are X-ray pulsars with soft gamma-ray bursting activity. According to the magnetar model, SGRs may be associated with star-quakes. The deformation of the star during the outburst could produce GWs (see section 1.2.3), while HENs could potentially emerge from hadron-loaded flares (see section 1.1.4).

A more exotic class of sources are cosmic strings, topological defects formed during phase transitions in the early Universe. Emission of gravitational waves is considered the main channel for cosmic string loops to decay. In particular, cosmic string cusps appear to be potential sources of gravitational waves due to the very large Lorentz factor achieved when they contract. Cosmic strings and topological defects in general are also of interest to high energy neutrino astronomy as they can produce particles, including neutrinos, up to the Planck scale [75].

1.3.3 Time delay between gravitational wave and high-energy neutrino emissions

The scenarios evoked in the previous sections are connected to GRBs. GRBs provide an interesting astrophysical scenario where the delay between GW and HEN emissions can be characterized. A conservative estimate of this delay determines the baseline duration over which GW and HEN are declared in coincidence. A statistical estimate has been obtained in [76] based

on GRBs mainly observed by BATSE, Swift and Fermi LAT. In this article, we considered the duration of the different emission processes to constrain the size of the time search window. Figure 1.13 summarizes the assumptions and modelling of [76]. This leads to an upper bound on the size of $\Delta t_{GW+HEN} = [-500s, +500s]$ the time search window. The latter is conservative enough to encompass most theoretical models of GW and HEN emissions for GRBs. This time window will be used in both analyses presented in this work, see Chapters 4 and 5 for further details.

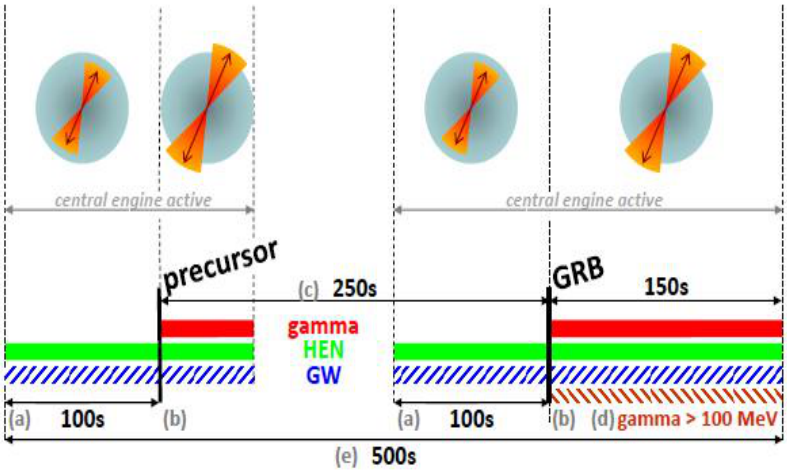

Figure 1.13 – Overview of the GRB emission processes and GW/HEN time search window. (a) Active central engine before the relativistic jet has broken out of star; (b) Active central engine with relativistic jet broken out of star; (c) Delay between onset of precursor and main burst; (d) Duration corresponding to 90% of GeV photon emission; (e) Time span of central engine activity. Possible GW/HEN emission between the precursor and the main GRB (no emission is shown on the figure) has no effect on the estimated time window. Overall, the considered processes allow for a maximum of 500s between the observation of a HEN and a GW transient, setting the time search window to [-500s; 500s]. (Adapted from [76])

REFERENCES

[1] E. Fermi, Z. Phys. 88 (1934) and Nuovo Cim. 11 (1934).

[2] C.L Cowen et al, Science, 124, 103 (1956).

[3] G. Danby et al, Phys. Rev. Lett. 9, 36, (1962);

[4] M. L. Perl et al, Phys. Rev. Lett 35, 1489, (1975).

[5] K. Kodama et al, Phys. Lett. B, 504, 218-224, (2001).

[6] B.T. Cleveland et al., Astrop. Jour. 496 505 (1998).

[7] J. N. Bahcall and R. Davis, PASP, 112, 770, 429-433, (2000).

[8] The Kamiokande II collaboration, Phys. Rev. Lett. 58 1490 (1987) and Phys. Rev. D38 448 (1988).

[9] M. S. Longair, newblock High-energy astrophysics, Cambridge University Press (2011).

[10] J. Beringer et al, Phys. Rev. D86, 010001 (2012).

[11] K. Greisen, Phys. Rev. Lett. 16, 748 (1966).

[12] G. T. Zatsepin and V. A. Kuzmin, JETP Lett. 4, 78 (1966).

[13] J. Abraham et al, Phys. Rev. Lett. 104:091101, (2010).

[14] E. Waxman, NIM A 827, 15c-25c (2009).

[15] D. Allard, e-Print: arXiv:1111.3290 (2011).

[16] G. Decerprit, D. Allard, A&A, 535, A66 (2011).

[17] E. Waxman and J. N. Bahcall, Phys. Rev. D 59 023002 (1999).

REFERENCES

[18] K. Mannheim, R.J. Protheroe and J.P. Rachen, Phys. Rev. D 63 (2001).

[19] http://www.mpi-hd.mpg.de/hfm/HESS/.

[20] http://fermi.gsfc.nasa.gov/

[21] W. Bednarek et al, New Astron. Rev. 49 (2005).

[22] A. Levinson and E. Waxman, Phys. Rev. Lett., 87, 171101 (2001).

[23] C. Distefano, Astrophys. J., 575:378-383, (2002).

[24] S. Galata, PhD thesis, Université Aix-Marseille (2012).

[25] W. Bednarek, Astrophys. J. 631 466 (2005).

[26] H. R. Christiansen et al, Phys. Rev. D73, 063012, (2006).

[27] D. Eichler, MNRAS, 335, 883, (2003).

[28] F. Aharonian et al, Astron. Astrophys. 425 13-17, (2004).

[29] F. Aharonian et al, Nature 439 695 (2006).

[30] F. Aharonian, et al, A&A 448, L43 (2006).

[31] D. Horns et al, A&A 451, L51-L54 (2006).

[32] C. Hazard et al, Nature 197 1037-1039 (1963).

[33] F. Halzen, astro-ph/0506248 (2005).

[34] J. Abraham et al, Science 318, 938-943 (2007).

[35] F. Aharonian et al, Nature 440, 1018 (2006).

[36] W. Benbow et al, Proceedings of the 30th ICRC, Merida, Mexique, (2007).

[37] A. Loeb and E. Waxman, JCAP 0605 003 (2006).

[38] W. S. Paciesas et al, Astrophys. J. Supp., 122, 465-495, (1999).

[39] E. Costa et al, Nature, 387, 783-785, (1997).

[40] T. Piran, Rev. Mod. Phys. 76, 1143-1210, 2004.

[41] E. Waxman and J. N. Bahcall, Astrophys. J., 541, 707-711, (2000).

[42] A. Levinson and D. Eichler, Astrophys. J., 594, L19-L22, (2003).

[43] R. Abbasi et al, Nature 484 351-354 (2012).

[44] E. Waxman and J. N. Bahcall, Phys. Rev. Lett 78, 2292-2295, (1997).

[45] J. N. Bahcall and E. Waxman, Phys. Rev. D64, 023002 (2001).

[46] Particle Data Group, Phys. Let. B 592 1 (2004).

[47] F. Zwicky, Helv. Phys. Acta, 6-110 (1933).

[48] G. Lim, PhD thesis, University of Amsterdam (2012).

[49] J. Wheeler, K. Ford, newblock Geons, Black Holes, & Quantum Foam: a life in physics, W. W. Norton, New York, (1998).

[50] M. Maggiore, newblock Gravitational Waves Volume 1. Theory and Experiments , Oxford University Press, (2007).

[51] R. A. Hulse J. H. Taylor, Astrophys. J., 195, L51-L53 (1975).

[52] J. M. Weisberg, D. J. Nice, and J. H. Taylor, Astrophys. J. 722, 1030-1034 (2010).

[53] , http://arxiv.org/abs/astro-ph/0609417.

[54] L. Blanchet, Living Rev. Relat., 5 (2002).

[55] A. Buonanno et al, Phys. Rev. D75, 124018 (2002).

[56] B. S. Sathyaprakash and B. F. Schutz, Living Rev. Relat, 12 (2009).

[57] J. Abadie et al, Class. Quantum Grav., 27, 173001 (2010).

[58] C. D. Ott, Class. Quantum Grav., 27, 063001 (2009).

[59] P. Sutton, LSC Technical Paper, P1000041 (2010).

[60] L. F. Chris and C.B. N. Kimberly, Living Rev. Relat., 14, 1 (2011).

[61] M. B. Davies et al., Astrophys. J., 579 L63, (2002).

[62] V. M. Kaspi, Proc. Nat. Acad. Sci. 107, 7147 (2010).

[63] K. Ioka, MNRAS, 327, 639-662 (2001).

[64] A. Corsi and J. B. Owen, Phys. Rev. D83, 104014 (2011).

[65] S. Ando et al, submitted to Rev. Mod. Phys. arXiv:1203.5192.

[66] S. Razzaque et al, Mod. Phys. Lett., 20, A2351 (2005).

[67] Z. Paragi et al, Nature 463, 516-518 (2010).

[68] S. Ando and J. F. Beacom, Phys. Rev. Lett., 95, 061103 (2005).

[69] C. Fryer and K. New, Living Rev. Relat., 14, 1 (2011).

[70] M. Davies et al, Astrophys. J., 579, L63 (2002).

[71] W. H. Lee, and E. Ramirez-Ruiz, New J. Phys., 9, (2007).

[72] Z. B. Etienne et al., Phys. Rev. D79, 044024 (2009).

[73] É. É. Flanagan and S. A. Hughes, Phys. Rev. D57, 4535-4565 (1998).

[74] S. Kobayashi and P. Mészáros, Astrophys. J., 589, 861-870, (2003).

[75] T. Damour and A. Vilenkin, Phys. Rev. Lett. 85, 3761-3764 (2000).

[76] B. Bruny et al, Astropart. Phys., 35, 1-7 (2011).

CHAPTER 2

NEUTRINO TELESCOPES

2.1 Summary

With the advent of a new generation of observatories including the ANTARES neutrino telescope observational astrophysics is entering a new era. The ANTARES neutrino telescope gives access to new and unexplored observations of the Universe complementary to the standard photon-based astronomy. This chapter gives an introduction to the neutrino astronomy from an instrumental point-of-view ranging from the general detection principles to the description of the instruments currently in operation. We focus in the most part of this chapter on the ANTARES instrument.

2.2 Neutrino telescopes

2.2.1 General principles

The detection rate $\mathrm{T}(\mathrm{E}_{\mathrm{min}}, \theta)$ of charged leptons l (e, μ, τ) produced by neutrino interactions around the detector can be obtained by convoluting the incoming neutrino flux dN/dE_ν and the detection probability of these neutrinos:

$$\mathrm{T}(\mathrm{E}_{\mathrm{min}}, \theta) = \int_{\mathrm{E}_{\mathrm{min}}} \mathrm{P}_{\nu\to\mathrm{l}}(\mathrm{E}_\nu, \mathrm{E}_{\mathrm{min}})\mathrm{P}_{\mathrm{trans}}(\theta, \mathrm{E}_\nu)\frac{\mathrm{dN}}{\mathrm{dE}_\nu}\mathrm{dE}_\nu \tag{2.1}$$

where $\mathrm{P}_{\mathrm{trans}}(\theta, \mathrm{E}_\nu)$ is the transmissivity coefficient of a neutrino through the Earth and $\mathrm{P}_{\nu\to\mathrm{l}}(\mathrm{E}_\nu, \mathrm{E}_{\mathrm{min}})$ is the probability that a neutrino of energy E_ν creates a detectable lepton of energy greater or equal to $\mathrm{E}_{\mathrm{min}}$. This latter probability can be written as :

$$\mathrm{P}_{\nu\to\mathrm{l}} = \mathcal{N}\int_{\mathrm{E}_{\mathrm{min}}}^{\mathrm{E}_\nu} \mathrm{dE}_\mathrm{l}\frac{\mathrm{d}\sigma}{\mathrm{dE}_\mathrm{l}}\mathrm{R}_\mathrm{l}(\mathrm{E}_\mathrm{l}, \mathrm{E}_{\mathrm{min}}) \tag{2.2}$$

where $\mathcal{N}$ is the Avogadro number, $\frac{d\sigma}{dE_l}$ is the interaction cross section as a function of the neutrino energy and $R_l(E_l, E_{min})$ is the path length of the produced lepton. In the case of a muon ($\mathrm{l} = \mu$), this distance can be much greater than the detector size, contrarily to electrons and τ which are respectively absorbed or quickly desintegrated. This explains why the detection of muon neutrinos is favoured over the other flavors ("golden" channel). However, neutrino telescopes are also sensitive to electron and tau neutrinos and can in principle discriminate between flavors: tau-neutrino with energies $\geq 1PeV$ can indeed travel several meters before decaying producing a second shower, while electron-neutrino yields an electron which produces an electromagnetic shower.

In the following, we will concentrate on muon neutrino interactions and describe into more details the different terms of relation 2.2.

2.2.2 Neutrino interactions

After penetrating the Earth, the neutrino is subject to interactions with electrons and nuclei of atoms and molecules that constitute the rock, the sea or the ice. Neutrinos interact through only the weak interaction and have a small cross section ($10^{-38}cm^2$ at 1 GeV) [1]. Interactions at higher energy ($E_\nu > 10GeV$) are dominated by deep inelastic scattering onto atomic nuclei. When they interact, neutrinos are subject to two main [1] interaction processes: charged current (CC) interaction or neutral current (NC) interaction. While the former consists in an exchange of charged boson $W^\pm$, the second involves the exchange of a neutral boson Z^0 (see Figure 2.1 for illustration):

$$\begin{aligned} \nu_l(\overline{\nu}_l) + N &\longrightarrow l^-(l^+) + X \\ \nu_l + N &\longrightarrow \nu_l + X \end{aligned} \tag{2.3}$$

where l stands for any kind of leptons (e, μ, τ), $N \equiv \frac{n+p}{2}$ can be seen, for simplicity, as an isoscalar nucleon and X represents the hadronic products of the interaction. In the following we concentrate on the CC interaction which produces a charged lepton that will be later detected.

The differential cross section of the neutrino for this process can be expressed in terms of the parton distribution functions as follow [2, 3]:

$$\frac{d^2\sigma}{dxdy} = \frac{2G_F^2 M_N E_\nu}{\pi} \left(\frac{M_W^2}{Q^2 + M_W^2}\right)^2 \left[xq(Q^2, x) + x\overline{q}(Q^2, x)(1-y)^2\right] \tag{2.4}$$

where:

[1] we will not treat here the Glashow resonance $\overline{\nu}e \to W \to X$

- G_F is the Fermi constant.
- Q is the invariant momentum transfer.
- M_N and M_W are the nucleon and the intermediate-boson masses.
- $\nu = E_\nu - E_l$ is the fraction of energy carried by the boson in the laboratory frame.
- $x = \dfrac{Q^2}{2M_N\nu}$ and $y = \dfrac{\nu}{E_\nu}$ are the Bjorken scaling factors.
- $q(Q^2, x)$ and $\overline{q}(Q^2, x)$ represent the parton distribution functions (PDFs) describing the quark and anti-quark content of nucleon.

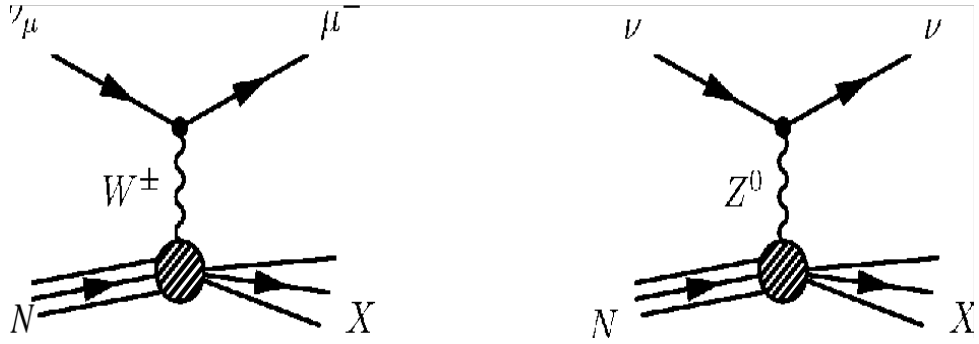

Figure 2.1 – Feynman diagram representation of the CC (left) and NC (right) interactions

Figure 2.2 left and right show the cross section of the ν and $\overline{\nu}$ interaction respectively. At energies $E_\nu > 10GeV$ the cross section increases linearly with energy while it follows a $\sigma \propto E_\nu^{0.4}$ relation at energies $E_\nu > 1PeV$. These different regimes arise from the non negligible value of Q^2 at high energy with respect to the mass propagator.

For muon neutrino interactions, the angle between the direction of the initial neutrino and the out-going muon in the charged-current channel is very small, the muon track and the parent neutrino are almost collinear. The angular difference between the direction of the primary ν_μ and the induced μ can be approximated by [4]:

$$\langle \theta_{\mu\nu} \rangle \approx \frac{0.7^\circ}{(E_\nu/TeV)^{0.6}} \tag{2.5}$$

During the propagation in the medium the muon track is further deflected as the muon undergoes multiple scattering. The mean angular deviation between the initial muon direction and

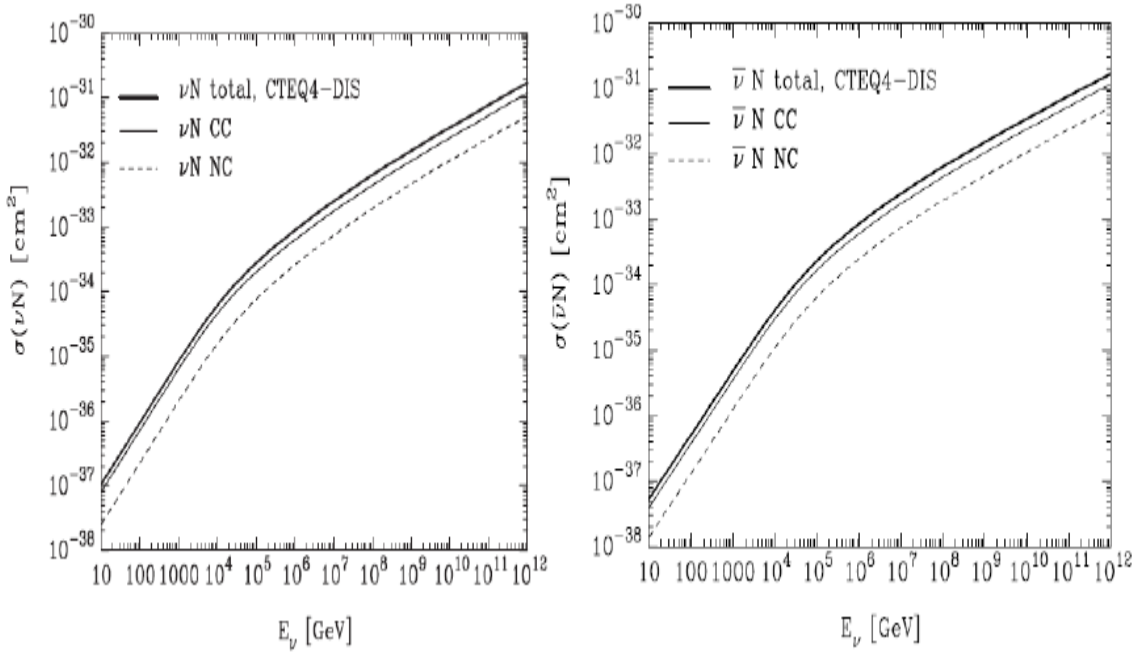

Figure 2.2 – The ν-N (left) and the $\overline{\nu} - N$ (right) cross section interaction as function of the energy

the direction after passing a distance x in the medium is described by [5]:

$$\Delta\theta_{ms} = \frac{13.6MeV}{E_\mu} z \sqrt{\frac{x}{X_0}} \left[1 + 0.038 ln\left(\frac{x}{X_0}\right)\right] \tag{2.6}$$

where X_0 is the radiation length[2] of the medium and $\Delta\theta_{ms}$ is given in radians and z is the charge number of the incident particle. The deviations due to the multiple scattering described by Equation (2.6) are generally smaller than the scattering angle in Equation (2.5). Therefore this allows the produced muon to somewhat preserve the original direction of the muon-neutrino. Indeed for neutrino energies larger than 1 TeV, the muon track is aligned with the incident neutrino within a degree. At higher energies ($\geq$ 10 TeV) the kinematics effects start to be negligible and the biggest uncertainty in the direction estimation comes from the calibration (timing and positioning) of the detector (see section 2.3.6).

2.2.3 Propagation of the neutrinos in the Earth

At high energies, as the cross section increases, neutrinos can be absorbed. Typically, the Earth becomes opaque to neutrinos at 70 TeV where the interaction length becomes comparable to the diameter of the Earth.

[2]For hadronic projectiles, the strong interactions also contribute to multiple scattering.

To quantify this effect, we take into account the profile of the earth density shown in Figure 2.3 [2]. Using this profile, 10 different layers whose density depends on the distance from the centre of the Earth are considered. The probability of a neutrino traveling a distance L (referred to as transmissivity coefficient Equation (2.2)), not to be absorbed, can be written in units of water-equivalent-length as:

$$P_{trans}(L) = e^{\frac{-L(\theta)}{\lambda}} \tag{2.7}$$

where $\lambda = 1/(\mathcal{N}\sigma_{tot})$ is the free mean path taking into account the total cross section. Figure 2.4 shows the absorption coefficient $(1 - P_{trans})$ as a function of energy and zenith angle in the Earth. These plots show that the absorption for neutrinos crossing horizontally a small amount of matter is negligible. Thus high energy neutrino telescopes are sensitive to high energy neutrinos ($> PeV$) mostly in that directions.

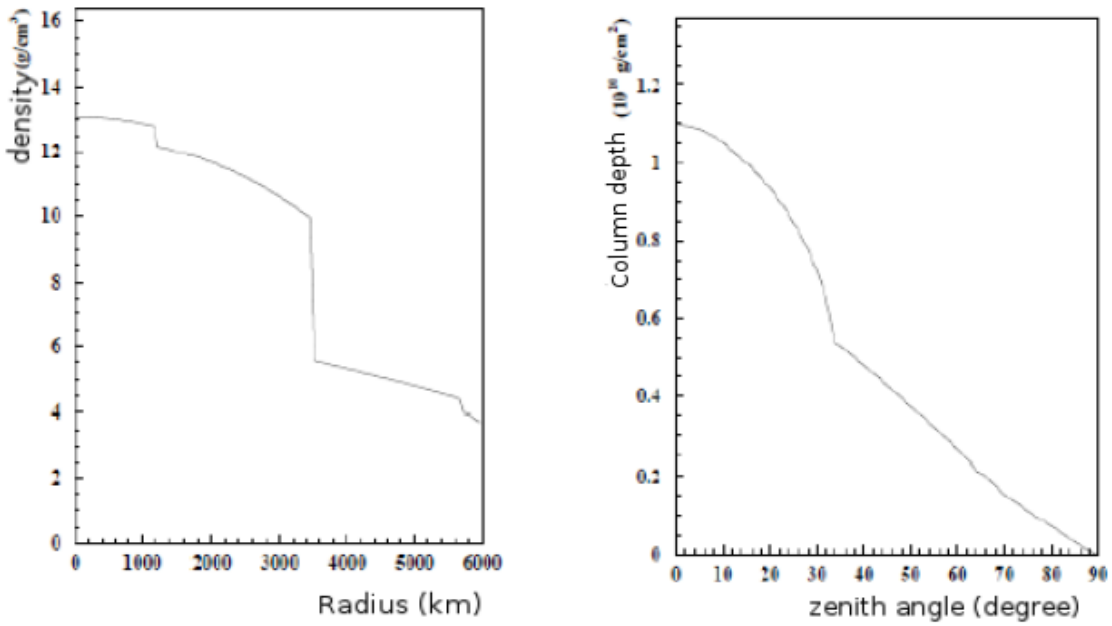

Figure 2.3 – Left: Density profile of the Earth according to the Preliminary Earth Model. Right: Thickness of the Earth as a function of the angle of incidence of the incoming neutrinos

2.2.4 Propagation of the muons in water and rocks

Depending on their energy and during their propagation in water or rock, muons lose energy due to various processes (see Figure 2.5). For E_μ <1 TeV the dominant process is the ionization, which can be described as a continuous process. At higher energies, muon lose their energy via stochastic phenomena such as bremsstrahlung, pair production and photonuclear interactions.

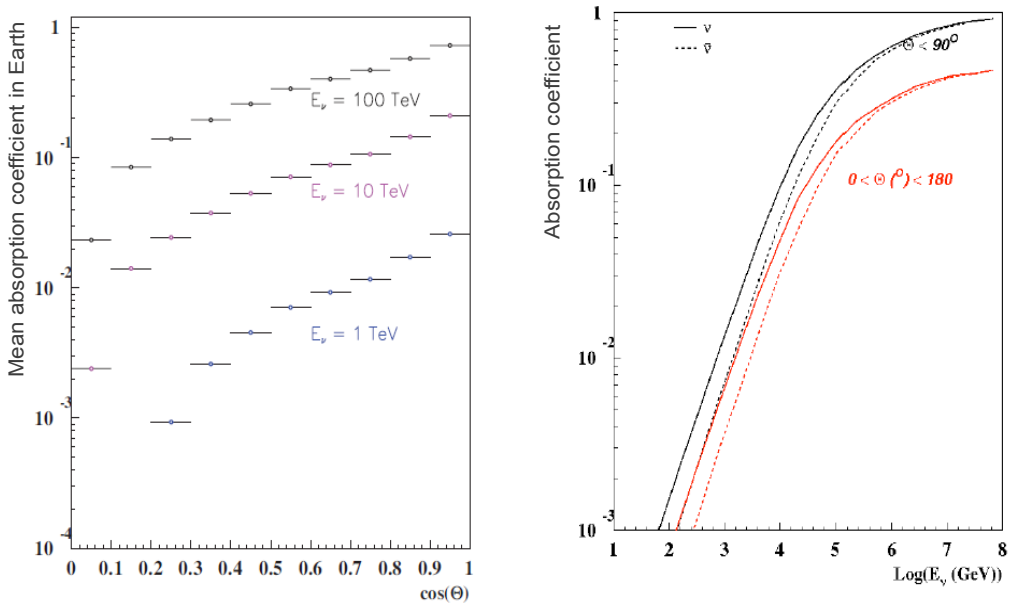

Figure 2.4 – Left: Mean absorption effect on neutrinos of energies: 1, 10 and 100 TeV as a function of the zenith angle θ_ν. Right: Absorption coefficient for upgoing neutrinos (black) and for the two hemisphere (red) as function of energy

- **Ionisation**: The continuous energy loss of muons passing through a medium at relatively low energy transfers to atomic electrons, ionising the material along the muon path. The energy loss is calculated using the Bethe-Bloch formula.

- **Bremsstrahlung:** In the electric field of a nucleus or atomic electrons, muons can radiate high energy photons.

- **Pair Production:** A muon can radiate a virtual photon which, again in the electric field of a nucleus, can convert into a real e^+e^- pair.

- **Photonuclear Interaction:** A muon can radiate a virtual photon which directly interacts with a nucleus in the muon propagation medium. The average energy loss for this process increases almost lineary with energy, and at TeV muon energies constitutes about 10% of the energy loss rate.

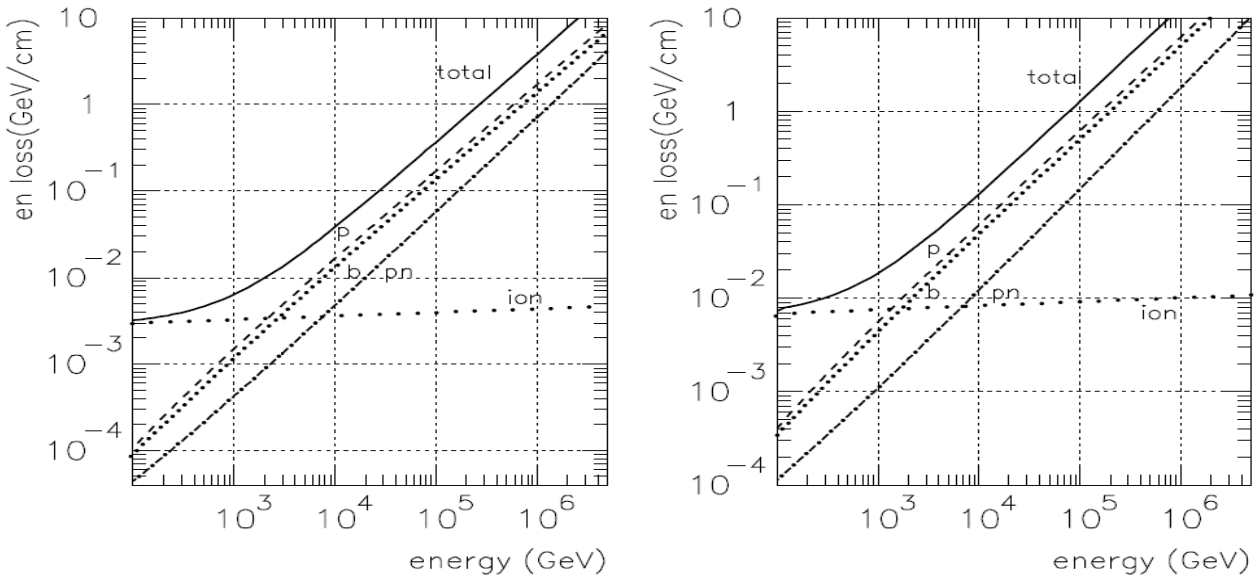

Figure 2.5 – Total and partial energy losses for muons in water (left) and standard rock (right) as a function of muon energy. Total energy loss : solid line; pair production (p): dashed line; bremsstrahlung (b): dotted line; photonuclear interaction (pn): dot-dashes; ionization (ion): large dots

The global contribution of all these processes to the mean energy loss of muons is given by [6]:

$$\left\langle -\frac{dE}{dx} \right\rangle = a(E) + b(E)E \tag{2.8}$$

where E is the total energy, a(E) is the contribution due to ionization and b(E) is due to the radiative processes. Both terms $a(E)$ and $b(E)$ are slowly varying functions of E at high energies. At low energies (<1 TeV) the dominant term comes from the ionization. In the approximation of a and b constant, the mean free path of a muon of energy E_μ until it reaches an energy E_{min} can be written as:

$$\mathrm{R_\mu(E_\mu, E_{min})} = \int_{\mathrm{E_{min}}}^{\mathrm{E_\mu}} \frac{1}{\left\langle \frac{\mathrm{dE}}{\mathrm{dX}} \right\rangle} \mathrm{dE} \approx \frac{1}{\mathrm{b}} \ln \frac{(\mathrm{a/b}) + \mathrm{E_\mu}}{(\mathrm{a/b}) + \mathrm{E_{min}}} \tag{2.9}$$

This gives an estimate of the distances which can be travelled by the muons. Nevertheless, in the high energy regime, the stochastic radiative processes enjoin to use Monte Carlo simulations to better reproduce the high energy losses. (see section 2.5).

2.2.5 Detection principle

Neutrino telescopes use sea water or ice as a detection medium to observe cosmic neutrinos. In parallel, these media act as a shield for down going particles of atmospheric origin, since muons

and neutrinos are the only particles able to reach deep underground or underwater. Other atmospheric and cosmic particles have either a short lifetime or a short interaction length and can not survive long in dense media.

A small fraction of the incoming high energy neutrino flux interacts, (following Equation (2.1)), with the nucleons that make up the matter (water, ice and rock) surrounding the detector. The induced muon-neutrino produces a relativistic muon, with a Lorentz factor $\beta > 1/n$. During its propagation, the muon produces an amount of Cherenkov light, see Figure 2.6 [7]. The Cherenkov radiation propagates in a cone whose opening angle θ_c depends on the particle velocity as:

$$cos\theta_c = \frac{1}{\beta n_{water}} \tag{2.10}$$

whith $n_{water} = 1.35$ for a wavelength of 450 nm and β=1, this formula leads to $\theta_c = 42°$. The emitted number of photons per unit of length x and wavelength λ (Equation (2.11)) increases with frequency [8]:

$$\frac{d^2N_\gamma}{dxd\lambda} = \frac{2\pi\alpha Z^2}{\lambda^2}(1 - \frac{1}{\beta^2 n^2_{water}}) \tag{2.11}$$

where α is the fine structure constant, Z the charge of the particle causing the emission and λ the wavelength of the emitted photons. Most part of photons is then produced in the ultraviolet region of the electromagnetic spectrum. Integrating Equation (2.11) between 300 nm and 600 nm, for which Cherenkov light contributes most to the signal from a muon, yields a quantity of $\simeq$350 photons emitted per centimeter of the track.

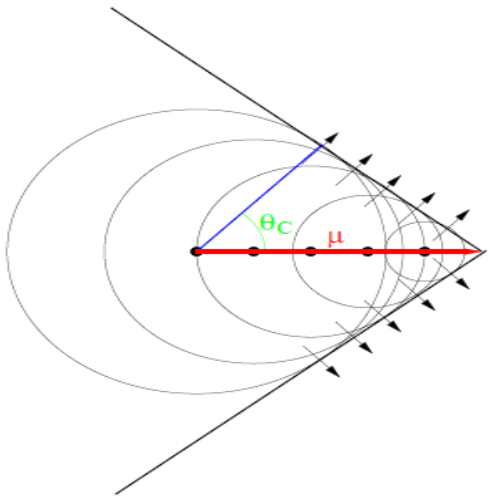

Figure 2.6 – Illustration of the Cherenkov effect. Local distortions of the charge configuration in the medium lead to the emission of electromagnetic waves. Individual contributions along the track (red line) interfere constructively on the envelope which forms a cone. Cherenkov photons (blue line) are emitted under the characteristic angle θ_C.

2.2.6 Overview of the past and current detectors

The BAIKAL neutrino telescope

The BAIKAL experiment [9] is a German-Russian collaboration. The detector is deployed at a depth of about 1km in the Siberian Baikal Lake. The experiment has been running since 1993, when three detection strings were immersed and put into operation. Since 1998 the detector was expanded to 18 strings with a total of 192 optical modules (OMs) (NT-200 detector. The detector is arranged around a central unit with the main electronic block and a calibration laser on the top of the layout that provides the support structures for the 18 strings which are distributed on a circular geometry with a radius of 22 m. Each of the strings measures 68.5 m. This setup was extended in 2005 by three additional strings of 200 m length with 36 PMTs at a distance of 100 m (NT-200+) to the detector center in order to increase the effective area for showers. Compared to neutrino telescopes in deep sea, the Baikal setup offers several advantages. Firstly, the operation in fresh water naturally reduces the background contributions from ^{40}K decays. Secondly, the maintenance of the detector is greatly alleviated by the possibility to use the frozen sea surface as a basis for deployment and recovery operations. The main disadvantages are the reduced absorption length of the water in Lake Baikal and the relatively low depth which leads to a larger atmospheric muon background compared to deep-sea telescopes.

The collaboration published the first limit on the neutrino diffuse flux from the Southern hemisphere using 1038 days of data [10]. The limit $\mathrm{dN/dE} < 8.1\,10^{-7} E^{-2} GeV^{-1} cm^{-2} s^{-1} sr^{-1}$ is obtained in the range of energy $20TeV \leq E \leq 50PeV$.
In order to further improve the sensitivity to cosmic signals, the collaboration envisages the enhancement of the telescope towards a Gigaton detector. An R&D and prototyping phase has started in this view.

The Antarctica neutrino telescopes

AMANDA: The AMANDA experiment [11] (Antarctica Muon and Neutrino Detector Array) started in 1990. It is located near the Scott-Amundsen South Pole station in Antarctica Ice. The experiment in its final configuration (AMANDA-II) consists of 19 strings immersed in the glacial ice at a depth ranging from 1500 m to 2000 m, carrying 677 OMs. Each OM is a glass pressure vessel, which contains an 8-inches hemispherical PMT and its electronics. AMANDA-B10, the inner core of 302 OMs placed on 10 strings, has been operating since 1997. The high level of light scattering at that depth limits considerably the performance of the detector. This affects especially the angular resolution that remains above few degrees. The optical

absorption length in the ice is typically 110 m at 400 nm with a strong wave-length dependence. The ice parameters vary strongly with depth due to horizontal ice layers, i.e. variations in the concentration of impurities which reflect past geological events and climate changes.
The AMANDA-II has been switched off early 2009 to allow for the extension to km-scale experiment IceCube. With 7 years of data taking, AMANDA-II collected a statistics of 6595 neutrino candidates and measured the spectrum of atmospheric neutrinos up to energies two orders of magnitude higher than in the previous experiments.

IceCube: The IceCube Neutrino Observatory is the successor of the AMANDA neutrino telescope. Construction of the IceCube Neutrino Observatory began at the geographic South Pole in the 2004-05 austral summer and was completed during the 2010-11 austral summer. IceCube consists of two parts: IceTop, a surface air shower array [12, 13], and IceCube, a muon and neutrino telescope [14] installed deep in the ice. The final configuration consists of 86 strings (IC86) of over 1000m length separated by 125m, with 5800 PMTs. Each string is comprised of light sensors called Digital Optical Modules (DOMs), which detect Cherenkov photons emitted by relativistic charged particles passing through ice. Each DOM is a spherical, pressure-resistant glass shell containing a 25 cm diameter Hamamatsu photomultiplier tube (PMT), a mu-metal grid for magnetic shielding of the PMT, and electronics for operation and control of the PMT as well as amplification, digitization, filtering, and calibration.
Each IceCube string is associated with an IceTop station, which consists of two cylindrical ice Cherenkov tanks separated by 10 m. Each tank has an inner diameter of 1.82 m, is 1.3 m high, and contains two down-facing DOMs, with center-to-center spacing of 58 cm, frozen in optically clear ice 90 cm in depth.

A large amount of data has already been acquired with smaller configurations throughout the installation period (IC22, IC40, IC59, IC79 and IC86), where for example IC22 denotes the 22-string configuration. Using the data from IC40, the atmospheric neutrino spectrum in the northern hemisphere has been measured up to 100 TeV. No point sources have been identified in a set of more than 10^5 neutrino candidates from both hemispheres. Searches for transient sources have set stringent limits on neutrino emission from gamma-ray bursts, and are now accompanied by an extensive neutrino-triggered follow-up program. A very large statistics of cosmic ray events has revealed an anisotropy in the cosmic ray flux at the 10^{-3} level in the 10-100TeV range. While no source of extra-terrestrial neutrinos has been found yet, the physics results obtained so far illustrate the very good performance of the detector.
Some of recent results published by the IceCube collaboration at the moment of writing this thesis can be found in [12, 15–17].

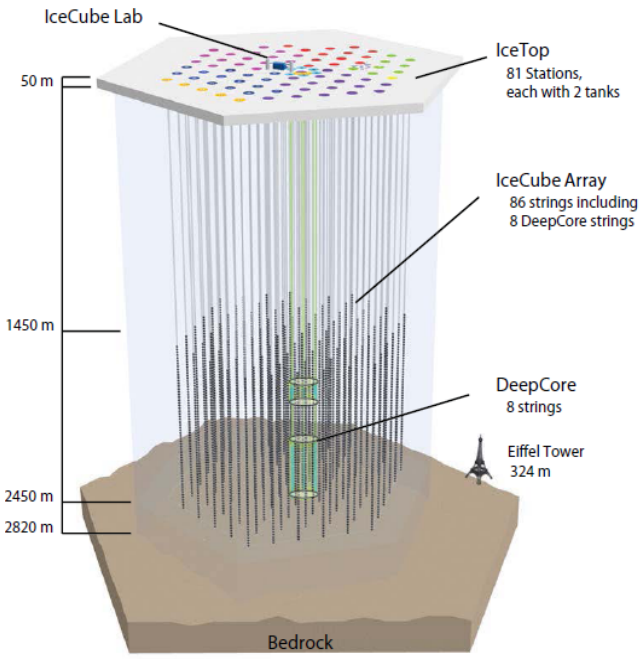

Figure 2.7 – The IceCube detector with its components DeepCore and IceTop in the final configuration (December 2010)

The Mediteranean neutrino telescopes

NESTOR: The Greek NESTOR (Neutrino Extended Submarine Telescope with Oceanographic Research) collaboration [18] initiated the first project for a neutrino telescope in the Mediterranean sea at a site located 18 km off the coast of Pylos at a depth of 4000 m. The chosen telescope design uses tower-like rigid support structures instead of flexible mooring strings. These towers consist of 12 layers made up of six arms each, which are laid out in a star-shaped form. On each of these arms one upward and one downward looking 13" PMT are mounted. A prototype version of a tower storey has been tested in 2003, and first atmospheric muon data were recorded. Some recent results from the NESTOR collaboration are published in [19].

NEMO: The Italian NEMO (Neutrino Mediterranean Observatory) project [20] has focused on research and design studies for a future km-scale detector in the Mediterranean sea. The NEMO design concept features a flexible tower structure of horizontal bars of 15 m length which are connected by ropes. At each end of the bars two PMTs are mounted, one locking downwards, the other one in the horizontal direction. The detection towers can be deployed as a compact object together with a socket and self unfurl in the sea. After the unfolding, adjacent bars are aligned perpendicular to each other. NEMO published results from a sample of data recorded in January 2007 [21].

The KM3NET neutrino telescope: The KM3NeT consortium [22] is a joint effort of the ANTARES (see next section), NEMO and NESTOR collaborations to construct a cost-effective next generation telescope of cubic-km size. The geometry of the detector [23] consists of a three-dimensional array of OMs attached to vertical structures (Detection Units, DUs). An array of DUs constitutes a detector building block. Several building blocks form the full detector of about 300 DUs. A DU, which is anchored to the sea floor and kept upright by a submerged buoy, could consist of horizontal bars equipped with 2 OMs, one at each end. Alternatively, vertical strings with single optical module could be a simpler design. This should be decided by the end of 2012. The DUs will anyway be connected to shore by an electro-optical cable, and the OMs will consist of 31 3-inch PMTs housed inside a 17-inch pressure-resistant glass sphere covering almost a 4π field of view.

2.3 The ANTARES neutrino telescope

The ANTARES neutrino telescope [24] is an underwater neutrino detector deployed in the Mediterranean Sea at a depth of 2500 m offshore from Toulon (France) for a design lifetime of about 10 years. It is the most sensitive high energy neutrino observatory studying the Southern Hemisphere, including the Galactic Center 2/3 of the time. The ANTARES field of view has a sky coverage of 3.5π sr (see Figure 2.8).

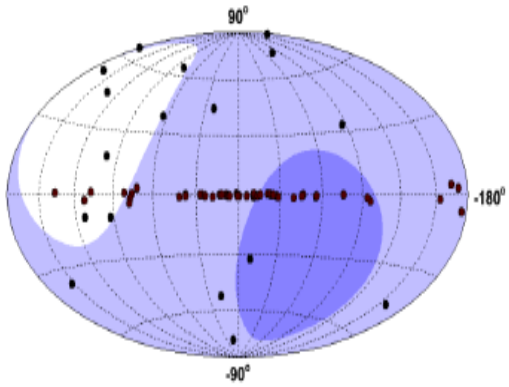

Figure 2.8 – Sky coverage of the ANTARES neutrino telescope. The blue area is seen 100% of the time by ANTARES while it is completely blind to the white area.

The ANTARES neutrino telescope consists of twelve lines with a sensitive area for high energy muons of more than 0.05 km^2 for $E \geq 100$ TeV. Its construction started with the installation of the first lines in 2006, and has been completed on May 30, 2008. The full structure is a three-dimensional array of photo-multipliers (PMT). In addition, a special instrumentation

line (IL), mostly dedicated to environmental studies, was put in operation in January 2008. This makes of the ANTARES detector an interesting observatory for Earth science, oceanographic and acoustic studies. The ANTARES Collaboration is a joint effort of about 29 laboratories from 8 countries (France, Germany, Italy, Morocco, the Netherlands, Romania, Russia and Spain).

2.3.1 Detector design

A detailed description of the ANTARES neutrino telescope is given in [24]. The basic elements of the detector are the optical modules (OMs). The later is the assembly of a pressure resistant glass sphere of diameter 43 cm housing a photomultiplier tube and the electronics needed to provide the necessary high voltage [25]. An exhaustive study of PMTs was carried out during the R&D phase, started in 1990, which led to the selection of the 10" Hamamatsu R7081-20 model. Three OMs make up a floor and five floors are grouped to form a sector. One string comprises five sectors.

The layout of the detector consists in a 3-dimensional array of optical modules (OMs) supported by flexible vertical strings anchored to the seabed with the Bottom String Socket (BSS) and are held vertical by a buoy at the top. A schematic overview of the detector string is shown in Figure 2.9. The PMTs are oriented downwards with an angle of 45° below the equator. This orientation gives high efficiency for tracks between upward vertical and horizontal directions, and minimize the effects due to the biofouling. The latter is caused by the adhesion of microorganisms, mostly bacteria, on the external surface.

The detector is operating since 2008 in its complete configuration of 12 strings with 25 floors (75 OMs by string). Eleven strings have a nominal configuration while the twelfth string is equipped with 20 storeys and completed by devices dedicated to acoustic detection. Thus, the total number of the OMs installed in the detector is 885. The strings are about 450m long and separated from each other by at least 60 meters. The distance between two adjacent floors is 14.5m. All strings are connected to a main junction box, which provides the connection to the 40km long cable to the shore station. All the electronics for one storey are housed in a pressure resistant titanium container making up the so-called Local Control Module (LCM). A photon that hits the photo-cathode of a PMT can induce an electrical signal on the anode. If the amplitude of the signal exceeds a certain voltage threshold corresponding typically to 0.3 photo-electron, the signal is read out and digitized by a custom designed front-end chip. Every OM is read out by an electronics board housed in the LCM carrying a pair of Analogue Ring Samplers (ARS). The later provides the time and amplitude of the signal, both essential to reconstruct the muon track direction and estimate its energy (section 2.6). Each sector

contains a Master Local Control Module (MLCM), that collects the data produced in the floors of a sector and sends them to the main jonction box.

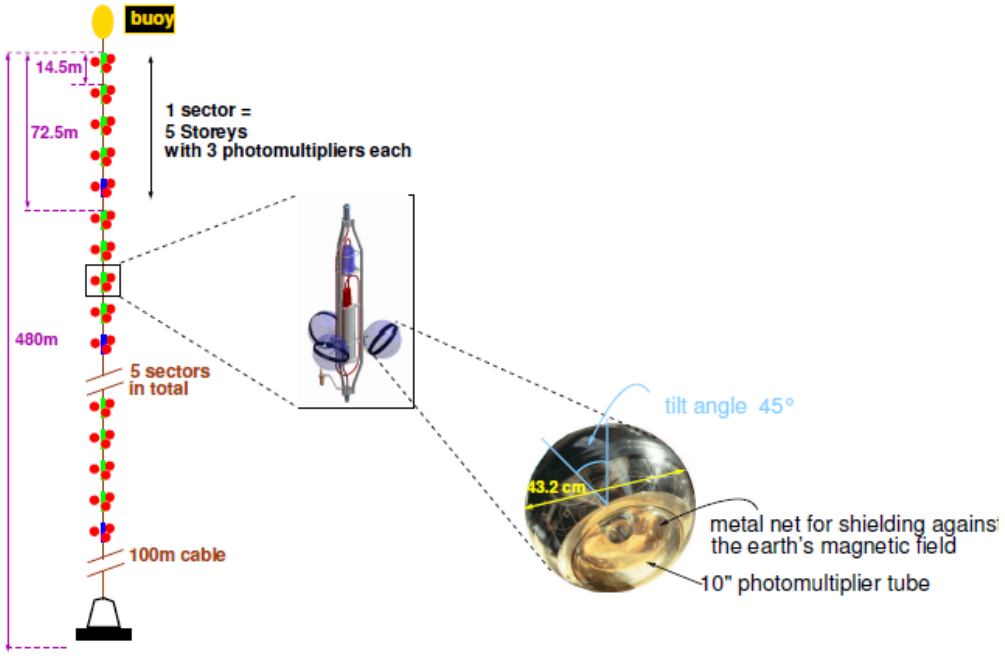

Figure 2.9 – A schematic view of ANTARES string.

2.3.2 ANTARES coordinates

The geographic site of ANTARES neutrino telescope is located at Latitude 42°47.935′N and Longitude 6°09.942′E. The convention for the detector coordinate system (UTM grid) [26, 27], shown in Figure 2.10, is a right-handed system with the x-axis pointing toward the East, the y-axis to the North and the z-axis parallel to the detector line going upwards. The origin is defined on the center of the detector on the sea floor. The direction of the particle track is defined by two angles:

- The angle θ is measured from the positive z-axis in a range [0, π]. Upgoing events have $\theta \leq 90°$, $\theta_{\uparrow} = 0°$, $\theta_{\rightarrow} = 90°$ and $\theta_{\downarrow} = 180°$.
- The azimuthal angle ϕ is measured from the positive x-axis and it increases counterclockwise towards the positive y-axis (East→North). ϕ is measured in a range $[-\pi, \pi]$.

To find the zenith of the source, θ should be rotated by 180° in space: zenith= 180° - θ. Elevation (also called altitude) can be used to denote the position of the source and is defined as "zenith - 90°".

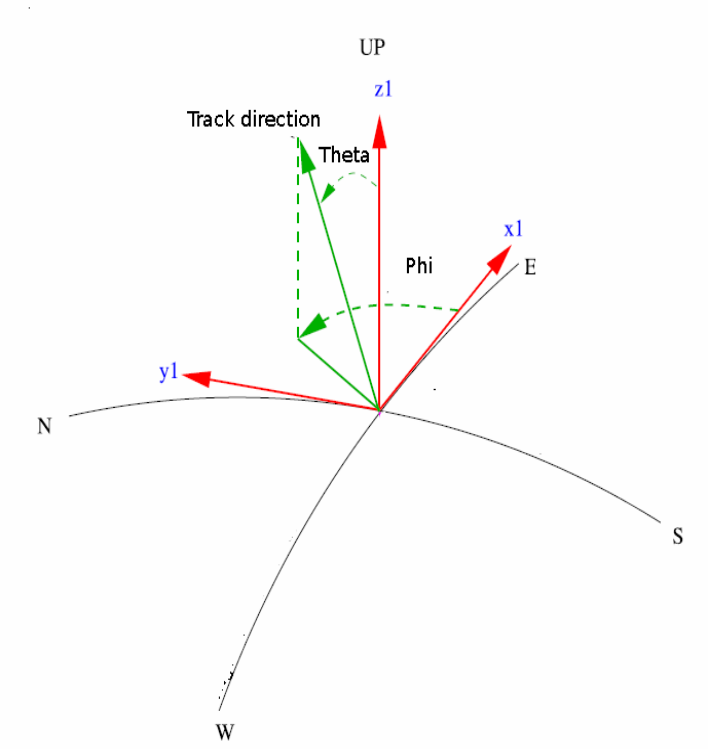

Figure 2.10 – Coordinate system of ANTARES

2.3.3 Background noise at the ANTARES site

Optical background: bioluminescence and ^{40}K

The Cherenkov radiation from $\nu-$induced muons is not the only light at the depth of the ANTARES site. Background light is produced by the decay of radioactive potassium-40 (^{40}K) and marine microorganisms (bioluminescence). The latter being enhanced in periods of high sea current. Figures 2.11 and 2.12 shows some examples of the sea current and the PMT rates. The ^{40}K decays into two channels:

$$^{40}K \longrightarrow ^{40}Ca + e^- + \overline{\nu}_e \tag{2.12}$$

$$\begin{aligned} ^{40}K + e^- &\longrightarrow ^{40}Ar^* + \nu_e \\ ^{40}Ar^* &\longrightarrow ^{40}Ar + \gamma \end{aligned} \tag{2.13}$$

The first decay channel (β decay) is the dominant decay mode of ^{40}K with a probability of 0.89. The average kinematic energy of the emitted electron is 1.12 MeV, enough to produce

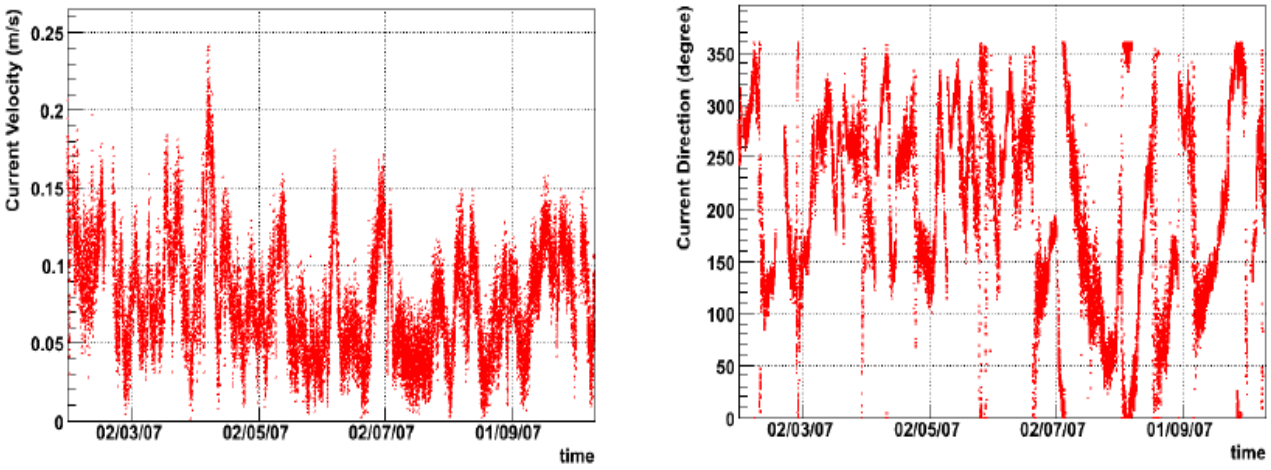

Figure 2.11 – Sea current velocity (left) and direction (right) in the ANTARES zone during the period going from February to November 2007.

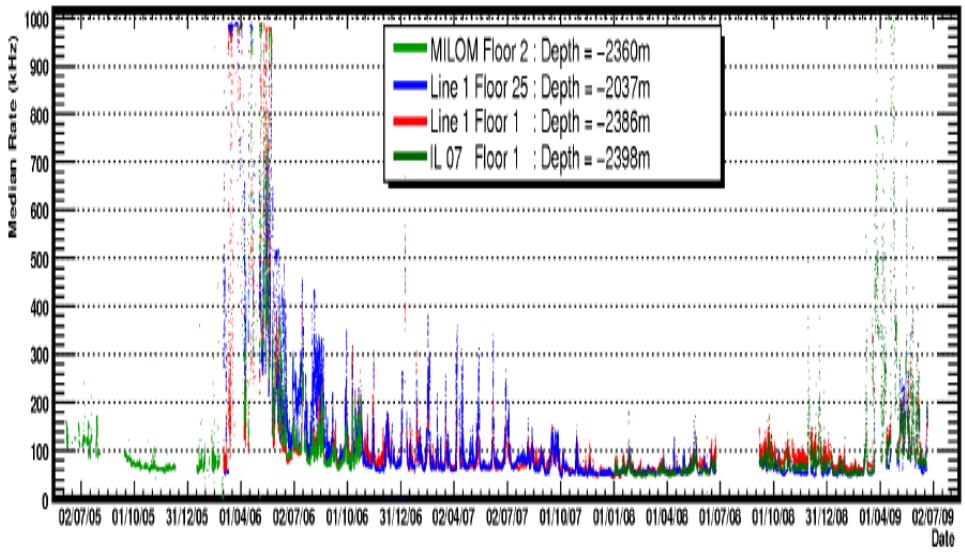

Figure 2.12 – Median single PMT background rates at different depth levels, monitored over four years of operation from 2005 and 2009.

Cherenkov light in water. The decay of the ^{40}K contibute to the PMT rates by a stable rate of around 30 kHz. In the second decay mode, the Cherenkov light comes from the Compton scattering of the 1.4 MeV photon emitted in the desexcitation of the ^{40}Ar.

2.3.4 Physical background: atmospheric muons and neutrinos

Cosmic ray interactions in the Earth's atmosphere above the detector produce energetic atmospheric muons (see section 1.1.2). When the muon energy is high enough, they can travel large

distances and reach the detector from above. The aim to build the detector in deep sea is to use the water as a shield against the flux of those downward going atmospheric muons. However, upward going atmospheric muons can not travel through the Earth. Everything a part from the desired cosmic neutrinos is considered as background in the detector and should be discarded with filtering algorithms and dedicated predefined cuts in order to increase the sensitivity to cosmic neutrinos. However, upward going atmospheric neutrinos are an irreducible background in the detector. Their flux is several orders of magnitude smaller than atmospheric muons as it is shown in Figure 2.13. As cosmic neutrinos have hard spectrum ($\frac{dN}{dE} \propto E^{-2}$) [28], in contrast with the atmospheric neutrinos ($\frac{dN}{dE} \propto E^{-3.7}$) [29], the neutrino energy could be used to eliminate atmospheric neutrinos (this will be discussed in Chapter 4).

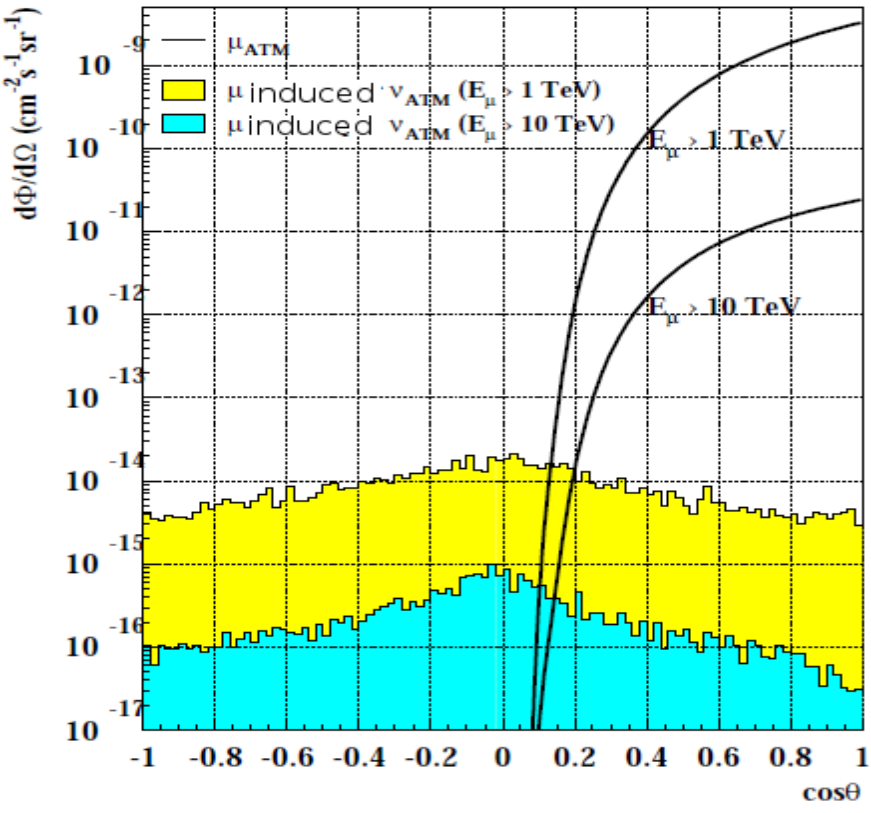

Figure 2.13 – Flux of atmospheric muons and muon induced by atmospheric neutrinos at 2300m water equivalent depth. In the downgoing direction ($cos\theta > 0$) the atmospheric muon flux is about 10^6 times higher than the neutrino-induced muon flux. The maximum near cosθ=0 in the neutrino induced muon spectrum reflects the increased probability of meson decay close to the horizon.

2.3.5 Trigger and DAQ systems

Data acquisition

The overall data rate being too heavy to be fully written on disk, filtering algorithms must be applied on-line to discard as much as possible the background and save as much as possible the signal events. Several filtering algorithms can be applied depending on the optical background rate, but the basic idea is to search in all directions a time sequence of hits compatible with the passing of a relativistic particle emitting Cherenkov radiation. This is done on shore with a trigger elaborated to process all data coming from the detector in quasi real time [30]. These hits are causally related in time and position, while time-position of hits produced by ^{40}K decays or bioluminescence are uncorrelated (caused by random processes).

The aim of the trigger is to select correlated hits in the ARS data stream for digitization[3], readout and transfer to the on-line data processing system on shore. Once the signal has been digitized in the ARS, it is sent to the Data Acquisition (DAQ) board for storage. The DAQ board collects data and sends them to the shore via an Ethernet port. Then, the characteristics of the hits are evaluated in order to discard most background hits, resulting in reduction of data rate by a factor of at least 10^4. Off-shore, the ARS data are organized in data frames. All frames that belong to the same time window are sent to the same processor in the processing farm, as sketched in Figure 2.14. The program buffers the frames in a queue to handle transmission delays in the network. When all frames of a particular time window have been collected, they are passed to the trigger algorithm. The complete collection of frames is referred to as a *time slice*. The time and charge of all hits in the data are determined using the known calibration constants of the detector (see section 2.3.6).

Trigger algorithms

The first level of trigger is a simple threshold of about 0.3 photo-electron[4] (pe) equivalent charge applied to the analog signal of the PMT. The corresponding digital data (time and charge) are then referred to as L0 hits.

The detection of two coincident photons by the same PMT generally results in a single hit with a charge that corresponds to $\simeq$2 pe. This is unlikely to happen as the result of random background hits, which are mainly produced by single photons and consequently have a charge that corresponds to a single pe. Therefore, the second level of trigger (L1) searches for hits with a large charge (greater than 3 pe or 10 pe depending on the detector's configuration), or

[3]Because of the length of the optical link to the shore, electrical signals cannot be transmitted in analog form, thus they must be formatted by the ARS.

[4]Equivalent to 45mV.

alternatively for coincidence of hits in the same storey (but different OMs) within 20 ns, (i.e local coincidence of L0 hits). The time window of 20 ns accommodates the difference in OM positions, uncertainties in the time calibration and some light scattering.

The two most frequently used algorithms both uses L1 hits as a starting point:

- The 3N trigger looks for causality relations in space-time between different "L1 hits" in $\pm 2.2\mu$s time window[5], roughly corresponding to the muon transit time across the detector. A minimum of 5 L1 hits (so at least 10 pe) in coincidence is required to write the event on disk, that is the overall L0 hits sequence during the $\pm 2.2\mu$s time window. The efficiency of the trigger (for the 12 line configuration) rapidly grows with the number of pe in the event. It reaches almost 100% for 40 detected photo-electrons. The purity of this filtering is evaluated at 90% by Monte Carlo simulations.

- The T3 filtering [31] condition can be added in case of low optical background. This algorithm is more open and therefore accepts more background hits, but allows for more efficient shower recognition. Instead of looking for hits that are causally connected, one searches for a T3 trigger cluster within a time window of $\pm$ 2μs. A T3 trigger cluster is defined as the occurrence of at least 2 L1 hits in two consecutive storeys within a coincidence time window. This time window is 100 ns in the case that the two storeys are adjacent, and 200 ns in the case of next to adjacent storeys.

In this context, it is important to mention that only the 3N trigger will be used in the results obtained with 2007 data presented in Chapter 4. However, in the results obtained with 2009-2010 data presented in Chapter 5 we use the T3 and 3N triggers.

2.3.6 Detector calibration and electronics

The precision on the muon track reconstruction (i.e., its time and its direction) requires a precise measurement of the arrival time of the photon, the position of the PMTs, the charge of the hits and the threshold voltage for the readout of the PMTs by associated front end electronics. These PMTs have been calibrated on-shore prior to the deployment. Below, we concentrate on the *in–situ* calibration system of the time and the PMT position. For the threshold and charge calibration, see for example [32].

Time calibration

ANTARES is designed to achieve an angular resolution smaller than 0.3° for muons above 10 TeV. This pointing accuracy is closely related to the precision in the determination of the

[5]More precisely 2.2 μs before the time of the first L1 hit up to 2.2 μs after the last L1 hit.

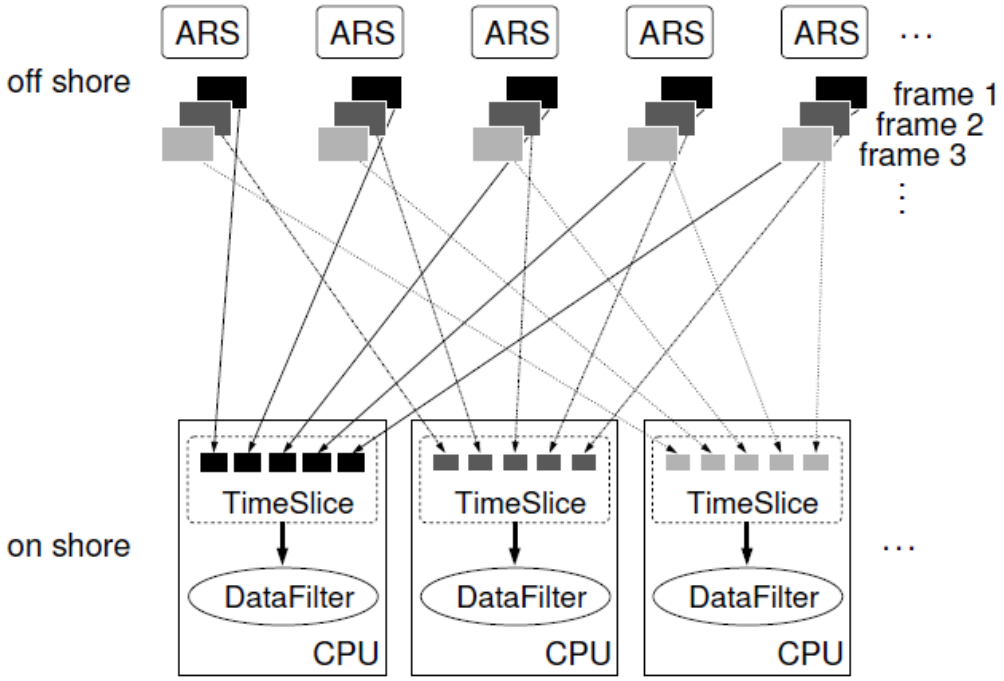

Figure 2.14 – A schematic view of the data collection on shore.

arrival time of the Cherenkov photons at the PMTs. Thus, a time calibration of the detector is necessary [33]. The calibration system includes a 20 MHz reference master clock on shore, LEDs installed inside each OM and Optical Beacons (OBs), equipped with LED or laser devices. The clock system provides a common signal to synchronize the readout of the OMs. Signal received from shore are converted and decoded by an electronics board inside the LCM and are then distributed over an electrical bus to the ARS chips. The relative offset of each local clock can be measured by using a calibration signal sent by the master clock and echoed back. The clock system assigns an absolute event time with a GPS master clock synchronization accuracy of 100 μs.

The optical beacon system is used to calibrate the relative offsets between the PM tubes. Four blue (472 nm) LED beacons on storeys 2, 9, 15 and 21 of each detector line and two green (592 nm) laser beacons on the BSS of L7 and L8 are used for this purpose. The LED beacons are used for intra-line calibration purposes while the laser beacon, being much more powerful and able to illuminate all the lines, is used for inter-line calibration. An initial set of time offsets is determined in the laboratory prior to deployment. After deployment, these values may change due to different factors such as temperature changes or stresses in the cables. Using the optical beacon system they are monitored every month and readjusted as necessary. A

second calibration system consisting of a blue (470 nm) LED inside each OM is used to measure time offsets between the PM tube photo-cathode and the read-out electronics. Internal LED and optical beacon measurements reveal less than 0.5 ns contribution of the electronics to the photon arrival time resolution. Thus, time resolution is dominated by the transit time spread of the PM tubes which is about 1.5 ns, and light scattering and chromatic dispersion, which depends on the distance travelled by the photon. The calibration system just described provides a relative time calibration of better than 1 ns.

Position calibration

The optical modules are hanged to strings that are freely floating in the sea water. Thus, orientations and positions of each PMT should be measured at every moment to enable their monitoring. This is done, every two minutes, by an acoustic system which is set up on the BSS of each string. A pulse of frequency 40-60 kHz is sent by an acoustic transmitter held on the BSS and is received by the hydrophones situated on each sector along the line allowing a real time localization in space of the OMs by triangulation. The orientation of each optical module frame is measured by a compass and a tilt-meter located inside the LCM container. Together, measurements from the tilt-meters, compasses and acoustic system provide a measurement of the relative position of the OMs with an accuracy of 10-20 cm [34].

2.4 Data quality

The selection of data is based on some quality criteria. Each run is tagged by some quality parameters that are stored in the ANTARES data base. The main flags are the 'SCAN' and the Quality-Basic (QB) flags. The former allows to check the run setup of each run as some of them are not write-protected in the database thus they may have been modified during the data taking. In this analysis we select all physics runs which have run setup protected against writing "$SCAN \neq 1$". The second parameter allows to define some crude criteria in order to detrmine the quality of the data. It can takes the following values (1, 2, 3 and 4), where each number stands for:

- QB = 1 : Defined to perform a basic selection, minimum requirement for a run to be included in the analysis.

- QB = 2 : It requires that at least 80% of the OMs expected to work at the time of the run are effectively working.

- QB = 3 : It requires a mean baseline rate over all active PMT $\leq$ 120 kHz AND a burst fraction $\leq$ 40%.
- QB = 4 : Same condition on baseline as in QB = 3 AND a burst fraction $\leq$ 20%.

The baseline rate, in kHz, represents the most probable counting rate of a given OM computed from the rate distributions (number of hits divided by the frame duration) in each PMT over the whole (typically few hours long) run. For one PMT the baseline is extracted from a gaussian fit on the left part of the distribution of the rates measured every 15 mn. The burst fraction, in percent, corresponds to the fraction of time during which the OM counting rates are larger than 20 % above the baseline rate [35].

For the analysis of 2007 (2009-2010) data presented in Chapter 4 (Chapter 5) we require a minimum QB value of 3 (1). Requirements about the external conditions (e.g. baseline, burst fraction and sea current), the configuration and behaviour of the detector during a given run (e.g. number of active units, L1 thresholds, alignment), and the properties of the run itself (e.g. duration, number of slices, trigger rates) can also be taken into account for the selection of runs.

2.5 Simulation chain

Simulation tools are one of the main ingredients needed to assess the performances of the detector. The simulation chain basically starts with the physics processes occurring in the atmosphere, Earth and underground, that can lead to the production of some detectable light in the detector, taking into account the probability of each process to occur. It also mimics the detector response to these processes. The particles that are simulated are the atmospheric muons and neutrinos induced by interactions of cosmic rays with the Earth's atmosphere, and cosmic neutrinos.

2.5.1 Simulation of high-energy neutrinos

These particles are generated using the program GENHEN [36]. The code generates a flux of neutrinos with uniformly distributed directions, within a zenith angle range $[\theta_{min}, \theta_{max}]$ and according to an arbitrary user input spectrum $E_\nu^{-\Gamma}$. The choice adopted in this work is $\theta \in [0, \pi]$, $\Gamma = 1.4$ and $E_\nu \in [10^2, 10^8] GeV$. GENHEN first generates the neutrino position, direction and energy. Neutrino interactions are simulated with LEPTO [37] for deep inelastic scattering (DIS) and RSQ [38] for resonant and quasi-elastic scattering (QES). The secondary particles resulting from the interaction that are able to produce detectable light are stored

for further usage. We introduce a volume within which the Cherenkov light is generated (see section 2.5.3), named *the can*. A schematic view of the can is shown in Figure 2.15.

The simulated flux of neutrinos arriving at the Earth is given per units of energy dE, solid angle $d\Omega$, area dS and time dt by the following relation:

$$\frac{d\Phi_\nu^{sim}}{dE_\nu d\Omega dS dt} = \frac{N_{total}}{t_{gen} V_{gen} I_\theta I_E E^\Gamma} \frac{1}{\sigma(E_\nu)\rho N_A} \frac{1}{P_{Earth}(E_\nu, \theta_\nu)} \tag{2.14}$$

where:

- N_{total} is the total number of generated events.
- Γ is the generation spectral index.
- $t_{gen}(s)$ is the arbitrary duration covered by the simulation.
- $V_{gen}(m^3)$ is the total generation volume of the Cherenkov light (in water equivalent units in this case)
- I_E is the energy phase space factor. It depends on the Γ chosen value:

$$I_E = \begin{cases} \dfrac{E_{max}}{E_{min}} & \text{if } \Gamma = 1 \\ \dfrac{E_{max}^{1-\Gamma} - E_{min}^{1-\Gamma}}{1-\Gamma} & \text{otherwise} \end{cases}$$

- $I_\theta(sr) = 2\pi \times (cos(\theta_{max}) - cos(\theta_{min}))$ is the angular phase space factor corresponding to the specified range of $cos(\theta_\nu)$.
- $\sigma(E_\nu)(m^2)$ is the charged current neutrino interaction cross-section.
- $\rho N_A(m^{-3})$ the number of target nucleons per unit volume.
- $P_{Earth}(E_\nu, \theta_\nu)$ is the probability of transmission through the Earth for a neutrino of given E_ν and θ_ν.

For a given flux model $\dfrac{d\Phi_\nu^{model}}{dE_\nu d\Omega dS dt}$ each event is reweighted by the ratio of two fluxes at the point (E_ν, θ_ν). That is, the event weight is defined as follow:

$$w_{event} = \frac{d\Phi_\nu^{model}}{dE_\nu d\Omega dS dt} \times \left(\frac{d\Phi_\nu^{sim}}{dE_\nu d\Omega dS dt} \right)^{-1} \tag{2.15}$$

The same sample of neutrinos, initially generated following a $E^{-1.4}$ spectrum, can be re-weighted using any user specified spectrum by assigning a different weight to each event, w_{event}. Three weighting parameters are introduced in the ANTARES convention of Monte Carlo simulations [39]. First, the weight $w1$ contains the projected area of the can onto the plane perpendicular to the neutrino direction. Second, the weight $w2$, is equal to $\frac{N_{total}}{t_{gen}} \times \left(\frac{d\Phi_\nu^{sim}}{dE_\nu d\Omega dS dt} \right)^{-1} \times F$, where F is thte number of second per year. It has units GeV.m^2.sr.s.year^{-1}. Third, the global weight $w3$ equivalent to w_{event}, is defined as follows:

$$w3 = w2 \times \frac{d\Phi_\nu^{model}}{dE_\nu d\Omega dS dt} \tag{2.16}$$

where $\frac{d\Phi_\nu^{model}}{dE_\nu d\Omega dS dt}$ is the differential flux of neutrinos before penetrating the Earth, in unit of GeV^{-1}.m^{-2}.sr^{-1}.s^{-1}. The global weight $w3$ has unit of year^{-1} which can be understood as "rate" per year.

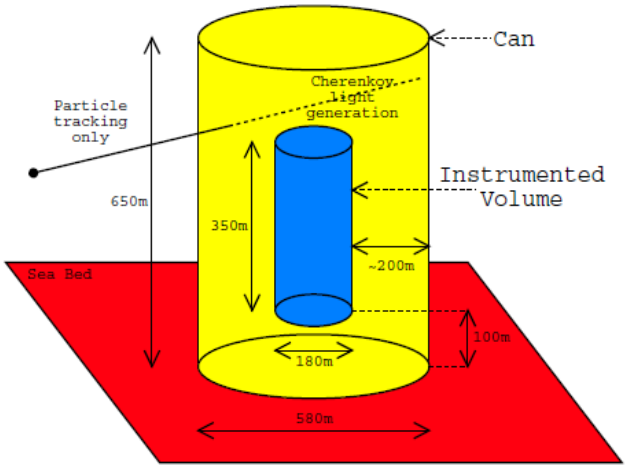

Figure 2.15 – Schematic view of the can, surrounding the instrumented volume.

2.5.2 Simulation of atmospheric muons

Apart from neutrinos, only atmospheric muons, as secondaries from hadronic showers, with energies typically above 500 GeV (1TeV) at the sea level can reach the detector (at a depth larger than 2000 m) for zenith angle $< 60°$ ($> 60°$) while the others are absorbed. The surviving events at sea level are characterized by a certain energy, direction and muon multiplicity. ANTARES Collaboration uses two independent approaches to simulate this atmospheric muon background:

Full simulation package: The program named CORSIKA[6] [40] is used to simulate high energetic primary cosmic radiation (protons, α particles and heavier nuclei) interactions in the atmosphere and the propagation of the secondary particles to sea level. Most of the particles emerging from these interactions are pions and kaons. The primary cosmic ray flux is generated following a diffuse flux $dN/dE \propto E^{-\Gamma}$ which allows a later re-weighting with a user specified flux model. CORSIKA offers the choice of the cosmic ray flux and their model of interactions in the atmosphere. To minimize the CPU time, the ANTARES collaboration has chosen to split the flux of the primary cosmic rays into 5 groups including the most abundant particles: proton, helium, carbon, magnesium and iron nuclei in an energy range from few TeV to 10^2 PeV and zenith range from 0° to 85°. Secondary particles such as photons, leptons, mesons and nuclei are also propagated to sea level. The development of the hadronic shower in the atmosphere is simulated with the QGSJET01 model [41]. In the analysis presented in chapter 4 we use the Battistoni parametrization of the primary cosmic rays [42]. CORSIKA allows to compare at each step the results of the simulation with data from other experiments which permits a well control of the systematics.

For the propagation of muons from sea level to the detector, the ANTARES collaboration uses the MUSIC[7] package [43]. MUSIC takes into account the interaction processes of muons with matter, i.e. bremsstrahlung, multiple scattering, ionization and pair production (see section 2.2.4). The energetic losses of muons can be modeled by the formula Equation (2.8). Ionization can be considered as a continuous process. As such, it is treated identically over the whole energy range, while the other processes are treated differently when a huge energy loss is induced. Energy losses are thus split into two parts: continuous energy losses (calculated with the Bethe-Bloch formula) and stochastic losses. These latter processes are taken into account when the fraction of energy lost by the muon is greater than 10^{-3}E. In MUSIC, muons are deflected by the three processes quoteed above except ionization.

Fast simulation package: This program named MUPAGE[8] [44] is based on a predefined parametrization of muon flux measured by several experiments. The parameters include the depth (from 1.5 km to 5 km, the zenith angle θ and, for muon showers, the multiplicity m and the distance of each muon with respect to the direction of the shower). The parametrization has been extracted from the full simulation package HEMAS [45, 46] and the hadronic interaction models were simulated using the DPMJet model [47]. MUPAGE generates events for a user specified data acquisition time, in such a way that no further weighting is needed. This

[6] COsmic Ray SImulation for KAscade
[7] MUon SImulation Code
[8] Atmospheric MUons from PArametric formulas: a fast GEnerator for neutrino telescopes

simulation provides the best data/MC agreement, hence it is used for the results presented in the Chapter 5.

2.5.3 Simulation of the Cherenkov light

The propagation of muons and electrons in water results in the emission of Cherenkov photons. Those are simulated using KM3 [48] and GEASIM codes. The former simulates the propagation of muons using the MUSIC package, the light and secondary particles emitted by these muons. The latter, generates the hits at the OMs by means of a full GEANT (version 3.21) simulation of photon production. In contrast of KM3, GEASIM neglects the photon scattering, thus it assumes their direction as a straight line. This assumption makes GEASIM faster than KM3. Hereafter we concentrate on the KM3 code which simulates the Cherenkov light from muons and electromagnetic showers in three steps:

1. **GEN**: includes a complete GEANT3 simulation of the Cherenkov light. It generates photons produced from short muon track segment (typically one meter) and electromagnetic showers. The Cherenkov photons (direct and scattered) are traced individually through water until absorption takes place. Their positions and times are recorded at concentric spheres of various radii centered on the origin of emission. The program output consists of some tables containing all the photons recorded at each spherical shell.

2. **HIT**: uses the output tables described above to create the hit distributions at the OMs for muon track segments and electron showers. The photon probabilities are computed taking into account the optical properties (absorption and scattering length and refractive index) measured at the ANTARES site [49]. Positions and times of arrival of photons at each OM are stored and used to convert the hit probability into photo-electron number using Poisson statistics. During this step, the orientation of the PMT with respect to the track direction, the position of the lines are taken into account.

3. **KM3MC**: At this level, the propagation of the muons already generated at the can surface is performed. It takes as input the detector description and uses the photon tables to calculate the number of photo-electrons produced in each PMT and their arrival time. Segments of about 1m are examined step by step taking into account the energy losses of the muon. If the energy lost by the muon is greater than the mean energy lost by ionization an electromagnetic shower is produced along the segment. This electromagnetic shower is treated independently using the table of electrons.

   Both GEN and HIT programs are run only once to generate the relevant tables of OM hit

probabilities. These tables are then stored on disk for subsequent use by KM3MC which is the program the end-user is most likely to use.

2.5.4 Generation of the optical background

The ANTARES neutrino telescope is located in an environment of high optical background produced by ^{40}K and bioluminescence at rates of about 100kHz per OM. The triggerEfficiency program [50] generates the background hits at the OMs according to the rates found in the raw data files. Then, it applies the same trigger criteria as for data to select candidate events in the Monte Carlo samples.

2.5.5 MC run by run approach

Recently the ANTARES collaboration has adopted a new Monte Carlo simulation approach in order to reproduce more realistic conditions of data taking following a run-by-run strategy [51]. The input information (run setup, mean rates, position and orientation of OMs, time and charge calibrations, ARS threshold and run duration) are taken from the data themselves and plugged into the simulation. This approach calls the simulation codes described in section 2.5.

Practically, $5{\times}10^8$ neutrinos are simulated using GENHEN package in the energy range of 100 GeV and 100 PeV. To simulate downgoing atmospheric muons we generate one tenth of the statistics of the corresponding data run using MUPAGE. The run-by-run MC simulation approach is used in the analysis described in Chapter 5.

2.6 Track reconstruction algorithm

The track reconstruction consists of finding values for the free parameters in the assumed model which most likely caused the outcome of the measurement. In the case of muon track reconstruction, the basic model is a straight line passing through the detector along which a muon moves with the speed of light producing a Cherenkov light on its way as shown in Figure 2.16 (right). The reconstruction takes a set of PMT hits within the three OMs on each storey of each string and deduces the best set of values for the track parameters that are, at a given time t_0, the position $\overrightarrow{p} = (x, y, z)$ and direction $\overrightarrow{d} = (sin(\theta)cos(\phi), sin(\theta)sin(\phi), cos(\theta))$ of the muon. By convention, the time t_0 is defined as the time when the muon passes through the plane perpendicular to its direction and containing the centre of gravity of the detector (see Figure 2.16 on the left).

The muon trajectory is then characterized by $N_{parameters} = 5$ independent parameters that must be estimated by a given reconstruction algorithm. In practice, an analytical expression

which connects the photon arrival times t_i^{th} to the track parameters is used:

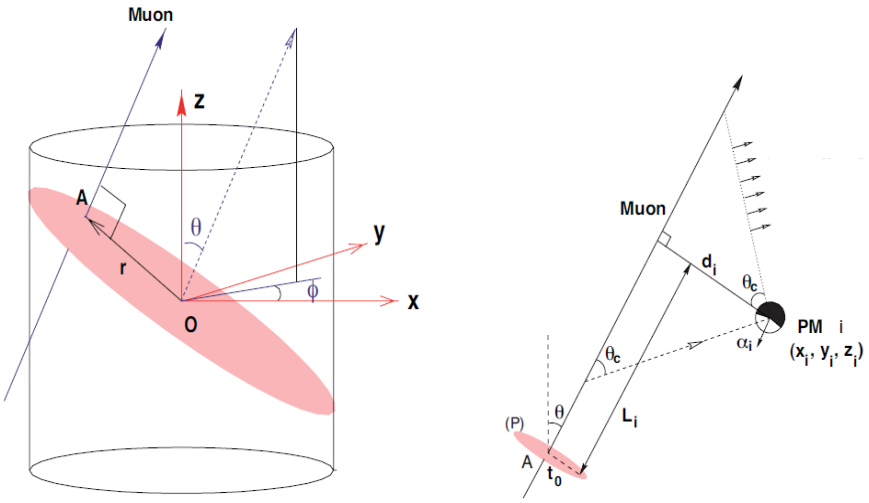

Figure 2.16 – Schematic view of the reconstruction strategy. Left: the geometrical description of the *can* and the coordinates used for the reconstruction. Right: the geometrical structure of the muon track induced by a muon-neutrino: definition of variables.

$$t_i^{th} = t_0 + t_{trans} + t_{trav} \tag{2.17}$$

where t_{trans} is the time it takes for the muon to reach the point where the light is emitted and t_{trav} is the time it takes for the photon to travel from that point to the OM. Using Figure 2.16 it follows:

$$t_{trans} = \frac{L_i}{c} - \frac{d_i}{c\,tan(\theta_c)}$$

$$t_{trav} = \frac{d_i}{v_g\,sin(\theta_c)}$$

where c is the velocity of light in vacuum and v_g is the group speed in water [52].

In the following we describe the two main reconstruction algorithms adopted by the ANTARES collaboration and used in this thesis. These methods assume that only a single muon crosses the detector. Therefore atmospheric muon bundles will be worse reconstructed and consequently removed by quality cut criteria.

2.6.1 In-situ reconstruction algorithm

The fast reconstruction algorithm called BBfit [53], convenient for the online use has been developed as a robust reconstruction method, which produces reliable results without precise

positioning calibration. Its strict hit selection leads to an accurate up-down separation while keeping a good efficiency. In BBfit, the exact geometry of the detector is ignored: the detector lines are straight (i.e lines are supposed unaffected by the sea current) and the 3 OMs of each storey are considered as a single OM centered onto the string. Thus, the hits altitude corresponds to the altitude of the optical modules.

As the first step, time and charge calibration (see section 2.3.6) is applied, the calibrated hit times and amplitudes being given in units of nano-seconds and photo-electrons (pe) respectively. For the selection of hits the algorithm uses the same criteria as those of the T3 trigger (see section 2.3.5). The algorithm requests a coincidence of 2 "L1 hits" in two adjacent floors (next-to-adjacent floors) within 80 ns (160 ns). Then, all hits of the same floor, in coincidence within 20 ns, are merged into one single hit. The time of the merged hit is the earliest time of the participating hits, and the charge is the combined charge of all merged hits. These merged hits are used for the reconstruction. The quality of the reconstruction is measured by a modified-χ^2 function, given by the Equation (2.18):

$$\chi^2 = \frac{Q}{N_{dof}} \tag{2.18}$$

where $N_{dof} = N_{hit} - N_{parameters}$ is the degrees of freedom, N_{hit} is the number of merged hits used in the fit, and

$$Q = \sum_{i=1}^{N_{hit}} \left[\frac{\Delta t^2}{\sigma_i^2} + \frac{q(q_i)d(d_{fit})}{< q > d_0} \right] \tag{2.19}$$

where σ_i is the timing error introduced to take into account the applied geometrical approximation and the occasional presence of late hits from small angle scattering or from electromagnetic processes. Its value is set to 10 ns for $q_i > 2.5$ pe and to 20 ns otherwise. The first term is a time residual, it exploits the difference time $\Delta t = (t_\gamma - t_i)$ between the hit time t_i and the expected arrival time of the photons t_γ from the muon track. The second term exploits the fact that an accumulation of storeys with high charges is expected on each detector line at its point of closest approach to the track. It depends on the measured amplitude q_i and the theoretical distances traveled by the detected photon d_{fit}. The chosen form gives an empirical penalty to the combination of high charge and large distance. The term $q(q_i) = q_0 q_i / \sqrt{q_0^2 + q_i'^2}$ is the amplitude of the hit corrected for the angular acceptance of the floor, i.e. $q' = 2q_i/(cos(\theta_\alpha)+1)$, where θ_α is the inclination of the photon track to the detector line, with an artificial saturation at 10pe. The term $d(d_{fit}) = \sqrt{d_{fit}^2 + d_1^2}$ is protected against small distance travelled by photons. One can assume the constant $q_0 d_1$ to be around 50m×photoelectron since the intensity

of the Cherenkov light decreases with the distance. The product $q.d$ is divided by the average corrected amplitude $< q >$, calculated from all hits which have been selected for the fit, to compensate for the fact that more energetic tracks or showers will produce more light at the same distance. The normalization d_0 balances the weight between the two terms. The value of d_0 has been chosen to be 50m, which is motivated by the fact that at this distance the typical signal in a PMT which points straight into the Cherenkov light front is of the order of one photoelectron.

The same quantity defined in Equation (2.18) is used to estimate a track or a shower (bright point) reconstruction parameters. The two cases differ in the way of calculating the expected arrival time of the photon at the PMT.

In the BBfit algorithm, events are split into four kinds: track reconstructed with a single line, track reconstructed with multiple lines, shower reconstructed with a single line and shower reconstructed with multiple lines. In the case of a single line reconstruction the azimuth information is lost leading to the estimate of only four parameters.

The azimuth degeneracy: In the case of tracks reconstructed using only two detector lines, an ambiguity is introduced on the reconstructed azimuth angle of the track, ϕ_{rec}. Thus two muon tracks are reconstructed both having the same zenith angle but different azimuth angle. The distribution of the hit times of the true track and of the track obtained by mirror symmetry with respect to the plane connecting the two lines, are identical. An illustration of this degeneracy is shown in Figure 2.17. The azimuth of the reconstructed original and mirror tracks are connected in the following way: $\phi_{mirror} = 2\phi_{lines} - \phi_{track}$, where ϕ_{lines} is the azimuth angle of the plane connecting the two lines.

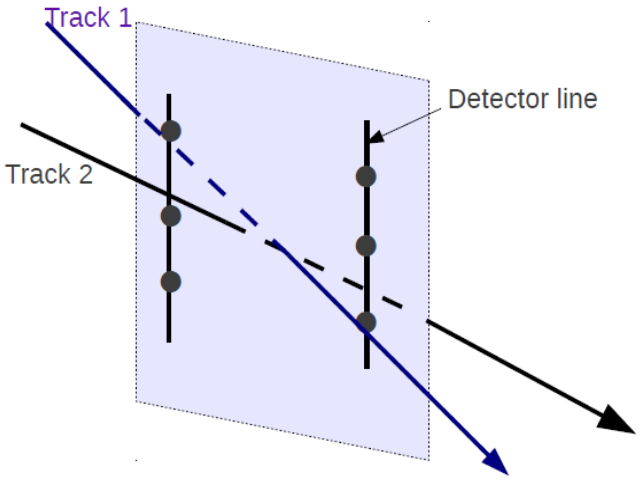

Figure 2.17 – Illustration of the azimuth degeneracy

The version of BBfit used in this thesis is $v3r6$. In this version we added the coordinates of the mirror track (named hereafter track(ϕ_{mirror})) in addition to the original one (named hereafter (track(ϕ_{track})). Previous versions provided only one solution randomly chosen among the two mirror tracks. This additional information permits to compare the *best*=Min ($track(\phi_{track}), track(\phi_{mirror})$) and the *random* (the one chosen randomly among the two solutions) track. Further details are presented in Chapter 4.

The choice between the tracks cannot be based on the χ^2 value since it is the same for both solutions. Thus to resolve the azimuth degeneracy, an intermediate reconstruction step was later introduced to BBfit. It consists of a temporary selection of all (raw) hits with time residuals less than 30ns for both tracks, over the whole detector. The sum of the charges of the two sets of selected hits is calculated and the track corresponding to the highest value is considered to be the correct one. The results presented in this thesis were completed before the implementation of this degeneracy breaking.

Bright point: When an electromagnetic or a hadronic shower is produced, it develops itself over a distance small compared to the spacing between detection storeys. As a consequence, light appears as if it was emitted isotropically from a bright point, and expanding with a velocity v_g. The four bright point parameters are therefore defined by the position of the emission point $\overrightarrow{P} = (x_0, y_0, z_0)$ and the emission time t_0. The spherical envelop of the light can then be fitted based on the simple relation:

$$v_g(t_i - t_0) = (\sqrt{(x_i - x_0)^2 + (y_i - y_0)^2 + (z_i - z_0)^2}$$

where t_i are the hit times, x_i, y_i the fixed horizontal positions of the lines and z_i the altitude of the PMT fired by the hit i.

The χ^2 of Equation 2.18 is then referred to as $b\chi^2$. Both the track χ^2 and the bright point $b\chi^2$ are used in the selection criteria of the final events to reject background: well reconstructed muons have a good χ^2 but poor $b\chi^2$ in contrast of background events.

2.6.2 Off-line reconstruction algorithm

A second more sophisticated and complex algorithm for the reconstruction of muon tracks, so-called Aafit, is based on the maximum likelihood method. Its full description is given in [54]. It consists of several stages:

Pre-selection of hits: This step allows to keep as much as possible hits that are most likely originating from a muon. The hits selected should verify the causality criterion given by the

following relation:

$$\Delta t_{ij} \leq \frac{d_{ij}}{v_g} + 20ns \tag{2.20}$$

where Δt_{ij} is the time difference between a hit i and the hit j with the largest amplitude, and d_{ij} is the distance between the OMs of the two hits. Hits with larger time differences cannot be related to the same muon, unless they have a residual larger than the safety factor 20ns [55], which is unlikely.

In order to reduce the impact of PMT afterpulses on the reconstruction, all the hits selected on the same OM using Equation (2.20) are merged within a time window of 300ns.

Pre-fit: The reconstruction procedure starts from a linear pre-fit based on the L1 hits, in order to provide a robust starting point for the further fitting procedure. At this stage, Aafit assumes that the hits occur on points that are located on the muon track, which allows to derive analytically a starting point from the minimization of the χ^2, although with a poor precision.

M-estimator fit: The M-estimators are a broad class of functions that allow parameter estimation even when the probability distribution that defines the problem is not exactly known. They are referred to as robust estimators when the result is insensitive to small variations of the underlying distribution assumed. The robustness of the M-estimator fit allows better estimate of a set of track parameters, using the residual Δt_i, and reduces the influence of outlier hits.

The output parameters of the prefit are used as seed in the M-estimator fit procedure which considers a sub-set of hits within 100m around the track estimated by the prefit and within a time window $\pm 150ns$ of the photon arrival times or a charge $\geq$2.3pe. The function that is maximized to estimate the track parameters is:

$$M = \sum_i \lambda \left(-2\sqrt{1 + A_i \frac{(t_i - t_i^{th})^2}{2}} \right) - (1 - \lambda) f_{ang}(\alpha_i) \tag{2.21}$$

where A_i is the hit amplitude, f_{ang} is the angular acceptance of the PMT as a function of the incident angle of the photon (with respect to the PMT axis) α_i. The λ parameter is set to 0.05 as the result of a Monte Carlo based optimization.

The maximum likelihood fit: The final fit procedure uses the principle of Maximum Likelihood (ML). It evaluates the theoretical arrival time of the photon at the OM i, t_i^{th}. Thus the time residual $\Delta t_i = t_i - t_i^{th}$, between the measured time and the expected time of the photon, is used to calculate the probability that the photon comes from the track. The track fitter searches for event direction for which the likelihood $\mathcal{L}$ takes maximum value. Under the

muon-like event assumption the following likelihood is calculated:

$$\mathcal{L} = \prod_i P(t_i|t_i^{th}) \tag{2.22}$$

Here $P(t_i|t_i^{th})$ is the statistical probability of observing t_i with the expectation of t_i^{th}. The probability of a hit with a certain residual Δt_i is described by a Probability Density Function (PDF). This PDF is a combination of a signal PDF and a background PDF. The first step

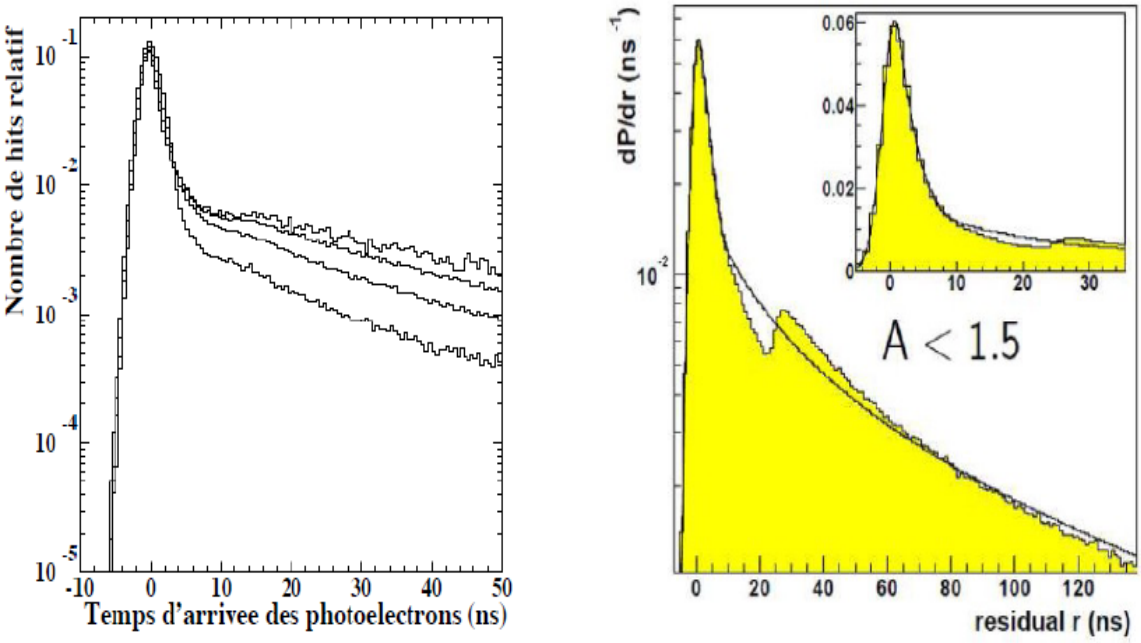

Figure 2.18 – Distributions of the time residuals used in the ML fit. Left: The curves correspond to four different muon energies, from the top to the bottom: 250, 50, 10 and 2 TeV. These PDFs do not take into account the background hits. The one used in the fit is the one for 10 TeV events. Right: An example of the full PDF used in final ML fit step for hit amplitudes <1.5pe. In yellow the histogram obtained by the Monte Carlo, the solid line is the parametrization used by the likelihood fit

of the ML fit is done using a signal only PDF as shown in Figure 2.18 (left). It takes into account the smearing on the hit times introduced by the transit time spread of the PMTs, which impacts the width of the peak around zero, and the scattering of light in water, which causes the long tail at positive values. An unphysical tail is present at values < -5ns, which was introduced to render the PDF differentiable at negative values. In this step hits with residual $\Delta t_i \in [-0.5R, R]$, where R is the root mean square of the residuals used in the M-estimator, are taken into account. Hits that are part of a coincidence or that have an amplitude larger than 2.5 pe are also selected.

The M-estimator and ML fit steps are repeated 9 times with some initial parameters inferred

from the pre-fit. Four starting points are obtained by rotating the pre-fit track by 25°. The rotation is done around the track point which is closest to the center of gravity of the selected hits. Four more trials are obtained by translating the starting point of the track by ±50 m in the direction $\overrightarrow{d} \times \widehat{z}$ (where $\overrightarrow{d}$ is the track direction) and by ±50 m in the direction of $\widehat{z}$. Among the 9 trials, the track with the best likelihood is stored. The number of the trials, N_{comp}, giving rise to compatible solutions (i.e with direction within 1° similar to the stored one) is used later in the analysis, as quality selection criterion.

The final fit uses an improved PDF using hits with time residual of ±250 ns (in order to add background hits), local coincidences and hits with amplitude larger than 2.5pe. An example of distribution of this PDF is shown in Figure 2.18 (right). At the output, the algorithm provides two quality parameters of the track. The first given by:

$$\Lambda = \frac{log\mathcal{L}}{N_{dof}} + 0.1(N_{comp} - 1) \tag{2.23}$$

where $N_{dof} = (N_{hits} - N_{parameters})$ is the number of degrees of freedom used in the fit. The second term acts as an ad hoc reward for fits with $N_{comp} > 1$. The second quality parameter is the angular error estimate, β, of the reconstructed track. This quality parameter is obtained from the fit of the likelihood and is given by:

$$\beta = \sqrt{\sigma_\theta^2 + sin^2\theta\sigma_\phi^2} \tag{2.24}$$

where σ_θ and σ_ϕ are the error estimates of the track's zenith and azimuth angles respectively. The use of these quality parameters for the event selection is studied in Chapter 5 for the data recorded during the 2009-2010 data taking period.

REFERENCES

[1] K.F Grieder, Cosmic Rays At Earth, Researcher's Reference Manual and Data Book, Elsevier (2001).

[2] R. Gandhi et al, Phys. Rev., D58, 093009, (1998).

[3] R. Gandhi et al, Astropart. Phys., 5, 81110, (1996).

[4] J. G. Learned and K. Mannheim, Annu. Rev. Nucl. Part. Sci, 50, 679-749 (2000).

[5] Particle Data Group, European Physics Journal C, 3, 144 (1998).

[6] P. H. Barrett et al, Rev. Mod. Phys. 24, 133178 (1952).

[7] P. Cerenkov, CRAc. Sci. U.S.S.R. 8, 451 (1934).

[8] J. D. Jackson, John Wiley and Sons, Inc (1998).

[9] G. V. Domogatsky, Nucl. Phys. Proc. Suppl. 91, 438 (2001).

[10] V. Aynutdinov et al, NIMA 602 (2009).

[11] E. Andres et al, Astropart. Phys. 13, 1-20 (2000).

[12] H. Kolanoski et al, ePrint: arXiv:1209.5610 (2012).

[13] R. Abbasi et al, Astrophys. J. Lett. 689, L65 (2008).

[14] J. Ahrens et al, Proc. of the 27th International Cosmic Ray Conference, Hamburg Germany, 1237 (2001).

[15] R. Abbasi et al, Nature 484, 351-354 (2012).

[16] R. Abbasi et al, ePrint: arXiv:1208.4861 (2012).

[17] S. Böser et al, ePrint: arXiv:1205.6405 (2012).

[18] G. Aggouras et al, Nucl. Phys. Proc. Suppl., 151, 279 (2006).

[19] L. K. Resvanis, J. Phys. Conf. Ser. 39, 447 (2006).

[20] C. Distefano et al, Astrophys. Space Sci., 309, 415-420 (2007).

[21] C. Distefano et al, Nucl. Phys. Proc. Suppl., 190, 109-114 (2009).

[22] U. F. Katz, NIM A567, 457-461 (2006).

[23] KM3NET collaboration, available on http://www.km3net.org/TDR/TDRKM3NeT.pdf.

[24] J.A. Aguilar et al, NIM A 656 11-38 (2011).

[25] M. Amram et al, NIM A484 369-383 (2002).

[26] P. Vernin, ANTARES internal note, ANTARES-SOFT-2008-002 (2008).

[27] P. Vernin, ANTARES internal note, ANTARES-SOFT-2007-018 (2007).

[28] E. Waxman and J. Bahcall, Phys. Rev. D 59 (1998).

[29] G. D. Barr et al, Phys. Rev. D70 023006 (2004).

[30] J.A. Aguilar et al, NIM A570 107 (2007).

[31] J. Carr et al, ANTARES internal note, ANTARES-SOFT-2007-016 (2007).

[32] A. Kouchner, HDR, Université Paris Diderot (2009).

[33] J.A. Aguilar et al, Astropart. Phys. 34 539-549 (2011).

[34] A. M. Brown et al, Proceedings of the 31st ICRC, Lódź, Poland (2009), e-Print: arXiv:0908.0814.

[35] S. Escoffier, ANTARES internal note, ANTARES-SITE/2005-001 (2005).

[36] D. Bailey, ANTARES internal note, ANTARES-SOFT-2002-004 (2002).

[37] G. Ingelman et al, Computer Phy. Communications 101, 108-134 (1997).

[38] G. D. Barr, PhD thesis, University of Oxford (1987).

[39] J. Brunner, ANTARES internal note, ANTARES-SOFT-1999-003 (1999).

[40] D. Heck et al, CORSIKA: a Monte Carlo code to simulate extensive air showers, TIB Hannover (1998).

[41] G. Bossard et al, Phys. Rev. D 63, 054030 (2001).

[42] G. Battistoni et al, Nucl. Phys. B (Proc. Suppl.) 70 367-370 (1999); Astropart. Phys. 12 315-333 (2000).

[43] P. Antonioli et al, Astropart. Phys., 7, 357368 (1997).

[44] G. Carminati et al, Comput. Phys. Commun., 179: 915923 (2008).

[45] E. Scapparone, arXiv/physics.9902043 (1998).

[46] Y. Becherini et al, Astropart. Phys., 25, 113 (2006).

[47] J. Ranft, Phys. Rev. D51 (1995) 64 (2000).

[48] D. Bailey, ANTARES internal note, ANTARES-SOFT-2002-006 (2002).

[49] S. Adrián-Martínez et al, Astropart. Phys., 35, 552557 (2012).

[50] M. de Jong, ANTARES-SOFT-2009-001 (2009).

[51] C. Rivière, ANTARES internal note, ANTARES-PHYS-2012-001 (2012).

[52] L. A. Kuzmichev, NIM A482, 304 (2002).

[53] J.A. Aguilar et al, Astropart. Phys. 34 652662 (2011).

[54] A. Heijboer, PhD thesis, Universiteit van Amsterdam (2004).

[55] S. Galata, PhD thesis, Université Aix-Marseille (2012).

CHAPTER 3

GRAVITATIONAL-WAVE INTERFEROMETRIC DETECTORS

3.1 Summary

After the detailed review of neutrino astronomy with the ANTARES neutrino telescope given in the previous chapter, we review in this chapter the observational astrophysics possible with the gravitational wave detectors such as Virgo and LIGO. This chapter first gives an introduction to gravitational-wave astronomy from an instrumental point-of-view ranging from the general detection principles to the description of the instruments currently in operation. Being LIGO and Virgo very similar we will focus on the Virgo detector. The main part of this chapter offers an introduction to the analysis techniques for gravitational wave (GW) data.

3.2 Detection principle

The idea of using interferometry to detect gravitational waves was first proposed by two Russian theorists, M. Gertsenshtein and V.I. Pustovoit in 1962 [1]. The applicability of this idea was thoroughly studied by R. Weiss [2] and further by D. Drever [3] leading to the general design followed in today's instruments.

As we have seen in section 1.2.1, gravitational wave exerts a strain on space-time. It thus affect the distances between freely falling test particles. The idea is to sense this deformation thanks to ultra-precise laser interferometry. Let us consider a Michelson-type interferometer in which two laser beams propagate along two orthogonal arms of lengths L_1 and L_2. An impinging GW is equivalent to a relative displacement of the end mirrors of the interferometer (used as test masses) $\delta\ell \equiv L_1 - L_2$. This is related to the GW amplitude $h = \delta\ell/L$ where L is the interferometer arm length. The relative displacement of the test masses induces a

phase shift between the two interfering beams, measurable at the interferometer output with a photodetection. Three fundamental noises limit the accuracy of this measurement:

- **Seismic noise:** is a *displacement noise* which results from the vibration of the ground below the instrument. The noise comes from the global and large-scale motion of the tectonic plates (including the *micro-seismic* dominated by the interaction of the plates with ocean waves) and from the local anthropic activity. Seismic noise rises rapidly toward low frequencies and limits the sensitivity below 10 Hz. The seismic noise is reduced using suspension systems, as the Virgo *super-attenuator* (see section 3.3).

- **Thermal noise:** is also a *displacement noise* which originates from the Brownian motion of the atoms that compose the mirrors and their suspensions. To reduce this noise both are made of material with a high mechanical quality factor. This noise limits the sensitivity in the frequency band around 100 Hz (where the sensitivity is maximum) and therefore limits the observational horizon of the instrument.

- **Shot noise** is a *sensing noise* which results from the quantum fluctuation of light. Those fluctuations can be interpreted as fluctuations in the phase shift at the photo-detector, thus they can mimic the GWs. The effect of the shot noise is reduced by increasing the number of photons in the interferometer. This is why high-power lasers are used and light is "recycled" thanks to the technique of power recycling. Several kilo-Watts of light power is stored in the initial GW interferometers.

The impact of those three noises can be reduced to reach the accuracy of $h_{noise} \sim 10^{-21}$. Several instruments have reached this objective after many years of preparation and construction involving a large number of scientists and engineers coming from many countries. We will describe the Virgo detector in more details in the next section. A next generation of instruments is under way and expected for 2015. The objective is a ten-fold improvement of the sensitivity over the first (and current) generation of instruments. This increases the accessible volume of the Universe (and hence the number of detectable sources) by a factor of 1000.

3.3 The Virgo detector

The Virgo interferometer [4] has been built by a collaboration between France and Italy. It is located near Pisa, Italy. The vertex of the Virgo detector is at elevation 53.238 m and at geographic coordinates 43°37′53″N and 10°30′16″E.

In short, Virgo consists in two orthogonal kilometric arms (3 km) illuminated by a laser source. The laser is a Nd:YAG with a wavelength $\lambda_L = 1064$ nm and output power $P \sim 10$ W in the initial Virgo design. An initial resonating optical cavity called *mode cleaner* performs both spatial filtering ("mode cleaning") and frequency stabilization of the input beam. The cleaned laser beam is sent to the beam splitter which separates the light into two identical beams directed to the two arms. To increase the optical path length the interferometer arms are replaced by Fabry-Perot resonating optical cavities. A simplified scheme of Virgo interferometer is shown in Figure 3.1. The relative position of the mirrors of the cavity is controlled so that the light after one round-trip is coherent in phase with the in-coming light from the beam splitter. The equivalent number of round trips or *finesse* is determined by the transmissivity and reflectivity of the input mirrors as well as by their optical losses. The finesse is about 50 in the initial Virgo design. The light beam propagates in an ultra-vacuum system to protect it from air density fluctuations. The two beams recombine and interfere at the beam splitter. The interferometer is tuned on the *dark fringe* by a control system which adjusts the position of the end mirrors accordingly. In the absence of GWs, the small fraction of light power that constitutes the dark fringe goes to a photo-detector that measures its intensity, while all the light that circulates in the arms (bright fringe) is reflected by the beam-splitter back toward the laser. Here, a semi-reflective *power-recycling* mirror feeds the bright fringe back into the interferometer in phase with in the in-coming light from the main laser.

In summary, Virgo is composed of six main mirrors (four large input and end mirrors, the beam splitter and the power recycling mirror) [5] and four resonating optical cavities (mode cleaner, two in the arms and the power recycling cavity). The main optics in the arms are mirrors of 350mm diameter, 100mm thickness and 20kg mass.

All the mirrors are suspended to a specific seismic isolation system, called *super-attenuator* [6]. At its heart is a chain of pendulums, each stage of which provides good attenuation of the vertical and horizontal ground vibrations. The overall attenuation is more than 10^{10} at frequencies ≤ 10 Hz.

3.4 Response of a gravitational wave interferometer

The response h of the interferometer to an impinging GW with polarization h_+ and $h_\times$ can be written as

$$h = F_+(\theta, \phi, \psi)h_+ + F_\times(\theta, \phi, \psi)h_\times \tag{3.1}$$

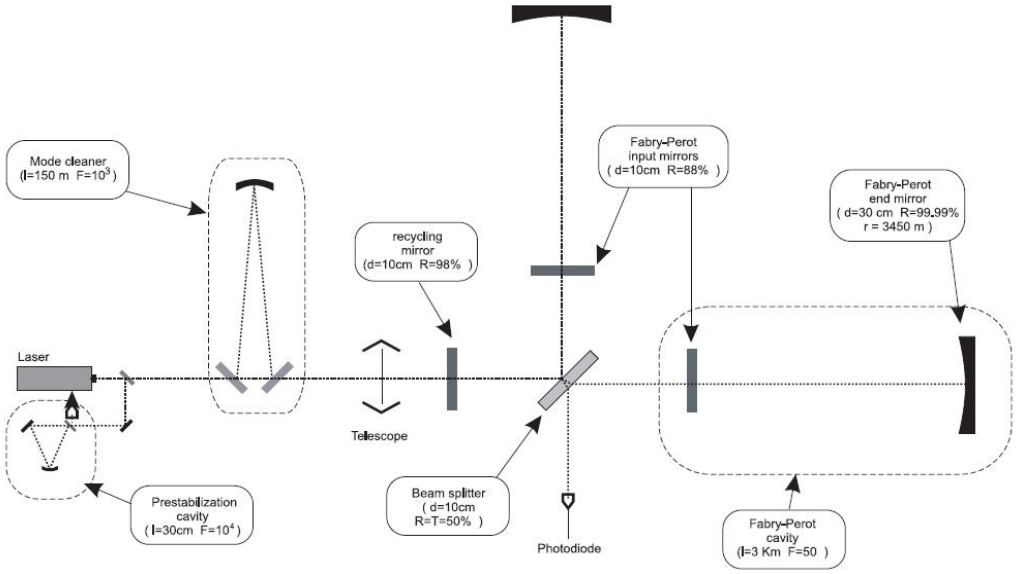

Figure 3.1 – The basic optical scheme of Virgo

where the antenna pattern F_+ and $F_\times$ are equal to

$$\begin{aligned} F_+(\theta,\phi,\psi) &= \frac{1}{2}(1+\cos^2\theta)\cos 2\phi\cos 2\psi - \cos\theta\sin 2\phi\sin 2\psi \\ F_\times(\theta,\phi,\psi) &= \frac{1}{2}(1+\cos^2\theta)\cos 2\phi\cos 2\psi + \cos\theta\sin 2\phi\sin 2\psi \end{aligned} \tag{3.2}$$

and are functions of the three angles θ, ϕ and ψ defined as follows. Let the Cartesian frame (x, y, z) have the origin on the beam-splitter and the arms of interferometer are along the x and y axes. The propagation plane of the GW is characterized by the frame (x', y', z'). In the prime coordinates the propagation of the GW coincides with the z' axis. Its sky location is defined by the polar angles θ and ϕ with respect to (x, y, z), see Figure 3.2. The polarization angle ψ is between the projection of the x arm onto the plane orthogonal to the direction of propagation and the x' axis.

The antenna pattern F_+ and $F_\times$ in Equations (3.2) encode the detector angular sensitivity (see Figure 3.3). Generally speaking, GW detectors have a very wide aperture and are hence non-directional. We see that the GW detector is blind to certain directions for any value for ψ, i.e., for $\phi = \pm\pi/4$ and $\theta = \pi/2$. This corresponds to the two bisectors of the detector arms. Conversely, the response $F_+^2 + F_\times^2$ is maximum for $\theta = 0$ or π i.e, a GW coming from the zenith.

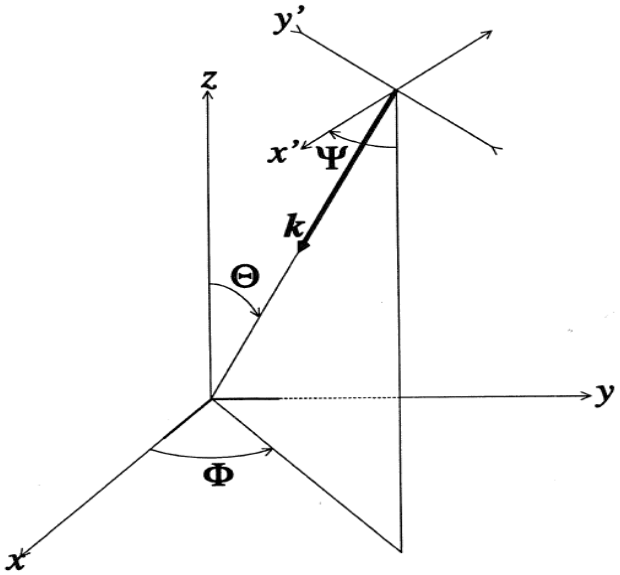

Figure 3.2 – The coordinate system used in Virgo in the computation of the antenna pattern functions. The origin coincides with beam-splitter and along the x and y axes. A rotation by an angle θ around y axis and ϕ around z axis brings the (x', y', z') frame onto the (x, y, z) frame

3.5 Astrophysical reach of a gravitational wave detector

An approximate yet realistic estimate of the astrophysical reach of GW detectors can be obtained by considering isotropic monochromatic source of GW [7]. We start from the expression of the GW flux and GW radiated energy given in Equations (1.22) and (1.24) respectively in section 1.2.2.

For monochromatic source emitting at frequency f_0, we have

$$F_{GW} \approx \frac{\pi c^3}{4GT} f_0^2 h_{rss}^2 \tag{3.3}$$

where $h_{rss}^2 \equiv \int_T h_+^2(t) + h_\times^2(t) dt$. Here we integrated over the duration T which corresponds to the entire duration of the considered GW transient.

Assuming that the source is isotropic, we get from Equation (1.24)

$$E_{GW} = \frac{\pi^2 c^3}{G} D_L^2 f_0^2 h_{rss}^2 \tag{3.4}$$

More realistically, the emission pattern may be linear (e.g., supernova core collapse)

$$h_+(t) \sim \sin^2 \iota s(t) \tag{3.5}$$

$$h_\times(t) \sim 0 \tag{3.6}$$

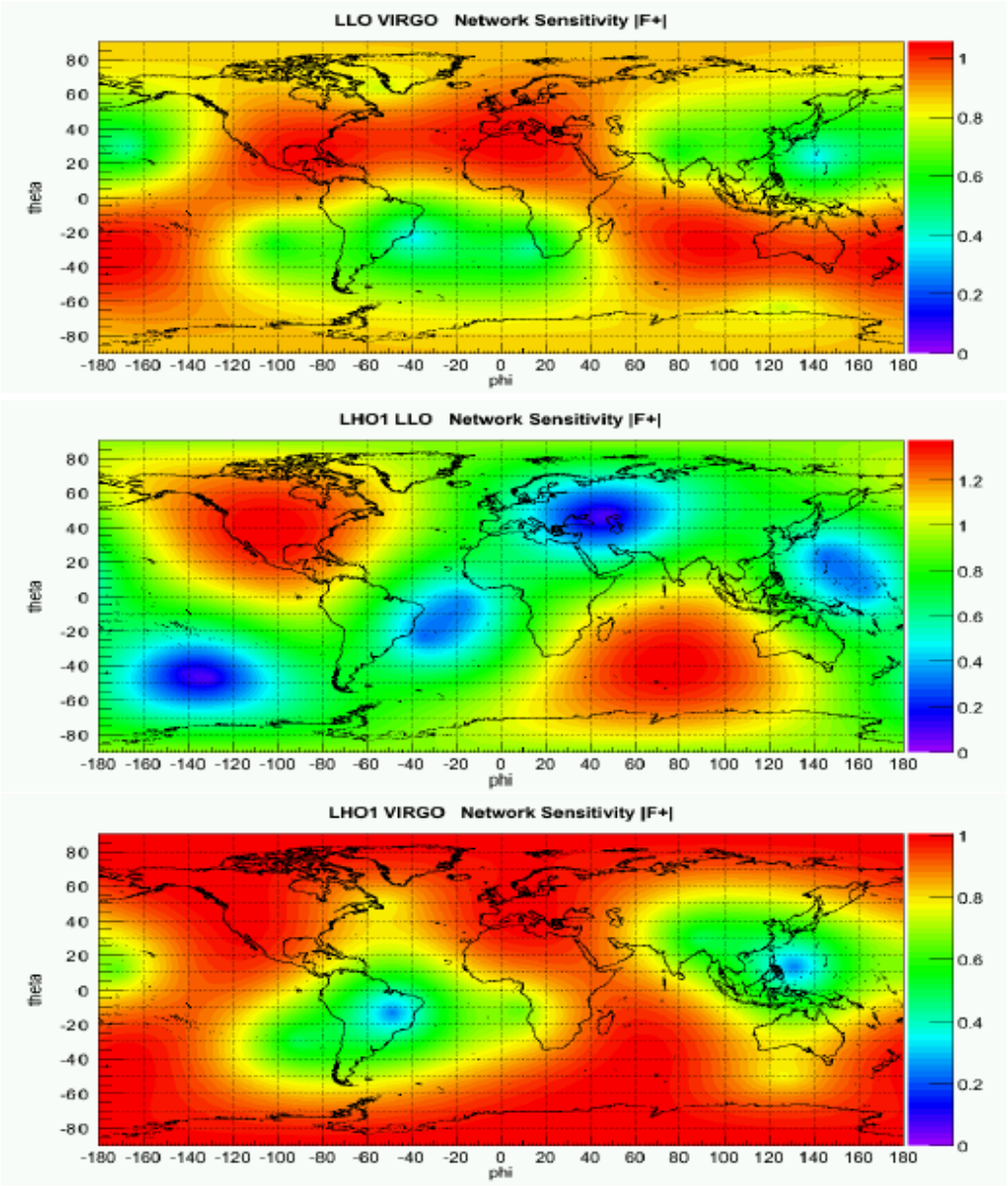

Figure 3.3 – The module of the plus component of the network antenna pattern considering the three couples of detectors: H1L1, H1V1, L1V1. The area which network are more sensitive (red colour) increase with respect to the single detector case. This immediately shows the advantage of using more than one detector.

or elliptical (e.g., binary mergers)

$$h_+(t) \sim (1+\cos^2\iota)/2A\cos\Phi(t) \tag{3.7}$$
$$h_\times(t) \sim \cos\iota A\sin\Phi(t) \tag{3.8}$$

In that case, it is easy to show that the Equation (3.4) holds

$$E_{GW} = \alpha\frac{\pi^2c^3}{G}D_L^2f_0^2h_{rss}^2 \tag{3.9}$$

with a rescaling factor α in section 1.2.2 whose value depends on the polarization pattern. We have $\alpha = 8/15$ and $\alpha = 2/5$ for linear and elliptical polarization respectively.

Let ρ define the signal-to-noise ratio (SNR),

$$\rho^2 \equiv \int\frac{|H(f)|^2}{S(f)}df \tag{3.10}$$

where $H(f)$ is the Fourier transform of the detector response $h(t) = F_+h_+(t) + F_\times h_\times(t)$ as defined in Equation (3.1). $S(f)$ is the two-sided noise power spectral density.

For monochromatic sources, it is easy to show that

$$\rho^2 \approx \beta^2\frac{h_{rss}^2}{S(f_0)} \tag{3.11}$$

where $\beta^2 = F_+^2 + F_\times^2$, $\beta^2 = F_+^2\sin^2\iota$ and $\beta^2 = F_+^2((1+\cos^2\iota)/2)^2 + F_\times^2\cos^2\iota$ for the isotropic, linear and elliptical emission patterns respectively as defined in Equations (3.5) and (3.7).

Combining Equations (3.11) and (1.24), we finally get

$$E_{GW} = \frac{\alpha}{\beta^2}\frac{\pi^2c^3}{G}D_L^2f_0^2S(f_0)\rho^2 \tag{3.12}$$

It can be checked numerically that $\alpha/\beta^2 \approx 2$ for all polarization cases [7].

Consider a burst source that releases $E_{gw} = 10^{-2}M_\odot$ (which is the typical order-of-magnitude for mergers of stellar-mass compact objects) at frequency $f = 50$ Hz where Virgo sensitivity is $S^{1/2}(f) \approx 8\times10^{-23}/\text{Hz}^{1/2}$. By inverting the above Equation (3.12), we can compute that this source is detectable with SNR $\rho = 10$ at $D_L \sim 11$ Mpc. This is compatible with the distance estimates for the horizon of binary mergers (see reference [8]).

3.6 Worldwide network of gravitational wave detectors

The first generation of interferometric GW detectors includes a total of five large-scale instruments. The French-Italian project Virgo presented earlier. The US-based Laser Interferometer Gravitational-Wave Observatory (LIGO), which includes three kilometric-scale instruments located in Livingston, Louisiana and Handford, Washington (the latter hosts two interferometers in the same vacuum enclosure). GEO, a German-British detector in operation near Hannover, Germany (see Figure 3.4).

Figure 3.4 – Geographic location of the interferometric detectors. This world map displays the location of the four sites of the first generation detectors (LIGO H and L, Virgo and GEO).

3.6.1 Source positioning

GW detectors are non-imaging instruments with a nearly omni-directional response. Source localization therefore requires multiple detectors, in order to use the measured time delay between detectors as well as the amplitude of the measured signal in each detector to triangulate a sky location. Several methods of localization have been investigated. The timing accuracy of a GW signal can be written as [9]:

$$\sigma_t \sim \frac{1}{2\pi\sigma_f\rho} \tag{3.13}$$

where σ_f is the effective bandwidth of the source and ρ is the SNR. For nominal values $\sigma_f = 100$ Hz and $\rho = 8$, timing accuracies are of the order of 0.1 ms. This can be compared to the light travel time between detectors (10–30 ms for the LIGO-Virgo network) to deduce the angular uncertainty for the triangulation of times of arrival. For example, for a binary coalescence signal at the threshold of detectability, [9] estimates a best-case localization of 20 deg^2 (90% containment), and a typical localization of twice this. Additional constraints provided by other

instruments with a better angular accuracy such as HEN telescopes can therefore significantly help improving the source localization.

3.6.2 Sensitivities reached so far and coordinated data takings

In 2007, LIGO and Virgo have concluded an agreement which includes the data sharing and coordination of their data takings. The first joint data taking is the LIGO fifth Science Run (or S5) and the first Virgo Science Run (or VSR1). The former started on November 4th, 2005 and ran until October 1, 2007; and the later began on May 18, 2007 until Sep 30, 2007. A second joint data taking with enhanced detectors, S6/VSR2-3, began on 7 July 2009 and ended on 20 October 2010.

We show in Figures 3.5 and 3.6 the strain sensitivity that these detectors reached during S5/VSR1 and S6/VSR2-3 respectively.

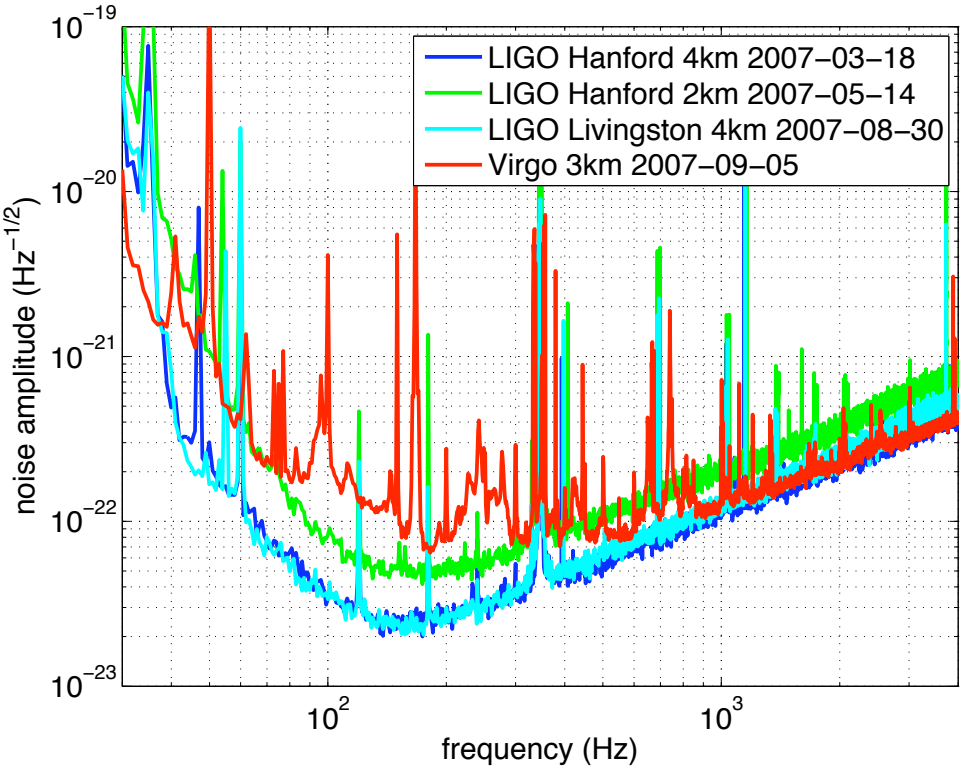

Figure 3.5 – Typical Virgo and LIGO sensitivity curves during the joint science run S5/VSR1

3.7 Analysis of gravitational wave data

The output of a GW detector is a time series which contains the response to an impinging GW $h(t)$ and the instrumental noise $n(t)$. The astrophysical sources are expected to be rare

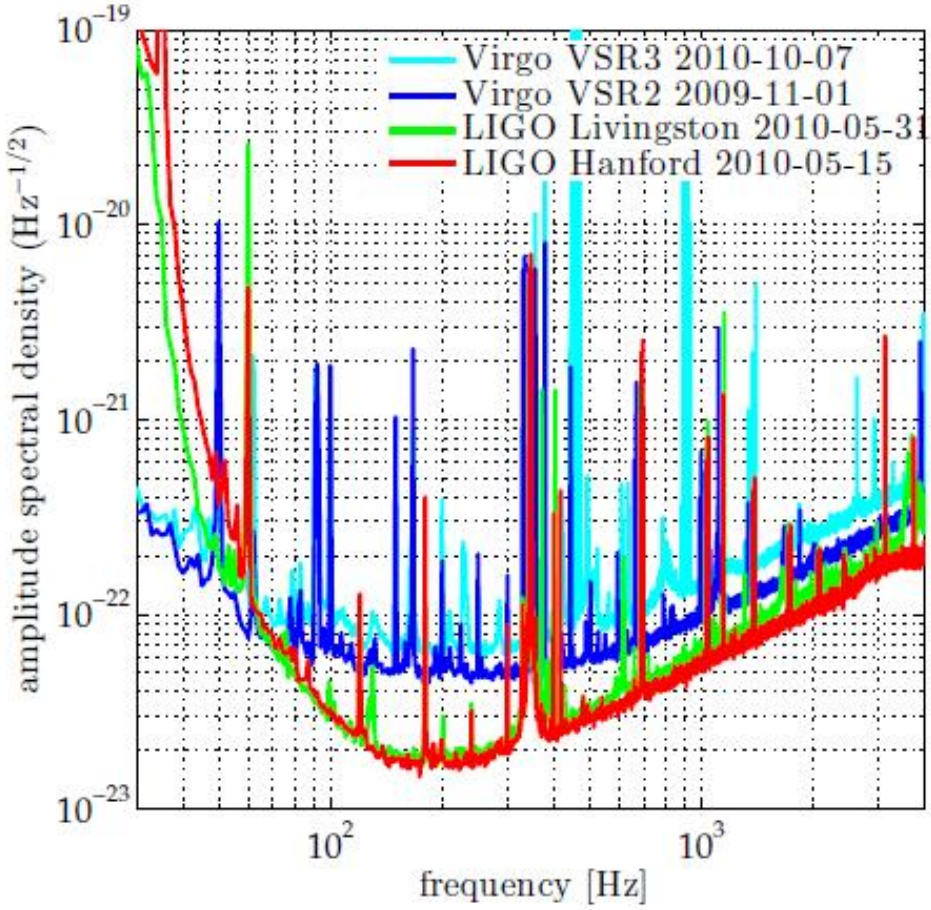

Figure 3.6 – Typical Virgo and LIGO sensitivity curves during the joint science run S6/VSR2-3

with signature at the limit of detectability. Efficient signal processing methods are thus required to detect the GW signal at low SNR.

Two distinct cases can be considered: (*i*) the GW signal is known to a good accuracy thanks to reliable astrophysical models; (*ii*) the GW signal is unknown or poorly known. In the first case, it can be shown that under that the noise is stationary and Gaussian, the optimal detection method is the *matched filtering*. Essentially this consists in cross-correlating the data with the expected signal. A detection is made when an excess of correlation is observed. In the second case (unmodelled burst signals), *time-frequency* techniques are used to extract transient signals from the background noise. We considered that the joint sources of GW and HEN falls in the latter category.

In this section, we give a general overview of the methods and techniques used for the detection of GW bursts. We also introduce in the section two algorithms used to search for GW bursts: the *X-pipeline* and *coherent WaveBurst* (cWB). Both those methods have been

used in the context of the joint GW and HEN searches we present in Chapters 4 and 5.

3.7.1 Wavelets and time-frequency analysis

Fourier transform decomposes a signal into its frequency components. The power spectrum provides information about frequency only. The temporal localization is cancelled. A time-frequency distribution is a transform that maps a 1-D signal into a 2-D time-frequency map, which describes the evolution of spectra over time. Each pixel in this map represents the signal power at a given time and frequency.

There exists various ways to produce such representation. Short-term Fourier analysis or wavelet based transforms are the most commonly used. This consists in replacing the Fourier basis composed of long-duration complex exponentials by short duration signals called wavelets concentrated about a given time and frequency. The time-frequency representation results from the projection of the signals on the wavelet basis.

Stationary background noise is associated with a homogeneous wavelet representation while transient signals appears as a localized excess of power. This can be used to detect GW transients by searching for clusters of connected time-frequency pixels (associated with an outstanding power). An example of the time-frequency representation of a transient is given in Figure 3.7.

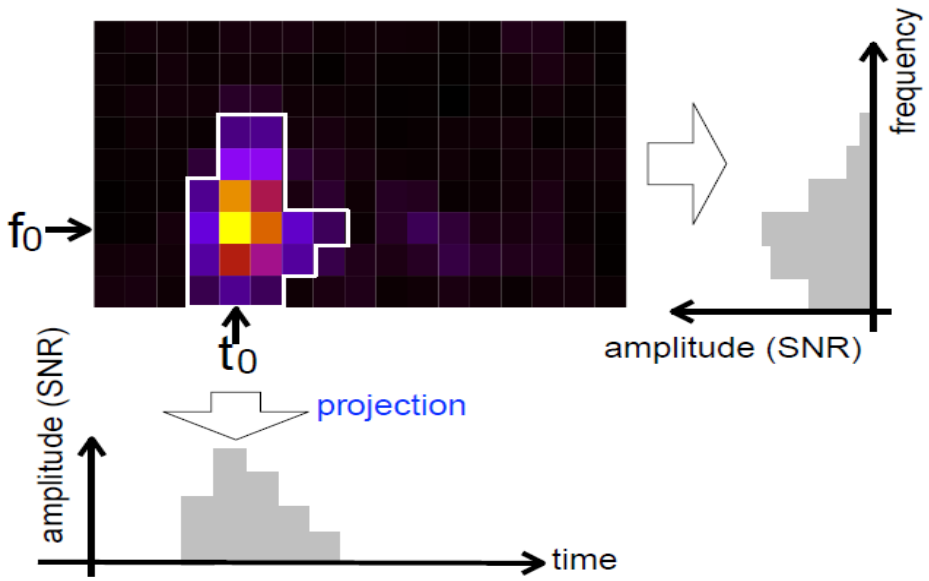

Figure 3.7 – Time-frequency representation and its projection to time- and frequency-axis respectively. (source: [10])

3.7.2 Multi-detector analysis

In the previous section, we described the basic methods used for the analysis of the data stream from a single detector. In the following, we will be interested in aspects specifically related to multiple data streams. The availability of multiple data streams impacts on the way the data are analyzed at different levels.

Coherent analysis of multiple data stream

Coherent excess power methods used to search for unmodelled GW bursts require that the signals received by all detectors are *consistent* in time *and* phase. Concretely this is realized by combining the data streams from multiple detectors, taking into account the antenna response and noise level of each detector so that the sum operates constructively for a GW burst from a given sky direction. The data stream which results from this coherent combination maximises the signal-to-noise ratio (SNR). It is used to produce a time-frequency map of the signal energy (equivalently, the SNR), which is then scanned for transient excursions (or *events*) that may be GW signals. Each event is characterised by a measure of significance, based on energy and/or correlation between detectors, as well as its time-frequency properties. Another outcome from this type of analysis is the probability (pseudo-)distribution over the sky usually referred to *sky map* from which the most likely location of the source can be extracted (see Figure 3.8).

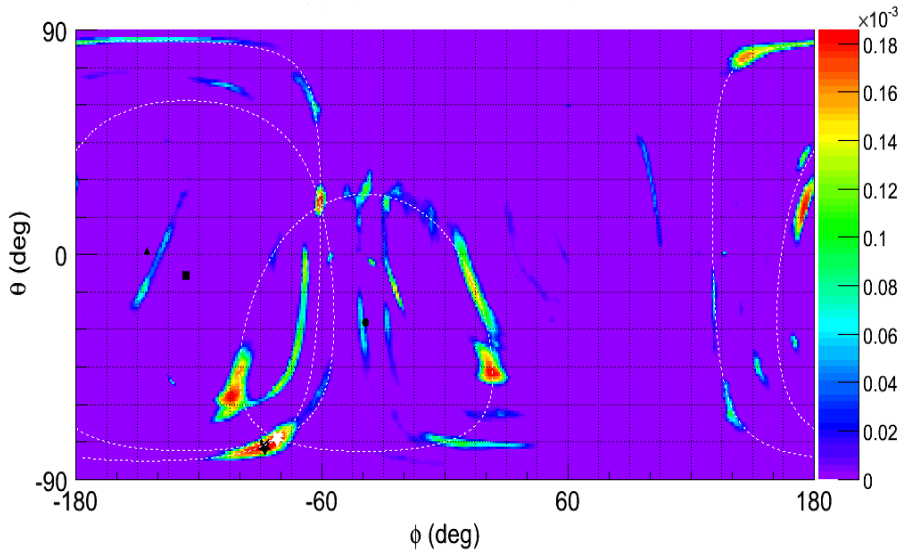

Figure 3.8 – An example of sky map of network statistics for a three detector networks. (source [11])

Mitigation of non-Gaussian/non-stationary noise with multiple data

Fundamental noises presented above are expected to be Gaussian and stationary. However, the real instrument noise is dominated by an overwhelming fraction of non-Gaussian non-stationary noises from various origins. It consists in a large number of transient noise excursions commonly called *glitches*. Glitches are produced by a variety of environmental and instrumental processes, such local seismic noise or saturations in feedback control systems. Since glitches occasionally occur nearly simultaneously in separate detectors by chance, they can mimic a gravitational-wave signal.

The population of glitches are difficult to model. The size and the large complexity of GW detectors makes this modelling even more difficult. GW detectors being extended instruments over kilometers, it is hard to completely isolate them from the outside world and the surrounding anthropic activity. Therefore, the accurate modelling of the non-Gaussian/non-stationary noise background is for now out-of-reach. It has to be mitigated and this can be done at least partially by using multiple data.

It is possible to calculate combinings of the data from multiple detectors where the GW signals from all detectors interfere destructively in the sum. The GW signal thus cancels, but not background glitches. The energy in these "null" stream(s) may be used to reject or down-weight events not consistent with a gravitational wave. The success of such tests depend critically on having several independent detectors of comparable sensitivity. The cross-correlation with auxiliary non-GW sensitive channels (which monitors the global status and environment of the GW detector) provides also an important resource for background rejection.

Use of multiple data for background estimation

We explained earlier that the accurate modelling of non-Gaussian non-stationary noise is out-of-reach. The remaining part of the glitches that cannot be identified by the coherent techniques described in the previous section constitutes the dominating background noise in burst searches. This background has to be estimated. However, GW signals cannot be turned off: the detectors cannot be shielded from them. Therefore, we don't have "noise-only" data at disposal for background estimation.

Nevertheless, the background can be estimated thanks to the availability of multiple data streams by time shifting one detector's data with respect to the others by a delay much longer than the time-of-flight between detectors. Time shifts only leave triggers due to random coincidences in detector noise and erase the contribution from real GW signals. By repeating the analysis many times with different time-shifts, we get an accurate estimate of the rate of background events.

3.7.3 Sensitivity estimate

We test the performance of the search algorithms by repeatedly adding fake gravitational wave signals to the raw data stream and estimating the detection efficiency of each "injected" waveform models. The astrophysical origin and waveform morphology, of the gravitational wave bursts we search for in this work are a priori unknown. A broad range of signal waveforms were considered for the analysis of 2007 data presented in Chapter 4. These include astrophysically-motivated waveforms as well as ad-hoc waveforms. The list of test signals includes:

- ***Sine-Gaussian waveforms*** both linearly polarized

$$h_+(t+t_0) = h_0 \exp(-t^2/(4\tau^2)\cos(2\pi f_0 t) \tag{3.14}$$
$$h_\times(t+t_0) = 0 \tag{3.15}$$

  or circularly polarized

$$h_+(t+t_0) = \frac{1+\cos^2\iota}{2} h_0 \exp(-t^2/(4\tau^2))\cos(2\pi f_0 t) \tag{3.16}$$
$$h_\times(t+t_0) = \quad \cos\iota \quad h_0 \exp(-t^2/(4\tau^2))\sin(2\pi f_0 t). \tag{3.17}$$

  The latter case mimics at least qualitatively the expected GW emission from the final part (merger and ringdown) of the coalescence of a neutron-star and/or black-hole binary. It also provides a reasonable model for the GW emission from some of the extreme scenarios considered for core-collapse supernovae described in section 1.3.1.

  In the above equations, f_0 is the central frequency, t_0 is the central time and the decay time $\tau \equiv Q/(\sqrt{2\pi}f)$. Q is the effective number of cycles of the waveforms with values ranging from 2 to 100.

- ***White noise bursts*** are bandpassed random time-series of selected duration with independent polarization amplitudes. White noise bursts can be considered as a limiting case: their waveform does not help to distinguish them from the detector noise. The only discrimant property used to detect them is that they are correlated signatures in the various detector data.

- ***Ring-down waveforms*** are expected from processes like f-modes of NS, or during the ring-down of newly formed BH/NS during the post merger phase after coalescence, or produced in SN star-quakes related to Soft Gamma Repeaters (SGR). They are characterized by their frequency f_0, duration τ or Q (similarly to SG) and polarization. They

have the following expression:

$$h_+(t+t_0) = \sin(2\pi f_0 t)\exp(-t/\tau) \tag{3.18}$$

$$h_\times(t+t_0) = \cos(2\pi f_0 t)\exp(-t/\tau) \tag{3.19}$$

Figure 3.9 illustrates the various families of waveforms injected into data for simulation studies in time and time-frequency demain.

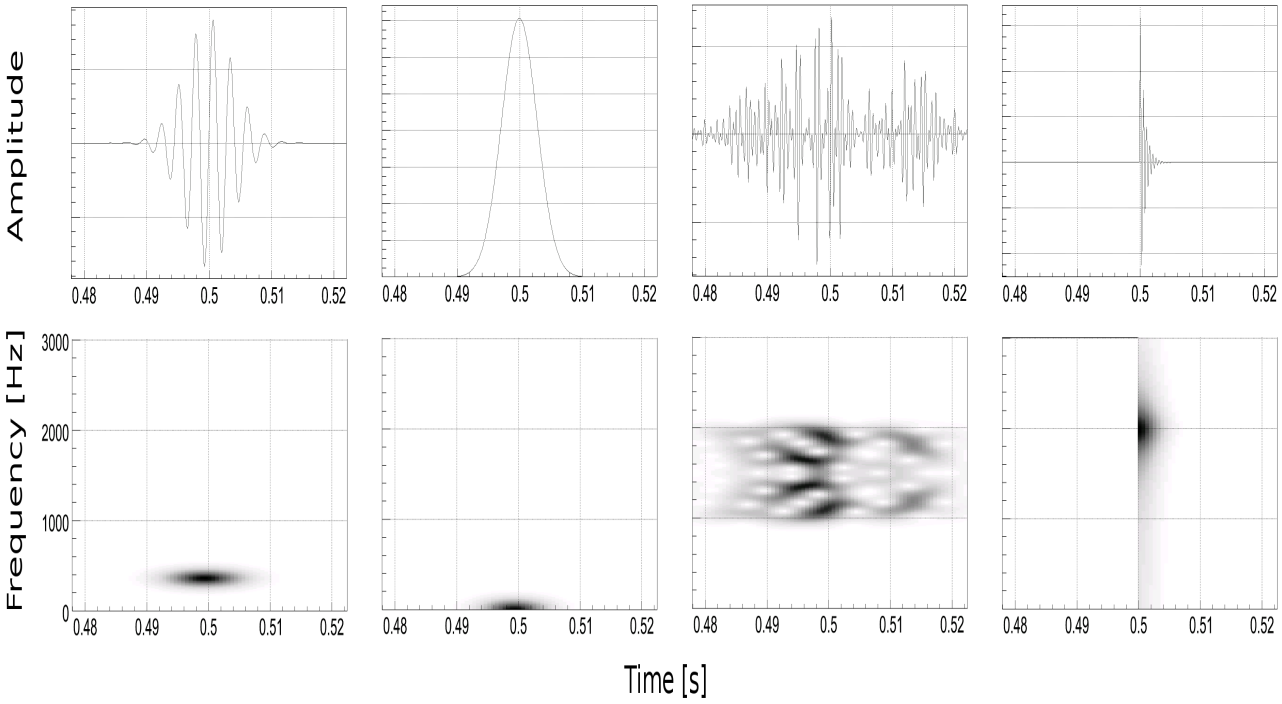

Figure 3.9 – Representation of waveforms in the time domain (top row) and a time-frequency domain (the bottom row). From left to right: a 361 Hz $Q = 9$ sine-Gaussian, a $\tau = 4.0$ ms Gaussian waveform, a white noise burst with a bandwidth of 1000-2000 Hz and characteristic duration of $\tau = 20$ ms and, finally, a ringdown waveform with a frequency of 2000 Hz and $\tau = 1$ ms. (source: [13])

3.7.4 Data analysis methods to search for gravitational wave bursts

The X-pipeline algorithm

X-pipeline is an analysis algorithm for interferometric gravitational wave detection. It deals with unmodelled gravitational wave bursts associated with external astrophysical triggers such as gamma rays or neutrinos. The X-pipeline processes data *coherently* from an arbitrary network of GW detectors in the frequency band 64-500 Hz.

For a specific time and direction, the X-pipeline reads the appropriate GW data and Fourier transforms it. Then for each specified direction it makes a time-frequency map of the time-series data, and computes the different statistics for each time-frequency bin, mainly coherent energies. After that, the X-pipeline looks at a fixed percentage (e.g. 1%) of bins with the highest value of the detection statistics (measured coherent energy) and marks those bins as black bins, see Figure 3.10. Black bins that share a common side are grouped together into clusters which are considered a candidate detection event [12].

X-pipeline algorithm is used, with a slightly modifications that will be discussed later, in this work to analyse the ANTARES, LIGO and Virgo data from 2007. Results are presented in Chapter 4.

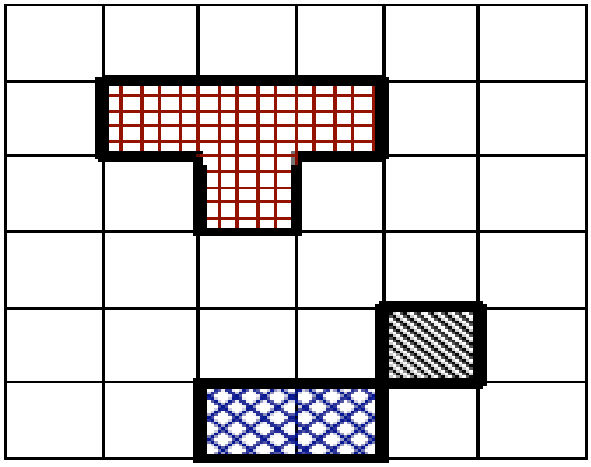

Figure 3.10 – A time frequency map with "black" pixels grouped into 3 clusters. Nearest-neighbor black pixels (those that share an edge) are grouped into a single cluster. Each cluster in this image is denoted by a different color and hatching pattern. (Source [12])

The coherent WaveBurst algorithm (cWB)

coherent WaveBurst (cWB) [14, 15] is, in contrast with the X-pipeline, an un-triggered (all–sky) search algorithm for detecting gravitational wave burst. It uses the constraint likelihood approach [16] to construct a least-squares fit of the two GW polarizations to the combined data from a network of detectors in the frequency band 64-5000 Hz. The cWB analysis is performed in several steps. First, detector data is decomposed into a time-frequency representation and then whitened and conditioned to remove narrow-band noise features. Events are identified by clustering time-frequency pixels with significant energy which is coherent among detectors and characterized using test statistics derived from a constrained (regulated) likelihood (which is also a measure of the signal energy detected in the network and is calculated as described

in [16]). Two statistics are computed by cWB. The first is a network correlation coefficient net_{cc}, which is a measure of the degree of correlation between the detectors. The second is the coherent network amplitude ρ and is proportional to the signal-to-noise ratio. The latter is used to rank events within a homogeneous sub-period.

A triggered version of cWB, named *skymask coherent WaveBurst* (s-cWB), has been developed and used in the analysis presented in Chapter 5. Further details about the s-cWB are discussed in Chapter 5.

REFERENCES

[1] E. Gertsenshtein and V. I. Pustovoit, Soviet Physics JETP 43, 605-607 (1962).

[2] R. Weiss, Quarterly Progress Report, Research Laboratory of Electronics, MIT 105: 54 (1972).

[3] P. Saulson, Fundamentals of Interferometric Gravitational Wave Detectors, World Scientific, (1994).

[4] F. Acernese et al, Class. Quantum Grav. 25, 114045 (2008).

[5] F. Beauville, Virgo Technical Paper, VIR-NOT-ROM-1390-262.

[6] F. Acernese et al, Astropart. Phys. 33, 182-9 (2010).

[7] P. J. Sutton, LSC Technical Paper, P1000041.

[8] J. Abadie et al, e-Print, arXiv:1203.2674 [gr-qc] (Mar. 2012).

[9] S. Fairhurst, New J. Phys., 11, 123006, (2009).

[10] H. Ryota et al, 12th GWDAW (Gravitational Wave Data Analysis Workshop), arXiv:0804.0296 [gr-qc] (2008).

[11] http://www.ligo.org/science/GW100916/.

[12] P. J. Sutton et al, New J. Phys. 12 053034 (2010).

[13] J. Abadie et al, Phys. Rev. D 85, 122007 (2012).

[14] S. Klimenko et al, Class. Quantum Grav. 25, 114029, (2008).

[15] M. Drago, PhD thesis, Università degli Studi di Padova (2010).

[16] S. Klimenko et al, Phys. Rev. D 72, 122002 (2005).

CHAPTER 4

GW+HEN ANALYSIS OF 5L–S5/VSR1

4.1 Summary

In this chapter we present the first joint search for gravitational-wave bursts associated with high energy neutrinos. Contrarily to the analysis presented in chapter 5, this first search was not jointly optimized: we used the neutrino candidate list obtained for a point source search and looked for possible concomitant, both in time and direction, GW signal using an algorithm specially designed for this kind of *triggered* searches. In this chapter, we describe the method used for this first search and take special care to the description of the neutrino candidate selection using the 2007 data set of ANTARES, LIGO and VIRGO detectors. All detectors were running in their initial sensitivity: ANTARES was running in 5-lines (5L) configuration; LIGO and VIRGO were just finishing their first science runs (S5) and (VSR1) respectively. The outcome of this first search is submitted for publication in the Astrophysical journal [1] and has led to several public presentations [2]. No significant coincident events were observed. We placed limits on the density of joint HEN+GW emission events in the local universe, and compare them with densities of merger and core-collapse events.

4.2 High energy neutrino triggered search procedure

The outline of the proposed search procedure [3–6] is shown in diagram 4.1. The GW+HEN joint search is performed by combining GW and HEN data using a *triggered* analysis [7, 8]. Using the latter, the search for GW signals is then restricted to an astrophysically motivated range of arrival times around the neutrino time and in its estimated direction. Compared to a classical method where GW signals are searched for with random arrival time, triggered searches can be run with a lower event detection threshold thanks to the reduction in the volume of analyzed data. This leads to a higher detection probability at a fixed false alarm probability

and better limits in the absence of detection. Similarly, the *a priori* knowledge of the source direction allows for searching only a small part of the sky and vetoing candidate events at times not consistent with the expected GW arrival time. In fact, the number of accidental coincidences between GW detectors decreases as the size of the search window decreases. This part of the sky is referred to as *angular search window* (or ASW) and is described in section 4.4.1. Thus, the use of an external trigger can be a very effective tool for a successful search of GW signals.

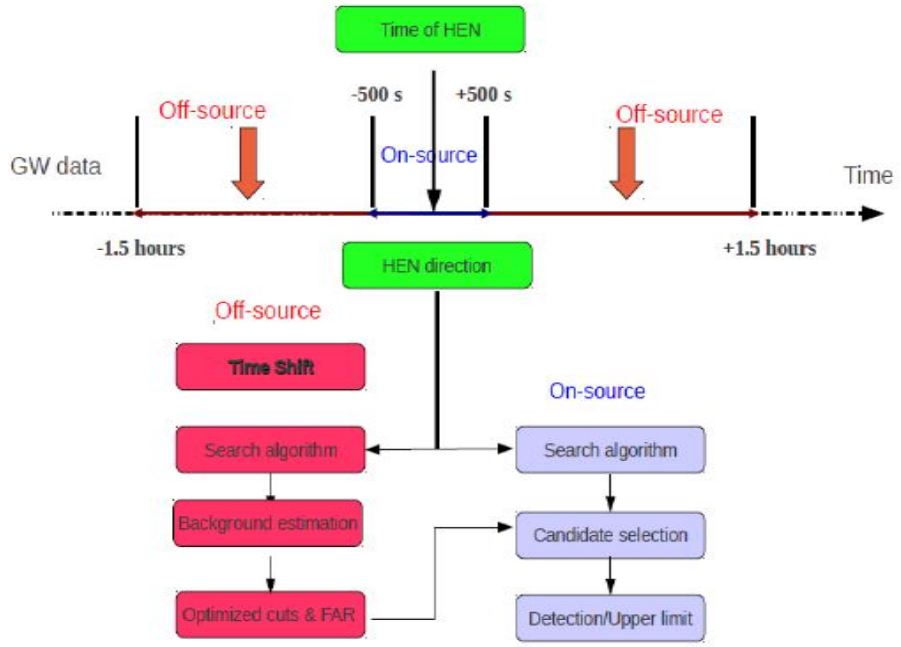

Figure 4.1 – Schematic flow diagram of a HEN-triggered search for GWs. Each neutrino candidate (with its time and directional information) provided by ANTARES acts as an external trigger for the GW algorithm, which searches the combined GW data flow from all active interferometers (ITFs) for a possible concomitant signal. The size of the spatial search window is related to the angular accuracy associated to each HEN candidate. The background estimation and the optimization of the selection strategy are performed using time-shifted data from the off-source region in order to avoid contamination by a potential GW signal. Once the search parameters are tuned, the box is opened and the analysis is applied to the on-source data set.

In the present analysis, the external trigger is a neutrino candidate provided by ANTARES. The neutrino candidate, used as input for the GW+HEN joint search, is characterized by a set of parameters: its sky position $\overrightarrow{d}$, as given by the direction of the reconstructed muon track, the associated (and possibly direction-dependent) point-spread function of the detector (PSF), the neutrino arrival time, which defines the trigger time t_0, and the range of possible time delays (positive and negative) Δt between the neutrino signal and the associated GW signal, which is astrophysically motivated, as discussed in section 1.3.3. The latter quantity is referred to as the *on-source* window for the neutrino; this is the time interval which is searched

for GW candidate signals. To estimate the significance of the resulting GW candidates, the background rate has to be approximated using time-shift analysis as described in section 3.7.2. This background study is performed in an *off-source* window (shown in red on the diagram of Figure 4.1) around the time of the neutrino candidates.

The GW data used in this thesis are the LIGO S5 runs and VIRGO VSR1 runs (see section 3.2). These data are selected from periods where the detectors H1, H2, and V1 were in science mode, i.e. usable for the detection of GW. The LIGO fifth "science run" (S5) ranges from November 4, 2005 until September 30, 2007 [9, 10]. Over one year of science-quality data were collected with all three LIGO interferometers in simultaneous operation at their design sensitivity, with duty factors of 75%, 76%, and 65% for H1, H2, and L1 respectively. The Virgo detector started its first science run, VSR1 [11], on May 18, 2007. The Virgo duty factor over VSR1 was 78%. The GW data used in this analysis cover the period between January 27 and September 30, 2007.

4.3 Selection of High Energy Neutrino candidates

4.3.1 The ANTARES data and Monte Carlo sample

The 5L data sample of ANTARES ranges from January 27 to December 4, 2007 [12]. This analysis is restricted to the data taking period overlapping with the science runs of VIRO and LIGO detectors: January 27 to September 30, 2007.

The ANTARES sample is composed of the so-called silver runs selected by data quality criteria applied on all runs. The silver data set is obtained by accepting a baseline rate up to 120 kHz and a burst fraction up to 40% (cf paragraph 2.4). For each detector configuration at least 80% of OMs are required to be active over the full run. This means that among 375 channels a minimum of 300 OMs were active during the 5L period. Taking into account all the above mentioned criteria and the 20% dead time present in the on-line trigger at that period [13, 14], the remaining active time is T_{obs}= 104 days. The final common observation time, considering the duty cycle of the LIGO-Virgo detectors, reduces to T_{obs}^{com}= 91.36 days. The events are triggered with the $3N$ filter (section 2.3.5). The raw data are processed with the BBfit $v3r6$ (section 2.6.1). The set of calibration used for these data are shown in the table 4.1.

In the following we will distinguish between events reconstructed with 2-lines (2L) and those reconstructed with 3-lines and more (3L+). This distinction comes from the presence of two mirror tracks in the case of events reconstructed with 2L, for BBfit $v3r6$. As mentioned in

first run → last run	Calibration set
25700 → 27640	2007:L5:V4.0
27729 → 29763	2007:L5:V4.1

Table 4.1 – Calibration sets used to calibrate data

section 2.6.1 this version allows access to both mirror tracks. This is a crucial improvement for the present triggered search as it allows to reduce the size of the search window and consequently the background rate. This improvement is illustrated in section 4.4.1
Various Monte Carlo files are simulated as described in section 2.5. In this thesis the neutrino sample is simulated by GENHEN and weighted according to the Bartol flux for atmospheric neutrinos and an E^{-2} spectrum for cosmic neutrinos. The sample of atmospheric muons is simulated with CORSIKA and weighted with the Battistoni flux. All the MC files used in this analysis are processed by TriggerEfficiency with the 3N trigger. In Figure 4.2 we show the distributions of the nadir angle θ (as introduced in section 2.3.2) for data and MC samples. The colour code of the nadir distributions is the following:

- Turquoise curve: the MC truth for down-going atmospheric muons, which have been simulated within $90° \leqslant \theta \leqslant 180°$.
- Red curve: the reconstructed θ for MC atmospheric muons.
- Green curve: the MC truth for atmospheric neutrinos, which have been simulated in the range $0° \leqslant \theta \leqslant 90°$.
- Blue curve: the reconstructed θ for MC atmospheric neutrinos.
- Black curve: data.

The red curve extends over the whole range of θ in contrast of MC truth, showing that the majority of events with $\theta \leqslant 90°$ are atmospheric muons misreconstructed as up-going. Cuts based on the above parameters will be studied in the next section to remove these misreconstructed muons and select a sample of data with optimized discovery potential.

4.3.2 Event selection criteria

The first step of the selection is to keep only upgoing tracks:

cut 1: $\theta \leqslant 90°$

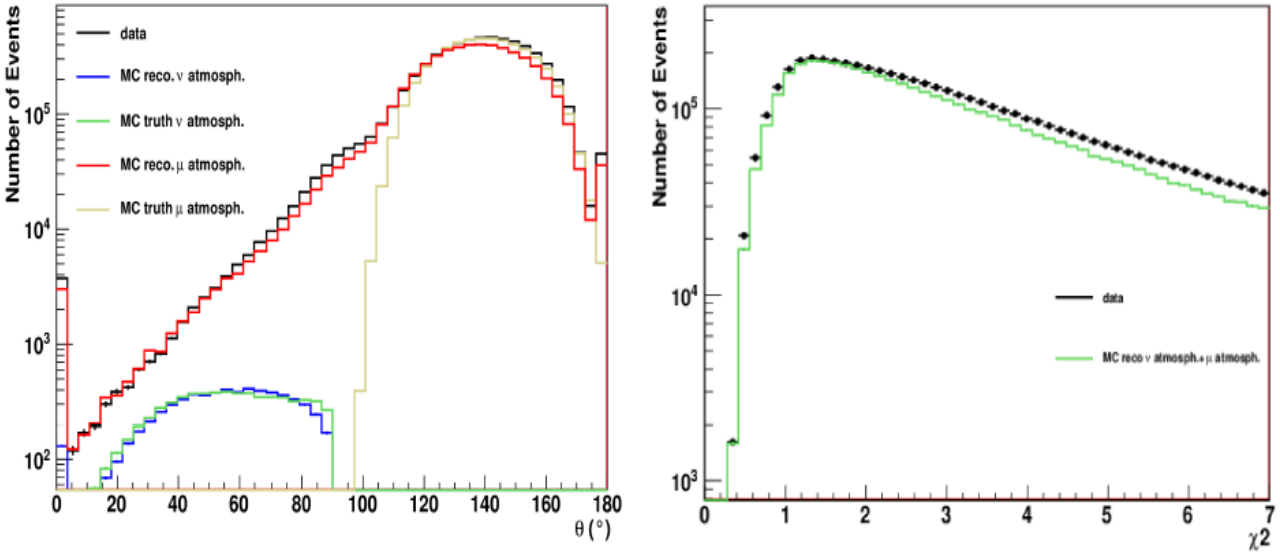

Figure 4.2 – Left: distributions of nadir θ for the data and MC. The colour code is explained in the text. We see that part of the atmospheric muons are reconstructed as upgoing while they are downgoing. Those are known as *misreconstructed* atmospheric muons. Right: distribution of the track χ^2 for data and MC including all the reconstructed events.

The subsequent steps are motivated by the will to distinguish remaining misreconstructed atmospheric muons from the desired muons originating from the interaction of upgoing neutrinos around the detector. The parameters used for this selection are the quality parameters $\chi 2$, $b\chi^2$ presented in section 2.6.1, whose distributions are illustrated in Figure 4.3.

After selecting the events passing the cuts, it is easy to compute with the MC simulations, the effective surface that represents the detector sensitivity for the given set of cuts. The neutrinos effective area is defined as the ratio of the rate of selected events to the neutrino flux at Earth:

$$A_\nu^{eff}(E_\nu, \theta) = \frac{N_{sel}}{N_{gen}} \times V_{generation}(E_\nu, \theta) \times (\rho . N_A) \times \sigma(E_\nu) \times P_{Earth}(E_\nu, \theta_\nu) \qquad (4.1)$$

Where N_{sel} and N_{gen} stand for the selected and generated events respectively. While, $V_{generation}$, ρ, N_A, P_{Earth} were introduced in section 2.5. For illustration purposes, we show in Figure 4.9 the neutrino effective area as function of neutrino energy.

In the present analysis, the final cuts on $\chi 2$ and $b\chi^2$ are derived in such a way to maximize the chances to discover a point-like source of HEN following the prescriptions detailed in [15, 16]. The objective is to maximize the so-called discovery potential. In order to do so we minimize the model discovery factor (MDF) that is defined, for a point source at declination δ, emitting

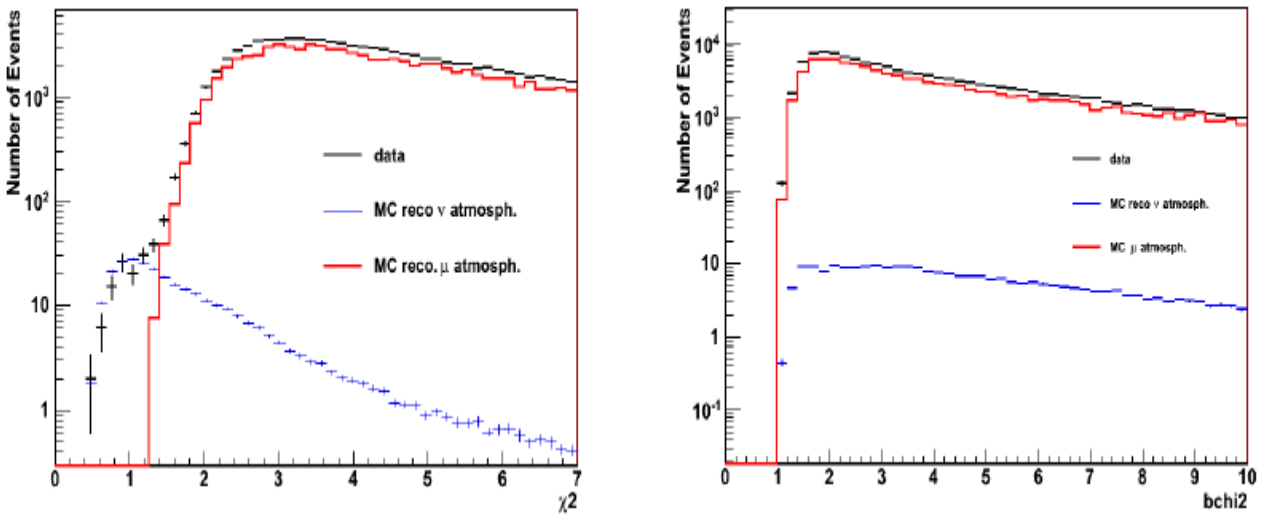

Figure 4.3 – Distributions of the track χ^2 (left) and the bright point $b\chi^2$ for Data and MC including all the events reconstructed as upgoing.

a power law flux with spectral index γ, as:

$$E^{\gamma}\frac{d\Phi(\delta)}{dEdSdt} = \frac{N_{sig}(\delta)}{A_{eff}(\delta) \times \Delta t \times \int_{E_{min}}^{E_{max}} E^{-\gamma} dE} \tag{4.2}$$

where:

- $N_{sig}(\delta)$ is the average expected number of signal events needed to have a 50% probability to make a discovery at the 5σ level.
- $A_{eff}(\delta)$ is the effective area as defined by Equation (4.1).
- Δt is the live time of selected runs.
- $[E_{min}; E_{max}]$ is the simulated events energy range.

Several combinations of values were tried for the maximization of the discovery potential:

- χ^2: 1.4, 1.6, 1.8, 2.0, 2.2, 2.4, 2.6.
- $b\chi^2$: 1.0, 1.4, 1.8, 2.2, 2.6.

Examples are shown in Figure 4.4 for a variety of cuts on χ^2 and for different nadir angle ranges, applying a cut on $b\chi^2 \geq 1.8$. Figure 4.5 shows other examples for 2 other cuts on $b\chi^2$.

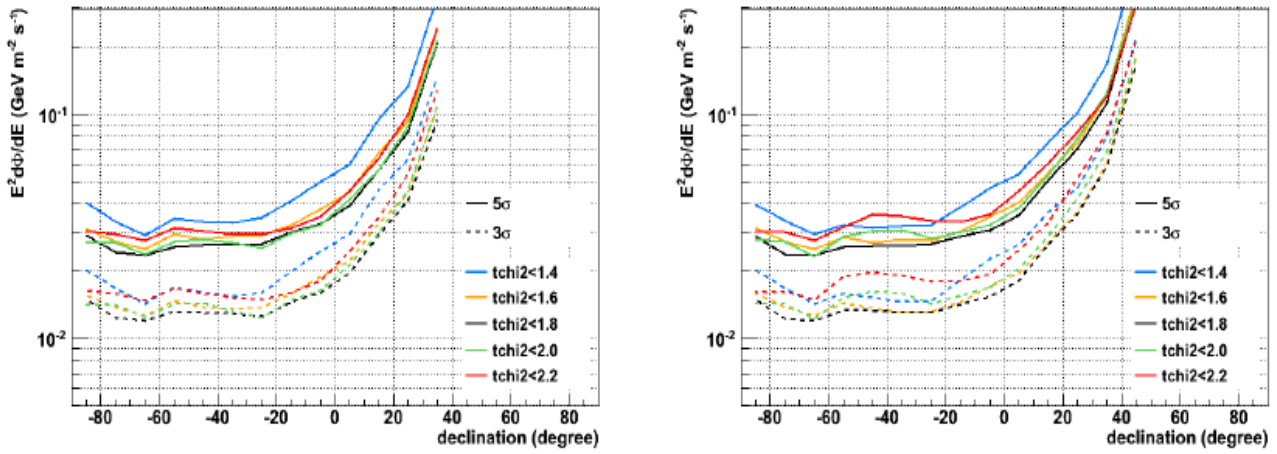

Figure 4.4 – Model discovery factor, for different values of χ^2 (labeled "tchi2" in the legend), for $b\chi^2 \geq 1.8$ and $\theta \leq 80°$ (left), $\theta \leq 90°$ (right). (Source [16])

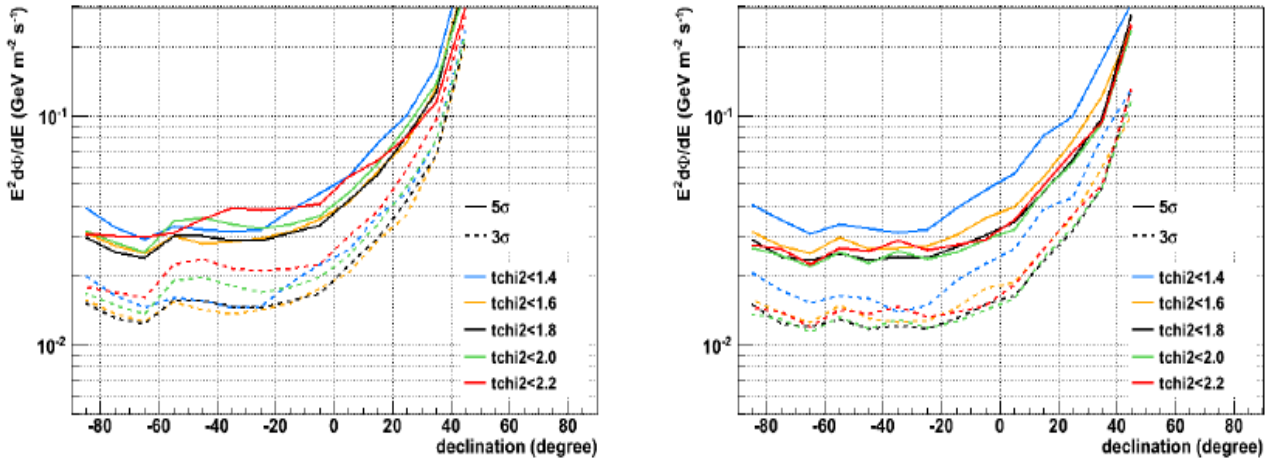

Figure 4.5 – Model discovery factor, for different values of χ^2 (labeled "tchi2" in the legend), for $\theta \leq 90°$ and $b\chi^2 \geq 1.0$ (left), then $b\chi^2 \geq 2.6$ (right). (Source [16])

At this stage the following cuts $\theta \leq 90°$, $\chi^2 \leq 1.8$ and $b\chi^2 \geq 2.2$ yield one of the best discovery potentials for a large declination band. However, applying these cuts implies a relatively high contamination of atmospheric muons close to the horizon, i.e. $80° < \theta \leq 90°$. To reduce this contamination it has been decided to apply a tighter χ^2 cut in this specific nadir θ range. Thus, the final chosen cuts are:

cut 2: $b\chi^2 \geq 2.2$. This cut is illustrated in Figure 4.6. This rejects events from large electromagnetic showers likely to appear in downgoing muon bundles.

cut 3: Further cuts are applied on the track depending on the arrival direction of the candidate: $\chi^2 \leq 1.8$ when $\theta \leq 80°$ and $\chi^2 \leq 1.4$ when $80° \leq \theta \leq 90°$. Figure 4.7 illustrates the discrimination power of these cuts for both nadir ranges.

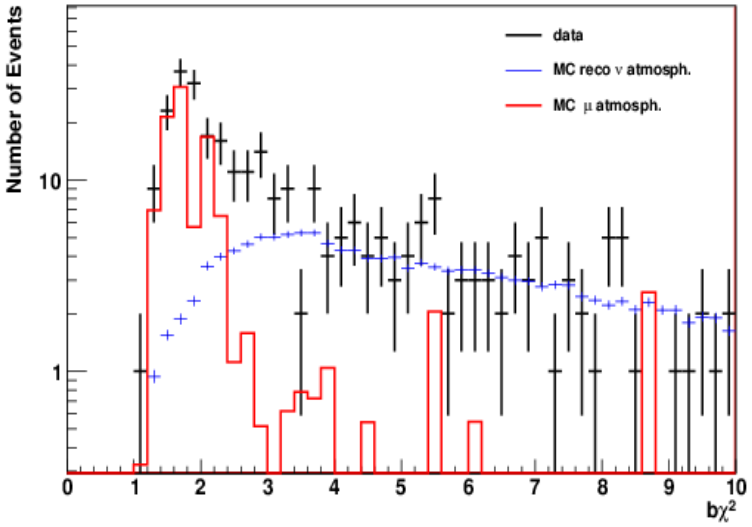

Figure 4.6 – Bright point fit distributions for up-going events for data and MC where **cut 3** has been applied. Since a bright point is a point-like light source which emits a isotropic light flash at a given moment, events with a very good bright-points fit are not retained as they are not compatible with a muon track. This is more likely to happen with mis reconstructed atmospheric muons.

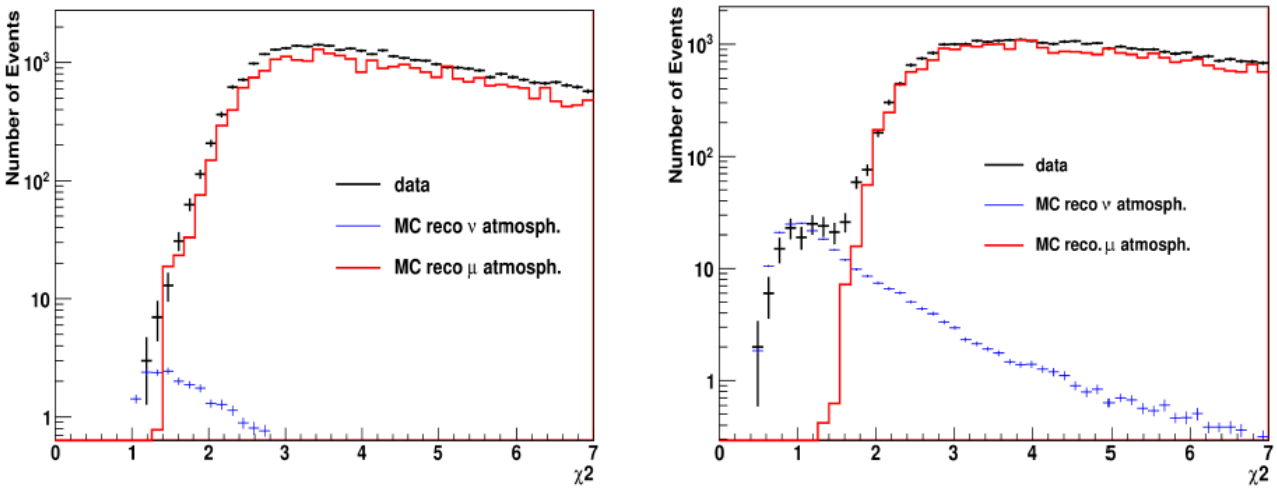

Figure 4.7 – Quality distributions of the track fit for up-going events for data and MC in the range of $\theta \leq 80°$ (right) and in the range $80° \leq \theta \leq 90°$ (left). The cut on $b\chi^2 \geq 2.2$ is applied in both cases.

In this section we have described a set of cuts derived from MC sample to discriminate between the true neutrino signal and the background of atmospheric muons. We have shown that using two quality fit values χ^2 $\leq$1.8 when θ $\leq$80°, and χ^2 $\leq$ 1.4 when 80° $\leq$ θ $\leq$90° allows to cut out most misreconstructed upward going muons. The percentage of remaining atmospheric muons (or contamination) in the final data sample is estimated to be roughly less than 20%.

Figures 4.8 shows the distributions of the nadir angle and the sine of the declination for the events selected with the final cuts, which are globally consistent with the MC expectations.

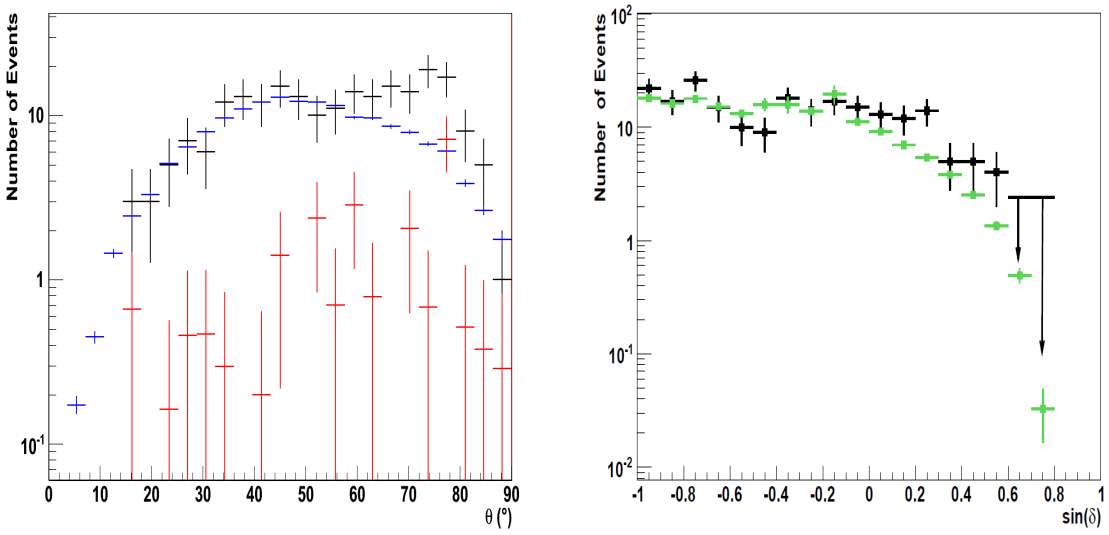

Figure 4.8 – Left: θ distributions for data and MC samples (blue: atmospheric neutrinos, red: atmospheric muons). Right: distributions of the sine of the declination for data (black) and MC (green: total atmospheric background). All cuts are applied.

The corresponding effective surface, as defined by Equation (4.1) is shown on Figure 4.9 as a function of the neutrino energy. To characterize further the potential physics yield of the selected sample, we define the sensitivity as the median 90% upper limit obtained over an ensemble of simulated experiments with zero-signal assumption. The sensitivity of the HEN search has been quantified for the whole 5 line data period. It depends on the declination of the potential source. Figure 4.10 shows the sensitivity for the search using the selection criteria described above and assuming an E^{-2} spectrum. From the curve it's shown that the best sensitivity is estimated to be $E^2 \frac{dN}{dE} \approx 10^{-6}$ GeV cm^{-2} s^{-1}.

In the next section, we discuss into details the angular accuracy that can be expected applying the present cuts. This angular accuracy not only depends on the reconstruction parameters, but also on the energy of the selected events. We discussed in chapter 1 that

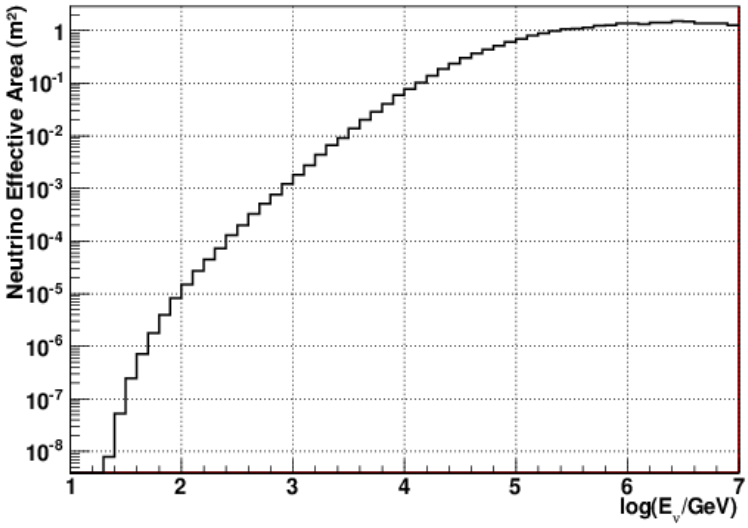

Figure 4.9 – The effective area for neutrinos as a function of the neutrino energy. The sensitivity of the detector for up-going neutrinos increases with energy due to the rise of neutrino cross-section. Above an energy of 1 PeV the sensitivity saturates at about 1 m^2 as the increasing neutrino cross-section and the Earth absorption cancel out.

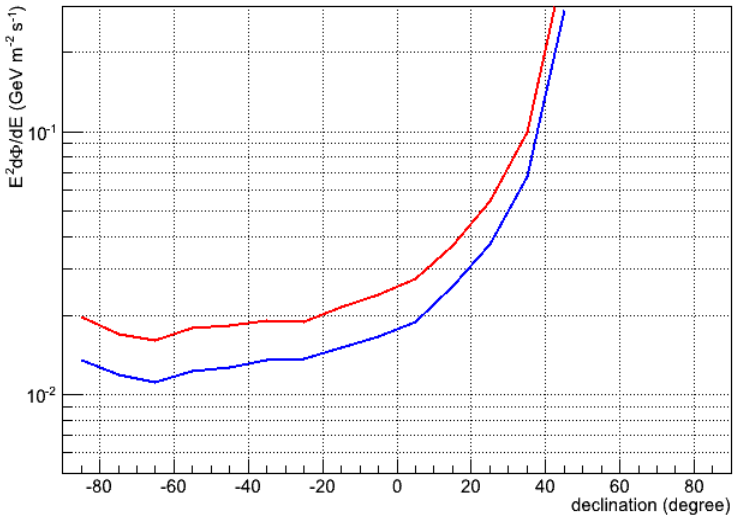

Figure 4.10 – Sensitivity, after applying all the above described cuts, for the whole 5Line period (blue) and for the GW+HEN joint time of observation (red).

the energy of the high energy neutrino, when correctly reconstructed, can indeed be a good indicator of whether the candidate is of cosmic or atmospheric origin. This is illustrated with the present sample in Figure 4.11.

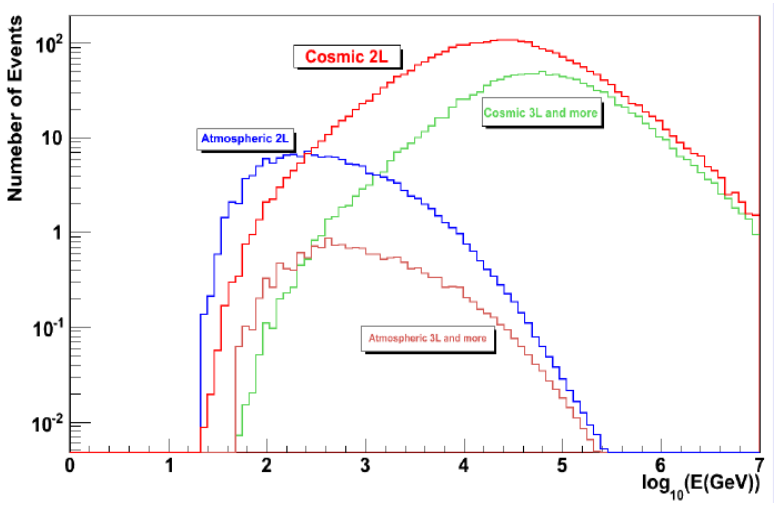

Figure 4.11 – Distributions of energy for atmospheric and cosmic (according to an $E-2$ spectrum) neutrinos. The 2L and 3L+ case are presented separately.

The approach used in this analysis is to use the number of hits as an energy estimator of the candidate. Figure 4.12 shows that the number of hits and the MC energy of the neutrino candidate are correlated. On basis of event-by-event selection, we shall associate to each event in the final list an energy (in term of number of hits) in addition to the basic characteristics discussed in section 4.4.2. For illustration purposes the distributions of the number of hits used by the reconstruction for both MC and data, after applying all cuts, are shown in Figure 4.13.

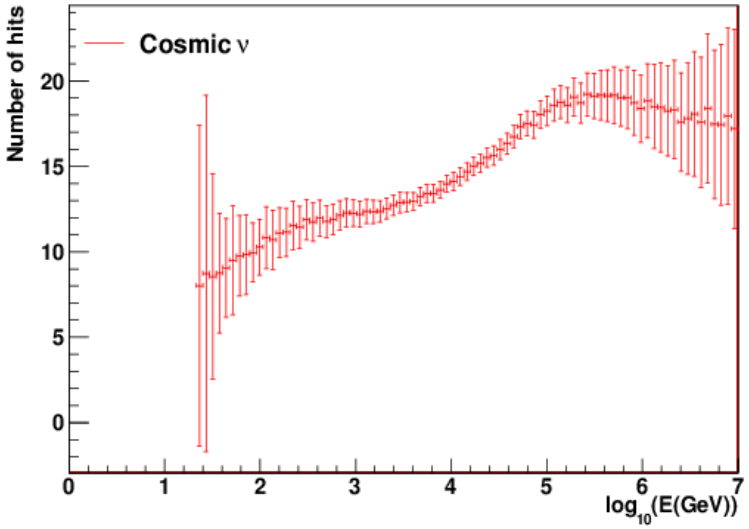

Figure 4.12 – Number of hits versus neutrino energy for cosmic (E^{-2}) neutrinos.

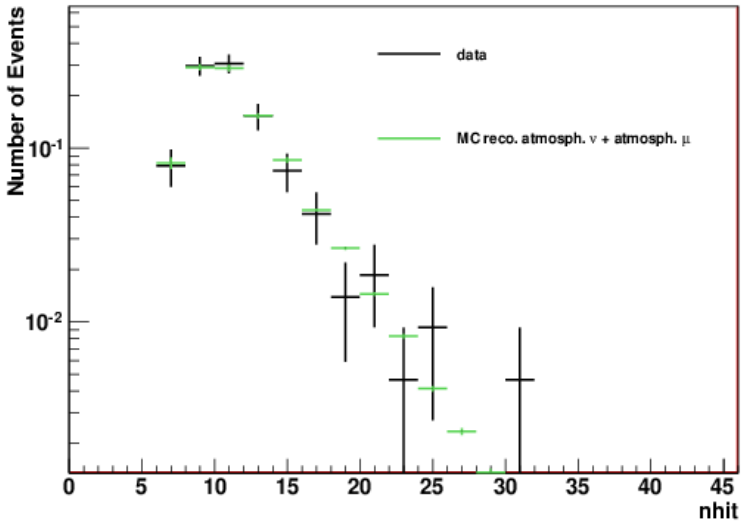

Figure 4.13 – Number of hits used in the fit for up-going events after applying the cuts described in the text.

4.4 High energy neutrino horizon

In this section we estimate the horizon d_ν of the ANTARES neutrino telescope given the cuts presented above and assuming certain models of sources, namely long-GRBs (LGRB) and short-GRBs (SGRB). These models are presented in section 1.9 and the associated neutrino fluxes are plotted in Figure 4.14. The detectability of each kind of source also depends on its distance to the observer.

Let $N_\nu(\theta, \phi, d_\nu)$ be the expected number of detected neutrino events from a source located at a distance d_ν and with local coordinates (θ, ϕ):

$$N_\nu(\theta, \phi, d_\nu) = \left(\frac{d_s}{d_\nu(\theta, \phi)}\right)^2 T \int_{E_\nu^{min}}^{E_\nu^{Max}} A_\nu^{eff}(E_\nu, \theta, \phi) \times \frac{d\Phi(E_\nu, \theta, \phi)}{dE_\nu} dE_\nu, \tag{4.3}$$

where $A_\nu^{eff}(E_\nu, \theta, \phi)$ is the neutrino effective area of the detector, $(\Phi_\nu(E_\nu, \theta, \phi)$ the reference theoretical flux at Earth for a source located at a distance d_s, and T is the average duration of a GRB in the considered model. Note that we have omitted here the redshift energy loss of neutrinos, which is negligible for sources at $z < 1$. Rearranging the Equation (4.3) gives:

$$d_\nu(\theta, \phi, N_\nu) = d_s . \sqrt{\frac{\int_{E_\nu^{min}}^{E_\nu^{Max}} A_\nu^{eff}(E_\nu, \theta, \phi) . \frac{d\Phi(E_\nu, \theta, \phi)}{dE_\nu} . dE_\nu}{N_\nu}} \tag{4.4}$$

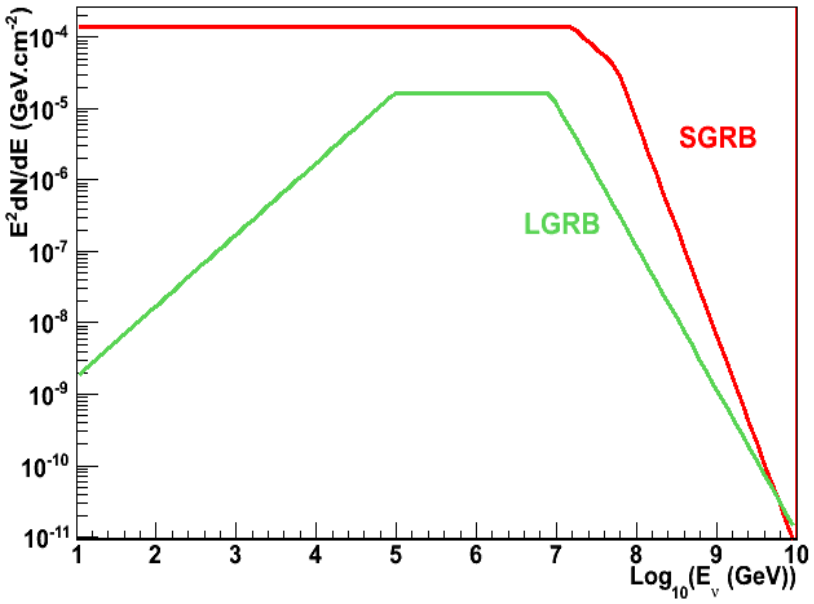

Figure 4.14 – Flux spectrum of LGRB (z=2) and SHRB (z=1) used in this thesis.

We then define $d_\nu^{50\%}$ as the distance at which the probability to observe at least one event from the considered source is 50%:

$$P(\geq 1|N_\nu) = 1 - P(0|N_\nu) = 50\% \tag{4.5}$$

where N_ν is the number of expected events as given by Equation (4.3) and $P(0|N_\nu)$ follows the Poisson statistics:

$$P(n|N_\nu) = \frac{(N_\nu)^n \exp(N_\nu)}{n!} \quad ; n > 0 \tag{4.6}$$

The 50% probability corresponds to the value $N_\nu = 0.7$.

Our approach allows the calculation of the HEN horizon on a event-by-event basis. For this we use the effective area $A_\nu^{eff}(E_\nu, \theta, \phi)$ calculated in bins of (θ, ϕ) and of in bins of energy (ranging between $[10, 10^7]$GeV). We finally compute numerically $d_\nu^{50\%}$ given d_s, using Equation (4.4) and $N_\nu = 0.7$.

For both cases (LGRB and SGRB), we assume d_s= 21 Mpc (equivalent to z = 0.005). We find in average $d_\nu^{50\%}$=12.4 Mpc for the former and $d_\nu^{50\%}$= 4.3 Mpc for the latter. The full distributions of $d_\nu^{50\%}$ for the selected sample of neutrinos are shown in Figure 4.15.

Alternatively, we show on Figure 4.16 the probability to observe one event at least, as a

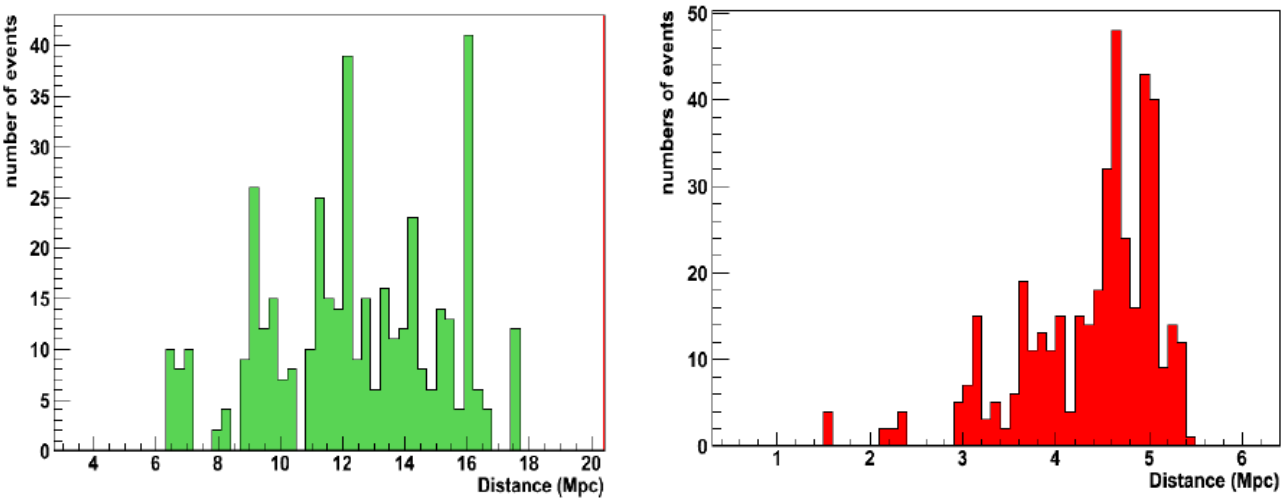

Figure 4.15 – Neutrino horizon calculated for selected sample according to the cuts described in section 4.3.2. On the left is result for long-GRB and on the right for short-GRB.

function of the source distance. This stands for standard LGRB and SGRB. The probability is averaged over all possible locations on the sky.

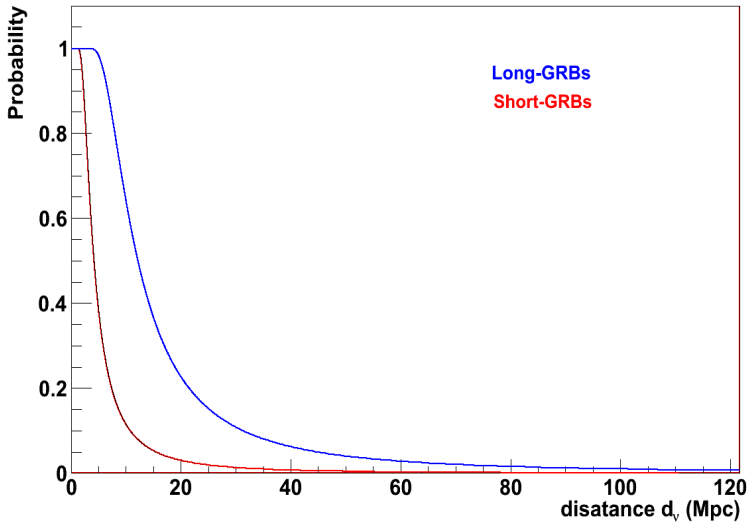

Figure 4.16 – Probability to detect a source as a function of its distance, for LGRB (blue curve) and SGRB (red curve).

4.4.1 Angular resolution and angular search window

The angular resolution is related to the error on the reconstructed track direction. It is defined as the median of the distribution of the space angle ψ between the true neutrino direction and

the reconstructed track and is obtained from MC sample obtained with the cuts defined in the previous section and weighted according to an E^{-2} flux. In the case of events reconstructed with 2 lines, we determine the angular difference of both mirror tracks with respect to the true MC direction. The minimum of those two values, which corresponds to the best track (as defined in section 2.6.1) is used to determine the angular resolution. This method allows to significantly improve the angular resolution as illustrated in Figure 4.17 and sketched in Figure 4.18.

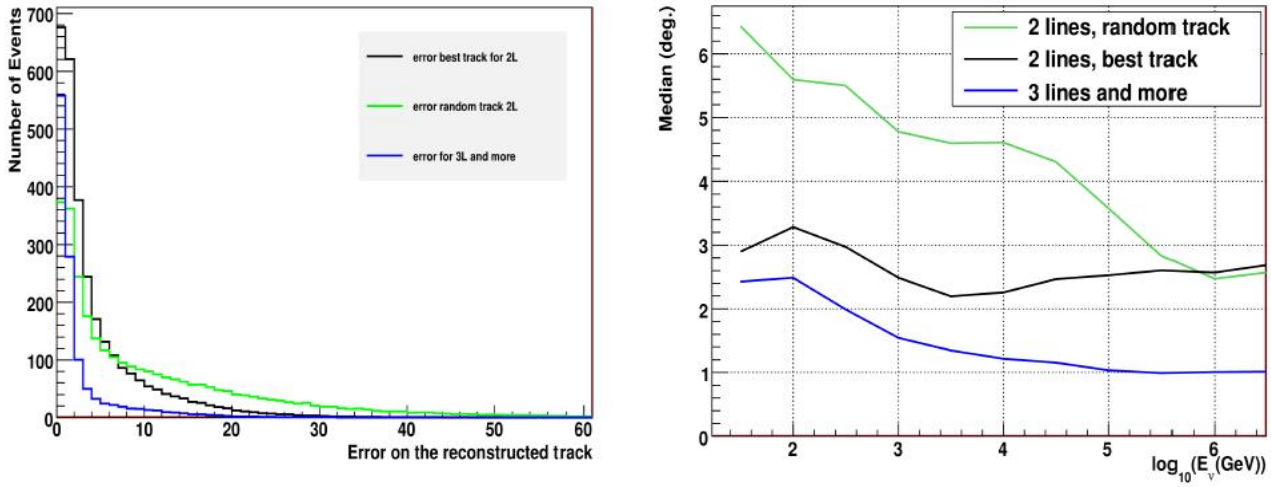

Figure 4.17 – Left: distribution of angular error between the neutrino direction and the reconstructed track for an E^{-2} flux. At low energies the error is dominated by the kinematics of neutrino interactions (see section 2.2.2). The median of this distribution is shown on the right plot as function of the neutrino energy (right). Both plots show the values obtained for the best and random tracks in the case of events reconstructed with 2 lines.

The uncertainty on the neutrino arrival direction has to be accounted for in the GW coherent analysis. This is done by defining, on an event-by-event basis, an angular search window (ASW) and the associated ψ distribution. This distribution is needed by the X-pipeline to compute the significance of an hypothetical signal for the scanned directions inside the ASW. The radius of this window is defined as the 90% (ASW90%) quantile of the ψ distribution. The following method is used to calculate the ASW90%:

- We calculate the ψ distribution for the selected MC sample in bins of declination and number of hits. We create 18 bins in declination range with steps of 10 degrees and, for each bin of declination, we create 16 bins in number of hits with step of 1 hit.

- For each distribution error we compute the 90% quantile of the distribution. The corresponding value is the ASW90%.

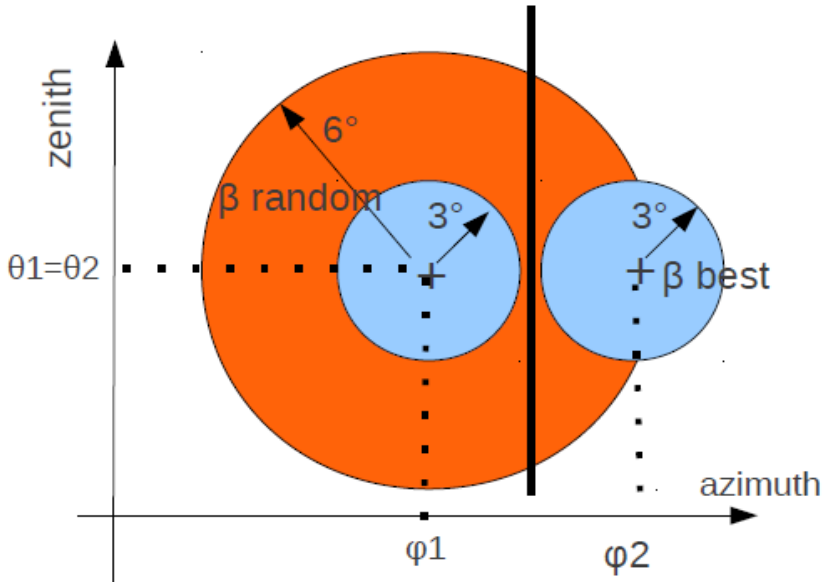

Figure 4.18 – Example (arbitrary values) of the projected angular resolution in local coordinates as obtained for the best (blue) and random (orange) track. The black line illustrates the plane containing the 2 detector lines used for reconstruction.

- We fit the ψ distribution by a log-normal function given by Eq. 4.7:

$$\mathcal{F}(x) = \frac{1}{\sqrt{2}} \frac{e^{-((\ln((x-\theta)/m))^2/2\sigma^2}}{(x-\theta)\sigma} \tag{4.7}$$

  with $x \geq \theta$ and $\sigma \geq 0$. θ is the location parameters, σ is related to the shape of the distribution and m is a scaling parameter.

  In Figure 4.19 is shown an example of the ψ distribution fitted by log-normal distribution for a given bin of declination.

  The fit is carried out until the 90% quantiles which is the limit radius used for GW searches. The output fit parameters are added to the HEN candidates list (see section 4.4.2).

In the 2L case, the best track distribution is used to determine the ASW90%. This allows for a substantial reduction of the solid angle to be scanned by the GW search algorithm, as can be deduced from the sketch of Figure 4.18. This can be further quantified by computing the ratio R as defined by:

$$R = \frac{\Omega_{best}}{\Omega_{random}} \tag{4.8}$$

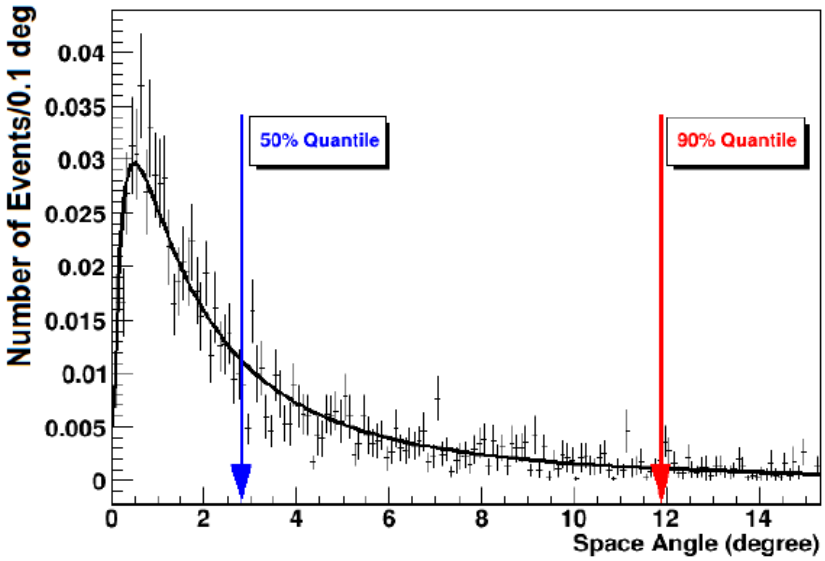

Figure 4.19 – Error distribution on the HEN arrival direction for a bin of declination between -30° and -20° and number of hits=9 together with the fitted log-normal. The arrows indicate the 50^{th} (median) and the 90^{th} (ASW90%) of the distribution.

where

$$\Omega_{best} = 2 \times 2\pi(1 - \cos(ASW90_{best})) \tag{4.9}$$

And

$$\Omega_{random} = 2\pi(1 - \cos(ASW90_{random})) \tag{4.10}$$

are the solid angles associated to the $ASW90_{best}$ and $ASW90_{random}$ respectively. The ratio between the $ASW90_{best}$ and $ASW90_{random}$ is plotted in Figure 4.20. We see from the curve that the size of the best angular search window $ASW90_{best}$ is in average 44.6% of the size of the random one, which justifies our approach.

The ASW50% (median) and ASW90% are plotted in the Figure 4.21. This Figure shows the improvement on the ASW90% derived from the approach described above. A single circular region of radius ASW90%=30 degrees encompasses the two mirror tracks, while the individual mirror tracks are contained in a circular region of radius ASW90%=12.5 degrees. The solid angle to be analyzed is 0.84 sr in the first case while it is $2 \times 0.15 = 0.30$ in the second case. The distinction of the two mirror tracks allows us to reduce the search window by a factor of almost 3. We show also the Point Spread Function (PSF) in Figure 4.22.

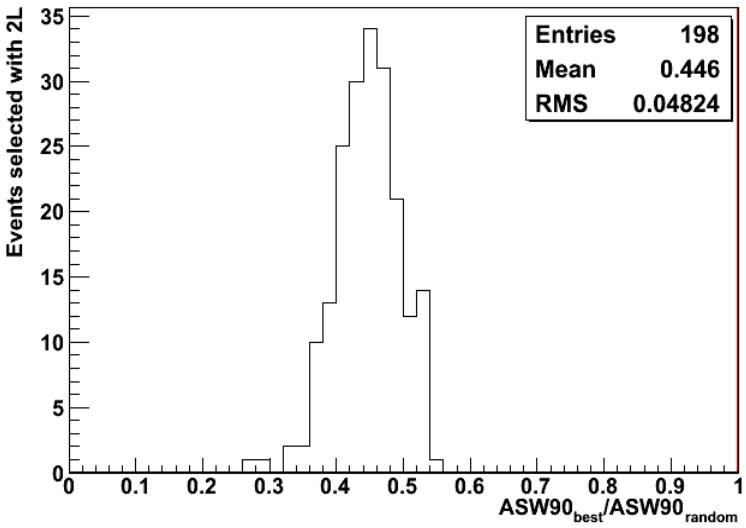

Figure 4.20 – Ratio between $ASW90_{best}$ and $ASW90_{random}$, ignoring any overlap between the search windows associated to each mirror solutions.

4.4.2 List of neutrino candidates

After applying the set of cuts described in the previous sections to the 181 runs corresponding to 104 days equivalent live time to the present analysis period, 414 neutrino candidates remain, which are listed in [17]. In this sample we have separated events reconstructed with exactly 2 lines from those reconstructed with at least 3 lines. This strategy is imposed to take into account the mirror track for events reconstructed with exactly 2 lines. The main informations

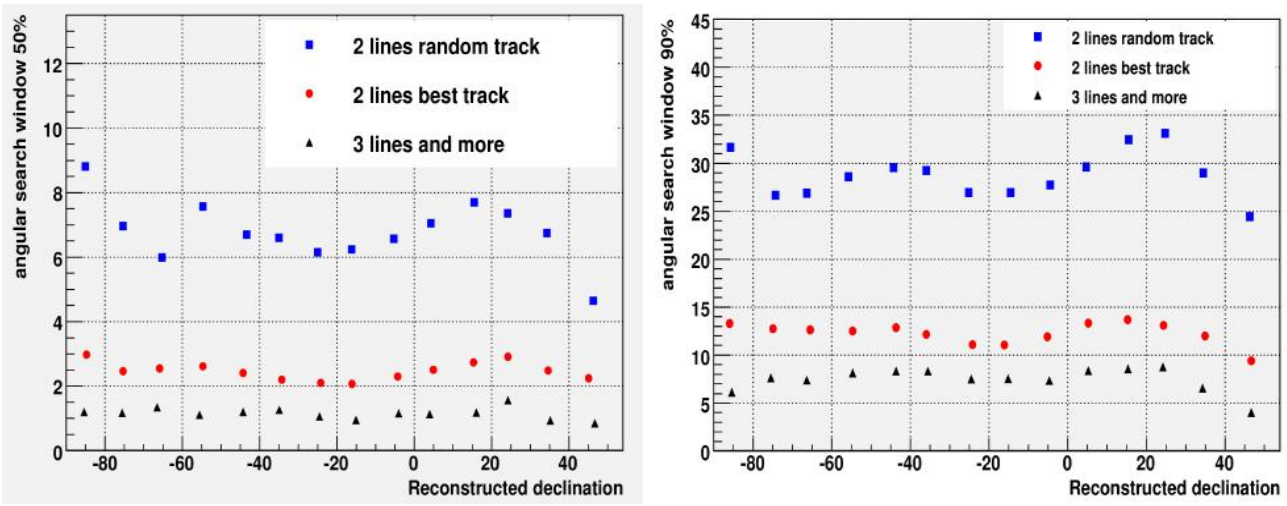

Figure 4.21 – ASW50% (left) and ASW90% (right) as function of declination

in the event list correspond to:

- The neutrino arrival time in Julian Day specified for epoch J2000, which is used also for the computation of the celestial coordinates (right ascension and declination). It is the sum of the UTC event time, computed from the start time of the run, and the product of the frame duration and the frame index;
- The equatorial coordinates (α, δ) of each candidate (computed using ConvertCoordinates libraries from the ANTARES local coordinates (θ, ϕ));
- The number of lines and the number of hits used in the fit of the track;
- The angular search windows for both 50% and 90% quantiles;
- The log-normal fit parameters obtained by fitting the angular error distribution in bins of event declination and number of hits, as explained in section 4.4.1.

The equatorial coordinates (α, δ) and the galactic coordinates of the selected candidates are shown in Figures 4.24 and 4.25 respectively. Due to the geographical location of the detector, the part of the sky with declination greater than 48° is always above the horizon and is thus never observed by the ANTARES telescope. In contrast, the part of the celestial sphere with declination below -48°, is always visible. The region in between is visible during some fraction of the day. This visibility factor convoluted to the intrinsic acceptance of the detector is shown in galactic coordinates in the Figure 4.26.

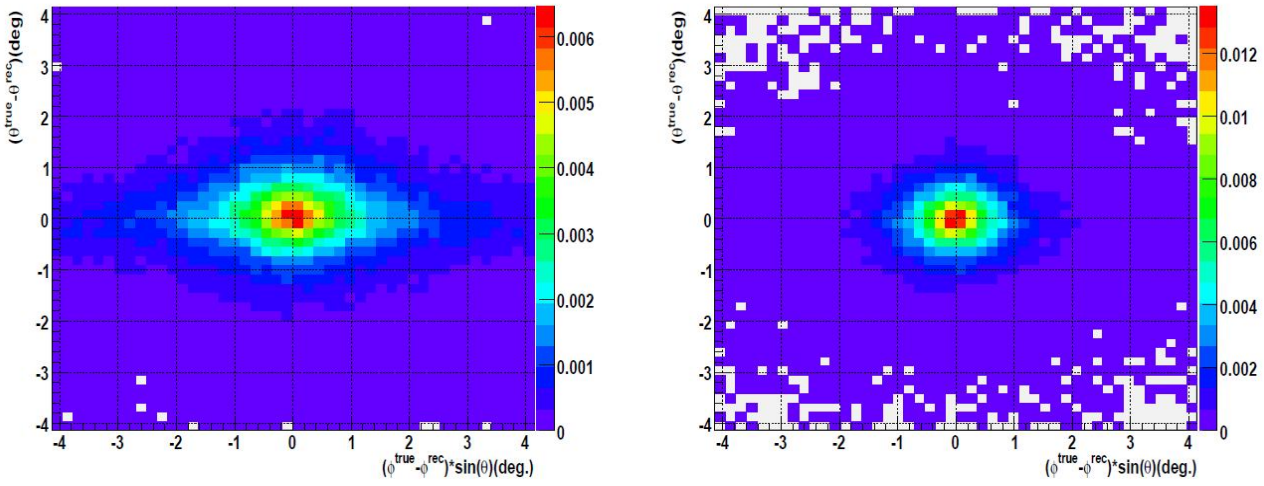

Figure 4.22 – PSF of the ANTARES neutrino telescope, on the left for event selected with 2L (best track) and, on the right for events selected with 3L+.

Of the HEN candidate events, 158 occurred at times when at least two gravitational-wave detectors were operating. Since two or more detectors are required to discriminate GW signals from background noise (as described in section 4.5), in the following we consider only these remaining 158 HEN candidates: 144 2-line events and 14 3-line events. We show in Figure 4.23 the distribution of the ASW90% of these events.

4.5 Coincidence with gravitational waves

4.5.1 Gravitational wave event analysis

Once the list of HEN candidates has been established, they can be fed as external triggers into the X-pipeline to search for GW signals in coincidence with them. The GW dataset used is described in section 4.2. We now concentrate on the preprocessing of the GW dataset using a *coherent triggered* method. The triggered search requires several components provided by the neutrino candidate event, especially time and directional informations. This adopted procedure follows the one used in [18] where the GRB triggers are replaced by neutrino candidates. All the detectors operating at the time of the trigger and passing the data-quality requirements are used in the analysis.

As described in section 4.2 the dataset can be split into two parts: *on-source* and *off-source* data. The former serve to generate GW triggers in coincidence with the neutrino candidates,

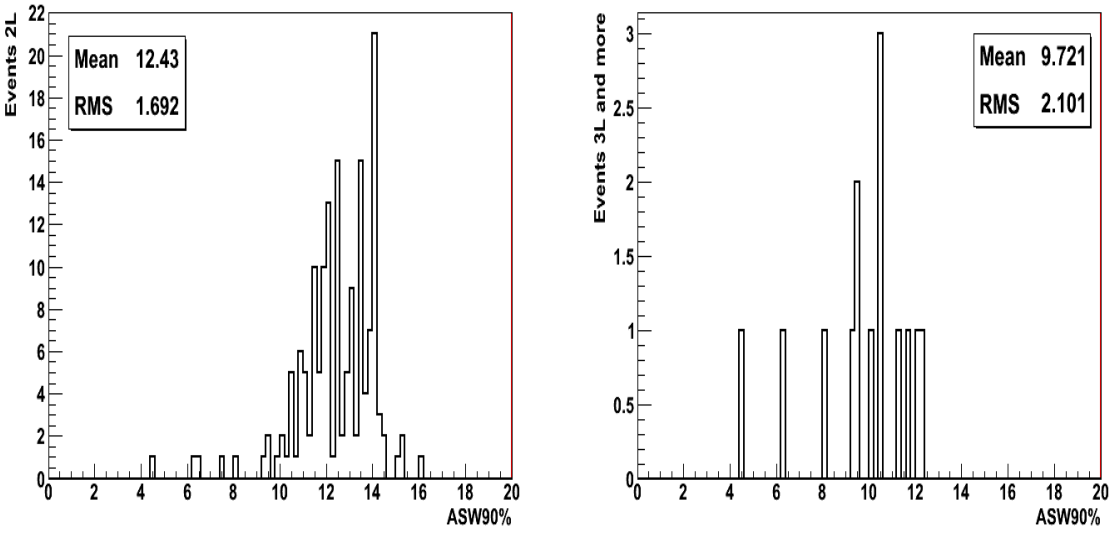

Figure 4.23 – ASW90% of the remaining 158 neutrino candidates. Left: events reconstructed with 2 lines. Right: events reconstructed with at least 3 lines.

while the latter are used to optimize the search parameters, to measure the expected false alarm rate and to standardize statistics derived from the on-source window. The on-source data consists of a segment from each interferometer data. The data segments are time-delayed according to the sky location being analysed so that a GW signal from that direction would appear simultaneous in each data stream.

In the context of the joint GW+HEN searches, the source emits a collimated jet pointing to Earth. This gives a quite strong indication about the source core dynamics and its orientation. In particular, it is natural to associate this direction to the source angular momentum. This motivates the assumption of a circular polarization of the incoming gravitational wave to separate the signals from noise. While some of the considered source models do not predict a circularly polarized GW, we expect the loss in sensitivity in that case to be relatively small. In addition to the marginalized circular polarization sum, other combinations of the data are constructed. Of particular importance are the"null" combinations designed to cancel out the GW signal from the given sky location; comparison to corresponding incoherent combinations provides powerful tests for identifying events due to background noise fluctuations glitches, as described in [19]. For each combination, the event cluster is assigned a combined energy as the sum of the energy values of its constituent pixels. This defines a first ranking statistics for the events. In addition, GW events are characterized by their duration, central time, bandwidth, and central frequency. Also, a second ranking statistic is computed based on a

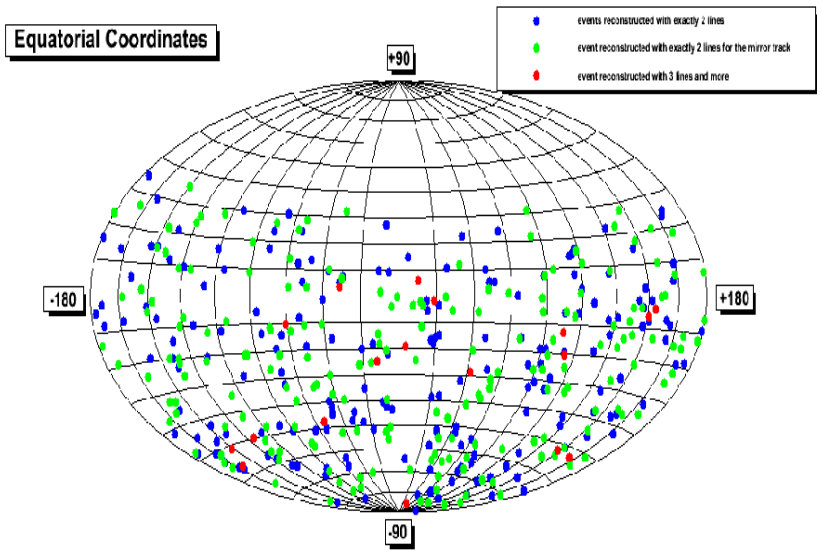

Figure 4.24 – Sky-map showing the reconstructed declination and right ascension of all the selected events. The blue and green dots correspond to the two possible directions of events reconstructed with exactly 2 lines. The red dots represent the coordinates of the events reconstructed with 3 lines and more.

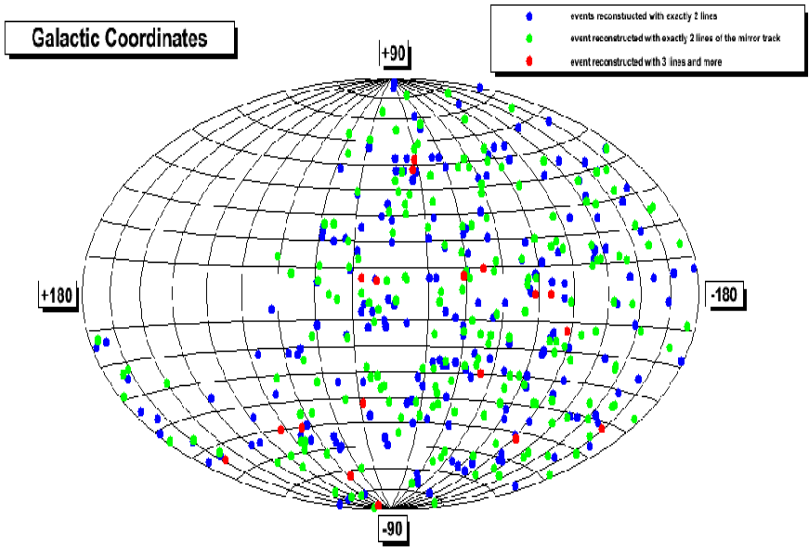

Figure 4.25 – Sky-map showing the selected events in galactic coordinates: The blue and green dots correspond to the two possible directions of events reconstructed with exactly 2 lines. The red dots represent the coordinates of the events reconstructed with 3 lines and more.

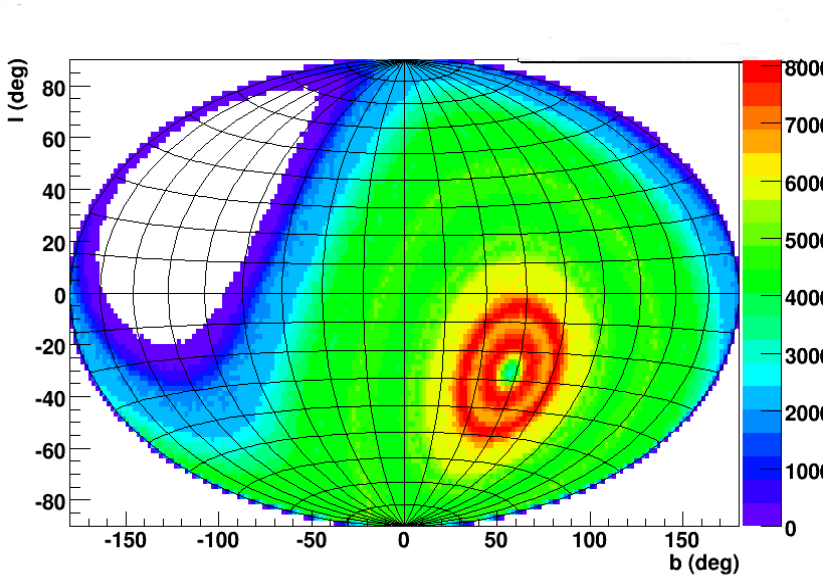

Figure 4.26 – Acceptance of the ANTARES detector in galactic coordinates, taking into account the visibility factor due to the rotational Earth motion. This quantity is the number of detected events for a given (arbitrary) flux. Only the relative values are relevant.

maximum-likelihood analysis of the event assuming a power-law distributed background noise with no assumption on the GW polarization. In practice this statistic is often found to provide signal-noise separation due to the non-Gaussian nature of the GW detector noise.

The time-frequency (TF) analysis (see section 3.7.1) is repeated for Fourier transform lengths of 1/128, 1/64, 1/32, 1/16, 1/8, 1/4 s, to maximize the sensitivity to GW signals of different durations. It is also repeated over a discrete grid of sky positions covering most of the source sky location probability distribution. A simple regular grid is used here, composed of concentric circles around the best estimate of the neutrino sky location, which covers 90% of the sky location probability distribution (see Figure 4.27). This grid is designed such that the maximum relative timing error between any pair of GW detectors is less that 0.5 ms. Finally, the events are decimated to a rate of 0.25 Hz before being written to disk.

GW triggers are produced independently for each sky position grid point. The detection statistic, written as a log-likelihood ratio between a signal and a background model, is penalized by the probability $\mathcal{F}(\overrightarrow{d})$ of the trial sky location being the true one, by adding the logarithm of that probability to the detection statistic. The reconstructed source sky position for a given signal is the sky position for which the trigger has the largest penalized detection statistic. Only that maximal trigger is kept by the analysis of the grid of sky positions.

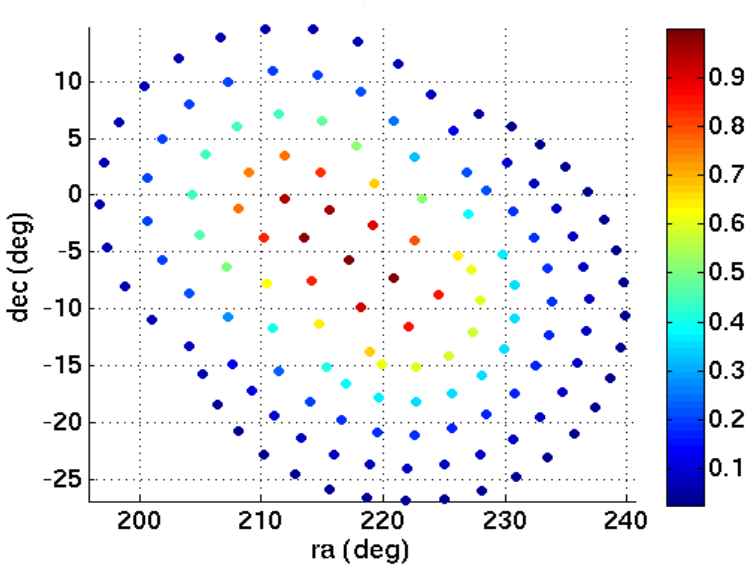

Figure 4.27 – The estimated neutrino locations and their uncertainties may give rise to overlapping regions on the sky. Searching for one point and its mirror image at once. The color bar shows the probability distribution. (Source [20])

The *off-source* window is defined as all data within ± 1.5 hours of the neutrino time, excluding the *on-source* interval. The statistical features in the off-source window are similar to the ones in the on-source window. In order to enlarge the background sample, we also repeat the off-source analysis after applying time shifts of multiples of 6 s to the data from one or more detectors. With such time slides, we were able to produce $O(10^3)$ background trials for

each HEN.

To assess the sensitivity of this joint search, the analysis is repeated with injections of simulated GW signals to the on-source data. The amplitudes and morphologies tested are discussed in section 4.6.2.

4.5.2 GW search optimization

As we stated in section 3.7.2, the sensitivity of searches for gravitational-wave bursts is limited by noise (gliches included). The trigger rejection operates in two steps, namely a data preselection followed by a glitch removal procedure. To reduce this background, events that overlap in time within known instrumental and/or environmental disturbances are vetoed. In addition to this, GW consistency tests comparing the coherent and incoherent energies are applied to each event [19]. These tests are applied to the on-source, off-source and injection events. The events failing one or more of these tests are discarded.

The thresholds are optimized by testing a preset range of thresholds and selecting those which give the best overall detection efficiency at a fixed false alarm probability of 1% when applied to a random sample of background and injection events (the on-source events are *not* used; i.e., this is a blind analysis). These tests also determine which of the two ranking statistics discussed in section 4.5 (based on circularly polarized GW energy or power law noise) gives the better detection efficiency. The winner is selected as the final ranking statistic.

Once the thresholds have been fixed, these consistency tests are applied to the on-source events and to the remaining off-source and injection events (those not used for tuning). The surviving on-source event with the largest significance (highest energy or power law statistic) is taken to be the best candidate for a gravitational wave signal and is referred to as the loudest event [21]. All surviving on-source events are assigned a false alarm probability by comparison to the distribution of loudest events from the off-source trials. Any on-source event with probability $p < 0.01$ is subjected to additional checks to try to determine the origin of the event and additional background time slide trials are performed to improve the accuracy of the false alarm probability estimate. After the p values have been determined for the loudest events associated with each of the 158 HEN events, the collective set of p values is tested for consistency with the null hypothesis (no GW signal) using the binomial test, discussed in section 4.5.4. We also set a frequentist upper limit on the strength of gravitational waves associated with each neutrino trigger, as discussed in section 4.6.2.

4.5.3 Low-frequency and high-frequency GW analyses

The analysis procedure described in the previous section has been implemented in the X-Pipeline. Given our knowledge of possible GW sources discussed in chapter 1, the most likely detectable signals at extra-galactic distances are in the low-frequency band (LF, $f \lesssim$ 500 Hz), where the detectors have maximum sensitivity (see Figure 3.5). At the same time, the computational cost of the X-Pipeline analysis increases at high frequencies. This is due in part to the extra data to be analyzed, but also to the need for finer-resolution sky grids to keep time delay errors much smaller than one GW period. We therefore split the gravitational wave band into two regions: 60-500 Hz and 500-2000 Hz.

The low-frequency band is analyzed for all HEN events. Such a search is computationally feasible while covering the highest-sensitivity region of the GW detectors. However, compact objects such as neutron stars or collapsar cores have characteristic frequencies for GW emission above 500 Hz. Such emissions might be detectable from galactic sources such as soft gamma repeater giant flares, or possibly from nearby galaxies. Since the computational cost in the high-frequency range for all HEN events is prohibitive with the current analysis pipeline, we perform the 500-2000 Hz (high frequency HL) analysis on the 3L+ HEN events only. The 3L+ events are a small subset ($\sim$ 10%) of the total trigger list and have the smallest sky position uncertainties, and therefore the smallest computational cost for processing. To further reduce this cost, we use the same sky grid for the high-frequency search as was used at low frequencies, after determining that the loss of sensitivity is acceptable. The HF analysis is performed independently of the low-frequency analysis (e.g. independent tuning, background estimation) using the identical automated procedure.

4.5.4 Binomial test

A quantitative analysis of the significance of any gravitational-wave event must take into account the trial factor due to the number of neutrino events analyzed. We use the *binomial test* [22], as the statistical method to look for a GW signature associated with individual neutrino candidates. Under the null hypothesis, the false alarm probabilities (FAPs) p for each HEN loudest event are expected to be uniformly distributed between 0 and 1. The binomial test compares the measured p values (in the on-source window) to the null distribution to determine if there is an excess which may have been due to the cumulative effect of weak GW signals.

The binomial test considers a number of events, N_{tail}, among the total number of events in the sample, N, that have to be tested and sorts their probabilities $p_{i\in[1,N_{\text{tail}}]}$ in increasing order (i.e. decreasing significance): $p_1 \leq p_2 \leq p_3 \leq ... \leq p_N$. For each of these probabilities, p_i, we

compute the cumulative binomial probability $P_{\geq i}(p_i)$ for getting i or more events at least as significant as p_i:

$$\begin{aligned} P_{\geq i}(p_i) &= \sum_{j=i}^{N} P_j(p_i) \\ &= 1 - \sum_{j=0}^{i-1} P_j(p_i) \end{aligned} \tag{4.11}$$

where $P_j(p_i)$ denotes the probability for getting j successes in N trials:

$$P_j(p_i) = \frac{N!}{(N-j)!j!} p_i^j (1-p_i)^{N-j} \,. \tag{4.12}$$

and N is the number of neutrino candidates analyzed. The lowest $P_{\geq i}(p_i)$ for $i \in [1, N_{\rm tail}]$ will point to the most significant deviation from the null hypothesis. To assess the significance of the deviation, we repeat the test using p values drawn from a uniform distribution and count the fraction of such trials which give a lowest $P_{\geq i}(p_i)$ smaller than that computed from the true measured p values.

4.6 GW+HEN joint search results

4.6.1 Individual GW searches

After applying several quality criteria to both the GW and the HEN data a list of neutrino candidates was retained for further search of possible concomitant GW signals. Out of this list, 158 neutrinos (reconstructed with 2L) have been analyzed in the low frequency (LF) range, and 14 (reconstructed with a least 3L) have been analyzed in both the LF and the high frequency (HF) range. We choose $N_{\rm tail}$ to be 5% of N; i.e., $N_{\rm tail} = 8$ for the low frequency band and $N_{\rm tail} = 1$ for the high frequency band.

The smallest FAP was found to be ($p = 0.01$), in the LF range. The corresponding neutrino trigger was localized on the sky by ANTARES telescope in direction (α, δ)=(204.4, -13.03) on Wed Sep 12, 2007. Additional time shifts totaling 18064 background trials yielded a refined FAP of $p = 0.004$, which is not significant given a trial factor of 158. This event came from the analysis of the H1, H2, and V1 data. Follow-up checks were performed, including checks of detector performance at the time indicated by monitoring programs and operator logs and

scans of data from detector and environmental monitoring equipment to look for anomalous behavior. While these checks did not uncover a physical cause for the event, they did reveal that it occurred during a glitching period in V1. We conclude that we have no clear gravitational wave burst signal associated with any of our sample of 158 neutrino events. The full analysis is therefore consistent with no GW events being present. Figures 4.28 and 4.29 show the cumulative distribution of p-values measured in the LF and HF analyses. In both cases the measured p-values are consistent with the null hypothesis. We also found no candidates in the HF band.

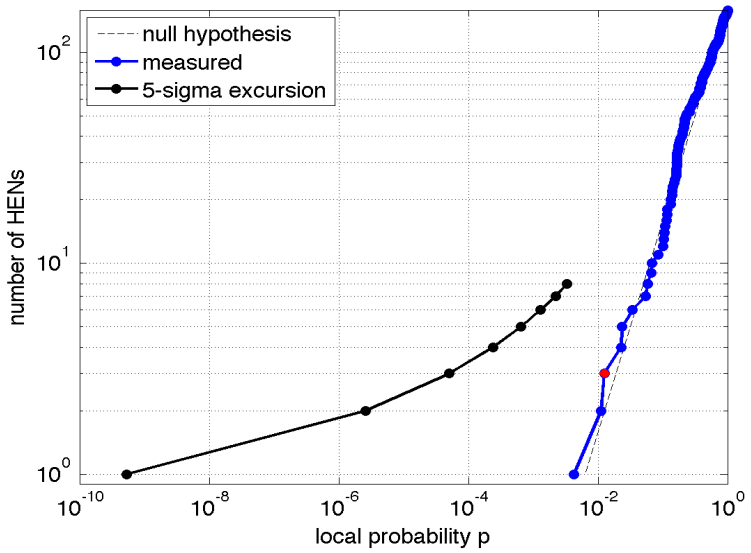

Figure 4.28 – Distribution of observed p values for the loudest GW event associated with each neutrino analysed in the low frequency analysis. The red dot indicates the largest deviation of the low p tail from the uniform distribution null hypothesis; this occurs due to having the three loudest events below $p_3 \sim 0.013$. Deviations this large or larger occur in approximately 64% of experiments under the null hypothesis. The black line shows the threshold for a 5-sigma deviation from the null hypothesis.

4.6.2 GW upper limits

The sensitivity of the GW search is determined by a Monte-Carlo study. For each neutrino trigger, we add simulated GW signals to the on-source data and repeat the analysis described in section 4.5. We consider that the simulated signal is detected if it produces an event louder than the loudest on-source event after all event tests have been applied. We define a 90% confidence level lower limit on the distance to the source as the maximum distance $D_{90\%}$ such that for any distance $D \leq D_{90\%}$ the probability of detection is 0.9 or greater.

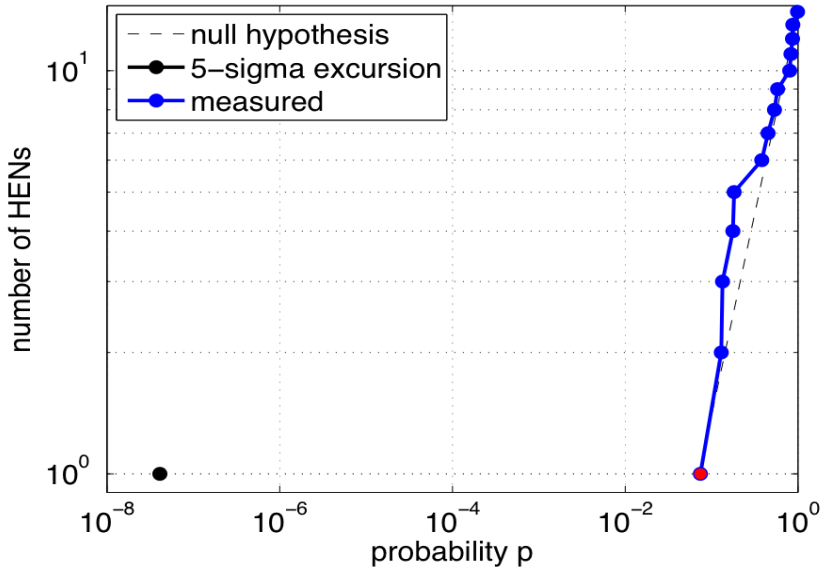

Figure 4.29 – Distribution of observed p values for the loudest GW event associated with each neutrino analysed in the high frequency analysis. The red dot indicates the largest deviation of the low p tail from the uniform distribution null hypothesis; since $N_{\rm tail} = 1$, this is constrained to occur for p_1. Deviations this large or larger occur in approximately 66% of experiments under the null hypothesis. The black dot shows the threshold for a 5-sigma deviation from the null hypothesis.

Injected waveforms: We added different burst-type signals to the raw data. The *ad hoc* waveforms are Gaussian-modulated sinusoids already introduced in section 3.7.3:

$$h_+ = \frac{(1+\cos^2\iota)}{2}\frac{h_{\rm rss}}{(2\pi\tau^2)^{\frac{1}{4}}}e^{-\frac{(t-t_0)^2}{4\tau^2}}\cos 2\pi f_0(t-t_0)\,, \tag{4.13}$$

$$h_\times = \cos\iota\frac{h_{\rm rss}}{(2\pi\tau^2)^{\frac{1}{4}}}e^{-\frac{(t-t_0)^2}{4\tau^2}}\sin 2\pi f_0(t-t_0)\,. \tag{4.14}$$

Here f_0 is the central frequency, t_0 is the central time, and we chose $\tau = 1/f_0$ as the duration. We use central frequencies of 100 Hz, 150 Hz, and 300 Hz for the low-frequency analysis and 554 Hz and 1000 Hz for the high-frequency search. The quantity $h_{\rm rss}$ is the root-sum-square signal amplitude:

$$h_{\rm rss} \equiv \sqrt{\int h_+^2(t) + h_\times^2(t)dt}\,. \tag{4.15}$$

This amplitude is related to the total energy $E_{\rm GW}$ in the gravitational-wave burst by:

$$E_{\rm GW} = \frac{2}{5}\frac{\pi^2 c^3}{G}h_{\rm rss}^2 f_0^2 D^2\,. \tag{4.16}$$

This waveform is consistent with the GW emission from a rotating system viewed from an inclination angle ι to the rotational axis. We select the inclination uniformly in $\cos\iota$ with $\iota \in [0°, 5°]$. This corresponds to a nearly on-axis system, such as would be expected for association with an observed long GRB. For astrophysical injections we use the gravitational-wave emission of inspiraling neutron star and black hole binaries, which are widely thought to be the progenitors of short GRBs. Specifically, we use the post-Newtonian model for the inspiral of a double neutron star system with component masses $m_1 = m_2 = 1.35M_\odot$, and the one for a black-hole-neutron-star system with $m_1 = 5M_\odot$, $m_2 = 1.35M_\odot$, as discussed in Chapter 1. We set the component spins to zero in each case. Motivated by estimates of the jet opening angle for short GRBs, we select the inclination uniformly in $\cos\iota$ with $\iota \in [0°, 30°]$.

For each HEN trigger, the injections are distributed uniformly in time over the on-source window. The injection sky positions are selected randomly following the estimated probability distribution (see Eq. 4.7) for the HEN trigger, to account for the uncertainty in the true HEN direction of incidence. The polarization angle (orientation of the rotational axis on the sky) is distributed uniformly. Finally, the amplitude and arrival time at each detector is perturbed randomly to simulate the effect of calibration errors in the LIGO and Virgo detectors.

Exclusion distances: For each waveform type (sine-Gaussians at 100, 150, 300, 554, 1000 Hz, and $1.35M_\odot$-$1.35M_\odot$ and $5M_\odot$-$1.35M_\odot$ inspirals), injections are performed over a range of amplitudes. For the inspiral signals, each amplitude corresponds to a well-defined distance. We can associate a physical distance to each amplitude for the sine-Gaussian waveforms as well, by assuming a fixed energy in gravitational waves. For concreteness, we select $E_{\rm GW} = 10^{-2}M_\odot c^2$. This value corresponds to the optimistic limit of possible gravitational-wave emission by various processes in the collapsing cores of rapidly rotating massive stars [23–26]; more conservative estimates based on 3D simulations have been made in [27–31].

The exclusion distance is defined as the largest distance at which in 90% of the cases the event corresponding to the GW signal would be louder than the loudest on-source event found in the data. For each type of gravitational wave simulated, the distributions of exclusion distances for our neutrino sample are shown in Figures 4.30 and 4.31. For binary neutron star systems of $(1.35 - 1.35)M_\odot$ and black hole - neutron star systems of $(5 - 1.35)M_\odot$ typical distance limits are 5 Mpc and 10 Mpc respectively. For the sine-Gaussian waveforms in the low-frequency band the typical distance limits are between 5 Mpc and 17 Mpc, while for those in the high-frequency band the typical limits are of order 1 Mpc.

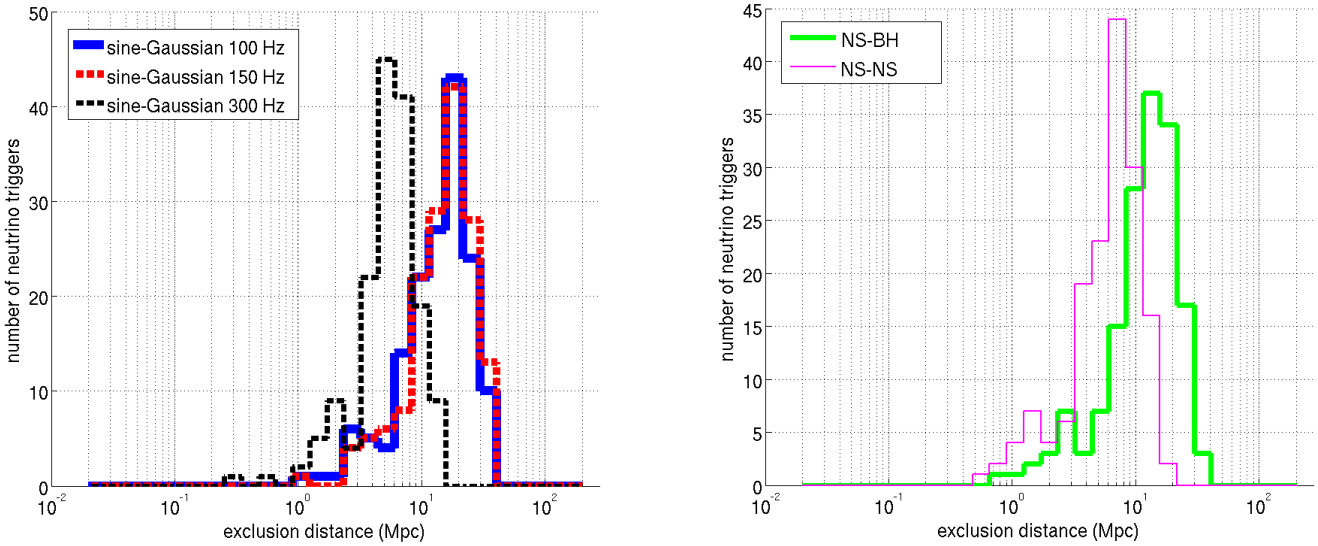

Figure 4.30 – Low-frequency analysis: the left plot is the histogram for the sample of analyzed neutrinos of the distance exclusions at the 90% confidence level for the 3 types of circular sine-Gaussian models considered: 100 Hz, 150 Hz and 300 Hz. A standard siren gravitational wave emission of $E_{GW} = 10^{-2}\, M_{\odot}\, c^2$ is assumed. The right plot shows histogram across the sample of analyzed neutrinos of the distance exclusions at the 90% confidence level for the 2 families of binary inspiral models considered: NS-NS and BH-NS.

4.7 Astrophysical implications

4.7.1 Upper limits on joint source populations

The present search for GW and HEN correlations in space and time revealed no evidence for coincident events. In accordance with the Poisson statistics, this implies a 90% confidence level upper limit on the rate of detectable coincidences of $2.3/T_{\rm obs}^{\rm com}$, where $T_{\rm obs}^{\rm com} \approx 91.36$ days is the duration of coincident observations. This can be expressed as a limit on the rate density (number per unit time per unit volume) $\rho_{\text{GW-HEN}}$ of objects which would yield coincident GW and HEN signals:

$$\rho_{\text{GW-HEN}} V_{\text{GW-HEN}} \leq \frac{2.3}{T_{\rm obs}} \,. \tag{4.17}$$

In this expression, $V_{\text{GW-HEN}}$ is the volume of universe probed by the present analysis for typical GW-HEN sources and 2.3 is the in accordance with the a Poisson process. This volume is related to the GW and HEN detection efficiencies as a function of distance, and must be estimated for typical emission models. We take as fiducial sources two classes of objects: the final merger phase of the coalescence of two compact objects (short GRB-like), or the collapse

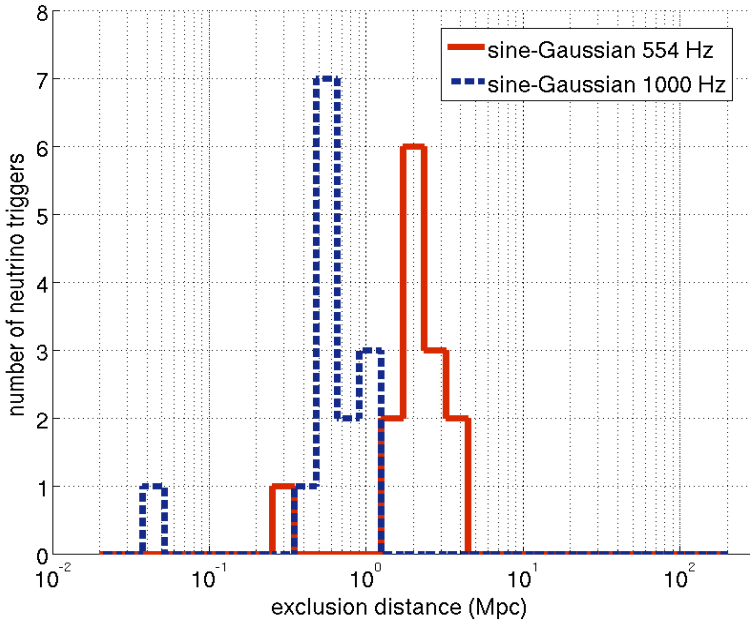

Figure 4.31 – High-frequency analysis: the histogram for the sample of analysed neutrinos of the distance exclusions at the 90% confidence level for the 2 frequencies of circular sine-Gaussian models considered: 554 Hz and 1000 Hz.

of a massive object (long GRB-like), both followed by the emission of a relativistic hadronic jet. The corresponding HEN and GW detection horizons (or exclusion distances) have been estimated respectively in sections 4.4 and 4.6.2. In the case of short GRBs, $d_{HEN} \sim 4.41$ Mpc and $d_{GW} \sim$ 5-10 Mpc depending on the binary masses, while for long GRBs they increase to $d_{HEN} \sim 12.55$ Mpc and $d_{GW} \sim$ 10-20 Mpc (under the optimistic assumption of $E_{\rm GW} = 10^{-2} M_{\odot} c^2$). The effective volume probed by the GW+HEN joint analysis can be written as:

$$V_{GWHEN} = \int_0^{\infty} P_{GWHEN}(r)\, 2\pi\, r^2 dr \int_{-\pi/2}^{\pi/2} \epsilon_{HEN}(\delta) \cos\delta d\delta \tag{4.18}$$

where $P_{GWHEN}(r) = P_{HEN}(r) \times P_{GW}(r)$ is the detection probability for a joint emitter and $\epsilon(\delta)$ is the visibility in ANTARES of a source at declination δ. This integral effectively extends until a certain distance $d_{GWHEN} \simeq min(d_{HEN}, d_{GW})$. As $d_{GW} > d_{HEN}$ for the sources considered hereabove, we approximate $P_{GW}(r)$ by a step function ($P_{GW}(r) = 1$ for $r < d_{GW}$, 0 elsewhere) and fold it with the probability $P_{HEN}(r)$ to detect at least one neutrino from the source (as described in section 4.4 and Figure 4.16). From Eq. 4.17 one can then derive approximate limits on the population density of joint GW+HEN emitters: $\rho^{\rm SGRB}_{\rm GW\text{-}HEN} \lesssim 10^{-2}{\rm Mpc}^{-3}\ {\rm yr}^{-1}$ for

SGRB-like sources, and $\rho^{\mathrm{LGRB}}_{\text{GW-HEN}} \lesssim 10^{-3}\mathrm{Mpc}^{-3}\ \mathrm{yr}^{-1}$ for LGRB-like sources.

4.7.2 Comparison of limits with existing estimates

[32, 33] suggest a local rate density of SGRB of $\rho_{\mathrm{SGRB}} \lesssim 10^{-9}\mathrm{Mpc}^{-3}\ \mathrm{yr}^{-1}$, and the abundance of binary neutron star mergers, their assumed progenitors, is estimated to be $\rho_{\mathrm{NS+NS}} \sim 10^{-6}\mathrm{Mpc}^{-3}\ \mathrm{yr}^{-1}$ [34], well below the reach of the present search ($\rho^{\mathrm{SGRB}}_{\text{GW-HEN}} \lesssim 10^{-2}\mathrm{Mpc}^{-3}\ \mathrm{yr}^{-1}$). With $T_{\mathrm{obs}} = 1$ year, an improvement of a factor 10 on the detection distance is required in order to be able to constrain the fraction of mergers producing coincident GW+HEN signals. [32] estimate a total rate of long GRBs of $\rho_{\mathrm{LGRB}} \sim 3 \times 10^{-8}\mathrm{Mpc}^{-3}\ \mathrm{yr}^{-1}$; these sources are closely related to Type II and Type Ibc core-collapse supernovae. The local rate of SNIbc is $\rho_{\mathrm{SNIbc}} \sim 2 \times 10^{-5}\mathrm{Mpc}^{-3}\ \mathrm{yr}^{-1}$, whereas $\rho_{\mathrm{SNII}} \sim 2 \times 10^{-4}\mathrm{Mpc}^{-3}\ \mathrm{yr}^{-1}$, relatively close to the obtained limit $\rho^{\mathrm{LGRB}}_{\text{GW-HEN}} \lesssim 10^{-3}\mathrm{Mpc}^{-3}\ \mathrm{yr}^{-1}$ under our optimistic assumptions of GW emission in this scenario. A factor 10 only is required in order to constrain the fraction of star collapses producing coincident GW-HEN signals, which translates into a required improvement of 2 on the detection distance.

4.8 Conclusions

In this chapter we have described the first joint GW+HEN search using coincident data taken in 2007 from the ANTARES neutrino telescope and the Virgo/LIGO GW interferometers. The absence of GW triggers in coincidence with a list of preselected HEN candidate events has allowed to establish limits on the rate density $\rho_{\text{GW-HEN}}$ of joint GW+HEN emitting systems. These limits are however not stringent enough to constrain the density of realistic, known candidate GW+HEN progenitors such as binary neutron star mergers or Type II/Ibc core-collapse supernovae. An increased sensitivity can be achieved by performing similar coincidence analyses using other data sets provided by the same instruments. The next chapter presents an improved analysis method applied to the joint data sample collected by ANTARES in its 12L configuration concomitantly with science runs conducted with enhanced Virgo and LIGO interferometers in 2009-2010. This analysis is described in chapter 5.

REFERENCES

[1] S. Adrian-Martinez et al, arXiv:1205.3018, (2012).

[2] B. Bouhou, Proceedings of the VLVNT11 conference, arXiv:1201.2840 (2011).

[3] T. Pradier, arXiv:0807.2567v1 (2008).

[4] V. V. Elewyck et al, Int. J. Mod. Phys. D18:1655-1659, (2009).

[5] B. Bouhou et al, Proceedings of SF2A'11, G. Alecian et al. Eds, 63-68 (2011).

[6] S. Ando et al, submitted to Rev. Mod. Phys. arXiv:1203.5192.

[7] S. D. Mohanty et al, Class. Quantum Grav. 21 5, S765-S774 (2004).

[8] K. Hayama et al, Class. Quantum Grav. 24, S681-S688, (2007).

[9] J. Abadie et al, Astrophys. J., 715, 1453-1461 (2010).

[10] J. Abadie et al, Phys. Rev. D 81, 52010 (2001).

[11] F. Arcenese et al, Class. Quantum Grav., 24, S671 (2007).

[12] B. Baret et al, ANTARES internal note ANTARS-PHY-2011- (2011).

[13] http://marantares.in2p3.fr:8080/ANALYSIS/125,

[14] P. Claire, PhD thesis, Université Paris Diderot, (2009).

[15] G. Halladjian et al, ANTARES internal note, ANTARES-PHYS-2010-002 (2010).

[16] G. Halladjian et al, PhD thesis, Université de la Méditerranée Aix-Marseille II (2010).

[17] http://antares.in2p3.fr/users/bbouhou/internal/HEN_list_2007_Updated_v2.txt,

[18] B. Abbott et al, Astrophys. J., 715, 1438 (2010).

[19] M. Was et al, Phys. Rev. D 86, 022003 (2012).

[20] I. Di Palma, Proceedings of TAUP 2011, J. Phys. Conf. Ser. 375, 060002 (2012).

[21] P. Brady et al., Class. Quantum Grav. 21, S1775 (2004).

[22] B. Abbott et al, Phys. Rev. D, 77, 062004 (2008).

[23] C. Fryer et al, Astrophys. J., 565 430-446 (2002).

[24] S. Kobayashi and P. Mészáros, Astrophys. J., 589 861–870 (2003).

[25] A. L. Piro and E. Pfahl, Astrophys. J. 658 1173 (2007).

[26] C. Fryer and K. New, Living Rev. Relat., 14 1 (2011).

[27] H. Dimmelmeier et al, Phys. Rev. D, 78 065056 (2008).

[28] C. D. Ott, Class. Quantum Grav., 26 063001 (2009).

[29] S. Scheidegger et al, A&A 514 A51 (2010).

[30] C. Ott et al, Phys. Rev. Lett, 106 161103 (2011).

[31] T. Takiwaki and K. Kotake, Astrophys. J., 743 1 (2011).

[32] Guetta, et al., Astropart. Phys. 20 429-455 (2004).

[33] E. Nakar, Phys. Rept., 442, 166 (2007).

[34] R. O'Shaughnessy et al, Astrophys. J., 716 615 (2010).

[35] G. M. Harry et al, Class. Quantum Grav. 27 084006 (2010).

[36] S. Braccini et al., Astropart. Phys. 23, 557 (2005).

[37] P. Meszaros, Astron. Astrophys. Suppl. Ser., 138, 533 (1999).

[38] G. J. Feldman and R. D. Cousins, Phys. Rev. D 57, 3873 (1998).

[39] E. Waxman, Lect. Notes Phys., 576, 122 (2001).

[40] J. Abadie et al., Phys. Rev. D 81 102001 (2010).

[41] K. Kotake et al, Rep. Prog. Phys., 69 971-1143 (2006).

CHAPTER 5

GW+HEN ANALYSIS FOR 12L–S6/VSR2-3

5.1 Summary

We have presented in the previous chapter results from the first joint search for gravitational-wave bursts associated with high energy neutrinos using the ANTARES, the Virgo and the LIGO data from 2007. In this chapter we present results from the analysis of their 2009-2010 data. A new method is proposed. The neutrinos are selected by a joint optimisation procedure taking into account efficiencies to the neutrino and gravitational-wave signals. The neutrinos have been reconstructed with a more sophisticated reconstruction algorithm, labelled Aafit, in contrast of the robust one (Bbfit) used in the previous search (Chapter 4). The search for GW in coincidence with these neutrinos are done using a specific GW search algorithm, labelled skymask-cWB, specifically prepared for this joint search. Below we describe further these data, the search strategies adopted and the final results.

5.2 Data set

5.2.1 Description of ANTARES data

We select from the database 2184 runs from July 7th, 2009 through October 20th, 2010. This list of runs has been selected using data quality (DQ) requirement (see section 2.4). That is, we select all runs with QualityBasic flag greater than 1 (QB$\geq$1) and runs with run setup "physics". We discard all runs with duration <5 minutes. Taking into account these DQ criteria we get a duty cycle of 56%. Figure 5.1 shows the distribution of run numbers selected for the analysis. The total observation time (using only neutrino side) is $T \equiv 266$ days.

A Monte Carlo simulation is performed to match the realistic condition of the data taking following the run by run approach (see section 2.5.5). These information (runsetup, mean rates, alignment, high rate veto, run duration) are taken from the data runs themselves and plugged

into the simulation. This method has been adopted recently by the ANTARES collaboration and is used by all ongoing analyses. A total of 5×10^8 neutrinos are simulated using the GENHEN package in the energy range 100 GeV-100 PeV, with an energy spectrum $dN/dE \propto E^{-\gamma}$, where $\gamma = 1.4$, and in all zenith directions. The spectrum used to simulate neutrinos permits a later re-weighting according to a user specified flux. In this analysis the same neutrino sample is weighted differently to be used as atmospheric neutrinos according to the Bartol flux [2] or as astrophysical signal according to the GRB diffuse flux of Waxman and Bahcall [3] (see section 1.1.4) or E^{-2} flux [4]. The simulation of atmospheric muons is performed using Mupage package (see section 2.5). In this analysis we select all the events passing the 3N or T3 trigger's condition (see section 2.3.5). These events are then reconstructed with the Aafit reconstruction algorithm (see section 2.6.2).

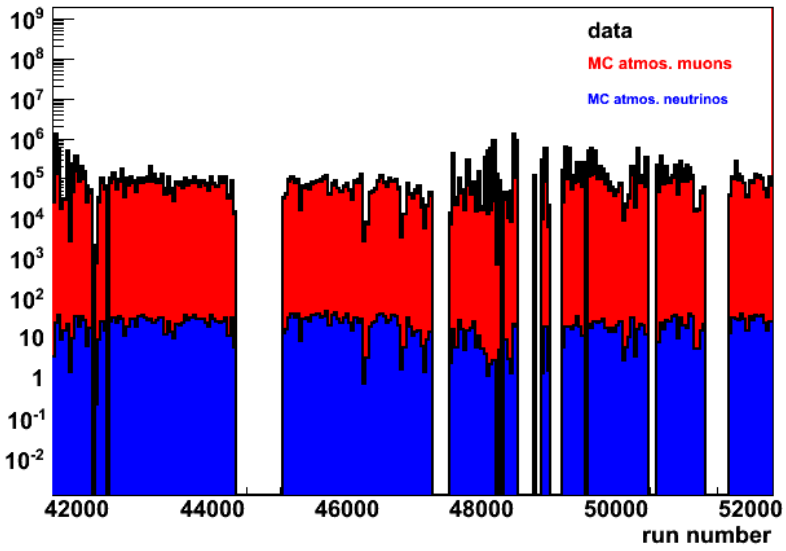

Figure 5.1 – Run numbers that passes the DQ requirements described in the text.

5.2.2 Description of Virgo and LIGO data

The GW data used in this search are the S6-VSR2/3 LIGO-Virgo data. Three detectors participated to this data taking namely LIGO-Livingston (L1), LIGO-Hanford (H1) and Virgo (V1). These data were collected between July 07, 2009 and October 21, 2010. LIGO S6 and Virgo VSR data are divided into four parts:

- Period A (S6A-VSR2): running from Tue July 7, 2009 at 21:00 UTC to Tue Sept. 1,2009 at 00:00 UTC.

- Period B (S6B-VSR2): running from Saturday Sep 26, 2009 12:46:33 UTC, Friday Jan 8, 2010 22:00:00 UTC.

- Period C (S6C) : running from Friday Jan 8, 2010 22:00:00 UTC to Saturday Jun 26, 2010 00:00:00 UTC.

- Period D (S6D-VSR3): running from Saturday Jun 26 2010 00:00:00 UTC to Wednesday Oct 20 2010 15:00:00 UTC.

This search aims at detecting bursts of gravitational waves in the frequency range from 64 Hz to 2 kHz. Note that the detectors are most sensitive at about $\sim$ 200 Hz as can be seen from Figure 5.2. The sensitivity in the selected frequency range is within a factor of 10 of the best sensitivity. Each curve in Figure 5.2 shows the amplitude spectral density as a function of frequency. The vertical "spikes" are from mechanical vibrations in parts of the detector. The sensitivity of a detector can be expressed in terms of the amplitude spectral density, which is the square root of the power spectral density, since the strength of a gravitational wave signal is proportional to the strain induced in the interferometer. We use the calibrated data with LSC tag `LDAS_C02` and the Virgo tag `HrecV2` and `HrecV3`. The calibration uncertainty is estimated to be 20% in amplitude and 10 degrees in phase for LIGO and 5.5% in amplitude and 3 degrees in phase for Virgo. The data quality flags [5] aim at eliminating periods where data have poor quality (some or all of the detectors was particularly noisy e.g., due to internal malfunctioning and/or environmental disturbances).

5.2.3 The ANTARES, the Virgo and the LIGO joint data set

The search requests at least two GW detectors in operation. The concomitant data taking period between S6VSR2/3 and ANTARES 12L goes from July 7th, 2009 up to October 20th 2010 with some in between periods where one or no interferometer (IFO) was in science mode. In this period, the observation time for each IFO network is: 44.7 days (H1L1V1), 33.5 days (H1L1), 23.1 days (L1V1) and 27.4 days (H1V1). The sum of these partial periods gives the total concomitant observation time of $\tau \equiv$128.7 days.

5.3 Gravitational wave event generation

For this analysis we rely on a new detection pipeline `skymask coherent WaveBurst` which is a variant of the coherent WaveBurst (cWB) pipeline, presented in section 3.7.4 developed for the purpose of this search.

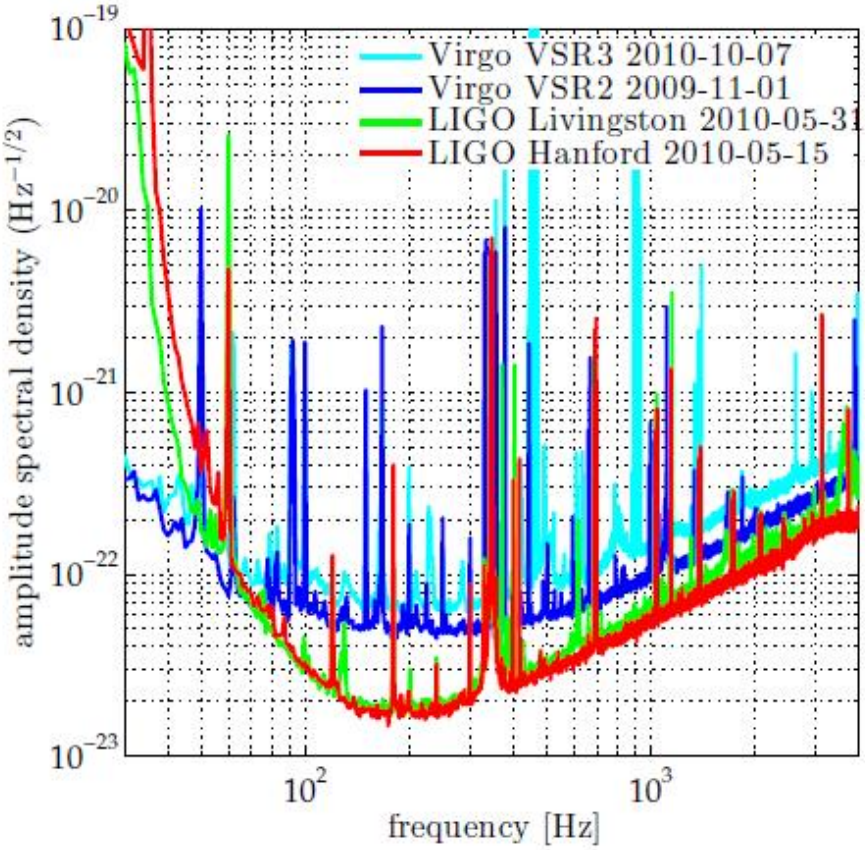

Figure 5.2 – Sensitivity of LIGO-Virgo during the S6-VSR2/3 period.

5.3.1 Skymask coherent WaveBurst pipeline

This pipeline has been developed to overcome limitations of earlier analysis schemes presented in section 3.7.4. In particular, it takes into account the lessons learned from the first ANTARES–LIGO/Virgo joint search (see Chapter 4) [6] based on the X-pipeline algorithm.

Core collapse supernovae being one of the potential source targets, the frequency bandwidth should extend to 2 kHz at least. We also expect many more neutrino candidate for this data set, of the order of $\mathcal{O}(10^3)$, which is an order-of-magnitude increase with respect to the previous analysis. The current implementation of the X-pipeline used for the first search would require a very large computing power to perform the analysis in a realistic time.

This is why we developed "skymask coherent Wave-Burst" (in short, s-cWB) [7], a variant of the cWB pipeline which reconstructs GW events only in an *a priori* sky area specified by a *sky mask*. This enables the analysis of periods with two GW detectors only (see Figure 5.4 for an illustration). We are thus able to cover the whole livetime. This pipeline is also computationally more efficient than the X-pipeline thus enabling the broadband analysis (up to 2 kHz) for order

of thousands of neutrino triggers.

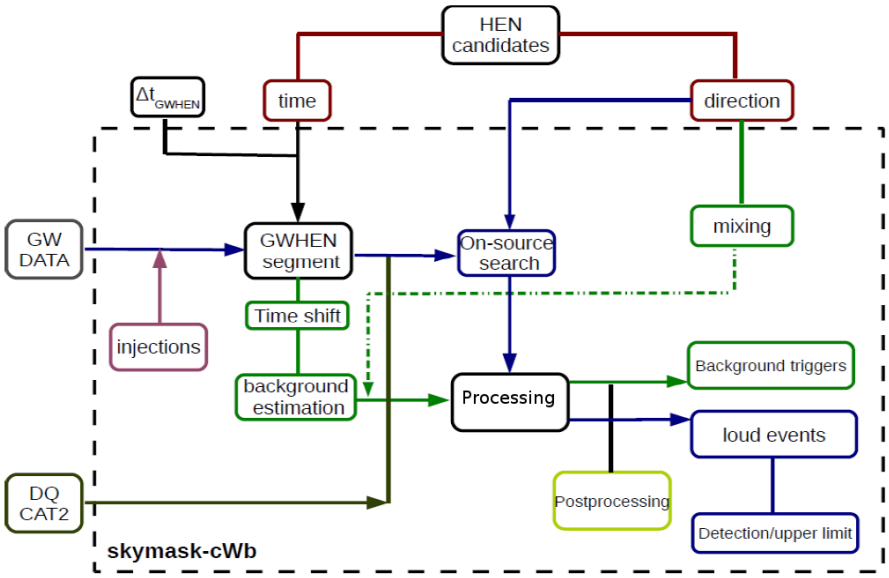

Figure 5.3 – Schematic outline of the GW+HEN 12LS6VSR2-3 analysis pipeline.

As discussed in section 4.2 the time and direction of the neutrino candidates are exploited as input to the s-cWB pipeline. s-cWB selects GW data segments of length ΔT centered about the t_ν, i.e *on-source* window (see section 4.2). It also takes into account the ASW associated to the direction of the neutrino candidate. The search for GW signal is thus restricted to areas on the sky defined by the provided ASW90% instead of scanning the whole sky. A grid, of same resolution as cWB, i.e 0.4×0.4 degree, is used within the ASW90% (see section 4.4.1). The neutrino PSF is taken into account as a probability distribution: each event inside this angular search window is weighted according to the PSF. Figure 5.3 shows a schematic view of the s-cWB pipeline used in this analysis. s-cWB defines the same coherent statistics as cWB, the most relevant ones for this study are the network correlation amplitude ρ, the network correlation coefficient net_{cc} and the network energy disbalance net_{ED}. While cuts on net_{cc} and net_{ED} are used to distinguish noise outliers from genuine GW signals, the final event selection is done through a cut over the statistic ρ which characterises the event significance [8]. We refer the reader to appendix B for the mathematical definition of those statistics.

5.3.2 Background estimation

The method used in the cWB for background study is described in [9]. For completeness, we now describe the general principle. We remind that in a coherent analysis such as s-cWB, time delays are applied to each data streams in order to compensate the time taken by the wave to

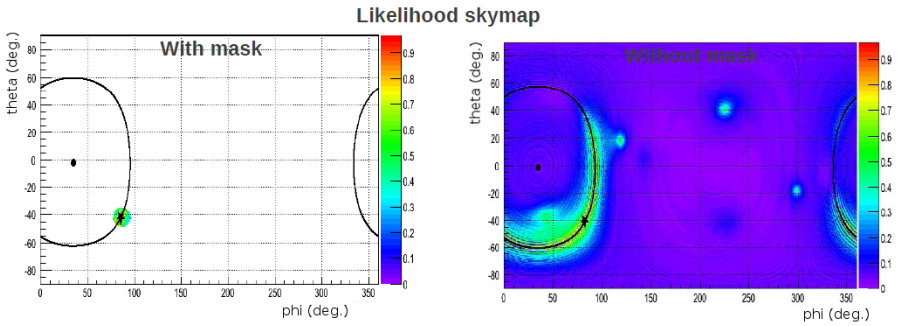

Figure 5.4 – Likelihood skymap of the reconstructed GW events in the case of 2 IFOs, without neutrino skymask (right) and with skymask (left).

propagate from one detector to the other. Thanks to this operation, GW signals from a given source direction are thus aligned in time. The time delays are necessarily smaller than the time-of-flight (at the speed of light) between Virgo and LIGO is about to 27 ms and 10 ms for the Handford and Livingston detector respectively. The method used for background estimation consists in applying additional and non-physical time-shifts to one or more GW data streams as described in section 3.7.2. The time-shifts applied for the background estimation are much larger than the time-of-flight added to the noise auto-correlation time scale (which dominate the sum). These time-shifts erases any correlation between pairs of GW detectors due to any GW signal. The analysis is repeated over several time-shifted data set. The distribution of the resulting events provides an estimate of the experiment background.

In addition to the time-shift analysis s-cWB allows the possibility to estimate background using mixing skymasks and/or combine both methods. While skymask mixing is convenient numerically, we observed that it has limitations because it introduces correlation between trials especially in the case of two-detector network. We consider it as an option for the final analysis. The analysis cuts are tuned based on the estimated background.

We evaluated the background and performance of s-cWB over a simulated neutrino test sample. This study is approximately representative of the final analysis using real neutrino candidate events. The fake neutrino set consisted in 1000 events randomly generated uniformly distributed over the entire sky and during the S6A/VSR2 period. The neutrino localisation uncertainties were chosen to mimick that of 2007 neutrino sample (see chapter 4). We used the modelled 'g'-search which is optimized for circularly polarized GW signals and we disabled regulation. We performed multiple (101) time-shift and (70) skymask mixing experiments between L1, H1 and V1 detectors. This leads to the background estimates presented in Figure 5.5. We adjusted the rejection cuts on net_{cc} and net_{ED} to mitigate the long background tails due to the absence of regulation. For an objective FAR of 10^{-7} Hz we therefore need a selection

cut $\rho \geq \rho_{threshold} = 3.25$.

5.3.3 Sensitivity estimates

In order to test the performance of the s-cWB we add simulated signals of various amplitudes and waveforms to data (see section 3.7.3). The simulated signals are produced using the Burst-MDC package described in [10].

For each neutrino candidate, we simulate randomly a set of source position according to the PSF. Fake signals are added every $\sim$ 100 seconds mimicking the GW signature from sources at those position. We test the probability of detection and correct recovery for various amplitudes by applying multiplicative factors from weak to strong signals covering the full range from 0 to 100 % efficiency. The resulting data stream is processed identically to the standard analysis.

For each waveform, we evaluate the efficiency for detection as a function of the gravitational wave strain h_{rss} which is the incoherent sum of the "+" and "×" polarizations defined in Equation (4.15), see Figure 5.6. As expected, the efficiencies are essentially 100% for large values of h_{rss}, consistent with noise and thus 0% efficiency for small h_{rss}, and transitioning over a narrow intermediate range of h_{rss}. The resulting curve is empirically fitted by a sigmoid curve in $\log_{10}(h_{rss})$.

We produced the efficiency curves associated to the analysis of the test neutrino sample

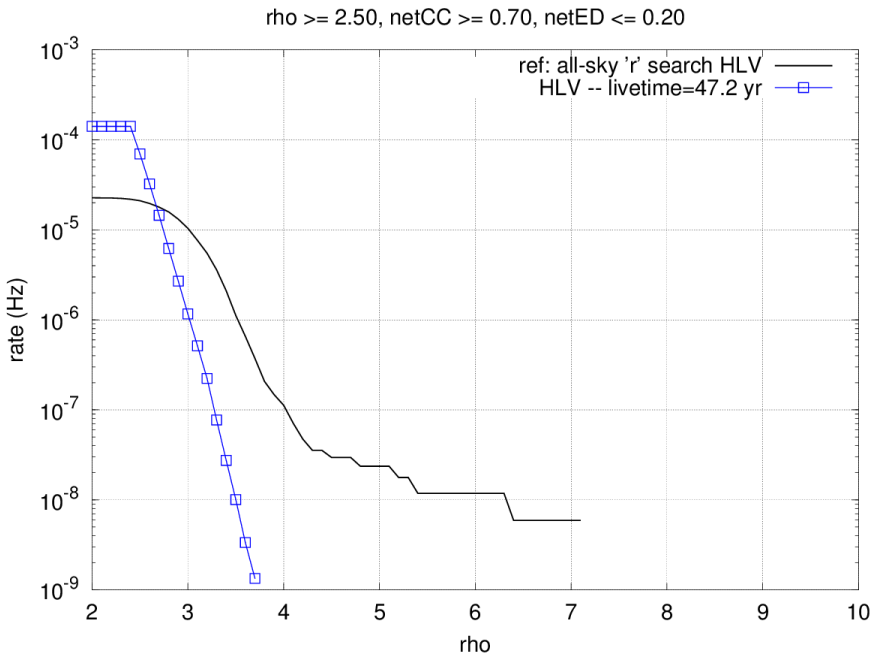

Figure 5.5 – Background estimate for the test neutrino sample as described in the text and considering triple detector network HLV compared to the all sky background for the same data taking.

introduced in the previous section. We performed multiple injections of circularly polarized Sine-Gaussian waveforms as in Equations (3.16) and (3.17) at four different frequencies i.e., 153, 100, 1053 and 1304 Hz. For selection cut corresponding to the FAR = 10^{-7} Hz we get $h_{rss}^{50\%} = 4.1 \times 10^{-22}/\sqrt{\text{Hz}}$ at 153 Hz. This can be compared to the result obtained with the X-pipeline in Chapter 4, namely $h_{rss}^{50\%} = 3 \times 10^{-22}/\sqrt{\text{Hz}}$ at the same frequency and for the same FAR requirement. Despite the absence of the (numerically expensive) event-by-event optimization of the cuts performed by the X-pipeline, the s-cWB performs at a comparable level.

5.4 Optimization procedures

The selection of the neutrino events can, in principle, be based on several approaches. Independently from the GW interferometers, the selection can be made in order to discard as much as possible misreconstructed atmospheric muons (resulting in a high purity sample of atmospheric neutrinos). Another criterion would be to filter the events in order to establish the best possible limit on some putative astrophysical neutrino flux (minimizing the so-called model rejection factor MRF). Reversely one can target a discovery by maximizing the model discovery

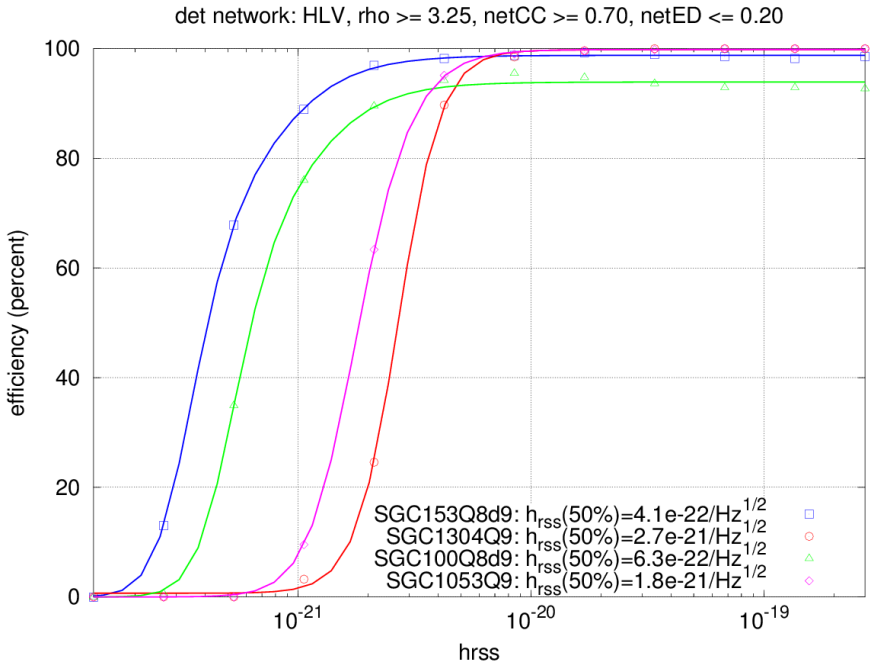

Figure 5.6 – Sensitivity estimate obtained with the test neutrino sample as described in the text and for triple detector network HLV.

potential MDP (minimizing the model discovery factor MDF) for this particular neutrino flux.

The third approach is completely dependent of the GW interferometers. This approach maximises a joint figure-of-merit (FOM) by combining the individual efficiencies of HEN and GW. FOM relies on our knowledge on the false alarm probability.

In the following subsections, we describe the three latter options. In the all cases, the signal is assumed to be a diffuse flux (as the sources of interest are distributed anywhere in the sky). We use the Waxman-Bahcall flux for unresolved GRBs, since the energy spectrum is supposed to be representative of generic long- and short-GRBs, (see section 1.1.4).

5.4.1 Model rejection factor and Model discovery potential

Model rejection factor (MRF): The model rejection factor (MRF) [11] is used in this search to optimize selection criteria in order to place the best upper limit on the signal from an assumed theoretical model. We use in this work the GRB diffuse flux of Waxman-Bahcall. The computation relies **only on Monte Carlo simulation sample** to estimate the expected background events (n_b) and true neutrino signal events (n_s). The authors in [11] introduce the *average upper limit* at 90% C.L, when n_s=0, as follows:

$$\overline{\mu}_{90}(n_b) = \sum_{n_{obs}}^{\infty} \mu_{90}(n_{obs}, n_b) \frac{(n_b)^{n_{obs}}}{n_{obs}!} exp(-n_b) \tag{5.1}$$

where $\mu_{90}(n_{obs}, n_b)$ is the Feldman-Cousins (F.C) upper limit [12]. That is, the best upper limit is obtained when the ratio between $\overline{\mu}_{90}(n_b)$ and n_s, labeled MRF, is minimum for a set of cuts:

$$MRF(\text{cuts}) = \frac{\overline{\mu}_{90}(n_b(\text{cuts}))}{n_s(\text{cuts})} \tag{5.2}$$

In this work we compute n_b and n_s against the reconstruction quality parameter Λ, introduced in section 2.6.2. It's worth noting that Λ and β are correlated as shown in Figure 5.7 right. We show also in Figure 5.8 distributions of β for upgoing events with and without cutting on Λ. Thus we decide not to use β in the optimisation. The distribution of Λ is shown in Figure 5.9 for only upgoing events. It's extrapolated to high Λ values using a Gaussian distribution.

With a number of background events of order of 10^4 for small Λ, the computation of $\overline{\mu}_{90}(n_{obs}, n_b)$ becomes considerably slow because of F.C. algorithm at high statistics. To speed up the computation time we model the upper limit by an analytical parameterization (see

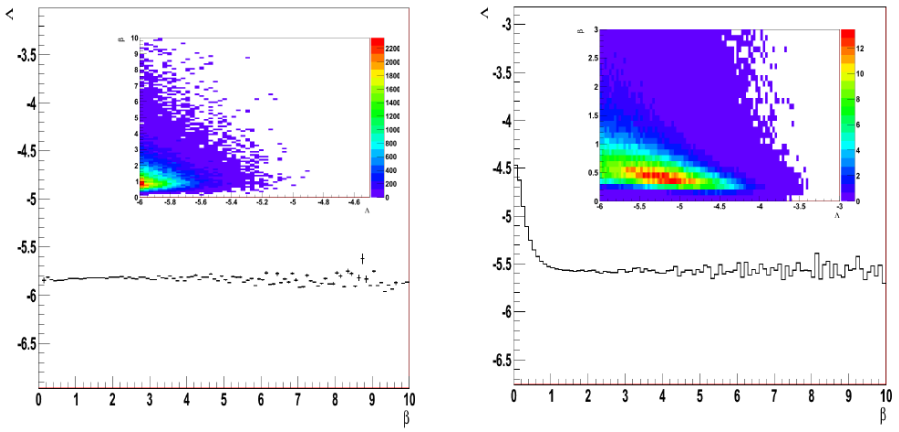

Figure 5.7 – Distribution of Λ as function of β parameter for atmospheric muons (left), for atmospheric neutrinos (right). Only upgoing events are selected.

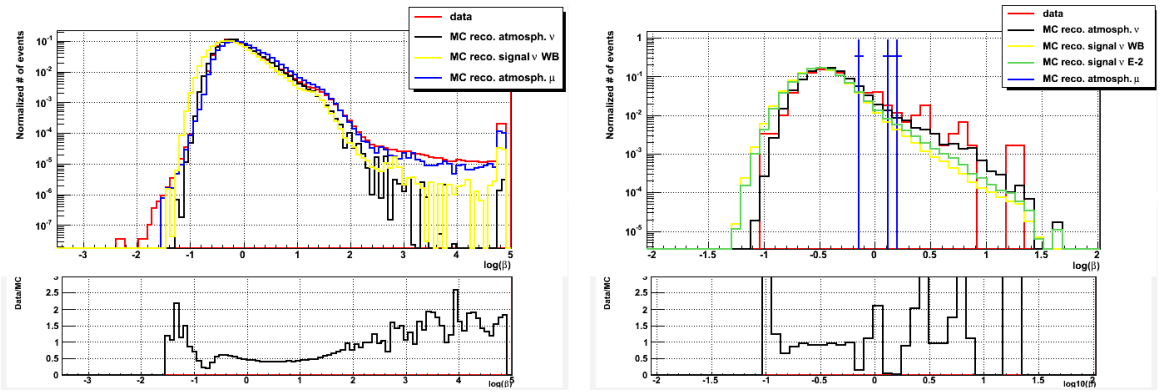

Figure 5.8 – Distributions of β parameter for data and MC without (top) and with (bottom) cut on Λ ($\Lambda > -5$). Only upgoing events are selected.

appendix A for further mathematical details):

$$\tilde{\mu}_Q(n_{obs}, n_b) = \left(\frac{-\sqrt{2}.Erf^{-1}(2Q-1) + \sqrt{2Erf^{-1}(2Q-1)^2 + 4n_{obs}}}{2} \right)^2 - n_b \tag{5.3}$$

where Erf is the error function and Q = 90% is the significance level. In analogy with Equation 5.1, $\tilde{\mu}_Q(n_{obs}, n_b)$ is weighted with its Poisson probability of occurrence. Thus the model rejection factor becomes:

$$\tilde{MRF}(\text{cuts}) = \frac{\bar{\tilde{\mu}}_{90\%}(n_b(\text{cuts}))}{n_s(\text{cuts})} \tag{5.4}$$

In Figure 5.10 is shown the modified ratio (Equation (5.4)) as function of Λ. We define Λ_{min} in such way the ratio Equation (5.4) is minimum. From the curve 5.10 we find a minimum for

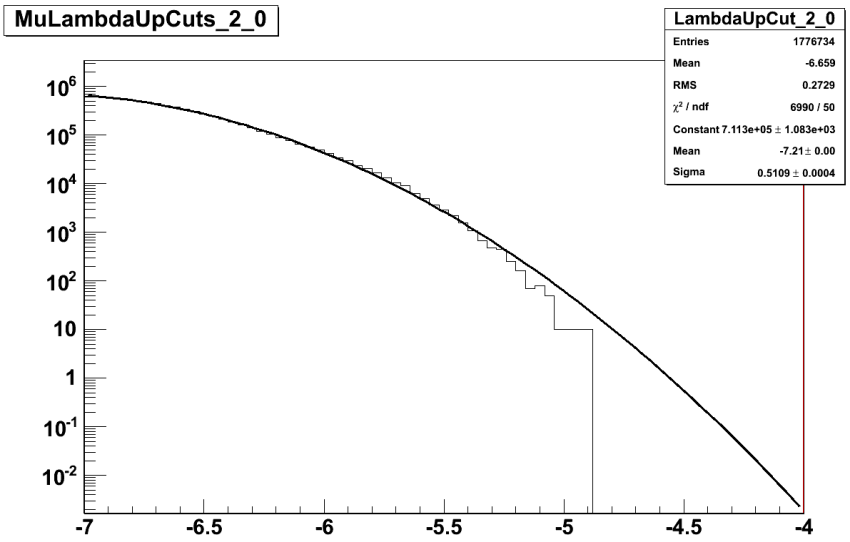

Figure 5.9 – Distribution of the track quality parameter Λ for misreconstructed atmospheric muons. The distribution is fitted by a Gaussian function.

$\Lambda_{min} = -4.1$. The final number of events passing Λ_{min} is ~ 20 events.

Model discovery potential: We report in this section a commonly used technique in high energy astrophysics, the so-called "Model Discovery Potential" (MDP) [13, 14], for optimizing quality cuts in order to maximize the probability of detecting an excursion of nσ (a "discovery")

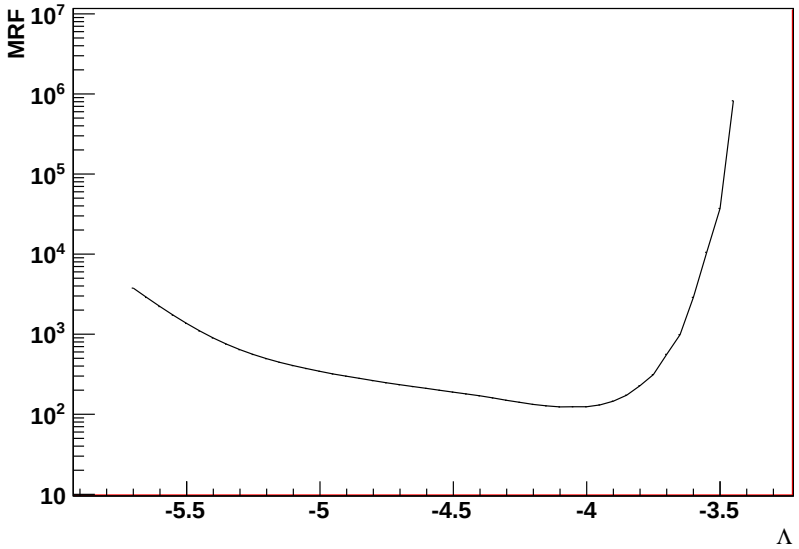

Figure 5.10 – MRF as a function of Λ completed as described in the text. The minimum value is found for $\Lambda = -4.1$

with a given C.L. We introduce n_{crit} the smallest number of events needed to claim a detection at a significance level α. A standard way to quantify this number is to calculate the probability for observing $\geq n_{crit}$ under the background only hypothesis:

$$\begin{aligned} P(\geq n_{crit}|\mu_b) &= \sum_{n=n_{obs}}^{\infty} P(n|\mu_b) \\ &= 1 - \sum_{n=0}^{n_{obs}-1} P(n|\mu_b) \end{aligned} \tag{5.5}$$

If $P(\geq n_{crit}|\mu_b) < 5.73 \times 10^{-7}$ we can report that we have a detection at 5σ level. This probability is called p_{value}, i.e $p = P(\geq n_{crit}|\mu_b)$. Small p_{value} is evidence against null hypothesis. If in addition to n_b a real signal μ_s is assumed then the probability that we would observe at least n_{crit} becomes:

$$\begin{aligned} P(\geq n_{crit}|\mu_b + \mu_s) &= \sum_{n=n_{obs}}^{\infty} P(n|\mu_b + \mu_s) \\ &= 1 - \sum_{n=0}^{n_{obs}-1} P(n|\mu_b + \mu_s) \\ &= 1 - \beta \end{aligned} \tag{5.6}$$

$1 - \beta$ is commonly known as the statistical power. Fixing $(1 - \beta)$ allows to calculate the corresponding value of μ_s for which Equation (5.6) is satisfied, i.e. μ_{lds}. We then define the model discovery factor (MDF) as the ratio between μ_{lds} and μ_s.

$$MDF(\Lambda) = \frac{\mu_{lds}(\Lambda)}{\mu_s(\Lambda)} \tag{5.7}$$

An optimization of the analysis which aims at minimizing the MDF against Λ for a given statistical power and a given significance (C.L.), has to be done numerically. From other side Punzi derived in [14] an analytical parameterization of μ_{lds} by approximation of Poisson distribution by Gaussian one:

$$S_{min} = \frac{cl^2 + 2\sigma\sqrt{n_b} + cl \times \sqrt{cl^2 + 4\sigma\sqrt{n_b} + 4n_b}}{2} \tag{5.8}$$

where σ and cl are the desired *number* of sigmas and C.L respectively (see Figure 5.11). Thus the MDF can be redefined by Equation (5.9):

$$M\tilde{D}F(\Lambda) = \frac{S_{min}}{\mu_s} \tag{5.9}$$

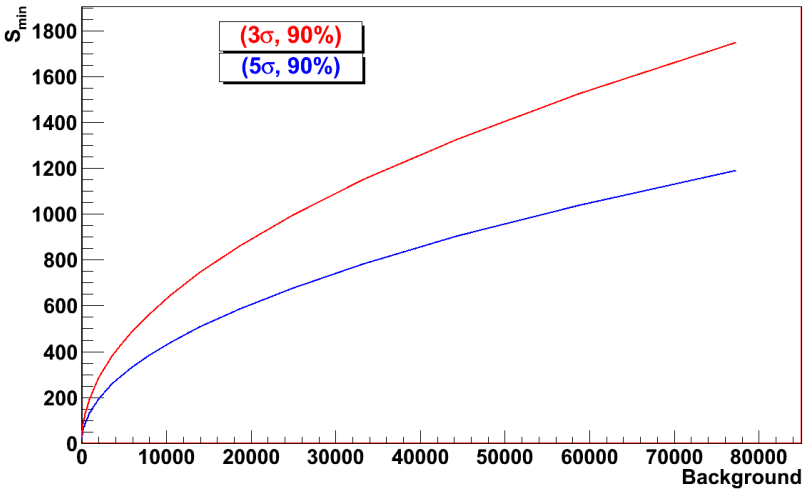

Figure 5.11 – Minimum number of signal events versus number of background events.

A study of MDF for a given (σ, cl) as a function of two reconstruction parameters, Λ and β is shown in Figure 5.12. It shows that the MDF has no clear minimum in the accessible parameter space. We confirm this with a 2D distribution of Λ vs β (insert in color in Figure 5.13), which shows the mean value of Λ for each bin in β. Figure 5.13 left shows that there is no minimum of the MDF as a function of β. On the contrary there is a clear minimum of the MDF as a function of Λ. Thus, we restrict this study to the only Λ parameter.

In this work we minimize Equation (5.9) against Λ. Figure 5.14 shows the result for different number of σ and number of cl. The minimum is obtained for $\Lambda_{min} = -4.9$ and is roughly the same whatever the assumed number of σ and cl. The number of events surviving this cut is ~ 600.

Figure 5.14 shows a rather flat behaviour of the MDF value against Λ (above -5.5). As a consequence the Λ value found to minimize the MRF is not far from the minimum value of the MDF. However, the optimal MRF cut shows a factor 2 loss in the detectable flux (proportional to the MDF) and the optimal cut for the MDF leads to a 3 times worse flux limit (proportional to the MRF). More over, these two approaches do not take into account the fact that we are

looking for common sources of GW and HEN. We conclude that none of these two approaches, often used in neutrino astrophysics, is fully satisfactory for our purpose. In the following section, we present a new optimization method that takes into account parameters from both GW and HEN data, as opposed to MRF and MDP approaches just described.

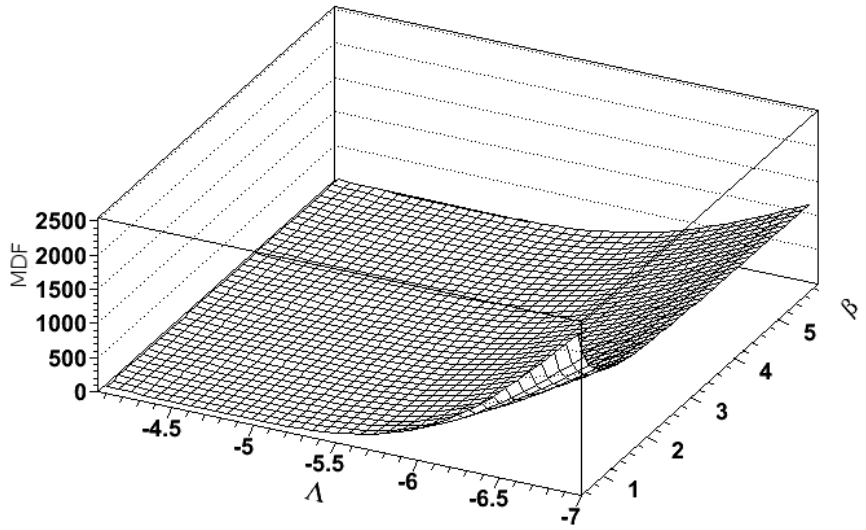

Figure 5.12 – The Model discovery factor in the two parameter space (β, Λ) for (3σ, 90%).

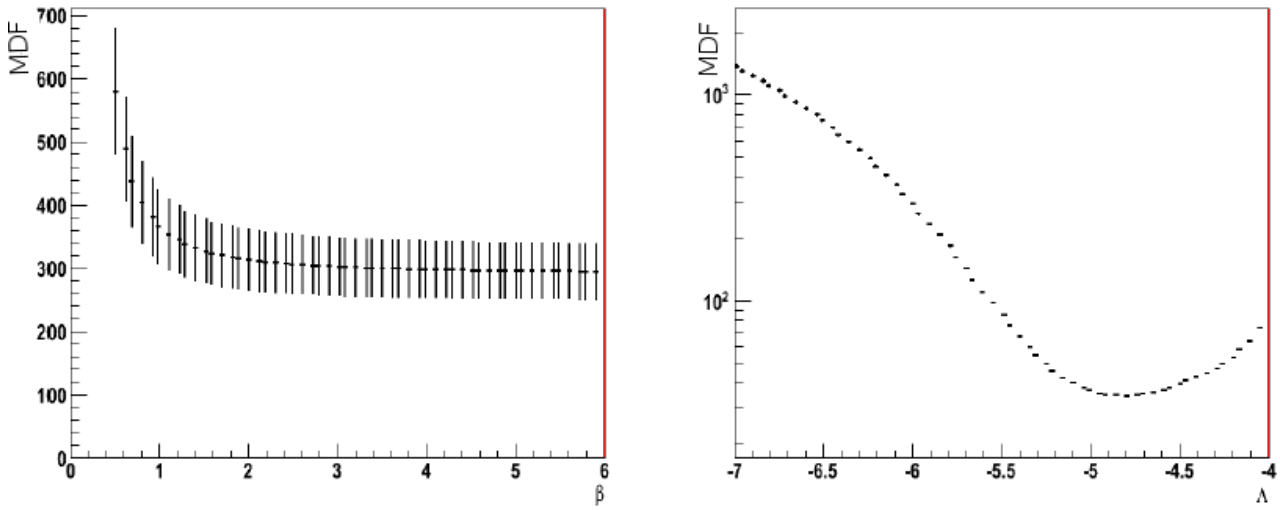

Figure 5.13 – Profile histogram of the MDF on β parameter (Left) and on Λ parameter (right).

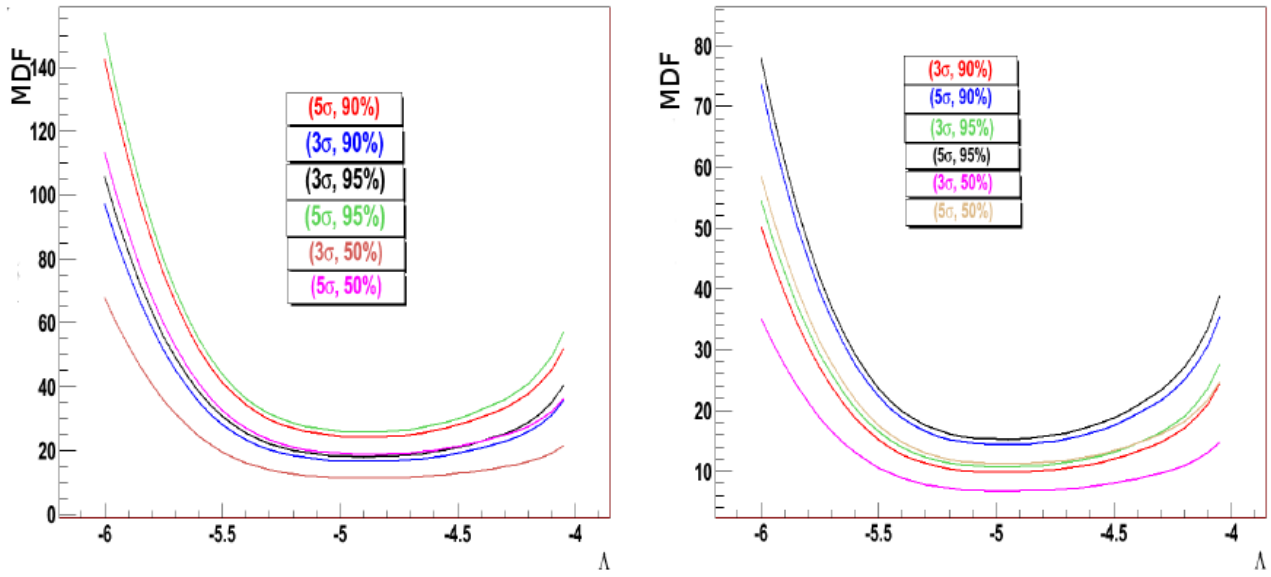

Figure 5.14 – The model discovery factor for different number of σ and cl as function of Λ, for W&B GRB diffuse flux (left) and E^{-2} flux (right). The curves show that the minimum of the MDF is independent of the number of sigma nσ and the C.L.

5.5 Description of the joint optimization strategy

The two selection procedures described above are not fully satisfactory since they only apply to the neutrino data and do not take into account the impact of the selection onto the GW search. Such independent selection criteria were used in the previous joint searches of HE neutrinos and GW (see chapter 4) leading to suboptimal searches. Here we propose a novel joint optimization procedure. The idea relies on the simple following arguments:

- The rational behind the concomitant search is to select as much as possible cosmic neutrino candidates and assess their cosmic nature by the observation of GW in time and space coincidence. In this view, the selection should leave large the efficiency to signal neutrinos which can be defined, by means of Monte Carlo simulations, as the ratio of selected events $N_{selected}$ (after cuts) over triggered events $N_{triggered}$:

$$\epsilon_\nu(\text{cuts}) = \frac{\text{N}_{\text{selected}}}{\text{N}_{\text{triggered}}} \tag{5.10}$$

  The cuts considered here are $cos\theta_{MC} \geq 0, cos\theta_{rec} \geq 0$. In order to increase ϵ_ν, loose cuts must be applied. This also considerably increases the number of selected background events.

- A too high number of these background events will result in an increased number of accidental coincidences FAR for a fixed set of cuts in the GW search. To avoid this situation, such triggered searches, are usually made with a fixed FAR. In order to keep this FAR constant, the higher the number of neutrino candidates to probe, the tighter the cuts should be applied on the GW side, leading to a poorer efficiency $\epsilon_{GW}(E_{GW}, r)$ for a given distance r and a model GW energy release. In other words this leads to a closer horizon for the GW search. In this case the probed distance for GW appears to depend on the neutrino selections cuts and one may write: $D \equiv D(cuts)$.

As a consequence, there should be a trade-off in these two approaches, which allows us to stick to the predefined FAR, with cuts that are optimal for the joint search.

5.5.1 Definition of the joint figure-of-merit

The approach adopted here is to apply the neutrino cuts to maximize the number $\mathcal{N}_{\mathrm{GWHEN}}$ of detectable sources emitting both GW and HEN. Let us assume that the sources are all identical and radiate E_{GW} in GW and emit a fluence φ_ν in HEN. Let us also assume that their population is isotropic so their density per unit time and volume R is a constant. The number of detectable sources is

$$\mathcal{N}_{\mathrm{GWHEN}}(\mathrm{cuts}) = \iint dt d^3\Omega\, \mathcal{R}(r,t)\epsilon_\nu(\mathrm{cuts})\epsilon_{GW}(\mathrm{cuts}; E_{GW}, r) \tag{5.11}$$

where $\mathcal{R}(r,t) = R\,\mathcal{P}(N_\nu > 0|\varphi_\nu/(4\pi r^2))$ is the density of detectable sources. From Poisson statistics, we get $\mathcal{P}(N_\nu > 0|\varphi_\nu/(4\pi r^2)) \propto 1/r^2$ in the limit of small fluxes.

The cuts being applied are connected to the methodologies in use for the muon track reconstruction on the HEN side and for the transient detection on the GW side. Those methodologies are detailed in section 5.3 for GW and in section 2.6 for HEN. We will optimize over the cut thresholds applied to the two following parameters: the quality of the muon track reconstruction Λ and a proxy to the signal-to-noise ratio ρ for the HEN and GW, respectively. We obtain

$$\mathcal{N}_{\mathrm{GWHEN}}(\Lambda, \rho_{threshold}) \propto \int_0^\infty 4\pi r^2 dr\, \frac{1}{r^2}\epsilon_\nu(\Lambda)\epsilon_{GW}(\rho_{threshold}; E_{GW}, r) \tag{5.12}$$

where we dropped the useless constants such as the global livetime τ of the experiment which results from the time integral.

The typical shape of $\epsilon_{GW}(\rho_{threshold}; E_{GW}, r)$ as a function of r for a given threshold and energy E_{GW} presents a rather sharp transition (less than a decade) from 100% to 0% (see e.g., Figures 3 and 4 of [15]). It can be reasonably well approximated by a step-like function with

the edge placed at the maximum distance $D(\rho_{threshold})$ at which a GW source is detectable, i.e., the GW *horizon*. Equation (5.12) can therefore be re-written as:

$$\mathcal{N}_{\text{GWHEN}}(\Lambda, \rho_{threshold}) \propto \epsilon_\nu(\Lambda) \int_0^{D(\rho_{threshold})} dr \tag{5.13}$$

The parameter $\rho_{threshold}$ sets a cut on the minimal detectable GW amplitude. For a GW "standard candle" emitted a given amount of energy in GW, it is inversely proportional to $D(\rho_{threshold})$. Therefore, we get

$$\mathcal{N}_{\text{GWHEN}}(\Lambda, \rho_{threshold}) \propto \epsilon_\nu(\Lambda)/\rho_{threshold} \tag{5.14}$$

As a conclusion, our aim is to tune the neutrino selection cuts in order to maximize the figure-of-merit given by the ratio $\epsilon_\nu(\Lambda)/\rho_{threshold}$.

5.5.2 Joint optimization procedure

We will now present the procedure for seeking the optimal cuts. Let the false-alarm probability FAP for the combined search be the probability of a fortuitous (time and spatial) coincidence of a GW and HEN background event. We define the working point of the optimization by setting a value for the FAP. Typically, we set FAP to 4.7×10^{-3} (which corresponds to a "2σ" excursion).

We scan the number N of neutrino candidates in the total livetime from a minimum to maximum value (typically from 10^2 to 10^4). There is a one-to-one correspondence between each selected N and a value for Λ. For each value of N, we compute the target GW false-alarm-rate FAR_{GW} from

$$\text{FAR}_{GW} = \frac{\text{FAP}}{N\Delta T}, \tag{5.15}$$

where ΔT is the duration of the temporal coincidence window (1000s).

We compute the GW background associated to a search triggered by N neutrino candidates. This is obtained thanks to the approximation using the all-sky GW background described in section 5.6.2. We deduce the value of $\rho_{threshold}$ for which the resulting background equals the target FAR_{GW}. At this point, the figure-of-merit defined in Equation (5.14) can be computed. The maximum value leads the optimal cuts for the considered range.

5.5.3 Dealing with non-stationary backgrounds

While an average signal neutrino efficiency $\langle\epsilon_\nu(\Lambda)\rangle$ valid for the full livetime period can be estimated, the GW background rate and sensitivity instead depends on the exact configuration

of the GW detector network which varies with time.

The whole livetime is divided into segments associated to a single configuration. Each period has a respective livetime τ_n such that the total livetime is $\tau = \sum_n \tau_n$. If we denote $f_n = \tau_n/\tau$, the respective livetime fraction, the average number of neutrino candidates falling in the segment n is therefore $N_n = f_n N$. Correspondingly, we divide the time integral in Equation (5.11) running over the whole livetime into segments

$$\mathcal{N}_{\mathrm{GWHEN}}(\mathrm{cuts}) = \sum_n \int_{\tau_n} dt \int d^3\Omega\, \mathcal{R}(r,t)\epsilon_\nu(\mathrm{cuts})\epsilon_{GW,n}(\mathrm{cuts}; E_{GW}, r) \tag{5.16}$$

Following the same steps described in section 5.5.1, we get

$$\mathcal{N}_{\mathrm{GWHEN}}(\Lambda, \rho_{threshold}) \propto \langle \epsilon_\nu(\Lambda) \rangle \sum_n f_n/\rho_{threshold,n} \tag{5.17}$$

where the thresholds $\rho_{threshold,n}$ corresponds to the false-alarm-rate $\mathrm{FAR}_{GW,n}$ for segment n.

The initial requirement on the FAP defines a global budget that has to be divided among the different segment analysis i.e., $\mathrm{FAP} = \sum_n \mathrm{FAP}_n$. It is natural to split this budget proportionally to the segment livetime, namely $\mathrm{FAP}_n = f_n \mathrm{FAP}$. In this setting, we thus have

$$\mathrm{FAR}_{GW,n} = \frac{\mathrm{FAP}_n}{N_n \Delta T} = \frac{\mathrm{FAP}}{N \Delta T} = \text{constant} \tag{5.18}$$

The overall optimization detailed in section 5.5.2 remains the same with the difference that $1/\rho_{threshold}$ is now replaced by $\sum_n f_n/\rho_{threshold,n}$.

5.6 Application of the joint optimization procedure

5.6.1 Efficiency to HEN

The first input to the joint optimization described above is the efficiency to neutrino candidates, i.e. ϵ_ν. It is obtained assuming the WB GRB diffuse flux (described in section 1.1.4) by means of MC simulations. The only parameter studied here is the quality of the reconstruction Λ, whose cumulative distributions are shown in Figure 5.15 for atmospheric muons, atmospheric neutrinos, and the studied WB flux of cosmic neutrinos. The MC distributions are compared to the data. The good agreement observed over the full range of Λ values allows us to proceed with the chosen optimization method. This agreement is obtained by applying a scaling factor of 0.8 to the atmospheric muons. Such correction is well within the uncertainty on theoretical

flux (30%) [16]. The obtained efficiency ϵ_ν is shown in Figure 5.16 as a function of the total number of selected events. The cuts considered here are $\cos\theta_{rec} \geq 0, \cos\theta_{MC} \geq 0$. The first cut ($\cos\theta_{rec} \geq 0$) permits to select events reconstructed as upgoing, while the second cut ($\cos\theta_{MC} \geq 0$) rejects those that are down-going reconstructed as upgoing (misreconstructed events). The inflection in the curves originates where the number of selected neutrino candidates starts to be dominated by misreconstructed atmospheric muons rather than atmospheric neutrinos.

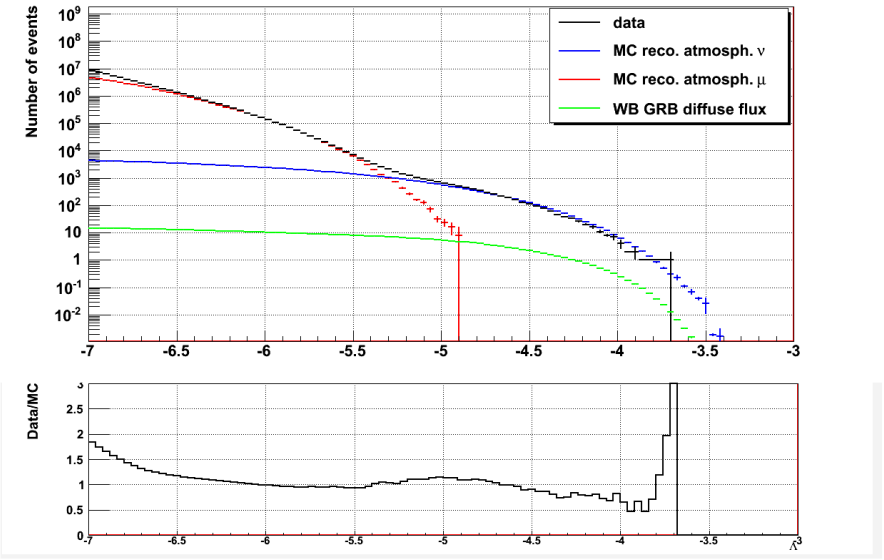

Figure 5.15 – Cumulative distribution of events, for the overall search period, as a function of Λ for the cuts described in the text. Curves of data and MC atmospheric muons and neutrinos are plotted. The distribution corresponding to the WB GRB diffuse flux is shown in green curve

The contamination (by atmospheric muons) and purity (with respect to the atmospheric neutrino sample) are shown as a function of number of neutrinos candidates in Figure 5.17.

5.6.2 Approximation of the GW background

Using s-cWB for the background estimation necessary for the cut optimization would be too much time consuming, due to high number of neutrino trials. Instead, we decided to approximate the background associated to the neutrino candidates by using the all-sky background(s).

If the GW background events are isotropically and Poisson distributed, it is easy to show that the background rate of triggered search should be rescaled by a factor $\sim (\Omega_{GW}^{1/2} + \Omega_{HEN}^{1/2})^2/(4\pi)$ where Ω_{GW} and Ω_{HEN} are the solid angles under the GW and HEN error-boxes (or PSF) respectively. This factor essentially results from an estimate of the probability that those two error boxes overlap if their central directions is chosen at random. The HEN error box

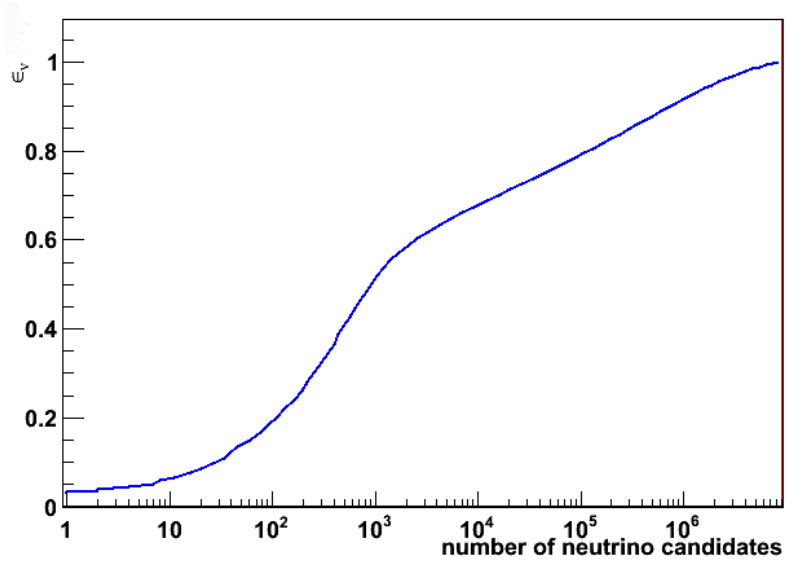

Figure 5.16 – Efficiency to neutrino candidates for WB GRB diffuse flux.

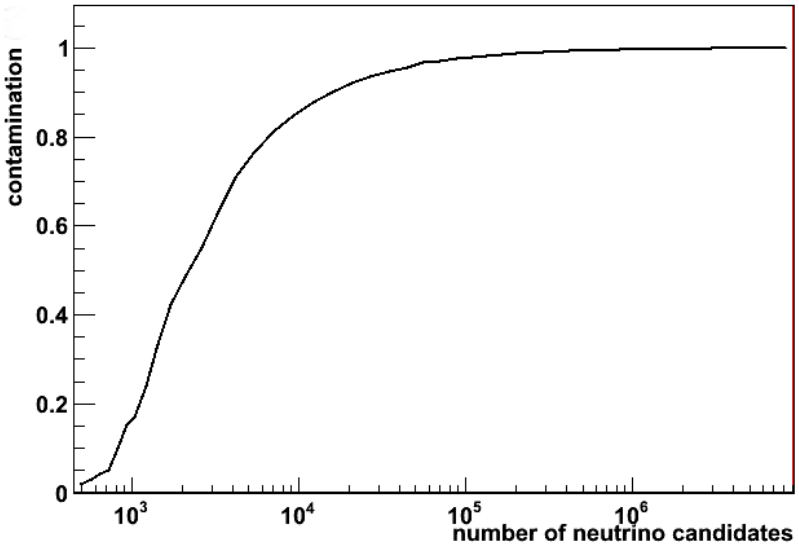

Figure 5.17 – Muon contamination of the neutrino sample for upgoing events in function of the number of candidates.

$\Omega^{1/2}_{HEN} = \sqrt{\pi}$ASW90% depends on the cut applied for the muon track reconstruction. In particular, it is a function of Λ and hence of N, the number of neutrino candidate. Ω_{GW} depends on the configuration of the GW detector network. We estimated that on average the sky map of a background event covers about 425 square degrees, which corresponds to a circular

region of radius about 12 degrees.

We checked this approximation with a Monte-Carlo simulation using a set of GW background triggers obtained for the all-sky S6A/VSR2 analysis. We cross-correlated many times these triggers with a random set of neutrino candidates of variable size. The backgrounds we obtain with this simulation are in rough agreement with the prediction obtained by rescaling the original all-sky background. However an additional factor is necessary to get a good fit of the joint predicted background. This factor estimated heuristically is $\sim aN+b$ where $a \approx 10^{-4}$ and $b \approx 0.5$ and N is the number of neutrino candidates. The result of background distributions is shown in Figure 5.18.

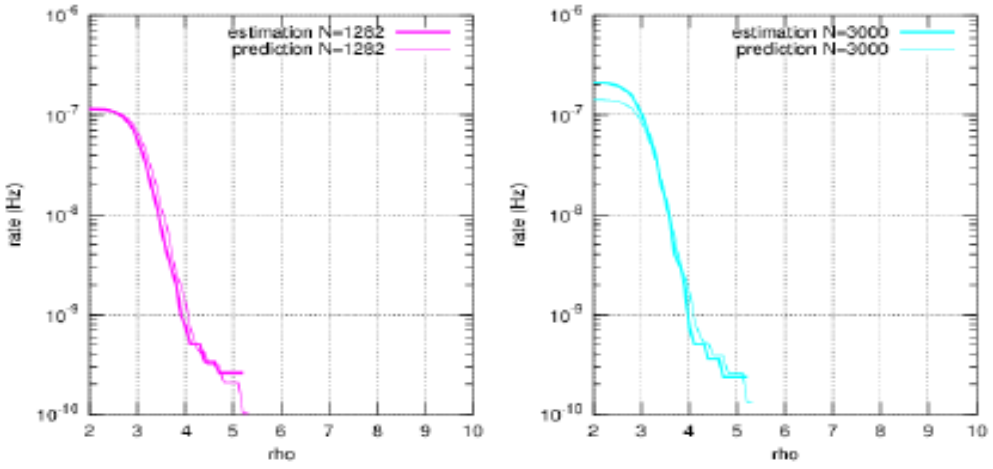

Figure 5.18 – Background distributions of the network correlated amplitude ρ for triggered search obtained by rescaling all-sky backgrounds

5.6.3 Results of the optimization

Study without cut on β

In this section, we summarize the results of the optimization procedure detailed in section 5.5.2. For simplicity, we restricted the optimization to periods with three operating GW detectors which is the most sensitive part of the data set. This corresponds to three separate runs labelled {"S6A/VSR2","S6B/VSR2", "S6D/VSR3"}. This corresponds to the respective livetimes τ_n ={6.9 days, 13.7 days, 24.1 days} and livetime percentages f_n ={5.36 %, 10.64 %, 18.72%}.

We use the approximation scheme described in the previous section 5.6.2 to compute the GW backgrounds for various N. The rescaling uses the neutrino angular window ASW$^{90\%}$ as a function of Λ parameter as shown in Figure 5.19. We deduce $\rho_{threshold,n}$ and the figure-of-merit

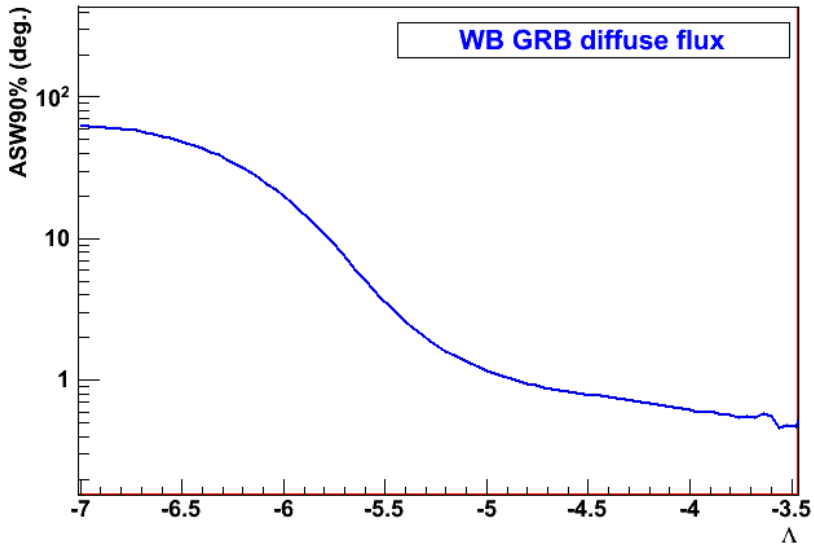

Figure 5.19 – The ASW90% used to estimate the GW background from the all-sky one. No cut on β is applied.

in Equation (5.17). Those quantities are shown as functions of the *total* number N of neutrino candidates (for the entire ANTARES livetime $T \approx 266$ days) in Figure 5.21. This number of neutrinos is taken from the data set and not from the MC sample. As such we are less dependent on the MC simulation and avoid problems of low statistics in the atmospheric muon MC sample. We see in Figure 5.20 that $\rho_{threshold,n}$ increases as a function of N as expected.

The number N of candidates (Λ) for the whole observation time τ that maximises the FOM is 3279 (-5.4). The angular search window is significantly better ASW90% = 2.6 degrees than the one used in 2007 joint search. In addition the efficiency ϵ_ν increases to about 62%.

Study against β parameter

The results presented in the previous section were obtained without any cut on the angular error estimate, β, of the reconstructed track. In this section we present an additional study by considering cuts on β. We choose the following cuts on $\beta < \{0.6°, 1°, 1.4°\}$ (see Figures 5.22).

The table 5.1 shows the atmospheric muon contamination, FOM and total number of candidates corresponding to the optimal $\{\Lambda, \beta\}$ cuts. The best FOM and hence sensitivity is obtained with no cut on β. However increasing the number of candidates leads to serious difficulties. Above of the order of 2000 candidates the estimation of GW background gets at the same time computationally very heavy and more difficult to estimate. Indeed, with growing number of candidates, the GW data segments used to estimate the background ρ distributions will begin

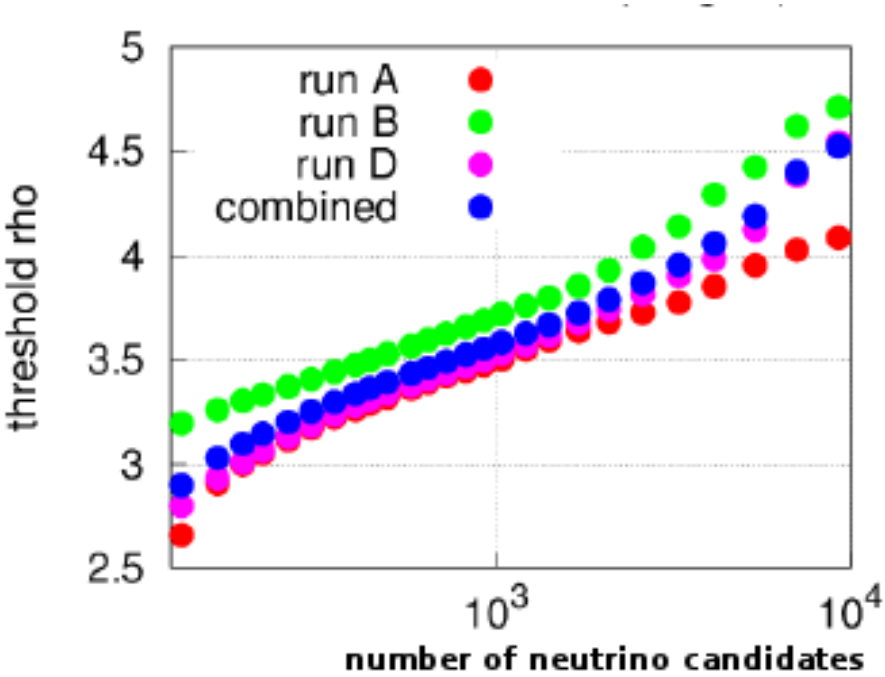

Figure 5.20 – Distributions of ρ as function of the number of neutrino candidates for the different GW data taking periods considered.

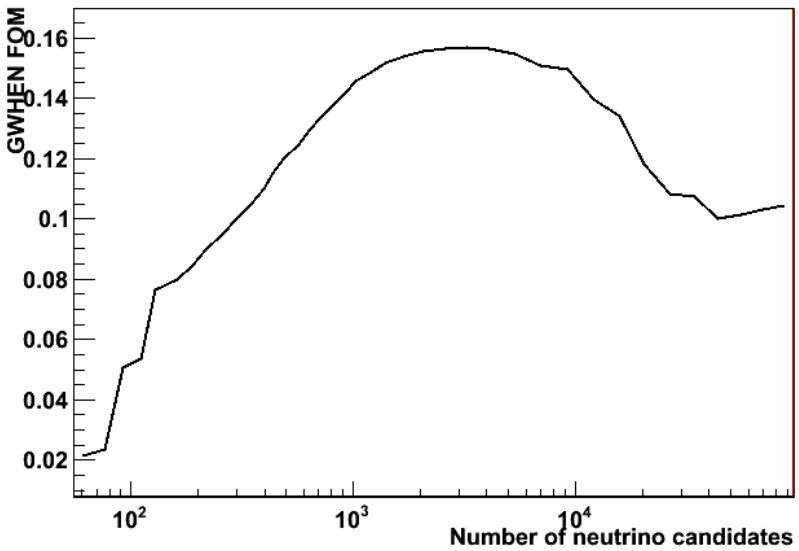

Figure 5.21 – FOM as a function of the number of neutrino candidates N without cut on β.

to overlap and correlation will appear. Given that with a β cut at 1 degree the loss in number of detectable sources (which is proportional to FOM) is just 2% with an affordable number of

candidates, we set the final cut values at $\Lambda > -5.44$ and $\beta < 1$. This can also be qualitatively justified by the fact that the contamination by atmospheric muons grows by 20% between $\beta < 1$ and no β cut. Since meanwhile the neutrino efficiency just marginally grows by 5%, most of the additional neutrino candidates brought by the reduction of the strength of the β cut will be mis-reconstructed atmospheric muons which will just make the GW background estimation more difficult.

$\Lambda >$	$\beta <$	Contamination (%)	ϵ_ν (%)	FOM	$ASW90\%$ (deg.)	MC N_ν	Data N_ν
-5.60	0.6	40.36	50	0.1358	1.3	1645	1699
-5.44	1.0	44.24	57	0.1525	1.7	1971	1986
-5.44	1.4	57.12	60	0.1547	2.0	2717	2633
-5.40	No cut	63.27	62	0.1564	2.6	3224	3279

Table 5.1 – Results of the joint optimization in term of FOM for each cut on Λ and β.

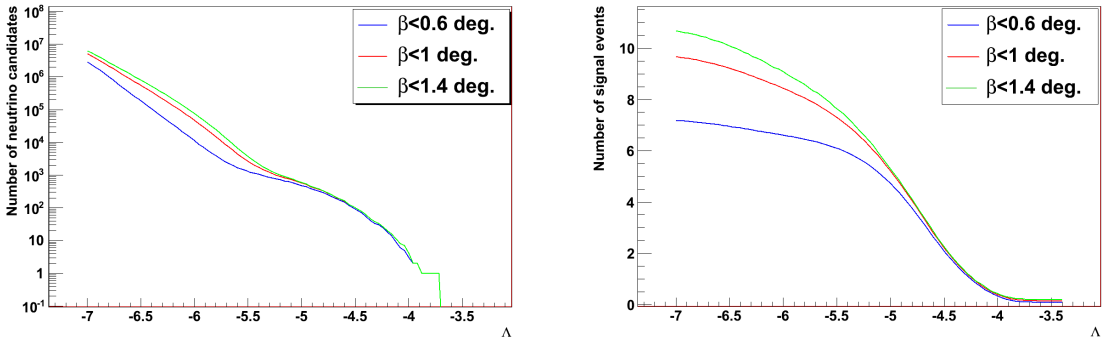

Figure 5.22 – Number of neutrino candidate events (Left) and signal WB GRB diffuse flux events (right) as function of Λ for different cuts on β

We compare Figure 5.25(left) the effective areas obtained with these different cuts and the one obtained with the cuts of the Point Source search ($\Lambda > -5.2$ and $\beta < 1°$). Figure 5.25(right) shows for comparison the ratio between the effective areas obtained in this work to the one obtained with the cuts applied in the search for the point sources [17]. We can see that the final set of cuts of this work gives a gain in effective area between 50% at low energy and almost 20% at high energy.

5.7 List of neutrino candidates

We present in this section the result obtained after applying the optimized cuts described in the previous sections. The list obtained consists in $N = 1986$ neutrino candidates.

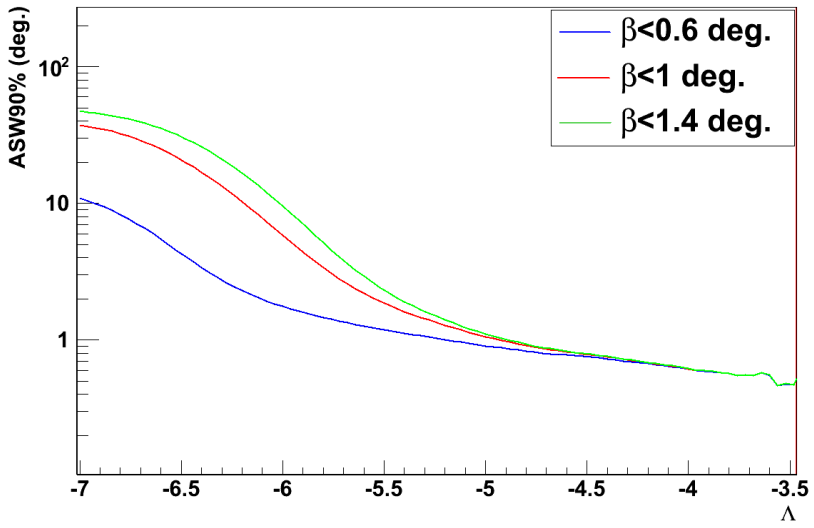

Figure 5.23 – Angular search window ($ASW90\%$) as function of Λ for different cuts on β

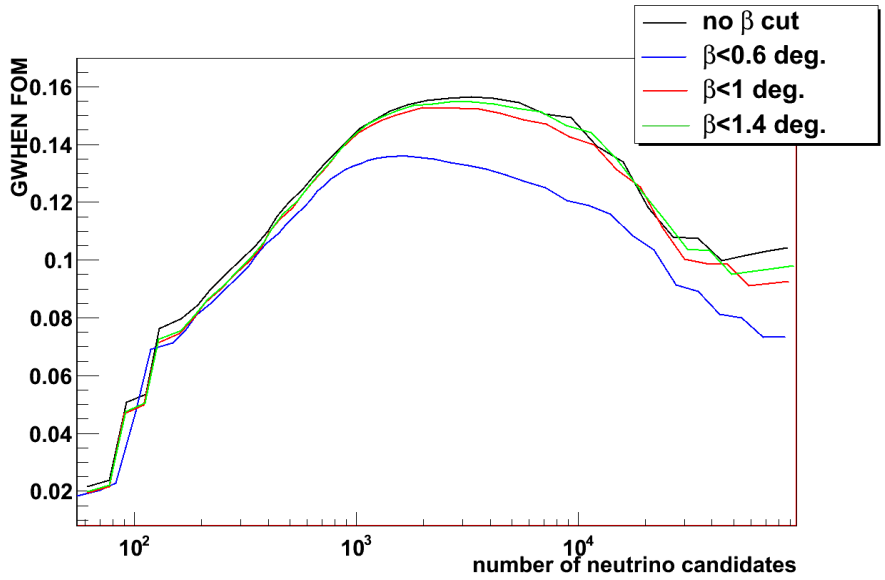

Figure 5.24 – Distribution of GWHEN FOM as a function of the number of neutrino candidates N, for different cuts on beta

The result consists in a list of neutrino candidates. Each of them is characterized by its arrival time, sky direction and associated error box. The following notations are adopted:

- Time t_i is given in Julian Day (or GPS)
- Reconstructed direction of the event $\overrightarrow{\mathbf{d}}_i = (\alpha_i, \delta_i)$ is given in equatorial coordinates, i.e. right ascension and declination. The skymap of the selected candidates is shown in Figure

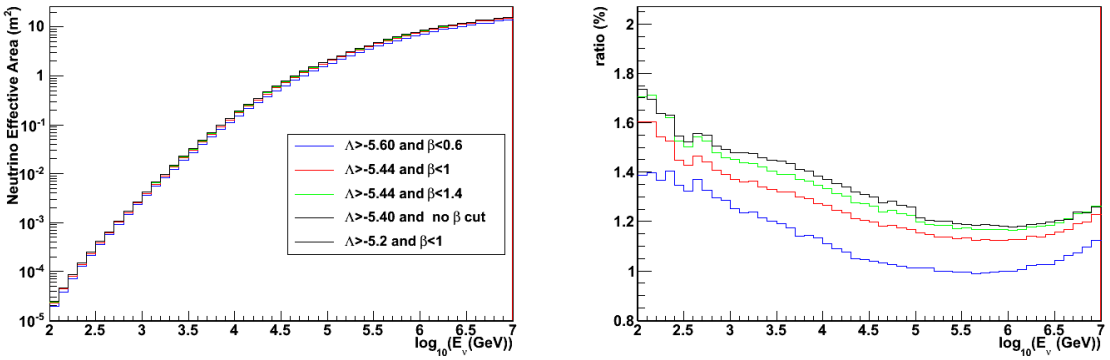

Figure 5.25 – Left: Neutrino effective areas as a function of neutrino energy. Right: ratio between GWHEN effective areas (corresponding to the different cuts in the text) and point-source one (after applying the corresponding cuts) as a function of neutrino energy.

5.26 in equatorial coordinates.

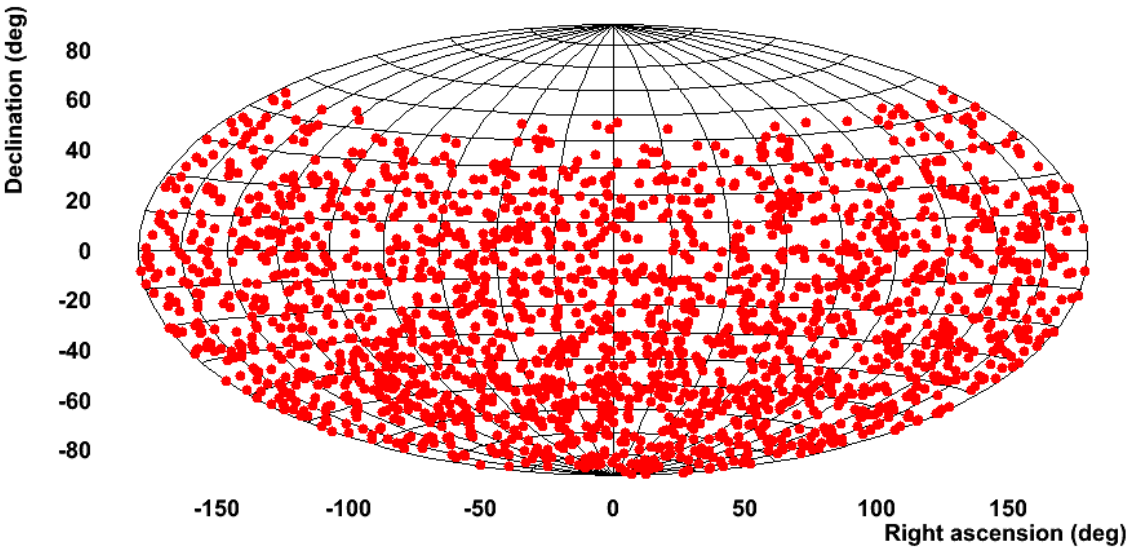

Figure 5.26 – Skymap of the final neutrino candidates selected for the analysis. The skymap is shown in equatorial coordinates.

- Energy estimator, given as the number of hits (or n^{hit}) used in the track fit. The distribution of the number of hits for data and MC is shown in Figure 5.27.

- ASW^{90}_{GWHEN} is a circle on the sky sphere with radius the 90% percentile of the distribution of space angles ψ between the reconstructed muon and the MC neutrino direction. It is computed from MC neutrino ANTARES simulation with the same selection cuts applied

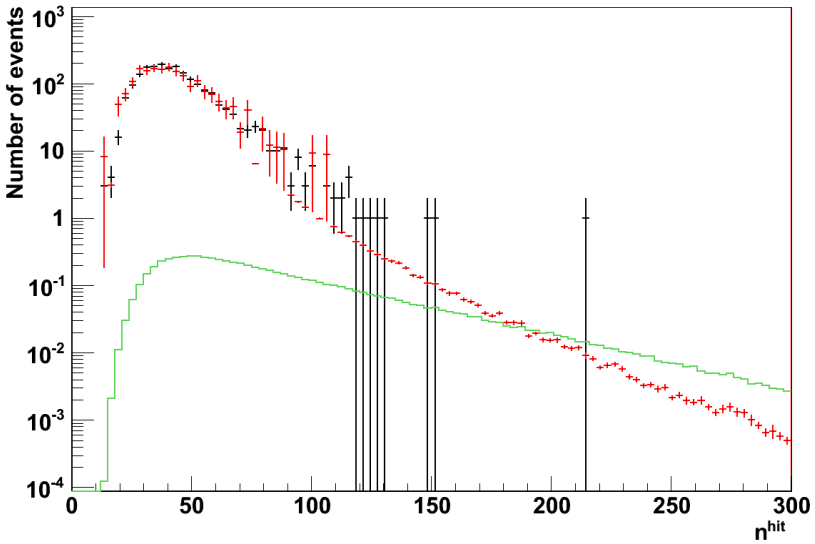

Figure 5.27 – Distribution of the number of hits used as proxy energy in this search. The black curve is the data, the red is the MC atmospheric background and the green is the MC distribution obtained for the WB GRB diffuse flux.

as that for the joint optimization and with an event weighting following the Waxman Bahcall GRB diffuse flux. This distribution is fitted with a log-normal function as defined hereafter:

$$P(\psi) = \frac{1}{\sqrt{2\pi}} \frac{\exp[-ln(\psi/m)^2/2\sigma^2]}{\sigma\psi} \tag{5.19}$$

where m and σ are respectively the so called scale and shape parameters. It can be linked to the neutrino bi-dimensional point spread function (PSF),

$$\mathcal{F}_i^{\mathrm{HEN}}(\vec{\mathbf{d}}) \equiv P(\vec{\mathbf{d}}\,|\vec{\mathbf{d}}_i) \propto \frac{1}{sin(\psi_i(\vec{\mathbf{d}}))} \frac{\exp[-ln(\psi_i(\vec{\mathbf{d}})/m)^2/2\sigma^2]}{\sigma\psi_i(\vec{\mathbf{d}})} \tag{5.20}$$

where $\psi_i(\vec{\mathbf{d}})$ is the space angle between the directions $\vec{\mathbf{d}}$ and $\vec{\mathbf{d}}_i$. An example of this point spread function can be seen on Figure 5.28.

In practice ASW^{90}_{GWHEN} (or equivalently $\mathcal{F}_i^{\mathrm{HEN}}$), m and σ can depend on several parameters like Λ (see Figure 5.19), the arrival direction of the neutrino, the number of hits, or the angular reconstruction error parameter β. Figure 5.29 shows the median of the space angle distribution as a function of declination. This quantity is to a good approximation independent of the declination and hence its variation with declination will not be used further to characterize events.

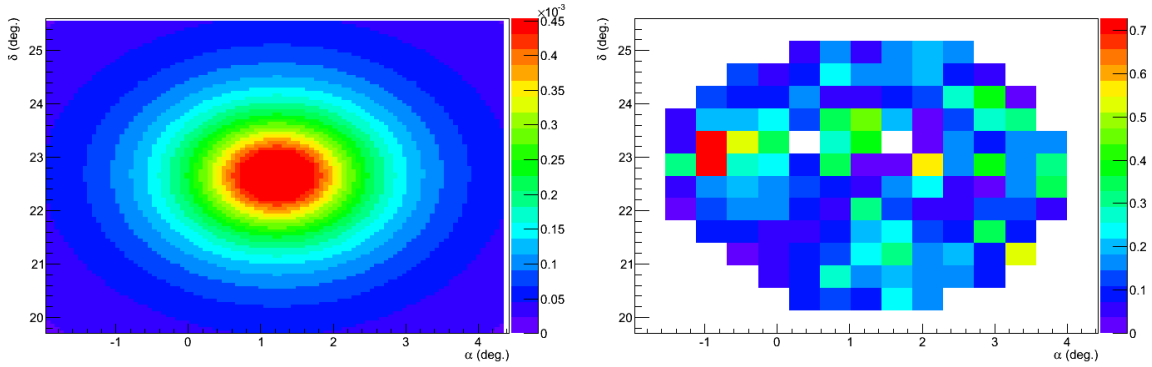

Figure 5.28 – Example of the neutrino PSF (left) and the corresponding GW skymap (right).

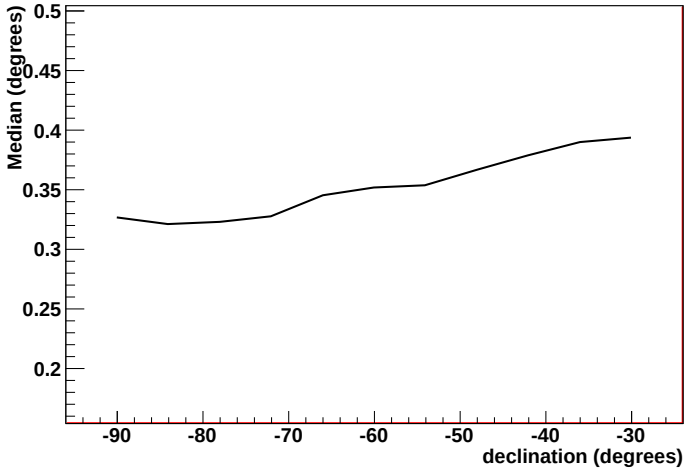

Figure 5.29 – The angular search window for 50% percentile as function of declination.

5.8 Procedure for the event post-processing and joint statistical treatment

The statistical analysis of the outcome of the joint search is based on the original proposal from [18], but different aspects are adapted to cope with the specificities of our study, in particular the use of sky masks (with typical size of a few squared degrees) in s-cWB.

Below we describe the different steps and define the relevant quantities that will be used in the final statistical treatment as well as in the estimation of the sensitivity and discovery power of the search.

The goal is to construct a test statistics based on the characteristics of each neutrino event

and its associated GW trigger and to compute their joint p-value (or equivalently their excess significance) relying on pseudo-experiment realizations of the search with no signal injected. The discovery potential will then be estimated with the same method but using pseudo experiments containing neutrinos following a WB energy spectrum and associated to GW signal injections. The pseudo experiments will be based on the neutrino characteristics and the combined test statistic described in sections 5.8.1 and 5.8.4.

5.8.1 Statistical characterisation of the neutrino candidates

In addition to the neutrino characteristics described above we compute the p-value of the neutrino event, denoted p_i^{HEN}. Since these will be considered independently, atmospheric and potential cosmic neutrinos differ only by their energy spectrum. As shown in Figure 5.30, we will use the simple energy estimator given by the number of hits n^{hit} of the reconstructed track. The p-value, i.e. the probability that the atmospheric background would produce an event with at least the number of hits of the considered event, is defined as:

$$p_i^{\mathrm{HEN}} = \frac{\int_{n_i^{hit}}^{\infty} P(n^{hit}) dn^{hit}}{\int_0^{\infty} P(n^{hit}) dn^{hit}} \tag{5.21}$$

where n_i^{hit} is the value corresponding to the event i and P the corresponding probability density function (or equivalently the not normalized distribution).

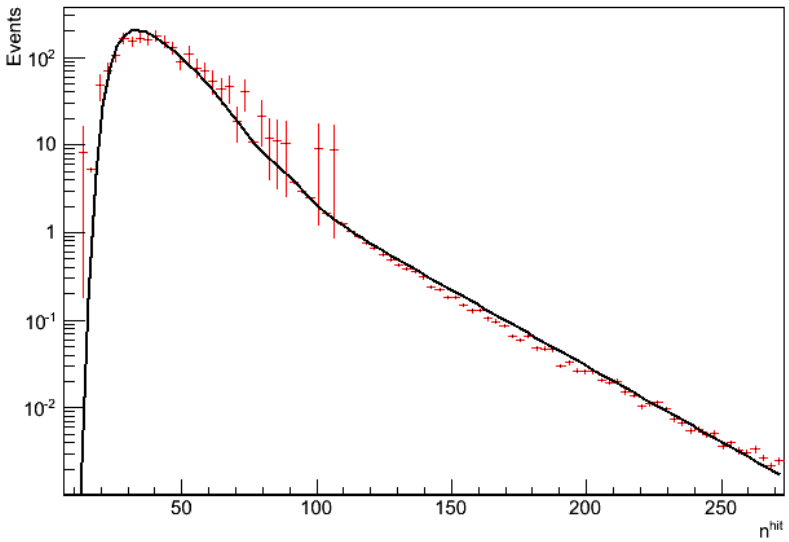

Figure 5.30 – Distribution (modified as described in the text) of n^{hit} together with the function used to fit it and evaluate the corresponding p-values.

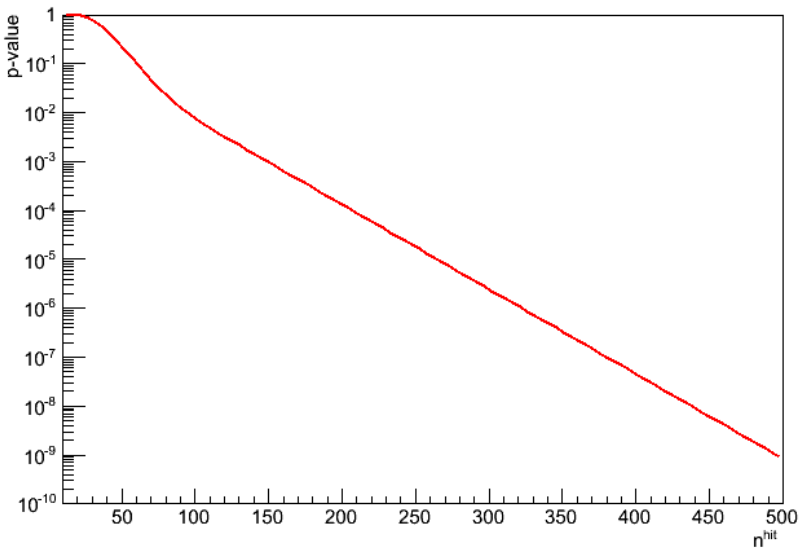

Figure 5.31 – Distribution of the HEN p-value as a function of n^{hit} estimated from MC simulation as defined in equation 5.21.

In practice the computation can be made with Monte Carlo simulations extrapolated to high values of n^{hit} if needed. Considering the overall contamination of atmospheric muons in the final sample (44%) and in order to compensate for the lack of statistics in the atmospheric muon simulation in the n^{hit} >100 region we conservatively choose to apply a penalty factor for the p-values obtained in the $n^{hit} > 100$ region. This is achieved by multiplying the atmospheric neutrino distribution by 1.7 in the considered $n^{hit} > 100$ region. The validity of this approach has been checked by relaxing the cuts and verifying the shape consistency of the muon and neutrino samples. The modified simulated n^{hit} distribution has been fitted with the following function:

$$P_{n^{hit}}(x) = exp(\sum_{n=0}^{4} p_n x^n) 1/(1 + exp(-p_5(x - p_6)))p_7 exp(p_8 x) \tag{5.22}$$

where p_n, n $\in$ [0, 8] are the fit parameters. The result is presented in Figure 5.30. The p-value as a function of n^{hit} can then be computed by numerical integration and is displayed in Figure 5.31.

Figures 5.32 and 5.33 show the local coordinates of the neutrino triggers together with the fitted functions which will be used to generate the pseudo experiments. The latter also allow us to draw the analysis exposure map, which is presented in Figure 5.34 in galactic coordinates.

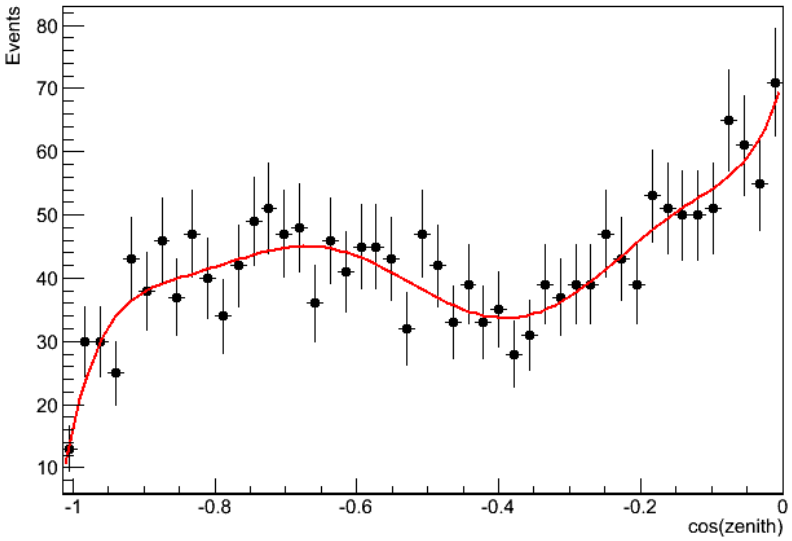

Figure 5.32 – Normalized distribution of the zenith angle for data together with the 7 degree polynomial used to fit it.

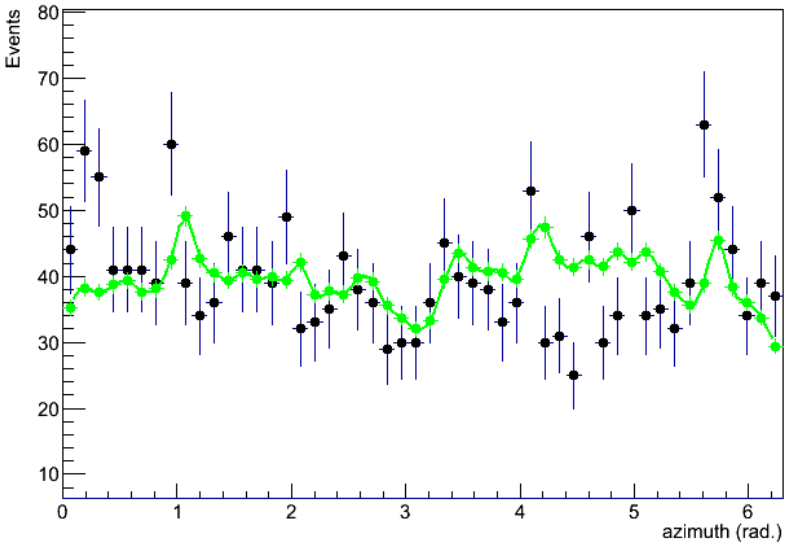

Figure 5.33 – Distribution of the azimuth for data together with the spline function used to parametrize it. This spline has been fitted on the neutrino Monte Carlo simulation (green points).

5.8.2 Statistical characterisation of the GW reconstructed events

For each of the selected neutrino events, s-cWB performs a search for GW around the neutrino time. The whole sky is not scanned but only the region corresponding to ASW90% centered on

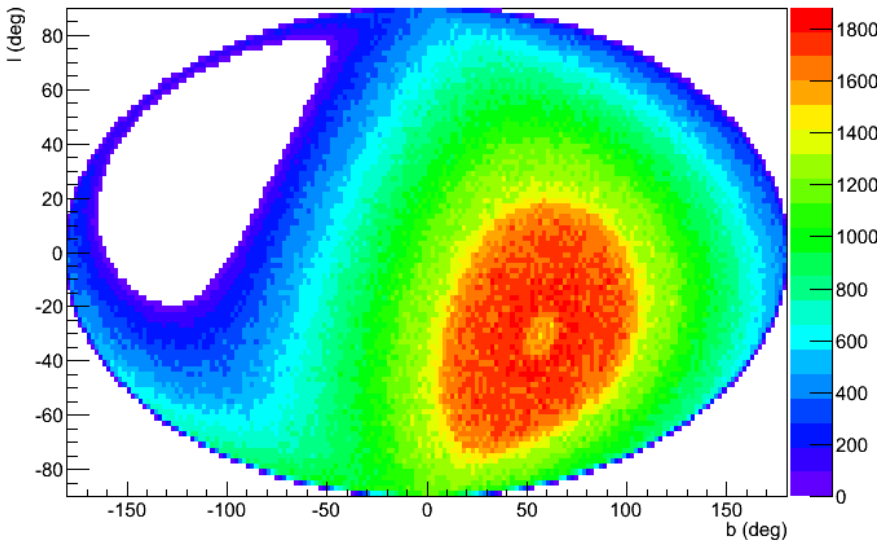

Figure 5.34 – Relative sky exposure map (arbitrary units) of ANTARES corresponding to the selected neutrino sample in Galactic coordinates.

the reconstructed arrival direction of the neutrino $\overrightarrow{\mathbf{d}_0}$. For each candidate, s-cWB will provide the GW skymap (SP) labeled hereafter $\mathcal{F}_i^{\mathrm{GW}}(\overrightarrow{\mathbf{d}})$ within ASW90% (see Figure 5.28 right for an example). These "sky-maps" will be made of pixels of $0.4° \times 0.4°$ each associated with the probability that a GW is coming from it. The following parameters, of each GW candidate, are provided by the s-cWB. The arrival time, the reconstructed sky location (θ, ϕ) in the Earth fixed frame with $\phi = 0°$ corresponding to the Greenwich Meridian, $\theta = 90°$ corresponding to the equator. Also it provides the value of ρ for each GW candidates. This latter will correspond to a false alarm rate $\mathrm{FAR_i}(\rho_\mathrm{i})$ as defined in sections 5.5.2 and 5.5.3. This will lead to a GW p-value indicating what is the probability that coherently combined GW interferometers background produces an event with at least this value of ρ_i, defined as:

$$p_i^{\mathrm{GW}} = 1 - P(0|\tau_i \times \mathrm{FAR_i}(\rho_i)) \tag{5.23}$$

where τ_i is the duration of the GW interferometers run corresponding to event i (see sections 5.5.2 and 5.5.3). The distributions are computed using $O(10^3)$ background realisations obtained with time shifts. The background distributions ρ of all detector configurations and run periods are presented in Figures 5.35 and 5.36. The corresponding p-value evolution for S6A run is shown in Figure 5.37.

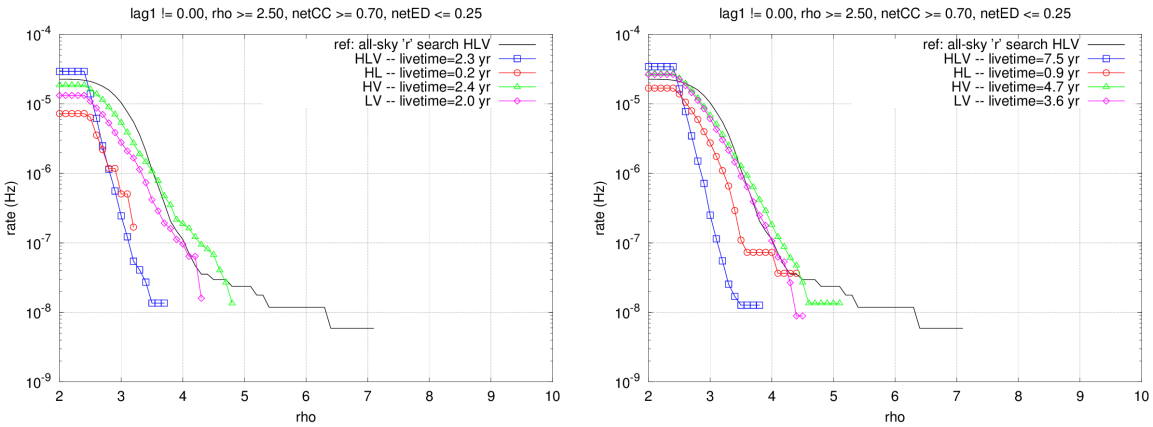

Figure 5.35 – Background estimate of the network correlated amplitude ρ for triggered search. Left: for the S6AVSR2-3 segments. Right: for the S6B segments

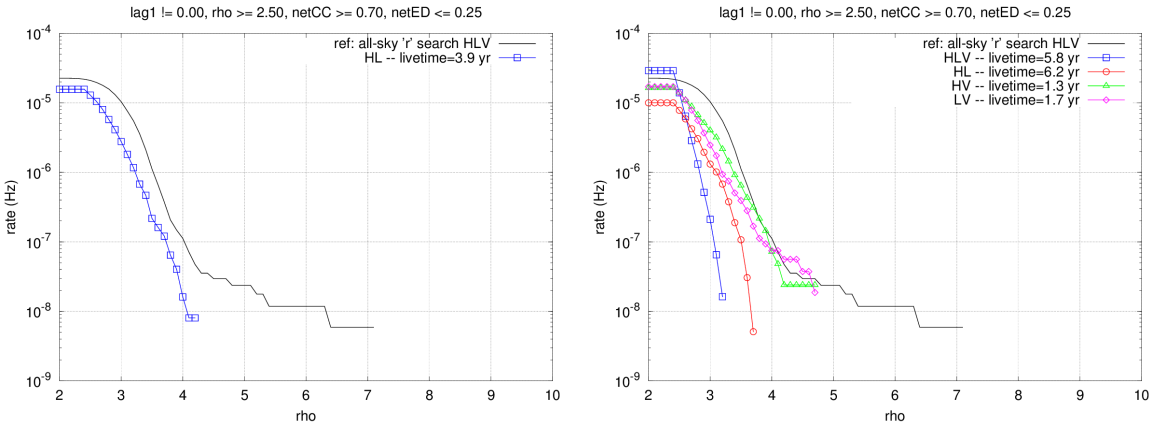

Figure 5.36 – Background estimate of the network correlated amplitude ρ for triggered search. Left: for the S6C segments. Right: for the S6D segments

5.8.3 Statistical characterisation of the joint candidates

The direction of the joint candidate event can be defined as the one maximizing the product of the HEN PSF and the GW SP: $\mathcal{F}_i^{\mathrm{GW}} \times \mathcal{F}_i^{\mathrm{HEN}}$.

The joint directional test statistic will rely on the marginalized likelihood of the joint event which is defined as:

$$ln(\mathcal{L}_i) = \int \mathcal{F}_i^{\mathrm{GW}}(\vec{x}) \times \mathcal{F}_i^{\mathrm{HEN}}(\vec{x}) d\vec{x} \tag{5.24}$$

Figure 5.38 shows an example of the joint likelihood. Figure 5.39 shows the distribution of P_{bg} of $\ln(\mathcal{L})$ for background estimated with the S6A data for three interferometers together with a Gaussian fit.

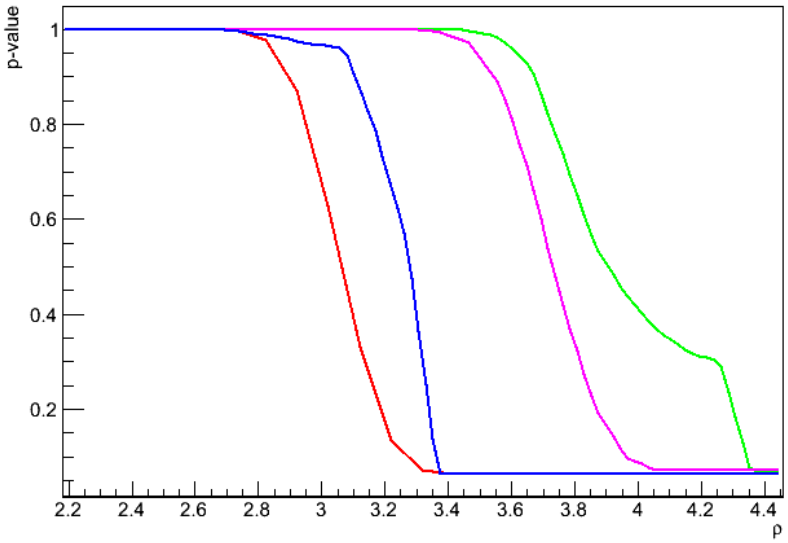

Figure 5.37 – The p-value as a function of ρ corresponding to S6A data and differents detector configurations HLV (bleu), HL (red), HV (green) and LV (magenta)

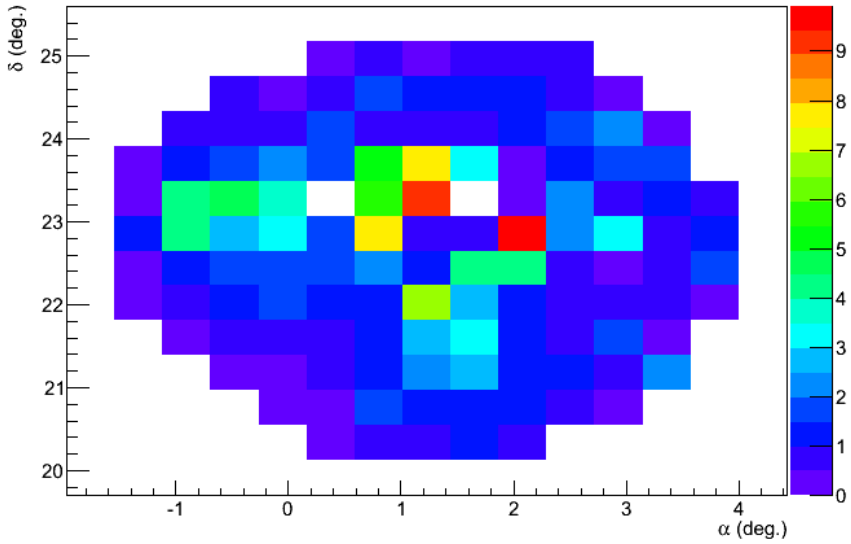

Figure 5.38 – Example of the joint likelihood obtained with the product of GW SP and HEN PSF

The p-value corresponding to the combined PSF-likelihood will be defined as:

$$p_i^{sky} = \int_{\mathcal{L}_i}^{\infty} P_{bg}(ln(\mathcal{L}))d\mathcal{L} \tag{5.25}$$

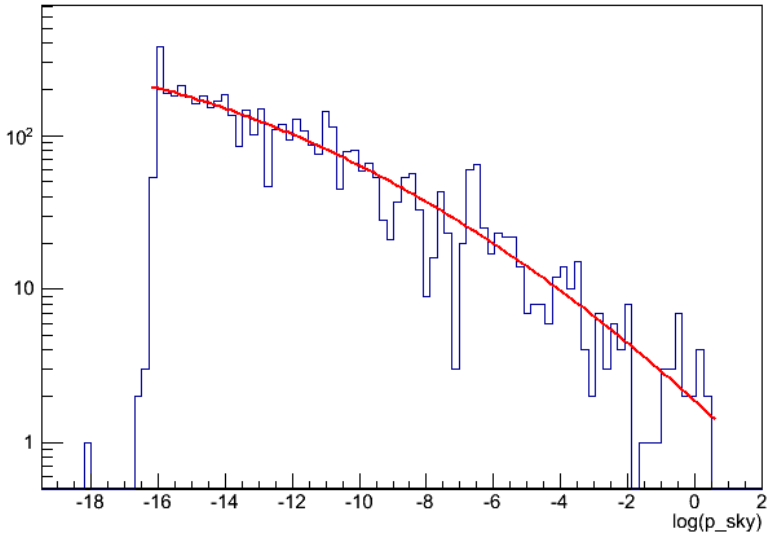

Figure 5.39 – Distribution of $ln(\mathcal{L})$ for background estimated with the S6A data for the detector network. The red curve corresponds to a Gaussian fit

and is determined by numerical integration of the fitting function. A dedicated fit will be performed for each S6 period and each interferometer configuration independently.

5.8.4 Final test statistic

All these p-values can be combined using Fisher's method [19] to construct a test statistic for each event i:

$$X_i^2 = -2\ln(p_i^{sky} \times p_i^{\mathrm{GW}} \times p_i^{\mathrm{HEN}}) \tag{5.26}$$

This variable behaves like a χ^2 with 6 degrees of freedom in case variables are independent. But since this is not guaranteed here and since p^{GW}, p^{HEN} and p^{sky} may not behave as proper p-values (i.e. be independently uniformly distributed in [0;1]), the significance of the final outcome of the search will be computed thanks to pseudo-experiment Monte Carlo realisations. In order to do so, the background probability density function of X^2 will be fitted for each S6 period and interferometer configuration. Figure 5.40 shows, for the particular case of S6A run and 3 interferometers configuration, the background distribution of the X^2 variable. It has been fitted with a "scaled χ^2" with 6 degrees of freedom and a general Γ distribution. The two functions obey to the following formula:

$$f(x;k;\theta) = \frac{1}{\theta^k}\frac{1}{\Gamma(k)}x^{k-1}e^{-x/\theta} \tag{5.27}$$

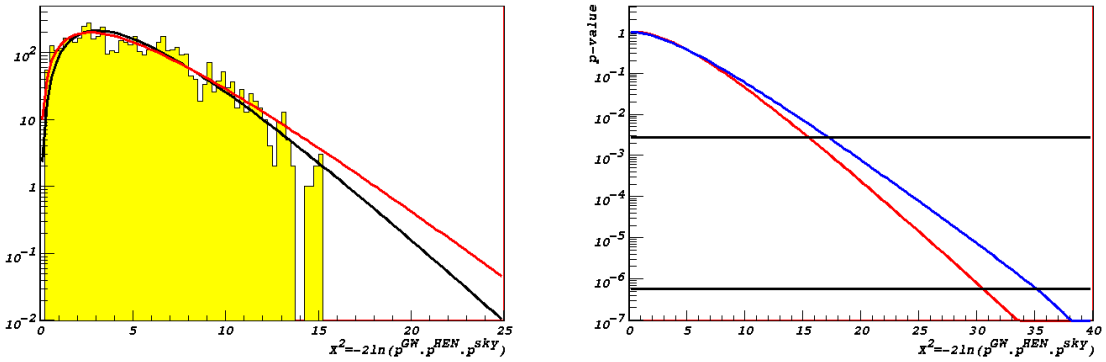

Figure 5.40 – Left: Background distribution of the X^2 for S6A with three interferometers. The black line is the scaled χ^2 and the red one the Γ distribution (see text). Right: corresponding p-value evolution of the Γ distribution (red) and scaled χ^2 (blue) together with lines corresponding to 3 (upper) and 5 (lower) sigma confidence levels.

The scaled χ^2 distribution has k=3 (from the 6 degrees of freedom), free θ (the scale parameter) and the fit gives a χ^2 per degree of freedom of 8.2. The general Γ distribution has both parameters free and the fit gives a slightly worse χ^2 per degree of freedom of 8.5. However, given the corresponding p-values evolution, displayed on the right panel of Figure 5.40, the most conservative choice for the pseudo experiments generation is the Γ distribution. The final result of the search will be the p-value of its most significant event i and is defined as:

$$p^{\mathrm{GWHEN}} = \int_{Max(X_i^2)}^{\infty} P_{bg}(max(X^2))dX^2 \tag{5.28}$$

where the probability density function $P_{bg}(max(X^2))$ is the result of Monte Carlo simulation of pseudo experiments of 1986 joint triggers.

5.8.5 Estimation of the horizon of detection

The detection horizon $D_{50\%}^{HEN}$ and $D_{50\%}^{GW}$ of each detector for a given model can be defined as the maximum distance for which there is at least a 50% chance probability that the signal would be detected. The common GW+HEN horizon will thus be:

$$D^{\mathrm{GWHEN}} = Min(D_{50\%}^{\mathrm{HEN}}, D_{50\%}^{\mathrm{GW}})$$

On the HEN side the horizon corresponds to the maximum distance at which there is a 50% chance probability to have at least one neutrino detected in ANTARES. On the GW side, the procedure is to generate a list of neutrinos with only one having the characteristics of a signal (i.e. with a WB n^{hit} distribution as shown by the green curve in Figure 5.27). This neutrino

has to be associated with a p_i^{GW} corresponding to an injected signal. This is repeated many times and the probability of detection will be the ratio of the number of realisations where $max(X_i^2)$ has a p-value lower than the threshold fixed at the end of last section. This detection power will correspond to the intensity of the GW injected in the data. An other interesting quantity would be to inject more and more signal neutrinos at a fixed GW signal intensity and see when the probability is above 50 percent. Once the GWHEN horizon is determined source population limit estimates will be set following the reasoning of section 4.7.

5.9 Conclusion

In this chapter we have described the second GW+HEN joint analysis using coincident data taken in 2009-2010 from the ANTARES neutrino telescope and the Virgo/LIGO GW interferometers. In particular we have detailed the methods specifically developed for this search. The joint optimisation procedure on GW and HEN data has led to a list of 1986 neutrino candidates maximizing the number of detectable joint sources. These neutrino events have been completely characterized with the main parameters needed for the coincidence search with GW (see section 5.7). Of these neutrino events, 775 candidates are associated with 2 or 3 interferometer configuration (i.e., HLV: 303, HV: 147, LV: 135 and HL: 190 neutrino candidates).

At the time of submission of this document, the analysis was not completed, some GW data processing being still necessary before launching the pseudo-experiment Monte Carlo simulations needed to set the final joint results. However, all technical steps and ingredients were well defined and presented in this chapter. The final results will be presented in a dedicated paper.

The analysis presented in this chapter has been obtained with improved algorithms and detectors with respect to the analysis of the 2007 data. The global improvement gain expected on the upper limit of population density of common HEN and GW emitters is estimated as follows:

- A gain of a factor 1.4 arises from the observation time (91.36 days and 128.7 days for 2007 and 2009-2010 data respectively).

- A gain of a factor ~ 5 comes from the improvement of the neutrino effective area with respect to 2007 analysis. Indeed, the horizon is imposed by ANTARES and the effective area of the detector has been multiplied by 3 leading to a gain of factor $\sqrt{3}$ on the distance and hence $\sqrt{3^3} \sim 5$ on the volume.

This implies a net improvement by a factor ~ 7 with respect to what is presented in section 4.7.1.

REFERENCES

[1] C. Rivière, ANTARES internal note, ANTARES-PHYS-2012-001 (2012).

[2] V. Agrawal et al, Phys. Rev. D, 53, 13141323 (1996).

[3] J. N. Bahcall and E. Waxman, Phys. Rev. D64, 023002 (2001).

[4] D. Guetta et al, Astropart. Phys. 20: 429-455 (2004).

[5] https://www.lsc-group.phys.uwm.edu/bursts/public/runs/s6/dqv/category_definer/H1L1V1-S6A_BURST_ALLSKY_OFFLINE-930960015-5011200.xml.

[6] S. Adrian-Martinez et al, arXiv: http://arxiv.org/abs/1205.3018, (2012).

[7] B. Bouhou et al, Poster at the Gravitational Wave Physics and Astronomy Workshop, Hanover (2012).

[8] J. Abadie et al, Phys. Rev., D81, 102001 (2010).

[9] M. Drago, PhD thesis, Università degli Studi di Padova.

[10] http://www.gravity.phys.uwm.edu/cgi-bin/cvs/viewcvs.cgi/matapps/src/simulation/BurstMDC/documentation/?cvsroot=lscsoft.

[11] G. C. Hill and K. Rawlins, Astropart. Phys., 19, 393-402 (2003).

[12] G. J. Feldman and R. D. Cousins, Phys. Rev. D57, 3873-3889 (1998).

[13] G. C. Hill et al, Oxford Physics, PHYSTAT2005 Proceedings (2006).

[14] G. Punzi, SLAC, PHYSTAT2003 Proceedings (2003).

[15] J. Abadie et al., Phys. Rev. D 85 122007, (2012).

[16] G. D. Barret al, Phys. Rev. D74, 094009 (2006).

[17] S. Adrián-Martínez et al, Astropart. J. 743: L14, (2012).

[18] B. baret et al, Phys. Rev. D85, 103004 (2012).

[19] R. A. Fisher, Statistical Methods for Research Workers, Oliver and Boyd (Edinburgh), (1925).

CONCLUSIONS

By pioneering with the combination of two non-photonic observations, gravitational waves and high-energy neutrinos, this thesis work initiated a new domain in multimessenger astronomy. We designed and assembled a complete pipeline allowing for the combined analysis of ANTARES and LIGO/Virgo data.

We did this in two steps. A first search was conducted on concomitant data taken during 2007. No significant coincident event was detected. This resulted in upper limits on the source population (including potential photon-dark or obscured sources only accessible through GW and HEN observations). To allow rapid progresses, we essentially relied on pre-existing analysis tools. Once the search completed, we identified the limitations and issues of those tools. This has led us to develop new and more sensitive analysis tools that are better suited to the observations at hand. These tools are now integrated in a new pipeline which we applied in the context of a second search using 2009-2010 data currently in progress. The improvements brought to this second search includes a new neutrino selection strategy relying on a combined figure of merit, which maximizes the number of common observable sources.

Some of the methodologies proposed here could be developed in other contexts, and even beyond the GW and HEN context. For instance, the pipeline skymask coherent WaveBurst could serve as a basis to other types of "triggered" GW follow-up burst searches (e.g., in coincidence with gamma-ray bursts). Another example is the optimization scheme which is fairly generic and may be used to optimize the other types of joint searches combining GW or HEN with other cosmic messengers (gamma-rays for instance).

The pathfinder developments done in this thesis pave the way for future collaborations involving the next generation of detectors. These projects include KM3NeT, the future km^3 neutrino telescope in the Mediterranean sea and the second generation of interferometric GW

detectors (advanced LIGO and advanced Virgo). The sensitivity of those instruments will be significantly improved with respect to their predecessors. There are reasonable chances that they will lead to actual observation in their respective channel.

APPENDIX A

DEMONSTRATION OF THE MRF APPROXIMATION

We follow Neymann's construction of confidence interval to have an estimation of the upper limit in case the computing time of Feldman Cousin limit is prohibitive. For a normal distribution, the probability that a measurement n_{obs} falls within the interval $[\mu + c, \mu + d]$, where μ is the mean and $c < 0$, is equivalent to the probability that a measurement μ falls within the interval $[n_{obs} - d, n_{obs} - c]$. Thus we write:

$$\begin{aligned} P(\mu + c_Q \leq n_{obs} \leq \mu + d) &= P(n_{obs} - d \leq \mu \leq n_{obs} - c_Q) \\ &= Q \\ &= erf(d) - erf(c_Q) \end{aligned} \tag{A.1}$$

where erf is the error function and Q is the significance level.

$$erf(x) \equiv \frac{1}{\sqrt{2\pi}} \int_{-\infty}^{x} e^{-t^2/2} dt \tag{A.2}$$

If $d \equiv \infty$

$$\begin{aligned} Q &= erf(\infty) - erf(c_Q) \\ &= 1 - erf(c_Q) \\ \Rightarrow c_Q &= erf^{-1}(1 - Q) \end{aligned} \tag{A.3}$$

From Eqs. A.1 and A.3 we write:

$$\mu \leq n_{obs} - erf^{-1}(1-Q) \tag{A.4}$$

Thus,

$$\mu_{max} = n_{obs} - erf^{-1}(1-Q) \tag{A.5}$$

Using the following relation [1]:

$$erf\left(\frac{x}{\sigma}\right) = \frac{1}{2} + \frac{1}{2}Erf\left(\frac{x}{\sqrt{2}\sigma}\right) \tag{A.6}$$

where σ is the standard deviations and Erf is given by:

$$Erf(x) = \frac{2}{\sqrt{\pi}}\int_0^x e^{-t^2}dt \tag{A.7}$$

we find that:

$$\mu_{max} = n_{obs} - \sqrt{2\mu}Erf^{-1}(1-2Q) \tag{A.8}$$

we can also write $\mu_{max} = n_s + n_b$ where n_s and n_b are the number of signal and background events respectively. We put $x = \sqrt{\mu_{max}} > 0$, thus

$$x^2 + \sqrt{2}Erf^{-1}(2Q-1)x - n_{obs} = 0 \tag{A.9}$$

resolving this equation we find:

$$\begin{aligned} x &= \frac{-\sqrt{2}Erf^{-1}(1-2Q) + \sqrt{2(Erf^{-1}(1-2Q))^2 + 4n_{obs}}}{2} \\ &= \sqrt{n_s + n_b} \end{aligned} \tag{A.10}$$

Finally:

$$n_s \equiv \tilde{\mu}_Q(n_{obs}, n_b) = \left[\frac{-\sqrt{2}Erf^{-1}(2Q-1) + \sqrt{2(Erf^{-1}(2Q-1))^2 + 4n_{obs}}}{2}\right]^2 - n_b \tag{A.11}$$

This approximation should be weighted with the Poisson probability of its occurence to get the new parametrization of *the average upper limit*:

$$\overline{\tilde{\mu}}_Q(n_b) = \sum_{n_{obs}}^{\infty} \tilde{\mu}_Q(n_{obs}, n_b)\frac{(n_b)^{n_{obs}}}{(n_{obs})!}exp(-n_b) \tag{A.12}$$

note that this approximation is applied for large values of $n_{obs} > n_{obs}^{crit}$ such that $|FC_{ul} - n_s|/FC_{ul} \leq 10\%$, where FC_{ul} is FC upper limit. Thus for $n_{obs} > n_{crit}$ we redefine the ratio to be minimized, in section 5.4.1 as follow:

$$M\tilde{R}F(\text{cuts}) = \frac{\overline{\tilde{\mu}}_Q(n_b(\text{cuts}))}{n_s(\text{cuts})} \tag{A.13}$$

REFERENCES

[1] W. J. Metzger, Statistical Methods in Data Analysis, HEN-343 (2002).

APPENDIX B

COHERENT WAVEBURST STATISTICS

We have discussed the coherent WaveBurst and the skymask-coherent WaveBurst pipelines in chapters 3 and 5 respectively. In this appendix we define the coherent statistics used in the identification of the GW triggers, i.e net_{cc}, net_{ED} and ρ.

We consider that we project the time-aligned data onto a complete wavelet basis. Let us denote $w[i,j]$ is the corresponding wavelet coefficients where i, j are the time-frequency indices. We do the same for the detector response $\xi[i,j] = F_+(\theta,\phi)w_+[i,j] + F_\times(\theta,\phi)w_\times[i,j]$ where $w_{+(\times)}[i,j]$ denotes the wavelet coefficients of the GW polarizations $h_{+(\times)}$. The antenna patterns $F_{+(\times)}$ are defined in Sec. 3.4. Let $\sigma[i,j]$ be the RMS noise in the time-frequency bin (i,j).

The log-likelihood functional is obtained assuming a Gaussian quasi-stationary noise and can be expressed in the wavelet domain as

$$L_{noise} = \sum_{i,j\in\Omega_{TF}} \left[\frac{w^2[i,j]}{\sigma^2[i,j]} - \frac{(w[i,j]-\xi[i,j])^2}{\sigma^2[i,j]} \right] \tag{B.1}$$

where Ω_{TF} is the time-frequency area selected for the analysis.

This expression in the case of a one-detector analysis. Eq. (B.1) can be generalized to K detectors

$$L_{noise} = \sum_{k=1}^{K} \sum_{i,j\in\Omega_{TF}} \left[\frac{w_k^2[i,j]}{\sigma_k^2[i,j]} - \frac{(w_k[i,j]-\xi_k[i,j])^2}{\sigma_k^2[i,j]} \right]. \tag{B.2}$$

Coherent WaveBurst relies on the maximum likelihood ratio statistic i.e., maximizing Eq. (B.2) over all sky locations (θ,ϕ). This quantity is a quadratic form of w, thus it can be expressed in a matrix form as follows

$$L_{noise}^{max}(\theta,\phi) = \sum_{n,m} L_{mn}, \tag{B.3}$$

where $L_{nm} = \sum_{i,j\in\Omega_{TF}} w_n[i,j]w_m[i,j]P_{nm}[i,j]$ and P is the orthogonal projector onto the GW

plane spanned by normalized antenna pattern vectors f_+ and $f_\times$ defined as follows

$$f_{+(\times)} = \left\{ \frac{F_{1+(\times)}(\theta,\phi)}{\sigma_1[i,j]}, .., \frac{F_{K+(\times)}(\theta,\phi))}{\sigma_K[i,j]} \right\}. \tag{B.4}$$

We refer to *coherent energy*

$$E_c = \sum_{m \neq n} L_{mn} \tag{B.5}$$

as the sum of the off-diagonal terms of the log-likelihood matrix. E_c measures the correlation between the detector responses to a common GW signal. We also defined the *reduced coherent energy* $e_c = \sum_{n \neq m} L_{nm}|r_{nm}|$ where the terms are weighted by the Pearson's coefficients

$$r_{nm} = \frac{L_{nm}}{\sqrt{L_{nn}L_{mm}}}. \tag{B.6}$$

By projecting the data onto the *null space* complementary to the GW plane, we define the null matrix $N_{nm} = E_{nm} - L_{nm}$ with $E_{nm} = w_n^2$ and the associated null energy

$$N_{null} = \sum_{n,m} N_{nm}. \tag{B.7}$$

Instrumental glitches have a small E_c and large N_{null}.

Finally, given these ingredients we can define the *network correlation coefficient*

$$net_{cc} = \frac{E_c}{N_{null} + |E_c|}, \tag{B.8}$$

the *coherent network amplitude*

$$\rho = \sqrt{\frac{e_c}{K} net_{cc}}, \tag{B.9}$$

and the *network energy disbalance*

$$net_{ED} = \sum_k \frac{|\Delta_k|}{E_c}, \tag{B.10}$$

where Δ_k is the energy disbalance for detector k.

While cuts on net_{cc} and net_{ED} are used to distinguish noise outliers from genuine GW signals, the final event selection is done through a cut over the statistic ρ which characterises the event significance (see chapter 5 for the application of these statistics).

APPENDIX C

LIST OF HIGH ENERGY NEUTRINO CANDIDATES FOR THE 2009-2010 DATA

```
# ID JD GPS RA[deg.] DEC[deg.] radius[deg.] location[deg.] scale[deg.] shape normalization nhit ASW_90[
## start S6A
0001 2455021.06199646 931094971 317.666 4.358 -1.1724e-01 4.7983e-01 5.2936e-01 3.8897e-02 51 0.9
0002 2455021.76038040 931155311 138.462 5.235 -1.3370e-01 8.5313e-01 6.3102e-01 3.7539e-02 30 2.4
0003 2455021.95309485 931171962 205.006 3.064 -9.2963e-02 5.6770e-01 6.3052e-01 3.8106e-02 44 1.4
0004 2455022.13148593 931187375 278.683 1.967 -1.2873e-01 4.3155e-01 4.6595e-01 3.9162e-02 57 0.7
0005 2455022.31313315 931203069 255.984 -46.786 -9.2963e-02 5.6770e-01 6.3052e-01 3.8106e-02 67 1.4
0006 2455022.44211534 931214213 118.664 28.874 -1.1909e-01 7.2127e-01 6.0423e-01 3.7507e-02 27 1.8
0007 2455022.45728516 931215524 157.294 -39.769 -9.2963e-02 5.6770e-01 6.3052e-01 3.8106e-02 53 1.4
0008 2455022.94472038 931257638 168.102 -42.850 -9.2963e-02 5.6770e-01 6.3052e-01 3.8106e-02 47 1.4
0009 2455023.18653782 931278531 272.997 -21.999 -9.2963e-02 5.6770e-01 6.3052e-01 3.8106e-02 50 1.4
0010 2455023.18998930 931278830 1.531 -28.790 -9.2963e-02 5.6770e-01 6.3052e-01 3.8106e-02 45 1.4
0011 2455023.37019701 931294400 334.105 -10.712 -9.2963e-02 5.6770e-01 6.3052e-01 3.8106e-02 48 1.4
0012 2455023.39396068 931296453 69.937 -17.854 -9.2963e-02 5.6770e-01 6.3052e-01 3.8106e-02 38 1.4
0013 2455023.40570083 931297467 32.350 -40.431 -9.2963e-02 5.6770e-01 6.3052e-01 3.8106e-02 45 1.4
0014 2455023.89575708 931339808 237.065 42.325 -9.2963e-02 5.6770e-01 6.3052e-01 3.8106e-02 67 1.4
0015 2455024.96057196 931431808 206.881 -5.697 -1.3370e-01 8.5313e-01 6.3102e-01 3.7539e-02 27 2.4
0016 2455028.74935072 931759158 192.449 -49.417 -9.2963e-02 5.6770e-01 6.3052e-01 3.8106e-02 46 1.4
0017 2455029.82388645 931851998 45.763 -56.811 -9.2963e-02 5.6770e-01 6.3052e-01 3.8106e-02 42 1.4
0018 2455030.16800912 931881730 74.591 14.647 -9.2963e-02 5.6770e-01 6.3052e-01 3.8106e-02 36 1.4
0019 2455030.27551389 931891019 29.548 7.599 -1.1724e-01 4.7983e-01 5.2936e-01 3.8897e-02 41 0.9
0020 2455030.33532665 931896187 51.484 -12.502 -1.1724e-01 4.7983e-01 5.2936e-01 3.8897e-02 62 0.9
0021 2455030.38375704 931900371 70.987 39.204 -1.1724e-01 4.7983e-01 5.2936e-01 3.8897e-02 31 0.9
0022 2455030.93817457 931948273 308.219 -48.184 -9.2963e-02 5.6770e-01 6.3052e-01 3.8106e-02 72 1.4
0023 2455031.60103568 932005544 206.992 -38.656 -9.2963e-02 5.6770e-01 6.3052e-01 3.8106e-02 38 1.4
0024 2455031.91920714 932033034 270.687 -44.455 -9.2963e-02 5.6770e-01 6.3052e-01 3.8106e-02 65 1.4
0025 2455032.08877353 932047685 2.736 -63.554 -9.2963e-02 5.6770e-01 6.3052e-01 3.8106e-02 57 1.4
0026 2455032.42253465 932076521 164.843 16.811 -9.2963e-02 5.6770e-01 6.3052e-01 3.8106e-02 43 1.4
0027 2455033.33583128 932155430 351.912 -40.016 -9.2963e-02 5.6770e-01 6.3052e-01 3.8106e-02 58 1.4
0028 2455033.57360678 932175974 174.370 43.050 -1.3370e-01 8.5313e-01 6.3102e-01 3.7539e-02 29 2.4
0029 2455033.61363238 932179432 227.699 -29.385 -9.2963e-02 5.6770e-01 6.3052e-01 3.8106e-02 38 1.4
0030 2455033.66610532 932183966 101.450 -43.373 -9.2963e-02 5.6770e-01 6.3052e-01 3.8106e-02 53 1.4
0031 2455034.45436583 932252072 109.591 -13.022 -9.2963e-02 5.6770e-01 6.3052e-01 3.8106e-02 87 1.4
0032 2455035.07953033 932306086 281.293 23.853 -1.1909e-01 7.2127e-01 6.0423e-01 3.7507e-02 22 1.8
0033 2455035.18161884 932314906 29.890 -63.436 -1.1724e-01 4.7983e-01 5.2936e-01 3.8897e-02 56 0.9
```

LIST OF HIGH ENERGY NEUTRINO CANDIDATES FOR THE 2009-2010 DATA

0034	2455035.40957799	932334602	101.450	32.177	-1.7861e+00	6.7827e+00	8.6368e-01	3.8440e-01	30	1.4
0035	2455035.64492418	932354936	247.231	-26.876	-9.2963e-02	5.6770e-01	6.3052e-01	3.8106e-02	35	1.4
0036	2455035.70030035	932359720	227.842	42.919	-9.2963e-02	5.6770e-01	6.3052e-01	3.8106e-02	46	1.4
0037	2455035.97026079	932383045	211.009	-59.338	-9.2963e-02	5.6770e-01	6.3052e-01	3.8106e-02	34	1.4
0038	2455036.00870766	932386367	242.953	-39.003	-9.2963e-02	5.6770e-01	6.3052e-01	3.8106e-02	67	1.4
0039	2455036.60298826	932437713	62.518	-47.951	-1.1724e-01	4.7983e-01	5.2936e-01	3.8897e-02	53	0.9
0040	2455036.60985464	932438306	102.326	15.432	-9.2963e-02	5.6770e-01	6.3052e-01	3.8106e-02	44	1.4
0041	2455036.63224016	932440240	272.965	-8.272	-9.2963e-02	5.6770e-01	6.3052e-01	3.8106e-02	59	1.4
0042	2455036.70911771	932446882	140.991	-37.795	-9.2963e-02	5.6770e-01	6.3052e-01	3.8106e-02	45	1.4
0043	2455036.71386641	932447293	197.929	-9.068	-1.1724e-01	4.7983e-01	5.2936e-01	3.8897e-02	72	0.9
0044	2455036.97629850	932469967	49.100	-45.947	-1.1724e-01	4.7983e-01	5.2936e-01	3.8897e-02	26	0.9
0045	2455036.99191191	932471316	260.728	1.668	-1.1724e-01	4.7983e-01	5.2936e-01	3.8897e-02	42	0.9
0046	2455037.07504211	932478498	181.562	-44.687	-5.8944e-02	2.9333e-01	5.7306e-01	3.8834e-02	110	0.6
0047	2455037.09645452	932480348	266.521	-55.111	-9.2963e-02	5.6770e-01	6.3052e-01	3.8106e-02	79	1.4
0048	2455037.42636007	932508852	135.162	-42.375	-1.1724e-01	4.7983e-01	5.2936e-01	3.8897e-02	45	0.9
0049	2455037.54148144	932518798	166.903	36.240	-9.2963e-02	5.6770e-01	6.3052e-01	3.8106e-02	38	1.4
0050	2455037.85645194	932546012	210.049	-5.290	-9.2963e-02	5.6770e-01	6.3052e-01	3.8106e-02	44	1.4
0051	2455038.44163643	932596572	120.888	13.742	-9.2963e-02	5.6770e-01	6.3052e-01	3.8106e-02	47	1.4
0052	2455038.95829055	932641211	278.848	31.341	-9.2963e-02	5.6770e-01	6.3052e-01	3.8106e-02	50	1.4
0053	2455038.97211600	932642405	163.861	-45.126	-9.2963e-02	5.6770e-01	6.3052e-01	3.8106e-02	37	1.4
0054	2455039.30290420	932670985	138.019	-66.930	-9.2963e-02	5.6770e-01	6.3052e-01	3.8106e-02	64	1.4
0055	2455041.87228627	932892980	323.880	-62.866	-9.2963e-02	5.6770e-01	6.3052e-01	3.8106e-02	53	1.4
0056	2455041.97123183	932901529	333.888	17.928	-1.3370e-01	8.5313e-01	6.3102e-01	3.7539e-02	29	2.4
0057	2455042.17163841	932918844	349.430	-6.478	-9.2963e-02	5.6770e-01	6.3052e-01	3.8106e-02	46	1.4
0058	2455042.35897386	932935030	124.059	6.046	-9.2963e-02	5.6770e-01	6.3052e-01	3.8106e-02	33	1.4
0059	2455042.45033082	932942923	3.545	-71.453	-1.3370e-01	8.5313e-01	6.3102e-01	3.7539e-02	30	2.4
0060	2455042.87758885	932979838	303.584	-28.374	-1.1724e-01	4.7983e-01	5.2936e-01	3.8897e-02	40	0.9
0061	2455042.89936669	932981720	250.252	-30.276	-9.2963e-02	5.6770e-01	6.3052e-01	3.8106e-02	37	1.4
0062	2455043.89864128	933068057	316.089	4.421	-9.2963e-02	5.6770e-01	6.3052e-01	3.8106e-02	36	1.4
0063	2455050.32408157	933623215	72.132	1.396	-5.8944e-02	2.9333e-01	5.7306e-01	3.8834e-02	114	0.6
0064	2455050.38858959	933628789	356.053	-31.259	-9.2963e-02	5.6770e-01	6.3052e-01	3.8106e-02	42	1.4
0065	2455050.40529145	933630232	313.438	-51.861	-9.2963e-02	5.6770e-01	6.3052e-01	3.8106e-02	55	1.4
0066	2455050.44870235	933633982	38.167	-55.362	-1.3370e-01	8.5313e-01	6.3102e-01	3.7539e-02	23	2.4
0067	2455052.47328426	933808906	115.206	-18.798	-1.1724e-01	4.7983e-01	5.2936e-01	3.8897e-02	47	0.9
0068	2455052.58433722	933818501	206.041	-45.213	-1.2873e-01	4.3155e-01	4.6595e-01	3.9162e-02	42	0.7
0069	2455052.85057939	933841505	166.502	-25.475	-1.2873e-01	4.3155e-01	4.6595e-01	3.9162e-02	60	0.7
0070	2455052.95932832	933850900	253.817	-75.759	-9.2963e-02	5.6770e-01	6.3052e-01	3.8106e-02	60	1.4
0071	2455052.97455143	933852216	286.417	37.666	-9.2963e-02	5.6770e-01	6.3052e-01	3.8106e-02	65	1.4
0072	2455053.41821454	933890548	20.185	-23.592	-9.2963e-02	5.6770e-01	6.3052e-01	3.8106e-02	59	1.4
0073	2455053.48363661	933896201	49.990	-19.411	-9.2963e-02	5.6770e-01	6.3052e-01	3.8106e-02	40	1.4
0074	2455053.53529934	933900664	187.949	-6.248	-1.1724e-01	4.7983e-01	5.2936e-01	3.8897e-02	52	0.9
0075	2455053.53684889	933900798	44.865	-25.779	-9.2963e-02	5.6770e-01	6.3052e-01	3.8106e-02	67	1.4
0076	2455053.74347266	933918651	163.514	13.204	-9.2963e-02	5.6770e-01	6.3052e-01	3.8106e-02	37	1.4
0077	2455053.74875280	933919107	78.440	-60.862	-9.2963e-02	5.6770e-01	6.3052e-01	3.8106e-02	34	1.4
0078	2455053.81557582	933924880	276.507	28.587	-9.2963e-02	5.6770e-01	6.3052e-01	3.8106e-02	85	1.4
0079	2455053.83153518	933926259	186.604	-39.316	-9.2963e-02	5.6770e-01	6.3052e-01	3.8106e-02	32	1.4
0080	2455054.19238734	933957437	79.365	-26.764	-9.2963e-02	5.6770e-01	6.3052e-01	3.8106e-02	29	1.4
0081	2455054.30248002	933966949	211.712	-45.529	-1.3370e-01	8.5313e-01	6.3102e-01	3.7539e-02	29	2.4
0082	2455054.32037523	933968495	41.278	31.473	-9.2963e-02	5.6770e-01	6.3052e-01	3.8106e-02	52	1.4
0083	2455054.65740359	933997614	289.824	-23.322	-9.2963e-02	5.6770e-01	6.3052e-01	3.8106e-02	34	1.4
0084	2455055.01582708	934028582	273.787	-44.754	-9.2963e-02	5.6770e-01	6.3052e-01	3.8106e-02	38	1.4
0085	2455057.10660147	934209225	355.481	-47.229	-1.1724e-01	4.7983e-01	5.2936e-01	3.8897e-02	40	0.9

```
0086 2455057.72174617 934262373 197.766 37.641 -9.2963e-02 5.6770e-01 6.3052e-01 3.8106e-02 32 1.4
0087 2455057.73197650 934263257 343.302 -21.717 -9.2963e-02 5.6770e-01 6.3052e-01 3.8106e-02 62 1.4
0088 2455057.77638293 934267094 18.317 -71.965 -1.1724e-01 4.7983e-01 5.2936e-01 3.8897e-02 36 0.9
0089 2455057.99678427 934286137 338.646 -57.019 -1.1724e-01 4.7983e-01 5.2936e-01 3.8897e-02 36 0.9
0090 2455058.10416152 934295414 25.851 14.336 -1.3370e-01 8.5313e-01 6.3102e-01 3.7539e-02 26 2.4
0091 2455058.18834888 934302688 178.236 -41.215 -9.2963e-02 5.6770e-01 6.3052e-01 3.8106e-02 46 1.4
0092 2455058.76158587 934352216 246.087 -39.107 -1.1724e-01 4.7983e-01 5.2936e-01 3.8897e-02 42 0.9
0093 2455058.86341465 934361014 3.491 -27.687 -9.2963e-02 5.6770e-01 6.3052e-01 3.8106e-02 72 1.4
0094 2455058.91450708 934365428 288.617 39.340 -9.2963e-02 5.6770e-01 6.3052e-01 3.8106e-02 30 1.4
0095 2455059.05793775 934377820 78.537 -81.132 -1.1724e-01 4.7983e-01 5.2936e-01 3.8897e-02 36 0.9
0096 2455059.14860678 934385654 296.207 -56.333 -1.1724e-01 4.7983e-01 5.2936e-01 3.8897e-02 35 0.9
0097 2455059.39256684 934406732 86.229 -5.943 -9.2963e-02 5.6770e-01 6.3052e-01 3.8106e-02 42 1.4
0098 2455059.55834199 934421055 110.022 -52.160 -1.2873e-01 4.3155e-01 4.6595e-01 3.9162e-02 41 0.7
0099 2455059.60484498 934425073 348.050 -74.294 -1.3370e-01 8.5313e-01 6.3102e-01 3.7539e-02 29 2.4
0100 2455059.72044919 934435061 88.907 -77.196 -1.2873e-01 4.3155e-01 4.6595e-01 3.9162e-02 59 0.7
0101 2455059.87421622 934448347 259.574 7.695 -1.3370e-01 8.5313e-01 6.3102e-01 3.7539e-02 25 2.4
0102 2455059.91445785 934451824 224.493 10.941 -9.2963e-02 5.6770e-01 6.3052e-01 3.8106e-02 49 1.4
0103 2455059.98885820 934458252 241.941 -37.187 -9.2963e-02 5.6770e-01 6.3052e-01 3.8106e-02 35 1.4
0104 2455060.09424206 934467357 323.311 -40.725 -9.2963e-02 5.6770e-01 6.3052e-01 3.8106e-02 42 1.4
0105 2455060.18410076 934475121 205.068 -72.845 -9.2963e-02 5.6770e-01 6.3052e-01 3.8106e-02 38 1.4
0106 2455060.25954351 934481639 9.288 -7.403 -9.2963e-02 5.6770e-01 6.3052e-01 3.8106e-02 42 1.4
0107 2455060.35331136 934489741 179.878 -53.666 -9.2963e-02 5.6770e-01 6.3052e-01 3.8106e-02 57 1.4
0108 2455060.52726260 934504770 47.437 -33.261 -9.2963e-02 5.6770e-01 6.3052e-01 3.8106e-02 55 1.4
0109 2455061.31263711 934572626 192.544 -55.694 -9.2963e-02 5.6770e-01 6.3052e-01 3.8106e-02 50 1.4
0110 2455061.44684815 934584222 72.470 -28.046 -9.2963e-02 5.6770e-01 6.3052e-01 3.8106e-02 42 1.4
0111 2455061.51759585 934590335 237.226 -9.551 -9.2963e-02 5.6770e-01 6.3052e-01 3.8106e-02 37 1.4
0112 2455061.55946493 934593952 202.888 33.499 -9.2963e-02 5.6770e-01 6.3052e-01 3.8106e-02 37 1.4
0113 2455061.73849454 934609420 19.756 -50.560 -9.2963e-02 5.6770e-01 6.3052e-01 3.8106e-02 51 1.4
0114 2455061.74870241 934610302 152.932 -6.469 -9.2963e-02 5.6770e-01 6.3052e-01 3.8106e-02 34 1.4
0115 2455061.83503097 934617761 298.604 -42.499 -9.2963e-02 5.6770e-01 6.3052e-01 3.8106e-02 25 1.4
0116 2455061.88976534 934622490 214.252 -34.716 -9.2963e-02 5.6770e-01 6.3052e-01 3.8106e-02 41 1.4
0117 2455061.94754236 934627482 357.669 13.929 -9.2963e-02 5.6770e-01 6.3052e-01 3.8106e-02 43 1.4
0118 2455062.02194877 934633911 172.194 -63.516 -9.2963e-02 5.6770e-01 6.3052e-01 3.8106e-02 32 1.4
0119 2455062.08912358 934639715 101.379 -14.331 -9.2963e-02 5.6770e-01 6.3052e-01 3.8106e-02 40 1.4
0120 2455062.21500284 934650591 295.537 -40.361 -9.2963e-02 5.6770e-01 6.3052e-01 3.8106e-02 33 1.4
0121 2455062.82701440 934703469 300.123 35.695 -9.2963e-02 5.6770e-01 6.3052e-01 3.8106e-02 34 1.4
0122 2455062.85720530 934706077 323.861 -6.029 -1.1909e-01 7.2127e-01 6.0423e-01 3.7507e-02 20 1.8
0123 2455062.88545185 934708518 263.884 8.358 -1.1909e-01 7.2127e-01 6.0423e-01 3.7507e-02 66 1.8
0124 2455062.89821627 934709620 245.558 16.387 -9.2963e-02 5.6770e-01 6.3052e-01 3.8106e-02 32 1.4
0125 2455062.97267542 934716054 285.690 27.039 -1.3370e-01 8.5313e-01 6.3102e-01 3.7539e-02 26 2.4
0126 2455063.17559712 934733586 25.934 -60.307 -1.1724e-01 4.7983e-01 5.2936e-01 3.8897e-02 43 0.9
0127 2455063.48054315 934759933 162.308 -30.704 -9.2963e-02 5.6770e-01 6.3052e-01 3.8106e-02 37 1.4
0128 2455063.57841217 934768389 314.799 -37.629 -9.2963e-02 5.6770e-01 6.3052e-01 3.8106e-02 35 1.4
0129 2455063.60847560 934770987 173.670 45.183 -1.1724e-01 4.7983e-01 5.2936e-01 3.8897e-02 57 0.9
0130 2455063.63467694 934773251 170.213 -13.859 -1.1724e-01 4.7983e-01 5.2936e-01 3.8897e-02 31 0.9
0131 2455063.68940751 934777979 233.357 -1.269 -1.1724e-01 4.7983e-01 5.2936e-01 3.8897e-02 37 0.9
0132 2455063.77603876 934785464 260.557 -19.652 -1.1724e-01 4.7983e-01 5.2936e-01 3.8897e-02 80 0.9
0133 2455063.78605218 934786329 138.906 -50.654 -9.2963e-02 5.6770e-01 6.3052e-01 3.8106e-02 58 1.4
0134 2455063.88720217 934795069 212.069 -22.876 -9.2963e-02 5.6770e-01 6.3052e-01 3.8106e-02 35 1.4
0135 2455064.04774615 934808940 335.759 44.453 -9.2963e-02 5.6770e-01 6.3052e-01 3.8106e-02 39 1.4
0136 2455064.14454310 934817303 288.283 -49.621 -9.2963e-02 5.6770e-01 6.3052e-01 3.8106e-02 36 1.4
0137 2455064.26502570 934827713 161.003 -8.728 -9.2963e-02 5.6770e-01 6.3052e-01 3.8106e-02 46 1.4
```

LIST OF HIGH ENERGY NEUTRINO CANDIDATES FOR THE 2009-2010 DATA

```
0138 2455064.56062293 934853252 38.039 -52.296 -9.2963e-02 5.6770e-01 6.3052e-01 3.8106e-02 74 1.4
0139 2455064.65752250 934861624 281.452 -16.760 -9.2963e-02 5.6770e-01 6.3052e-01 3.8106e-02 39 1.4
0140 2455064.78114668 934872306 257.829 -0.921 -9.2963e-02 5.6770e-01 6.3052e-01 3.8106e-02 35 1.4
0141 2455064.88179257 934881001 22.451 -15.508 -9.2963e-02 5.6770e-01 6.3052e-01 3.8106e-02 47 1.4
0142 2455064.95292887 934887148 146.216 -65.464 -9.2963e-02 5.6770e-01 6.3052e-01 3.8106e-02 40 1.4
0143 2455064.99601715 934890870 11.022 8.344 -9.2963e-02 5.6770e-01 6.3052e-01 3.8106e-02 41 1.4
0144 2455065.36133282 934922434 169.335 -47.674 -1.1724e-01 4.7983e-01 5.2936e-01 3.8897e-02 40 0.9
0145 2455065.60217816 934943243 165.957 -25.904 -1.1724e-01 4.7983e-01 5.2936e-01 3.8897e-02 56 0.9
0146 2455065.93864074 934972313 62.855 -28.983 -9.2963e-02 5.6770e-01 6.3052e-01 3.8106e-02 59 1.4
0147 2455066.39089495 935011388 176.976 -11.310 -1.1724e-01 4.7983e-01 5.2936e-01 3.8897e-02 36 0.9
0148 2455066.57591951 935027374 193.704 -21.759 -9.2963e-02 5.6770e-01 6.3052e-01 3.8106e-02 49 1.4
0149 2455066.61269078 935030551 3.471 -59.062 -9.2963e-02 5.6770e-01 6.3052e-01 3.8106e-02 71 1.4
0150 2455066.75797386 935043103 211.403 -49.385 -9.2963e-02 5.6770e-01 6.3052e-01 3.8106e-02 45 1.4
0151 2455066.77956388 935044969 235.841 17.491 -9.2963e-02 5.6770e-01 6.3052e-01 3.8106e-02 40 1.4
0152 2455067.01314266 935065150 289.079 -74.713 -9.2963e-02 5.6770e-01 6.3052e-01 3.8106e-02 44 1.4
0153 2455067.08142308 935071049 54.618 -13.711 -9.2963e-02 5.6770e-01 6.3052e-01 3.8106e-02 35 1.4
0154 2455067.11560343 935074003 234.943 -63.137 -1.3370e-01 8.5313e-01 6.3102e-01 3.7539e-02 29 2.4
0155 2455067.12042047 935074419 304.395 -12.814 -1.1909e-01 7.2127e-01 6.0423e-01 3.7507e-02 27 1.8
0156 2455067.15376586 935077300 21.271 -27.720 -1.2873e-01 4.3155e-01 4.6595e-01 3.9162e-02 45 0.7
0157 2455067.30991995 935090792 105.702 -6.759 -1.2873e-01 4.3155e-01 4.6595e-01 3.9162e-02 52 0.7
0158 2455070.47703972 935364431 265.930 -75.124 -9.2963e-02 5.6770e-01 6.3052e-01 3.8106e-02 41 1.4
0159 2455070.94445264 935404815 296.500 12.771 -1.1724e-01 4.7983e-01 5.2936e-01 3.8897e-02 39 0.9
0160 2455070.96791834 935406843 329.554 17.101 -1.1724e-01 4.7983e-01 5.2936e-01 3.8897e-02 45 0.9
0161 2455070.99781936 935409426 35.999 -50.428 -9.2963e-02 5.6770e-01 6.3052e-01 3.8106e-02 67 1.4
0162 2455071.13297930 935421104 91.198 -60.854 -1.3370e-01 8.5313e-01 6.3102e-01 3.7539e-02 25 2.4
0163 2455071.26768616 935432743 60.807 27.094 -9.2963e-02 5.6770e-01 6.3052e-01 3.8106e-02 51 1.4
0164 2455071.29632968 935435217 294.982 -48.854 -1.3370e-01 8.5313e-01 6.3102e-01 3.7539e-02 25 2.4
0165 2455071.32881274 935438024 197.670 -19.309 -1.1909e-01 7.2127e-01 6.0423e-01 3.7507e-02 28 1.8
0166 2455071.39038574 935443344 110.555 -56.593 -9.2963e-02 5.6770e-01 6.3052e-01 3.8106e-02 37 1.4
0167 2455071.40315053 935444447 60.000 19.101 -9.2963e-02 5.6770e-01 6.3052e-01 3.8106e-02 47 1.4
0168 2455071.76877458 935476037 285.997 1.892 -1.1724e-01 4.7983e-01 5.2936e-01 3.8897e-02 42 0.9
0169 2455071.82952120 935481285 6.548 -1.611 -9.2963e-02 5.6770e-01 6.3052e-01 3.8106e-02 32 1.4
0170 2455072.02111240 935497839 332.166 -27.354 -1.3370e-01 8.5313e-01 6.3102e-01 3.7539e-02 26 2.4
0171 2455072.08589852 935503436 267.489 -18.082 -9.2963e-02 5.6770e-01 6.3052e-01 3.8106e-02 53 1.4
0172 2455072.10148270 935504783 71.396 -42.301 -1.3370e-01 8.5313e-01 6.3102e-01 3.7539e-02 28 2.4
0173 2455072.42031869 935532330 42.345 -50.906 -9.2963e-02 5.6770e-01 6.3052e-01 3.8106e-02 50 1.4
0174 2455072.85751870 935570104 151.015 -64.369 -9.2963e-02 5.6770e-01 6.3052e-01 3.8106e-02 81 1.4
0175 2455072.87929551 935571986 302.403 -2.080 -1.1724e-01 4.7983e-01 5.2936e-01 3.8897e-02 38 0.9
0176 2455073.03755802 935585660 341.378 26.213 -1.2873e-01 4.3155e-01 4.6595e-01 3.9162e-02 38 0.7
0177 2455073.04830593 935586588 333.750 6.568 -9.2963e-02 5.6770e-01 6.3052e-01 3.8106e-02 73 1.4
0178 2455073.21274276 935600795 28.475 20.486 -1.1909e-01 7.2127e-01 6.0423e-01 3.7507e-02 28 1.8
0179 2455073.43171108 935619714 191.985 29.561 -9.2963e-02 5.6770e-01 6.3052e-01 3.8106e-02 34 1.4
0180 2455073.44068156 935620489 148.114 -0.467 -9.2963e-02 5.6770e-01 6.3052e-01 3.8106e-02 70 1.4
0181 2455073.46909432 935622944 195.280 -21.809 -9.2963e-02 5.6770e-01 6.3052e-01 3.8106e-02 32 1.4
0182 2455073.64250209 935637927 98.395 -50.232 -9.2963e-02 5.6770e-01 6.3052e-01 3.8106e-02 69 1.4
0183 2455073.64388251 935638046 264.339 28.544 -9.2963e-02 5.6770e-01 6.3052e-01 3.8106e-02 47 1.4
0184 2455073.69052558 935642076 180.486 -21.394 -9.2963e-02 5.6770e-01 6.3052e-01 3.8106e-02 38 1.4
0185 2455073.76116355 935648179 298.854 36.684 -9.2963e-02 5.6770e-01 6.3052e-01 3.8106e-02 48 1.4
0186 2455073.97565402 935666711 283.507 -12.569 -1.3370e-01 8.5313e-01 6.3102e-01 3.7539e-02 26 2.4
0187 2455074.16081558 935682709 1.175 -18.999 -9.2963e-02 5.6770e-01 6.3052e-01 3.8106e-02 34 1.4
0188 2455074.21222119 935687150 108.559 -53.956 -9.2963e-02 5.6770e-01 6.3052e-01 3.8106e-02 71 1.4
0189 2455074.32623248 935697001 298.966 -58.654 -9.2963e-02 5.6770e-01 6.3052e-01 3.8106e-02 37 1.4
```

```
0190 2455074.56496007 935717627 84.393 -37.166 -9.2963e-02 5.6770e-01 6.3052e-01 3.8106e-02 62 1.4
0191 2455074.57640119 935718616 79.034 -30.771 -9.2963e-02 5.6770e-01 6.3052e-01 3.8106e-02 38 1.4
0192 2455074.60422679 935721020 272.659 4.576 -9.2963e-02 5.6770e-01 6.3052e-01 3.8106e-02 75 1.4
0193 2455074.79432343 935737444 67.313 -48.050 -1.1724e-01 4.7983e-01 5.2936e-01 3.8897e-02 51 0.9
0194 2455075.10189846 935764019 8.468 1.425 -1.3370e-01 8.5313e-01 6.3102e-01 3.7539e-02 15 2.4
0195 2455075.17740608 935770542 14.325 29.555 -1.1724e-01 4.7983e-01 5.2936e-01 3.8897e-02 46 0.9
0196 2455075.21724744 935773985 348.538 -50.641 -1.3370e-01 8.5313e-01 6.3102e-01 3.7539e-02 29 2.4
0197 2455075.28702876 935780014 150.807 0.342 -1.3370e-01 8.5313e-01 6.3102e-01 3.7539e-02 30 2.4
0198 2455075.36731093 935786950 159.178 -34.961 -9.2963e-02 5.6770e-01 6.3052e-01 3.8106e-02 36 1.4
0199 2455075.38729420 935788677 26.551 -9.824 -9.2963e-02 5.6770e-01 6.3052e-01 3.8106e-02 66 1.4
0200 2455075.41695957 935791240 50.676 -64.237 -1.1909e-01 7.2127e-01 6.0423e-01 3.7507e-02 30 1.8
## stop S6A -- start
0201 2455075.56390515 935803936 186.645 -78.234 -9.2963e-02 5.6770e-01 6.3052e-01 3.8106e-02 39 1.4
0202 2455075.77641224 935822297 26.229 -51.325 -9.2963e-02 5.6770e-01 6.3052e-01 3.8106e-02 35 1.4
0203 2455075.99417841 935841112 42.364 11.601 -1.1909e-01 7.2127e-01 6.0423e-01 3.7507e-02 22 1.8
0204 2455075.99462135 935841150 292.792 -26.328 -9.2963e-02 5.6770e-01 6.3052e-01 3.8106e-02 35 1.4
0205 2455076.01741383 935843119 315.405 34.672 -9.2963e-02 5.6770e-01 6.3052e-01 3.8106e-02 44 1.4
0206 2455076.15557493 935855056 253.920 -64.226 -1.1724e-01 4.7983e-01 5.2936e-01 3.8897e-02 46 0.9
0207 2455076.18136926 935857285 160.419 -29.016 -1.1724e-01 4.7983e-01 5.2936e-01 3.8897e-02 34 0.9
0208 2455076.23681134 935862075 113.337 -57.305 -1.3370e-01 8.5313e-01 6.3102e-01 3.7539e-02 25 2.4
0209 2455076.27127798 935865053 307.233 -60.805 -9.2963e-02 5.6770e-01 6.3052e-01 3.8106e-02 72 1.4
0210 2455076.32513939 935869707 134.496 38.062 -9.2963e-02 5.6770e-01 6.3052e-01 3.8106e-02 51 1.4
0211 2455076.33399198 935870471 208.913 -12.640 -9.2963e-02 5.6770e-01 6.3052e-01 3.8106e-02 32 1.4
0212 2455076.35855125 935872593 147.308 -15.700 -9.2963e-02 5.6770e-01 6.3052e-01 3.8106e-02 32 1.4
0213 2455076.57486298 935891283 251.261 -16.281 -1.1724e-01 4.7983e-01 5.2936e-01 3.8897e-02 34 0.9
0214 2455076.58392926 935892066 118.896 2.822 -1.3370e-01 8.5313e-01 6.3102e-01 3.7539e-02 24 2.4
0215 2455076.77056074 935908191 274.193 -63.643 -9.2963e-02 5.6770e-01 6.3052e-01 3.8106e-02 47 1.4
0216 2455077.08998965 935935790 232.891 -61.107 -1.3370e-01 8.5313e-01 6.3102e-01 3.7539e-02 28 2.4
0217 2455077.29565244 935953559 99.410 -5.291 -1.3370e-01 8.5313e-01 6.3102e-01 3.7539e-02 32 2.4
0218 2455077.76187250 935993840 342.896 -9.615 -9.2963e-02 5.6770e-01 6.3052e-01 3.8106e-02 37 1.4
0219 2455077.79683288 935996861 196.981 -12.760 -9.2963e-02 5.6770e-01 6.3052e-01 3.8106e-02 38 1.4
0220 2455077.91146154 936006765 342.016 -46.411 -9.2963e-02 5.6770e-01 6.3052e-01 3.8106e-02 37 1.4
0221 2455078.11485758 936024338 41.640 46.071 -9.2963e-02 5.6770e-01 6.3052e-01 3.8106e-02 32 1.4
0222 2455078.14156621 936026646 282.452 -45.117 -9.2963e-02 5.6770e-01 6.3052e-01 3.8106e-02 54 1.4
0223 2455078.24965750 936035985 337.977 -49.741 -9.2963e-02 5.6770e-01 6.3052e-01 3.8106e-02 73 1.4
0224 2455078.31163506 936041340 182.403 -12.568 -9.2963e-02 5.6770e-01 6.3052e-01 3.8106e-02 28 1.4
0225 2455078.66255429 936071659 224.546 14.682 -9.2963e-02 5.6770e-01 6.3052e-01 3.8106e-02 53 1.4
0226 2455079.09997850 936109453 220.691 -78.436 -9.2963e-02 5.6770e-01 6.3052e-01 3.8106e-02 67 1.4
0227 2455079.14743735 936113553 235.278 -66.087 -1.3370e-01 8.5313e-01 6.3102e-01 3.7539e-02 24 2.4
0228 2455079.23722766 936121311 183.940 -49.505 -9.2963e-02 5.6770e-01 6.3052e-01 3.8106e-02 42 1.4
0229 2455079.30866599 936127483 21.285 -38.030 -9.2963e-02 5.6770e-01 6.3052e-01 3.8106e-02 53 1.4
0230 2455079.40743016 936136016 170.021 -12.730 -9.2963e-02 5.6770e-01 6.3052e-01 3.8106e-02 59 1.4
0231 2455079.47519614 936141871 63.018 -27.148 -1.1909e-01 7.2127e-01 6.0423e-01 3.7507e-02 25 1.8
0232 2455079.47590578 936141933 109.353 -43.789 -9.2963e-02 5.6770e-01 6.3052e-01 3.8106e-02 48 1.4
0233 2455079.56121105 936149303 132.409 1.719 -9.2963e-02 5.6770e-01 6.3052e-01 3.8106e-02 34 1.4
0234 2455079.57961689 936150893 219.567 44.493 -1.1724e-01 4.7983e-01 5.2936e-01 3.8897e-02 32 0.9
0235 2455079.60719435 936153276 105.653 -38.931 -9.2963e-02 5.6770e-01 6.3052e-01 3.8106e-02 37 1.4
0236 2455079.63811721 936155948 243.927 -85.337 -1.3370e-01 8.5313e-01 6.3102e-01 3.7539e-02 30 2.4
0237 2455079.78572540 936168701 340.634 -31.464 -9.2963e-02 5.6770e-01 6.3052e-01 3.8106e-02 49 1.4
0238 2455079.86039597 936175153 16.488 -32.619 -9.2963e-02 5.6770e-01 6.3052e-01 3.8106e-02 36 1.4
0239 2455079.91700502 936180044 241.291 -33.317 -1.1909e-01 7.2127e-01 6.0423e-01 3.7507e-02 20 1.8
0240 2455079.96408156 936184111 53.170 -4.564 -9.2963e-02 5.6770e-01 6.3052e-01 3.8106e-02 33 1.4
```

LIST OF HIGH ENERGY NEUTRINO CANDIDATES FOR THE 2009-2010 DATA

```
0241 2455079.99178393 936186505 53.833 -46.456 -1.3370e-01 8.5313e-01 6.3102e-01 3.7539e-02 23 2.4
0242 2455080.26754240 936210330 304.848 -63.157 -1.3370e-01 8.5313e-01 6.3102e-01 3.7539e-02 65 2.4
0243 2455080.30098932 936213220 200.562 -14.125 -9.2963e-02 5.6770e-01 6.3052e-01 3.8106e-02 33 1.4
0244 2455080.50745682 936231059 131.300 -53.602 -1.1724e-01 4.7983e-01 5.2936e-01 3.8897e-02 47 0.9
0245 2455080.61428536 936240289 171.795 19.682 -9.2963e-02 5.6770e-01 6.3052e-01 3.8106e-02 79 1.4
0246 2455080.65172297 936243523 346.127 -38.193 -1.3370e-01 8.5313e-01 6.3102e-01 3.7539e-02 25 2.4
0247 2455080.78975878 936255450 140.283 -42.237 -9.2963e-02 5.6770e-01 6.3052e-01 3.8106e-02 37 1.4
0248 2455080.81326229 936257480 153.269 -48.309 -9.2963e-02 5.6770e-01 6.3052e-01 3.8106e-02 56 1.4
0249 2455080.86532787 936261979 239.266 22.131 -9.2963e-02 5.6770e-01 6.3052e-01 3.8106e-02 32 1.4
0250 2455081.03265593 936276436 316.385 -27.710 -9.2963e-02 5.6770e-01 6.3052e-01 3.8106e-02 36 1.4
0251 2455081.17430312 936288674 145.492 -65.358 -1.3370e-01 8.5313e-01 6.3102e-01 3.7539e-02 29 2.4
0252 2455081.17518076 936288750 310.872 -35.986 -1.3370e-01 8.5313e-01 6.3102e-01 3.7539e-02 28 2.4
0253 2455081.27522467 936297394 33.006 -20.002 -9.2963e-02 5.6770e-01 6.3052e-01 3.8106e-02 51 1.4
0254 2455081.36548723 936305193 352.796 -38.440 -9.2963e-02 5.6770e-01 6.3052e-01 3.8106e-02 55 1.4
0255 2455081.42963220 936310735 172.399 -46.444 -1.1724e-01 4.7983e-01 5.2936e-01 3.8897e-02 44 0.9
0256 2455081.43810186 936311467 119.039 16.706 -1.1724e-01 4.7983e-01 5.2936e-01 3.8897e-02 42 0.9
0257 2455081.46934234 936314166 141.511 43.768 -9.2963e-02 5.6770e-01 6.3052e-01 3.8106e-02 41 1.4
0258 2455081.75732313 936339047 350.102 -7.725 -1.3370e-01 8.5313e-01 6.3102e-01 3.7539e-02 30 2.4
0259 2455081.87184067 936348942 2.549 24.156 -1.3370e-01 8.5313e-01 6.3102e-01 3.7539e-02 59 2.4
0260 2455082.03341998 936362902 8.738 -11.288 -9.2963e-02 5.6770e-01 6.3052e-01 3.8106e-02 37 1.4
0261 2455082.23583768 936380391 122.853 10.639 -9.2963e-02 5.6770e-01 6.3052e-01 3.8106e-02 37 1.4
0262 2455082.28760713 936384864 21.450 -56.564 -1.1724e-01 4.7983e-01 5.2936e-01 3.8897e-02 63 0.9
0263 2455082.53515656 936406252 197.978 -64.291 -1.2873e-01 4.3155e-01 4.6595e-01 3.9162e-02 44 0.7
0264 2455082.61202671 936412894 250.676 -9.426 -9.2963e-02 5.6770e-01 6.3052e-01 3.8106e-02 35 1.4
0265 2455082.63848570 936415180 187.983 16.341 -1.1724e-01 4.7983e-01 5.2936e-01 3.8897e-02 32 0.9
0266 2455082.67468045 936418307 274.678 -8.183 -9.2963e-02 5.6770e-01 6.3052e-01 3.8106e-02 38 1.4
0267 2455082.76755631 936426331 283.751 -21.164 -9.2963e-02 5.6770e-01 6.3052e-01 3.8106e-02 34 1.4
0268 2455082.92962440 936440334 316.109 -67.492 -9.2963e-02 5.6770e-01 6.3052e-01 3.8106e-02 42 1.4
0269 2455083.03701931 936449613 37.804 -45.552 -1.1724e-01 4.7983e-01 5.2936e-01 3.8897e-02 83 0.9
0270 2455083.05275481 936450973 5.566 -53.262 -1.2873e-01 4.3155e-01 4.6595e-01 3.9162e-02 60 0.7
0271 2455083.06745450 936452243 312.436 -15.372 -9.2963e-02 5.6770e-01 6.3052e-01 3.8106e-02 41 1.4
0272 2455083.18404952 936462316 355.395 -3.458 -9.2963e-02 5.6770e-01 6.3052e-01 3.8106e-02 62 1.4
0273 2455083.42293132 936482956 103.993 28.368 -1.1724e-01 4.7983e-01 5.2936e-01 3.8897e-02 44 0.9
0274 2455083.50672955 936490196 196.316 36.018 -1.3370e-01 8.5313e-01 6.3102e-01 3.7539e-02 29 2.4
0275 2455083.73577995 936509986 320.376 -43.986 -1.1724e-01 4.7983e-01 5.2936e-01 3.8897e-02 36 0.9
0276 2455083.73592252 936509998 195.708 8.432 -1.1724e-01 4.7983e-01 5.2936e-01 3.8897e-02 56 0.9
0277 2455083.73668266 936510064 314.963 23.670 -9.2963e-02 5.6770e-01 6.3052e-01 3.8106e-02 36 1.4
0278 2455083.80856309 936516274 220.616 -58.925 -1.1909e-01 7.2127e-01 6.0423e-01 3.7507e-02 31 1.8
0279 2455084.13393384 936544386 359.862 -42.770 -9.2963e-02 5.6770e-01 6.3052e-01 3.8106e-02 45 1.4
0280 2455084.29535617 936558333 149.835 -40.793 -1.1909e-01 7.2127e-01 6.0423e-01 3.7507e-02 29 1.8
0281 2455084.47954483 936574247 250.232 -29.542 -9.2963e-02 5.6770e-01 6.3052e-01 3.8106e-02 98 1.4
0282 2455084.52238013 936577948 86.300 -15.433 -9.2963e-02 5.6770e-01 6.3052e-01 3.8106e-02 50 1.4
0283 2455084.70065469 936593351 193.669 16.403 -9.2963e-02 5.6770e-01 6.3052e-01 3.8106e-02 36 1.4
0284 2455084.73734402 936596521 272.373 -12.385 -9.2963e-02 5.6770e-01 6.3052e-01 3.8106e-02 46 1.4
0285 2455084.93151646 936613298 11.085 -31.666 -9.2963e-02 5.6770e-01 6.3052e-01 3.8106e-02 44 1.4
0286 2455085.02272638 936621178 284.122 -4.322 -9.2963e-02 5.6770e-01 6.3052e-01 3.8106e-02 80 1.4
0287 2455085.17644877 936634460 39.562 4.080 -9.2963e-02 5.6770e-01 6.3052e-01 3.8106e-02 36 1.4
0288 2455085.39207416 936653090 149.682 -9.064 -9.2963e-02 5.6770e-01 6.3052e-01 3.8106e-02 33 1.4
0289 2455085.53667003 936665583 238.313 3.530 -9.2963e-02 5.6770e-01 6.3052e-01 3.8106e-02 42 1.4
0290 2455085.63388097 936673982 223.456 -13.145 -9.2963e-02 5.6770e-01 6.3052e-01 3.8106e-02 68 1.4
0291 2455085.81000029 936689199 258.033 28.657 -1.1724e-01 4.7983e-01 5.2936e-01 3.8897e-02 63 0.9
0292 2455085.81627549 936689741 181.333 -81.504 -9.2963e-02 5.6770e-01 6.3052e-01 3.8106e-02 44 1.4
```

```
0293 2455085.94696772 936701033 355.609 12.623 -9.2963e-02 5.6770e-01 6.3052e-01 3.8106e-02 37 1.4
0294 2455085.99814372 936705454 334.364 -73.035 -9.2963e-02 5.6770e-01 6.3052e-01 3.8106e-02 46 1.4
0295 2455086.33772210 936734794 51.412 -50.081 -9.2963e-02 5.6770e-01 6.3052e-01 3.8106e-02 41 1.4
0296 2455086.35776611 936736525 115.358 -1.712 -9.2963e-02 5.6770e-01 6.3052e-01 3.8106e-02 43 1.4
0297 2455086.40197481 936740345 212.435 -52.563 -5.8944e-02 2.9333e-01 5.7306e-01 3.8834e-02 101 0.6
0298 2455086.40866353 936740923 112.413 -1.239 -5.8944e-02 2.9333e-01 5.7306e-01 3.8834e-02 47 0.6
0299 2455086.48541717 936747555 131.185 -55.889 -1.3370e-01 8.5313e-01 6.3102e-01 3.7539e-02 28 2.4
0300 2455086.51202936 936749854 91.114 -85.172 -1.1724e-01 4.7983e-01 5.2936e-01 3.8897e-02 61 0.9
0301 2455086.81907830 936776383 272.525 -6.543 -9.2963e-02 5.6770e-01 6.3052e-01 3.8106e-02 56 1.4
0302 2455087.24479815 936813165 63.225 -16.889 -9.2963e-02 5.6770e-01 6.3052e-01 3.8106e-02 56 1.4
0303 2455087.38036137 936824878 215.603 -52.496 -1.1724e-01 4.7983e-01 5.2936e-01 3.8897e-02 33 0.9
0304 2455088.42721201 936915326 91.969 -36.275 -9.2963e-02 5.6770e-01 6.3052e-01 3.8106e-02 40 1.4
0305 2455088.46528086 936918615 132.251 -56.236 -9.2963e-02 5.6770e-01 6.3052e-01 3.8106e-02 66 1.4
0306 2455088.57025334 936927684 168.350 -16.421 -9.2963e-02 5.6770e-01 6.3052e-01 3.8106e-02 79 1.4
0307 2455089.41468143 937000643 245.913 -65.604 -9.2963e-02 5.6770e-01 6.3052e-01 3.8106e-02 45 1.4
0308 2455090.05202632 937055710 343.455 24.853 -9.2963e-02 5.6770e-01 6.3052e-01 3.8106e-02 38 1.4
0309 2455090.07066954 937057320 330.588 -13.538 -9.2963e-02 5.6770e-01 6.3052e-01 3.8106e-02 44 1.4
0310 2455090.07539159 937057728 2.778 6.638 -9.2963e-02 5.6770e-01 6.3052e-01 3.8106e-02 33 1.4
0311 2455090.08057983 937058177 328.174 16.945 -9.2963e-02 5.6770e-01 6.3052e-01 3.8106e-02 37 1.4
0312 2455090.11482057 937061135 307.431 -35.535 -9.2963e-02 5.6770e-01 6.3052e-01 3.8106e-02 42 1.4
0313 2455090.17635614 937066452 129.887 -15.388 -9.2963e-02 5.6770e-01 6.3052e-01 3.8106e-02 80 1.4
0314 2455090.26020686 937073696 99.595 -63.557 -9.2963e-02 5.6770e-01 6.3052e-01 3.8106e-02 50 1.4
0315 2455090.32316510 937079136 159.295 34.297 -9.2963e-02 5.6770e-01 6.3052e-01 3.8106e-02 47 1.4
0316 2455090.41727628 937087267 202.391 7.376 -9.2963e-02 5.6770e-01 6.3052e-01 3.8106e-02 45 1.4
0317 2455090.44945331 937090047 18.880 -41.386 -9.2963e-02 5.6770e-01 6.3052e-01 3.8106e-02 80 1.4
0318 2455090.46335818 937091249 271.916 -31.743 -9.2963e-02 5.6770e-01 6.3052e-01 3.8106e-02 58 1.4
0319 2455090.50333907 937094703 159.524 -15.889 -9.2963e-02 5.6770e-01 6.3052e-01 3.8106e-02 46 1.4
0320 2455091.11569909 937147611 181.766 -46.886 -9.2963e-02 5.6770e-01 6.3052e-01 3.8106e-02 39 1.4
0321 2455091.22797368 937157311 189.470 -64.559 -1.3370e-01 8.5313e-01 6.3102e-01 3.7539e-02 28 2.4
0322 2455091.24194602 937158519 93.087 -30.725 -9.2963e-02 5.6770e-01 6.3052e-01 3.8106e-02 45 1.4
0323 2455091.28544568 937162277 48.500 19.241 -1.3370e-01 8.5313e-01 6.3102e-01 3.7539e-02 31 2.4
0324 2455091.41615599 937173570 324.521 -48.735 -1.3370e-01 8.5313e-01 6.3102e-01 3.7539e-02 24 2.4
0325 2455091.44493275 937176057 229.094 -26.141 -9.2963e-02 5.6770e-01 6.3052e-01 3.8106e-02 42 1.4
0326 2455091.46355564 937177666 197.124 6.631 -1.3370e-01 8.5313e-01 6.3102e-01 3.7539e-02 23 2.4
0327 2455091.64030714 937192937 91.279 -40.405 -1.3370e-01 8.5313e-01 6.3102e-01 3.7539e-02 40 2.4
0328 2455091.76433502 937203653 187.982 -38.231 -1.1724e-01 4.7983e-01 5.2936e-01 3.8897e-02 36 0.9
0329 2455091.77363468 937204457 287.123 43.801 -9.2963e-02 5.6770e-01 6.3052e-01 3.8106e-02 42 1.4
0330 2455092.26310601 937246747 312.379 -64.703 -1.3370e-01 8.5313e-01 6.3102e-01 3.7539e-02 29 2.4
0331 2455092.38553911 937257325 43.981 -23.647 -1.3370e-01 8.5313e-01 6.3102e-01 3.7539e-02 55 2.4
0332 2455092.57538687 937273728 293.416 -31.917 -9.2963e-02 5.6770e-01 6.3052e-01 3.8106e-02 57 1.4
0333 2455092.63911316 937279234 260.435 27.843 -9.2963e-02 5.6770e-01 6.3052e-01 3.8106e-02 42 1.4
0334 2455092.81691255 937294596 353.786 12.035 -1.3370e-01 8.5313e-01 6.3102e-01 3.7539e-02 30 2.4
0335 2455092.82023761 937294883 186.894 -32.649 -9.2963e-02 5.6770e-01 6.3052e-01 3.8106e-02 33 1.4
0336 2455092.90980427 937302622 315.280 -0.447 -1.1724e-01 4.7983e-01 5.2936e-01 3.8897e-02 46 0.9
0337 2455092.94552705 937305708 298.898 -61.532 -9.2963e-02 5.6770e-01 6.3052e-01 3.8106e-02 88 1.4
0338 2455093.05334004 937315023 3.893 -7.564 -1.2873e-01 4.3155e-01 4.6595e-01 3.9162e-02 55 0.7
0339 2455093.29306832 937335736 193.268 -17.158 -1.3370e-01 8.5313e-01 6.3102e-01 3.7539e-02 22 2.4
0340 2455093.32564608 937338550 90.124 -5.205 -9.2963e-02 5.6770e-01 6.3052e-01 3.8106e-02 44 1.4
0341 2455093.40926251 937345775 317.116 -75.871 -9.2963e-02 5.6770e-01 6.3052e-01 3.8106e-02 33 1.4
0342 2455093.47608774 937351548 118.676 19.345 -1.1724e-01 4.7983e-01 5.2936e-01 3.8897e-02 57 0.9
0343 2455093.48161499 937352026 172.275 24.961 -9.2963e-02 5.6770e-01 6.3052e-01 3.8106e-02 70 1.4
0344 2455093.72319728 937372899 210.676 -15.984 -9.2963e-02 5.6770e-01 6.3052e-01 3.8106e-02 42 1.4
```

LIST OF HIGH ENERGY NEUTRINO CANDIDATES FOR THE 2009-2010 DATA

0345 2455093.85862360 937384600 289.632 28.662 -9.2963e-02 5.6770e-01 6.3052e-01 3.8106e-02 63 1.4
0346 2455094.04037710 937400303 45.899 30.911 -1.3370e-01 8.5313e-01 6.3102e-01 3.7539e-02 26 2.4
0347 2455094.09017880 937404606 73.479 -7.003 -1.1724e-01 4.7983e-01 5.2936e-01 3.8897e-02 40 0.9
0348 2455094.29038023 937421903 25.237 -8.833 -9.2963e-02 5.6770e-01 6.3052e-01 3.8106e-02 42 1.4
0349 2455094.43607690 937434492 210.009 -52.230 -9.2963e-02 5.6770e-01 6.3052e-01 3.8106e-02 54 1.4
0350 2455094.78884488 937464971 3.674 -48.582 -9.2963e-02 5.6770e-01 6.3052e-01 3.8106e-02 34 1.4
0351 2455094.92212449 937476486 353.805 -48.761 -1.1724e-01 4.7983e-01 5.2936e-01 3.8897e-02 51 0.9
0352 2455094.96444620 937480143 268.251 -11.069 -9.2963e-02 5.6770e-01 6.3052e-01 3.8106e-02 35 1.4
0353 2455095.02124958 937485050 21.663 1.555 -9.2963e-02 5.6770e-01 6.3052e-01 3.8106e-02 73 1.4
0354 2455095.08594664 937490640 95.314 -40.052 -9.2963e-02 5.6770e-01 6.3052e-01 3.8106e-02 37 1.4
0355 2455095.31074892 937510063 5.839 -69.210 -9.2963e-02 5.6770e-01 6.3052e-01 3.8106e-02 44 1.4
0356 2455095.40141202 937517896 51.941 -13.238 -9.2963e-02 5.6770e-01 6.3052e-01 3.8106e-02 58 1.4
0357 2455096.24040858 937590386 136.272 -47.028 -9.2963e-02 5.6770e-01 6.3052e-01 3.8106e-02 64 1.4
0358 2455096.29589030 937595179 146.780 -9.331 -9.2963e-02 5.6770e-01 6.3052e-01 3.8106e-02 40 1.4
0359 2455096.41449365 937605427 104.963 -33.021 -9.2963e-02 5.6770e-01 6.3052e-01 3.8106e-02 55 1.4
0360 2455096.52800333 937615234 128.593 -29.992 -9.2963e-02 5.6770e-01 6.3052e-01 3.8106e-02 32 1.4
0361 2455096.68391567 937628705 141.312 -39.629 -9.2963e-02 5.6770e-01 6.3052e-01 3.8106e-02 70 1.4
0362 2455097.45008271 937694902 228.978 -38.159 -9.2963e-02 5.6770e-01 6.3052e-01 3.8106e-02 32 1.4
0363 2455097.56872116 937705152 193.538 -2.264 -9.2963e-02 5.6770e-01 6.3052e-01 3.8106e-02 56 1.4
0364 2455098.16288293 937756488 148.194 -4.399 -9.2963e-02 5.6770e-01 6.3052e-01 3.8106e-02 35 1.4
0365 2455098.54092366 937789150 192.691 14.963 -9.2963e-02 5.6770e-01 6.3052e-01 3.8106e-02 40 1.4
0366 2455098.68646128 937801725 240.770 35.351 -9.2963e-02 5.6770e-01 6.3052e-01 3.8106e-02 48 1.4
0367 2455098.91636730 937821589 351.543 3.824 -9.2963e-02 5.6770e-01 6.3052e-01 3.8106e-02 36 1.4
0368 2455099.24073472 937849614 18.588 -14.617 -1.3370e-01 8.5313e-01 6.3102e-01 3.7539e-02 30 2.4
0369 2455099.59653242 937880355 296.078 0.247 -9.2963e-02 5.6770e-01 6.3052e-01 3.8106e-02 52 1.4
0370 2455099.63512643 937883689 175.922 0.378 -9.2963e-02 5.6770e-01 6.3052e-01 3.8106e-02 45 1.4
0371 2455099.79334823 937897360 93.697 -49.992 -1.1724e-01 4.7983e-01 5.2936e-01 3.8897e-02 40 0.9
0372 2455102.27178044 938111496 200.139 -27.965 -9.2963e-02 5.6770e-01 6.3052e-01 3.8106e-02 75 1.4
0373 2455102.27805785 938112039 67.798 22.646 -9.2963e-02 5.6770e-01 6.3052e-01 3.8106e-02 37 1.4
0374 2455102.35356275 938118562 132.628 -14.614 -9.2963e-02 5.6770e-01 6.3052e-01 3.8106e-02 40 1.4
0375 2455102.39752847 938122361 175.148 35.082 -9.2963e-02 5.6770e-01 6.3052e-01 3.8106e-02 41 1.4
0376 2455103.04918244 938178664 356.482 -3.559 -9.2963e-02 5.6770e-01 6.3052e-01 3.8106e-02 32 1.4
0377 2455103.40413438 938209332 278.252 -36.117 -9.2963e-02 5.6770e-01 6.3052e-01 3.8106e-02 38 1.4
0378 2455103.58586945 938225034 282.729 -79.220 -1.3370e-01 8.5313e-01 6.3102e-01 3.7539e-02 29 2.4
0379 2455103.78034553 938241836 204.419 -18.149 -9.2963e-02 5.6770e-01 6.3052e-01 3.8106e-02 36 1.4
0380 2455103.88545957 938250918 15.509 1.608 -9.2963e-02 5.6770e-01 6.3052e-01 3.8106e-02 52 1.4
0381 2455103.94084063 938255703 45.803 30.019 -9.2963e-02 5.6770e-01 6.3052e-01 3.8106e-02 47 1.4
0382 2455104.04120529 938264375 53.910 -56.310 -1.2873e-01 4.3155e-01 4.6595e-01 3.9162e-02 60 0.7
0383 2455104.16566846 938275128 288.279 -56.157 -9.2963e-02 5.6770e-01 6.3052e-01 3.8106e-02 74 1.4
0384 2455104.20894439 938278867 210.871 -51.328 -1.1724e-01 4.7983e-01 5.2936e-01 3.8897e-02 59 0.9
0385 2455104.23098445 938280772 63.085 -23.178 -9.2963e-02 5.6770e-01 6.3052e-01 3.8106e-02 33 1.4
0386 2455104.48051724 938302331 226.405 -28.934 -9.2963e-02 5.6770e-01 6.3052e-01 3.8106e-02 38 1.4
0387 2455104.68229967 938319765 288.159 -42.235 -1.1724e-01 4.7983e-01 5.2936e-01 3.8897e-02 75 0.9
0388 2455104.70328215 938321578 307.095 -6.614 -1.1724e-01 4.7983e-01 5.2936e-01 3.8897e-02 37 0.9
0389 2455104.90458370 938338971 8.751 -29.573 -9.2963e-02 5.6770e-01 6.3052e-01 3.8106e-02 51 1.4
0390 2455105.26904169 938370460 135.057 -0.240 -9.2963e-02 5.6770e-01 6.3052e-01 3.8106e-02 52 1.4
0391 2455105.47162534 938387963 76.853 -23.921 -1.3370e-01 8.5313e-01 6.3102e-01 3.7539e-02 24 2.4
0392 2455105.47359406 938388133 169.350 6.763 -1.1724e-01 4.7983e-01 5.2936e-01 3.8897e-02 37 0.9
0393 2455105.69289356 938407081 331.632 -21.688 -9.2963e-02 5.6770e-01 6.3052e-01 3.8106e-02 62 1.4
0394 2455106.09898691 938442167 349.394 -64.148 -1.3370e-01 8.5313e-01 6.3102e-01 3.7539e-02 30 2.4
0395 2455106.10501045 938442687 97.016 -14.779 -1.3370e-01 8.5313e-01 6.3102e-01 3.7539e-02 17 2.4
0396 2455106.13841955 938445574 20.880 -34.063 -1.3370e-01 8.5313e-01 6.3102e-01 3.7539e-02 18 2.4

```
0397 2455106.15760056 938447231 111.651 -66.684 -9.2963e-02 5.6770e-01 6.3052e-01 3.8106e-02 33 1.4
0398 2455106.15804839 938447270 308.309 -35.751 -1.1724e-01 4.7983e-01 5.2936e-01 3.8897e-02 55 0.9
0399 2455106.33725387 938462753 69.956 18.560 -1.3370e-01 8.5313e-01 6.3102e-01 3.7539e-02 29 2.4
0400 2455106.33770698 938462792 35.802 -64.301 -9.2963e-02 5.6770e-01 6.3052e-01 3.8106e-02 57 1.4
0401 2455106.38053544 938466493 230.019 -43.933 -1.1724e-01 4.7983e-01 5.2936e-01 3.8897e-02 35 0.9
0402 2455106.41301495 938469299 303.756 -66.111 -9.2963e-02 5.6770e-01 6.3052e-01 3.8106e-02 67 1.4
0403 2455106.43796736 938471455 173.146 22.524 -9.2963e-02 5.6770e-01 6.3052e-01 3.8106e-02 35 1.4
0404 2455106.59420504 938484954 267.949 15.123 -1.3370e-01 8.5313e-01 6.3102e-01 3.7539e-02 30 2.4
0405 2455106.59899067 938485367 186.962 -13.071 -1.3370e-01 8.5313e-01 6.3102e-01 3.7539e-02 20 2.4
0406 2455106.67855854 938492242 28.342 -53.398 -1.3370e-01 8.5313e-01 6.3102e-01 3.7539e-02 24 2.4
0407 2455106.68526612 938492821 183.389 -35.410 -1.3370e-01 8.5313e-01 6.3102e-01 3.7539e-02 27 2.4
0408 2455106.75716598 938499034 204.453 -8.382 -1.3370e-01 8.5313e-01 6.3102e-01 3.7539e-02 27 2.4
0409 2455106.93284884 938514213 6.804 17.120 -9.2963e-02 5.6770e-01 6.3052e-01 3.8106e-02 41 1.4
0410 2455106.94926794 938515631 275.171 -49.706 -1.3370e-01 8.5313e-01 6.3102e-01 3.7539e-02 31 2.4
0411 2455107.06586108 938525705 200.162 -51.684 -9.2963e-02 5.6770e-01 6.3052e-01 3.8106e-02 50 1.4
0412 2455107.06993162 938526057 89.805 -19.215 -1.3370e-01 8.5313e-01 6.3102e-01 3.7539e-02 26 2.4
0413 2455107.16309664 938534106 113.966 -2.746 -1.3370e-01 8.5313e-01 6.3102e-01 3.7539e-02 29 2.4
0414 2455107.22904195 938539804 47.678 -1.816 -9.2963e-02 5.6770e-01 6.3052e-01 3.8106e-02 33 1.4
0415 2455107.24446919 938541137 29.501 5.593 -9.2963e-02 5.6770e-01 6.3052e-01 3.8106e-02 52 1.4
0416 2455107.73067877 938583145 163.598 -27.937 -1.3370e-01 8.5313e-01 6.3102e-01 3.7539e-02 30 2.4
0417 2455107.74286200 938584198 15.701 -15.867 -9.2963e-02 5.6770e-01 6.3052e-01 3.8106e-02 52 1.4
0418 2455108.09088190 938614267 210.184 -75.982 -1.1909e-01 7.2127e-01 6.0423e-01 3.7507e-02 26 1.8
0419 2455108.13113839 938617745 76.988 -27.793 -1.1909e-01 7.2127e-01 6.0423e-01 3.7507e-02 27 1.8
0420 2455108.65188488 938662737 302.757 8.166 -9.2963e-02 5.6770e-01 6.3052e-01 3.8106e-02 34 1.4
0421 2455108.72213116 938668807 254.230 -49.669 -1.1724e-01 4.7983e-01 5.2936e-01 3.8897e-02 69 0.9
0422 2455108.77672014 938673523 233.790 16.947 -1.3370e-01 8.5313e-01 6.3102e-01 3.7539e-02 19 2.4
0423 2455108.93658872 938687336 88.782 -11.029 -9.2963e-02 5.6770e-01 6.3052e-01 3.8106e-02 38 1.4
0424 2455108.94028716 938687655 302.904 11.418 -1.3370e-01 8.5313e-01 6.3102e-01 3.7539e-02 30 2.4
0425 2455109.04694551 938696871 277.608 -35.585 -9.2963e-02 5.6770e-01 6.3052e-01 3.8106e-02 34 1.4
0426 2455109.27708373 938716755 42.313 12.270 -9.2963e-02 5.6770e-01 6.3052e-01 3.8106e-02 63 1.4
0427 2455109.27978510 938716988 81.125 24.193 -1.1724e-01 4.7983e-01 5.2936e-01 3.8897e-02 60 0.9
0428 2455109.30529717 938719192 245.768 -54.777 -9.2963e-02 5.6770e-01 6.3052e-01 3.8106e-02 48 1.4
0429 2455109.32126382 938720572 111.881 7.221 -1.1724e-01 4.7983e-01 5.2936e-01 3.8897e-02 46 0.9
0430 2455109.50827962 938736730 97.654 -76.296 -9.2963e-02 5.6770e-01 6.3052e-01 3.8106e-02 37 1.4
0431 2455109.64102689 938748199 150.037 -53.125 -9.2963e-02 5.6770e-01 6.3052e-01 3.8106e-02 28 1.4
0432 2455109.70997371 938754156 240.039 -55.760 -1.3370e-01 8.5313e-01 6.3102e-01 3.7539e-02 28 2.4
0433 2455109.78012252 938760217 191.092 -76.308 -9.2963e-02 5.6770e-01 6.3052e-01 3.8106e-02 48 1.4
0434 2455109.95262540 938775121 307.876 27.691 -9.2963e-02 5.6770e-01 6.3052e-01 3.8106e-02 38 1.4
0435 2455110.35278849 938809695 0.831 -83.787 -9.2963e-02 5.6770e-01 6.3052e-01 3.8106e-02 36 1.4
0436 2455110.39121065 938813015 231.918 -15.213 -9.2963e-02 5.6770e-01 6.3052e-01 3.8106e-02 70 1.4
0437 2455110.75548297 938844488 15.339 -17.305 -1.3370e-01 8.5313e-01 6.3102e-01 3.7539e-02 24 2.4
0438 2455110.76066198 938844936 77.634 -68.946 -1.1724e-01 4.7983e-01 5.2936e-01 3.8897e-02 58 0.9
0439 2455110.80497928 938848765 314.592 -2.379 -1.1724e-01 4.7983e-01 5.2936e-01 3.8897e-02 85 0.9
0440 2455110.91119889 938857942 262.753 2.770 -1.3370e-01 8.5313e-01 6.3102e-01 3.7539e-02 25 2.4
0441 2455110.99633956 938865298 78.485 25.500 -1.3370e-01 8.5313e-01 6.3102e-01 3.7539e-02 45 2.4
0442 2455111.07609910 938872189 62.979 -7.400 -1.1724e-01 4.7983e-01 5.2936e-01 3.8897e-02 42 0.9
0443 2455111.29796803 938891359 209.033 -50.034 -1.3370e-01 8.5313e-01 6.3102e-01 3.7539e-02 25 2.4
0444 2455111.31306605 938892663 224.628 -12.990 -1.3370e-01 8.5313e-01 6.3102e-01 3.7539e-02 26 2.4
0445 2455111.34094428 938895072 177.023 -21.854 -1.1724e-01 4.7983e-01 5.2936e-01 3.8897e-02 43 0.9
0446 2455111.52696723 938911144 221.214 -20.684 -1.2873e-01 4.3155e-01 4.6595e-01 3.9162e-02 77 0.7
0447 2455112.40857237 938987315 233.452 -14.584 -1.2873e-01 4.3155e-01 4.6595e-01 3.9162e-02 45 0.7
0448 2455112.49756440 938995004 126.204 -2.166 -9.2963e-02 5.6770e-01 6.3052e-01 3.8106e-02 35 1.4
```

LIST OF HIGH ENERGY NEUTRINO CANDIDATES FOR THE 2009-2010 DATA

0449 2455112.67848511 939010636 173.150 -48.876 -9.2963e-02 5.6770e-01 6.3052e-01 3.8106e-02 54 1.4
0450 2455112.80672018 939021715 200.152 -36.498 -9.2963e-02 5.6770e-01 6.3052e-01 3.8106e-02 54 1.4
0451 2455112.94746167 939033875 107.088 -34.198 -9.2963e-02 5.6770e-01 6.3052e-01 3.8106e-02 42 1.4
0452 2455113.29913474 939064260 146.416 39.410 -9.2963e-02 5.6770e-01 6.3052e-01 3.8106e-02 49 1.4
0453 2455113.52092373 939083422 170.341 6.919 -9.2963e-02 5.6770e-01 6.3052e-01 3.8106e-02 46 1.4
0454 2455113.66173084 939095588 356.420 -35.023 -9.2963e-02 5.6770e-01 6.3052e-01 3.8106e-02 40 1.4
0455 2455113.74950718 939103172 24.051 -14.475 -9.2963e-02 5.6770e-01 6.3052e-01 3.8106e-02 25 1.4
0456 2455113.87727032 939114211 72.400 -22.222 -1.1909e-01 7.2127e-01 6.0423e-01 3.7507e-02 29 1.8
0457 2455114.02079491 939126611 14.529 -34.800 -9.2963e-02 5.6770e-01 6.3052e-01 3.8106e-02 41 1.4
0458 2455114.08210711 939131909 131.171 -56.990 -9.2963e-02 5.6770e-01 6.3052e-01 3.8106e-02 39 1.4
0459 2455114.10003122 939133457 149.562 -23.916 -9.2963e-02 5.6770e-01 6.3052e-01 3.8106e-02 46 1.4
0460 2455114.47014329 939165435 171.940 -58.800 -1.1724e-01 4.7983e-01 5.2936e-01 3.8897e-02 72 0.9
0461 2455114.48221273 939166478 330.533 -41.798 -1.3370e-01 8.5313e-01 6.3102e-01 3.7539e-02 23 2.4
0462 2455114.61945104 939178335 299.100 -24.130 -1.1724e-01 4.7983e-01 5.2936e-01 3.8897e-02 46 0.9
0463 2455114.96373037 939208081 23.482 -38.374 -9.2963e-02 5.6770e-01 6.3052e-01 3.8106e-02 56 1.4
0464 2455115.20252461 939228713 7.009 -12.443 -9.2963e-02 5.6770e-01 6.3052e-01 3.8106e-02 33 1.4
0465 2455115.25815626 939233519 122.012 5.774 -9.2963e-02 5.6770e-01 6.3052e-01 3.8106e-02 40 1.4
0466 2455115.69694165 939271430 243.642 -31.468 -9.2963e-02 5.6770e-01 6.3052e-01 3.8106e-02 45 1.4
0467 2455115.73724370 939274912 339.596 30.885 -9.2963e-02 5.6770e-01 6.3052e-01 3.8106e-02 34 1.4
0468 2455115.77108010 939277836 251.583 -16.284 -1.3370e-01 8.5313e-01 6.3102e-01 3.7539e-02 29 2.4
0469 2455115.85696732 939285256 14.422 1.130 -9.2963e-02 5.6770e-01 6.3052e-01 3.8106e-02 34 1.4
0470 2455115.96788788 939294840 278.270 -83.675 -9.2963e-02 5.6770e-01 6.3052e-01 3.8106e-02 41 1.4
0471 2455115.96792188 939294843 237.923 -69.630 -1.3370e-01 8.5313e-01 6.3102e-01 3.7539e-02 30 2.4
0472 2455116.24429123 939318721 194.052 -28.568 -9.2963e-02 5.6770e-01 6.3052e-01 3.8106e-02 40 1.4
0473 2455116.42582425 939334406 351.379 -55.731 -9.2963e-02 5.6770e-01 6.3052e-01 3.8106e-02 56 1.4
0474 2455116.42960646 939334732 209.405 -17.414 -9.2963e-02 5.6770e-01 6.3052e-01 3.8106e-02 57 1.4
0475 2455116.59190139 939348755 164.209 -70.024 -9.2963e-02 5.6770e-01 6.3052e-01 3.8106e-02 53 1.4
0476 2455116.66839094 939355363 205.711 -67.549 -9.2963e-02 5.6770e-01 6.3052e-01 3.8106e-02 46 1.4
0477 2455116.72638818 939360374 89.399 -46.879 -9.2963e-02 5.6770e-01 6.3052e-01 3.8106e-02 41 1.4
0478 2455116.75696082 939363016 217.008 -18.117 -9.2963e-02 5.6770e-01 6.3052e-01 3.8106e-02 87 1.4
0479 2455116.91970536 939377077 299.273 -34.680 -9.2963e-02 5.6770e-01 6.3052e-01 3.8106e-02 40 1.4
0480 2455116.96917723 939381351 297.645 -0.251 -9.2963e-02 5.6770e-01 6.3052e-01 3.8106e-02 54 1.4
0481 2455117.11302713 939393780 58.528 -35.957 -1.1724e-01 4.7983e-01 5.2936e-01 3.8897e-02 44 0.9
0482 2455117.13440548 939395627 220.053 -52.071 -1.1724e-01 4.7983e-01 5.2936e-01 3.8897e-02 37 0.9
0483 2455117.30518671 939410383 87.764 -69.789 -9.2963e-02 5.6770e-01 6.3052e-01 3.8106e-02 42 1.4
0484 2455117.39428554 939418081 51.843 -27.383 -1.3370e-01 8.5313e-01 6.3102e-01 3.7539e-02 23 2.4
0485 2455117.41056783 939419488 62.812 -23.353 -9.2963e-02 5.6770e-01 6.3052e-01 3.8106e-02 42 1.4
0486 2455117.43264564 939421395 86.844 -31.075 -9.2963e-02 5.6770e-01 6.3052e-01 3.8106e-02 36 1.4
0487 2455117.44347119 939422330 222.113 -20.451 -1.2873e-01 4.3155e-01 4.6595e-01 3.9162e-02 46 0.7
0488 2455117.47784299 939425300 147.514 33.030 -9.2963e-02 5.6770e-01 6.3052e-01 3.8106e-02 58 1.4
0489 2455117.58490281 939434550 301.777 10.870 -9.2963e-02 5.6770e-01 6.3052e-01 3.8106e-02 37 1.4
0490 2455117.99339341 939469844 291.060 -38.797 -9.2963e-02 5.6770e-01 6.3052e-01 3.8106e-02 32 1.4
0491 2455118.09652087 939478754 339.369 -46.066 -9.2963e-02 5.6770e-01 6.3052e-01 3.8106e-02 37 1.4
0492 2455118.18926273 939486767 89.990 -53.063 -9.2963e-02 5.6770e-01 6.3052e-01 3.8106e-02 53 1.4
0493 2455118.71224171 939531952 10.798 -7.637 -9.2963e-02 5.6770e-01 6.3052e-01 3.8106e-02 40 1.4
0494 2455118.78390243 939538144 353.904 15.452 -9.2963e-02 5.6770e-01 6.3052e-01 3.8106e-02 61 1.4
0495 2455118.82267344 939541493 283.496 -49.890 -1.1909e-01 7.2127e-01 6.0423e-01 3.7507e-02 27 1.8
0496 2455118.83480135 939542541 31.539 -29.662 -1.1724e-01 4.7983e-01 5.2936e-01 3.8897e-02 69 0.9
0497 2455118.93664650 939551341 345.681 -26.193 -1.1724e-01 4.7983e-01 5.2936e-01 3.8897e-02 56 0.9
0498 2455118.95626420 939553036 0.772 26.750 -9.2963e-02 5.6770e-01 6.3052e-01 3.8106e-02 44 1.4
0499 2455118.98722376 939555711 31.086 44.150 -1.3370e-01 8.5313e-01 6.3102e-01 3.7539e-02 28 2.4
0500 2455119.06038976 939562032 107.194 -46.814 -1.1724e-01 4.7983e-01 5.2936e-01 3.8897e-02 43 0.9

```
0501 2455119.10381960 939565785 111.700 -29.431 -1.1724e-01 4.7983e-01 5.2936e-01 3.8897e-02 52 0.9
0502 2455119.23430143 939577058 98.321 19.419 -9.2963e-02 5.6770e-01 6.3052e-01 3.8106e-02 79 1.4
0503 2455119.50723823 939600640 117.050 -25.781 -9.2963e-02 5.6770e-01 6.3052e-01 3.8106e-02 36 1.4
0504 2455119.54814882 939604175 128.668 -73.127 -1.3370e-01 8.5313e-01 6.3102e-01 3.7539e-02 31 2.4
0505 2455119.60944940 939609471 103.082 -79.016 -1.3370e-01 8.5313e-01 6.3102e-01 3.7539e-02 26 2.4
0506 2455119.66618321 939614373 288.891 10.154 -1.3370e-01 8.5313e-01 6.3102e-01 3.7539e-02 27 2.4
0507 2455119.80532641 939626395 339.224 -13.088 -9.2963e-02 5.6770e-01 6.3052e-01 3.8106e-02 55 1.4
0508 2455119.85847406 939630987 13.254 -22.584 -9.2963e-02 5.6770e-01 6.3052e-01 3.8106e-02 32 1.4
0509 2455119.87126979 939632092 301.247 -15.812 -9.2963e-02 5.6770e-01 6.3052e-01 3.8106e-02 100 1.4
0510 2455120.14462516 939655710 38.322 27.279 -9.2963e-02 5.6770e-01 6.3052e-01 3.8106e-02 73 1.4
0511 2455120.43275522 939680605 214.461 -53.564 -1.1724e-01 4.7983e-01 5.2936e-01 3.8897e-02 53 0.9
0512 2455120.47931155 939684627 333.194 -46.537 -1.1724e-01 4.7983e-01 5.2936e-01 3.8897e-02 77 0.9
0513 2455120.49385715 939685884 227.452 45.373 -9.2963e-02 5.6770e-01 6.3052e-01 3.8106e-02 39 1.4
0514 2455120.69817599 939703537 6.947 -61.248 -9.2963e-02 5.6770e-01 6.3052e-01 3.8106e-02 35 1.4
0515 2455120.73808635 939706985 234.113 -47.606 -9.2963e-02 5.6770e-01 6.3052e-01 3.8106e-02 38 1.4
0516 2455120.81641992 939713753 294.394 24.516 -9.2963e-02 5.6770e-01 6.3052e-01 3.8106e-02 35 1.4
0517 2455120.89703852 939720719 256.611 -70.079 -1.1724e-01 4.7983e-01 5.2936e-01 3.8897e-02 33 0.9
0518 2455120.98134161 939728002 90.085 22.423 -1.1724e-01 4.7983e-01 5.2936e-01 3.8897e-02 50 0.9
0519 2455121.18227442 939745363 162.392 -43.568 -1.3370e-01 8.5313e-01 6.3102e-01 3.7539e-02 31 2.4
0520 2455121.33633591 939758674 90.349 5.215 -1.1724e-01 4.7983e-01 5.2936e-01 3.8897e-02 34 0.9
0521 2455121.77626935 939796684 280.168 -57.413 -1.1724e-01 4.7983e-01 5.2936e-01 3.8897e-02 72 0.9
0522 2455121.92770574 939809768 46.175 -18.464 -9.2963e-02 5.6770e-01 6.3052e-01 3.8106e-02 41 1.4
0523 2455122.35754073 939846906 121.636 5.775 -9.2963e-02 5.6770e-01 6.3052e-01 3.8106e-02 36 1.4
0524 2455122.53895372 939862580 233.077 -7.957 -1.1724e-01 4.7983e-01 5.2936e-01 3.8897e-02 37 0.9
0525 2455122.88976745 939892890 21.355 -24.817 -1.1724e-01 4.7983e-01 5.2936e-01 3.8897e-02 26 0.9
0526 2455122.96905831 939899741 349.006 31.298 -9.2963e-02 5.6770e-01 6.3052e-01 3.8106e-02 64 1.4
0527 2455123.17154615 939917236 250.627 -48.299 -9.2963e-02 5.6770e-01 6.3052e-01 3.8106e-02 68 1.4
0528 2455123.31624400 939929738 165.563 -5.823 -1.1909e-01 7.2127e-01 6.0423e-01 3.7507e-02 30 1.8
0529 2455123.43635652 939940116 273.038 -58.888 -9.2963e-02 5.6770e-01 6.3052e-01 3.8106e-02 53 1.4
0530 2455123.50894756 939946388 121.026 -53.723 -9.2963e-02 5.6770e-01 6.3052e-01 3.8106e-02 34 1.4
0531 2455123.77341984 939969238 242.247 -78.692 -9.2963e-02 5.6770e-01 6.3052e-01 3.8106e-02 42 1.4
0532 2455123.81395575 939972740 0.505 -50.354 -1.1724e-01 4.7983e-01 5.2936e-01 3.8897e-02 58 0.9
0533 2455123.84153899 939975123 3.414 14.939 -9.2963e-02 5.6770e-01 6.3052e-01 3.8106e-02 34 1.4
0534 2455124.41617295 940024772 218.431 17.849 -9.2963e-02 5.6770e-01 6.3052e-01 3.8106e-02 53 1.4
0535 2455124.42550676 940025578 278.630 -23.522 -9.2963e-02 5.6770e-01 6.3052e-01 3.8106e-02 80 1.4
0536 2455124.66281391 940046082 246.738 -75.528 -1.1724e-01 4.7983e-01 5.2936e-01 3.8897e-02 55 0.9
0537 2455124.73301856 940052147 308.761 -75.284 -9.2963e-02 5.6770e-01 6.3052e-01 3.8106e-02 78 1.4
0538 2455124.89469364 940066116 320.685 -33.509 -9.2963e-02 5.6770e-01 6.3052e-01 3.8106e-02 39 1.4
0539 2455124.99847915 940075083 51.269 -66.319 -1.3370e-01 8.5313e-01 6.3102e-01 3.7539e-02 21 2.4
0540 2455125.05026863 940079558 3.031 -9.007 -9.2963e-02 5.6770e-01 6.3052e-01 3.8106e-02 32 1.4
0541 2455125.13125508 940086555 31.563 8.618 -9.2963e-02 5.6770e-01 6.3052e-01 3.8106e-02 34 1.4
0542 2455125.17651380 940090465 346.590 -53.355 -1.1909e-01 7.2127e-01 6.0423e-01 3.7507e-02 31 1.8
0543 2455125.54695083 940122471 210.268 -65.801 -1.3370e-01 8.5313e-01 6.3102e-01 3.7539e-02 23 2.4
0544 2455125.67692770 940133701 243.164 16.606 -9.2963e-02 5.6770e-01 6.3052e-01 3.8106e-02 39 1.4
0545 2455125.78264708 940142835 9.373 -49.397 -1.1724e-01 4.7983e-01 5.2936e-01 3.8897e-02 58 0.9
0546 2455125.82050078 940146106 271.614 -68.371 -9.2963e-02 5.6770e-01 6.3052e-01 3.8106e-02 36 1.4
0547 2455125.86797558 940150208 26.170 39.099 -9.2963e-02 5.6770e-01 6.3052e-01 3.8106e-02 40 1.4
0548 2455126.16958920 940176267 26.159 -3.051 -9.2963e-02 5.6770e-01 6.3052e-01 3.8106e-02 44 1.4
0549 2455126.57395115 940211204 277.858 31.085 -1.1724e-01 4.7983e-01 5.2936e-01 3.8897e-02 45 0.9
0550 2455126.84745015 940234834 42.955 21.035 -1.1909e-01 7.2127e-01 6.0423e-01 3.7507e-02 26 1.8
0551 2455126.89342438 940238806 104.686 -34.039 -1.1724e-01 4.7983e-01 5.2936e-01 3.8897e-02 53 0.9
0552 2455126.90883151 940240138 40.048 -63.297 -9.2963e-02 5.6770e-01 6.3052e-01 3.8106e-02 41 1.4
```

LIST OF HIGH ENERGY NEUTRINO CANDIDATES FOR THE 2009-2010 DATA

0553	2455127.62431524	940301955	276.272	9.594	-1.2873e-01	4.3155e-01	4.6595e-01	3.9162e-02	64	0.7
0554	2455127.70146982	940308621	40.170	-42.834	-1.1724e-01	4.7983e-01	5.2936e-01	3.8897e-02	37	0.9
0555	2455127.78941914	940316220	317.629	37.671	-1.1724e-01	4.7983e-01	5.2936e-01	3.8897e-02	47	0.9
0556	2455128.37791950	940367067	226.634	-67.325	-9.2963e-02	5.6770e-01	6.3052e-01	3.8106e-02	41	1.4
0557	2455128.48421007	940376250	332.441	-29.655	-9.2963e-02	5.6770e-01	6.3052e-01	3.8106e-02	45	1.4
0558	2455128.49604244	940377273	222.078	42.240	-9.2963e-02	5.6770e-01	6.3052e-01	3.8106e-02	57	1.4
0559	2455128.87890660	940410352	33.977	-13.513	-9.2963e-02	5.6770e-01	6.3052e-01	3.8106e-02	34	1.4
0560	2455128.94782299	940416306	82.861	-28.278	-1.1724e-01	4.7983e-01	5.2936e-01	3.8897e-02	45	0.9
0561	2455128.99911445	940420738	28.863	39.702	-9.2963e-02	5.6770e-01	6.3052e-01	3.8106e-02	48	1.4
0562	2455129.23151505	940440817	63.399	-53.583	-9.2963e-02	5.6770e-01	6.3052e-01	3.8106e-02	36	1.4
0563	2455129.24410961	940441906	6.151	-58.770	-1.3370e-01	8.5313e-01	6.3102e-01	3.7539e-02	21	2.4
0564	2455129.42888012	940457870	165.708	-58.167	-1.3370e-01	8.5313e-01	6.3102e-01	3.7539e-02	25	2.4
0565	2455129.46803809	940461253	26.096	-57.126	-1.3370e-01	8.5313e-01	6.3102e-01	3.7539e-02	47	2.4
0566	2455129.63331953	940475533	260.848	-32.698	-1.3370e-01	8.5313e-01	6.3102e-01	3.7539e-02	36	2.4
0567	2455129.74693742	940485350	166.756	-58.293	-9.2963e-02	5.6770e-01	6.3052e-01	3.8106e-02	52	1.4
0568	2455129.85060141	940494306	65.732	-60.227	-9.2963e-02	5.6770e-01	6.3052e-01	3.8106e-02	43	1.4
0569	2455129.97996590	940505484	212.346	-48.187	-1.1724e-01	4.7983e-01	5.2936e-01	3.8897e-02	34	0.9
0570	2455130.04261403	940510896	313.204	-18.608	-1.3370e-01	8.5313e-01	6.3102e-01	3.7539e-02	21	2.4
0571	2455130.71697979	940569162	276.164	0.823	-1.1724e-01	4.7983e-01	5.2936e-01	3.8897e-02	44	0.9
0572	2455130.73928354	940571089	342.991	-32.316	-1.1724e-01	4.7983e-01	5.2936e-01	3.8897e-02	42	0.9
0573	2455130.90883162	940585738	90.482	-23.827	-9.2963e-02	5.6770e-01	6.3052e-01	3.8106e-02	94	1.4
0574	2455131.04302858	940597332	149.284	-3.053	-1.3370e-01	8.5313e-01	6.3102e-01	3.7539e-02	26	2.4
0575	2455131.09322920	940601670	25.112	15.380	-9.2963e-02	5.6770e-01	6.3052e-01	3.8106e-02	46	1.4
0576	2455131.09736405	940602027	330.097	-22.425	-1.3370e-01	8.5313e-01	6.3102e-01	3.7539e-02	26	2.4
0577	2455131.10132227	940602369	70.967	24.886	-9.2963e-02	5.6770e-01	6.3052e-01	3.8106e-02	40	1.4
0578	2455131.13305411	940605110	21.637	-26.976	-1.1724e-01	4.7983e-01	5.2936e-01	3.8897e-02	61	0.9
0579	2455131.46665416	940633933	27.225	-51.185	-1.1724e-01	4.7983e-01	5.2936e-01	3.8897e-02	84	0.9
0580	2455131.50656328	940637382	218.474	32.134	-9.2963e-02	5.6770e-01	6.3052e-01	3.8106e-02	45	1.4
0581	2455131.73572846	940657181	268.470	29.503	-9.2963e-02	5.6770e-01	6.3052e-01	3.8106e-02	67	1.4
0582	2455132.41269022	940715671	91.722	-16.046	-9.2963e-02	5.6770e-01	6.3052e-01	3.8106e-02	52	1.4
0583	2455132.71350595	940741661	230.084	-2.542	-9.2963e-02	5.6770e-01	6.3052e-01	3.8106e-02	40	1.4
0584	2455133.24511799	940787593	34.831	-10.815	-9.2963e-02	5.6770e-01	6.3052e-01	3.8106e-02	36	1.4
0585	2455133.86701904	940841325	181.531	-53.320	-1.3370e-01	8.5313e-01	6.3102e-01	3.7539e-02	29	2.4
0586	2455133.87178621	940841737	346.348	-25.473	-1.1724e-01	4.7983e-01	5.2936e-01	3.8897e-02	79	0.9
0587	2455133.93840643	940847493	359.884	-8.175	-9.2963e-02	5.6770e-01	6.3052e-01	3.8106e-02	66	1.4
0588	2455133.94025409	940847652	217.462	-56.767	-9.2963e-02	5.6770e-01	6.3052e-01	3.8106e-02	70	1.4
0589	2455133.94301469	940847891	317.600	-33.199	-9.2963e-02	5.6770e-01	6.3052e-01	3.8106e-02	66	1.4
0590	2455134.88193759	940929014	334.006	10.852	-9.2963e-02	5.6770e-01	6.3052e-01	3.8106e-02	42	1.4
0591	2455135.17944633	940954719	171.056	-40.090	-1.3370e-01	8.5313e-01	6.3102e-01	3.7539e-02	29	2.4
0592	2455135.27592074	940963054	136.558	34.198	-9.2963e-02	5.6770e-01	6.3052e-01	3.8106e-02	39	1.4
0593	2455135.30288916	940965384	134.181	-41.672	-1.1724e-01	4.7983e-01	5.2936e-01	3.8897e-02	51	0.9
0594	2455136.66749813	941083286	251.830	22.254	-9.2963e-02	5.6770e-01	6.3052e-01	3.8106e-02	42	1.4
0595	2455136.73338158	941088979	267.951	-18.728	-9.2963e-02	5.6770e-01	6.3052e-01	3.8106e-02	43	1.4
0596	2455136.90881518	941104136	325.566	29.975	-9.2963e-02	5.6770e-01	6.3052e-01	3.8106e-02	39	1.4
0597	2455137.01383289	941113210	107.265	-21.099	-1.1724e-01	4.7983e-01	5.2936e-01	3.8897e-02	89	0.9
0598	2455137.05125840	941116443	356.996	18.432	-1.3370e-01	8.5313e-01	6.3102e-01	3.7539e-02	14	2.4
0599	2455137.40940642	941147387	194.166	38.150	-1.1724e-01	4.7983e-01	5.2936e-01	3.8897e-02	53	0.9
0600	2455138.07224381	941204656	45.023	-73.484	-1.1724e-01	4.7983e-01	5.2936e-01	3.8897e-02	29	0.9
0601	2455138.22964691	941218256	187.377	22.481	-9.2963e-02	5.6770e-01	6.3052e-01	3.8106e-02	54	1.4
0602	2455138.49297261	941241007	319.308	-68.022	-9.2963e-02	5.6770e-01	6.3052e-01	3.8106e-02	41	1.4
0603	2455138.66407874	941255791	259.420	15.133	-9.2963e-02	5.6770e-01	6.3052e-01	3.8106e-02	32	1.4
0604	2455138.70878856	941259654	305.961	-56.371	-9.2963e-02	5.6770e-01	6.3052e-01	3.8106e-02	53	1.4

```
0605 2455138.80484908 941267953 267.146 6.146 -9.2963e-02 5.6770e-01 6.3052e-01 3.8106e-02 44 1.4
0606 2455139.17659348 941300072 188.397 -18.520 -9.2963e-02 5.6770e-01 6.3052e-01 3.8106e-02 33 1.4
0607 2455139.38663643 941318220 301.403 -39.883 -9.2963e-02 5.6770e-01 6.3052e-01 3.8106e-02 33 1.4
0608 2455139.55354005 941332640 120.588 -45.707 -9.2963e-02 5.6770e-01 6.3052e-01 3.8106e-02 32 1.4
0609 2455139.67658649 941343272 288.496 -10.161 -9.2963e-02 5.6770e-01 6.3052e-01 3.8106e-02 48 1.4
0610 2455139.84273192 941357627 30.147 4.845 -9.2963e-02 5.6770e-01 6.3052e-01 3.8106e-02 37 1.4
0611 2455139.93447511 941365553 288.410 -34.817 -1.2873e-01 4.3155e-01 4.6595e-01 3.9162e-02 38 0.7
0612 2455139.97019810 941368640 65.107 37.544 -9.2963e-02 5.6770e-01 6.3052e-01 3.8106e-02 54 1.4
0613 2455140.06783770 941377076 11.931 19.418 -9.2963e-02 5.6770e-01 6.3052e-01 3.8106e-02 39 1.4
0614 2455140.20084105 941388567 10.769 -43.905 -9.2963e-02 5.6770e-01 6.3052e-01 3.8106e-02 56 1.4
0615 2455140.23956732 941391913 108.903 -17.148 -9.2963e-02 5.6770e-01 6.3052e-01 3.8106e-02 38 1.4
0616 2455140.25011695 941392825 200.972 -60.354 -1.1724e-01 4.7983e-01 5.2936e-01 3.8897e-02 36 0.9
0617 2455140.56937111 941420408 289.436 -42.581 -1.1724e-01 4.7983e-01 5.2936e-01 3.8897e-02 48 0.9
0618 2455140.62746823 941425428 348.550 -19.841 -9.2963e-02 5.6770e-01 6.3052e-01 3.8106e-02 38 1.4
0619 2455140.99363963 941457065 38.911 23.479 -1.3370e-01 8.5313e-01 6.3102e-01 3.7539e-02 24 2.4
0620 2455176.36060023 944512770 195.011 -32.392 -9.2963e-02 5.6770e-01 6.3052e-01 3.8106e-02 46 1.4
0621 2455176.40237466 944516380 359.823 -65.837 -9.2963e-02 5.6770e-01 6.3052e-01 3.8106e-02 46 1.4
0622 2455176.46654245 944521924 257.082 4.281 -1.1724e-01 4.7983e-01 5.2936e-01 3.8897e-02 46 0.9
0623 2455176.60589619 944533964 303.881 -8.242 -1.1724e-01 4.7983e-01 5.2936e-01 3.8897e-02 49 0.9
0624 2455177.03758351 944571262 72.237 24.741 -9.2963e-02 5.6770e-01 6.3052e-01 3.8106e-02 44 1.4
0625 2455177.29581319 944593573 250.629 -28.328 -9.2963e-02 5.6770e-01 6.3052e-01 3.8106e-02 36 1.4
0626 2455177.37983646 944600832 264.444 2.125 -9.2963e-02 5.6770e-01 6.3052e-01 3.8106e-02 31 1.4
0627 2455177.47043999 944608661 185.947 16.929 -1.3370e-01 8.5313e-01 6.3102e-01 3.7539e-02 25 2.4
0628 2455177.49870100 944611102 257.049 -46.286 -1.1724e-01 4.7983e-01 5.2936e-01 3.8897e-02 42 0.9
0629 2455177.68067624 944626825 328.826 1.137 -9.2963e-02 5.6770e-01 6.3052e-01 3.8106e-02 49 1.4
0630 2455177.73889666 944631855 48.550 -8.711 -1.3370e-01 8.5313e-01 6.3102e-01 3.7539e-02 26 2.4
0631 2455177.96495108 944651386 250.890 -56.828 -1.1724e-01 4.7983e-01 5.2936e-01 3.8897e-02 36 0.9
0632 2455178.07888863 944661230 162.809 0.994 -1.1724e-01 4.7983e-01 5.2936e-01 3.8897e-02 42 0.9
0633 2455178.08458527 944661723 104.357 21.695 -9.2963e-02 5.6770e-01 6.3052e-01 3.8106e-02 33 1.4
0634 2455178.65448253 944710962 285.130 -27.855 -1.1724e-01 4.7983e-01 5.2936e-01 3.8897e-02 67 0.9
0635 2455178.66430116 944711810 301.419 -0.560 -1.1724e-01 4.7983e-01 5.2936e-01 3.8897e-02 68 0.9
0636 2455178.76675491 944720662 318.784 -31.718 -9.2963e-02 5.6770e-01 6.3052e-01 3.8106e-02 32 1.4
0637 2455178.87802147 944730276 13.866 32.173 -9.2963e-02 5.6770e-01 6.3052e-01 3.8106e-02 53 1.4
0638 2455179.05028598 944745159 10.291 -78.284 -9.2963e-02 5.6770e-01 6.3052e-01 3.8106e-02 42 1.4
0639 2455179.40395461 944775716 93.361 -46.081 -9.2963e-02 5.6770e-01 6.3052e-01 3.8106e-02 39 1.4
0640 2455179.40550306 944775850 97.663 -46.538 -9.2963e-02 5.6770e-01 6.3052e-01 3.8106e-02 40 1.4
0641 2455179.56627066 944789740 301.081 32.891 -9.2963e-02 5.6770e-01 6.3052e-01 3.8106e-02 48 1.4
0642 2455179.58936774 944791736 212.966 -3.599 -1.3370e-01 8.5313e-01 6.3102e-01 3.7539e-02 27 2.4
0643 2455179.73058975 944803937 87.161 -14.830 -9.2963e-02 5.6770e-01 6.3052e-01 3.8106e-02 45 1.4
0644 2455179.84496806 944813820 310.268 -36.443 -9.2963e-02 5.6770e-01 6.3052e-01 3.8106e-02 34 1.4
0645 2455179.85397646 944814598 207.057 -49.995 -9.2963e-02 5.6770e-01 6.3052e-01 3.8106e-02 73 1.4
0646 2455180.06707255 944833010 74.832 19.767 -1.3370e-01 8.5313e-01 6.3102e-01 3.7539e-02 31 2.4
0647 2455180.27510587 944850984 30.776 -51.459 -1.2873e-01 4.3155e-01 4.6595e-01 3.9162e-02 66 0.7
0648 2455180.32389121 944855199 175.448 18.109 -1.1724e-01 4.7983e-01 5.2936e-01 3.8897e-02 46 0.9
0649 2455180.64733940 944883145 128.707 -53.534 -1.1724e-01 4.7983e-01 5.2936e-01 3.8897e-02 35 0.9
0650 2455180.87835807 944903105 127.231 -43.494 -9.2963e-02 5.6770e-01 6.3052e-01 3.8106e-02 56 1.4
0651 2455180.88672615 944903828 334.541 -32.892 -9.2963e-02 5.6770e-01 6.3052e-01 3.8106e-02 37 1.4
0652 2455180.98455891 944912280 53.371 -21.714 -1.1724e-01 4.7983e-01 5.2936e-01 3.8897e-02 36 0.9
0653 2455181.06941845 944919612 169.837 -35.463 -9.2963e-02 5.6770e-01 6.3052e-01 3.8106e-02 33 1.4
0654 2455181.10539858 944922721 98.553 14.371 -9.2963e-02 5.6770e-01 6.3052e-01 3.8106e-02 37 1.4
0655 2455181.11092318 944923198 197.227 -62.747 -9.2963e-02 5.6770e-01 6.3052e-01 3.8106e-02 42 1.4
0656 2455181.25572826 944935709 54.726 -75.030 -9.2963e-02 5.6770e-01 6.3052e-01 3.8106e-02 43 1.4
```

LIST OF HIGH ENERGY NEUTRINO CANDIDATES FOR THE 2009-2010 DATA

0657	2455181.26114534	944936177	224.202	15.433	-1.1724e-01	4.7983e-01	5.2936e-01	3.8897e-02	35	0.9
0658	2455181.27213487	944937127	221.375	-39.836	-9.2963e-02	5.6770e-01	6.3052e-01	3.8106e-02	39	1.4
0659	2455181.39615310	944947842	331.913	-18.848	-9.2963e-02	5.6770e-01	6.3052e-01	3.8106e-02	63	1.4
0660	2455181.43261759	944950993	249.079	-9.585	-9.2963e-02	5.6770e-01	6.3052e-01	3.8106e-02	42	1.4
0661	2455181.52212712	944958726	203.664	4.713	-9.2963e-02	5.6770e-01	6.3052e-01	3.8106e-02	35	1.4
0662	2455181.52726115	944959170	303.200	15.620	-1.3370e-01	8.5313e-01	6.3102e-01	3.7539e-02	29	2.4
0663	2455181.68452047	944972757	66.048	-55.284	-9.2963e-02	5.6770e-01	6.3052e-01	3.8106e-02	44	1.4
0664	2455181.80611859	944983263	93.140	-38.941	-9.2963e-02	5.6770e-01	6.3052e-01	3.8106e-02	46	1.4
0665	2455181.81130490	944983711	278.108	-41.385	-9.2963e-02	5.6770e-01	6.3052e-01	3.8106e-02	49	1.4
0666	2455181.88721786	944990270	50.770	1.863	-1.1909e-01	7.2127e-01	6.0423e-01	3.7507e-02	27	1.8
0667	2455181.96213342	944996743	256.497	-62.777	-1.1909e-01	7.2127e-01	6.0423e-01	3.7507e-02	52	1.8
0668	2455182.25901530	945022393	280.095	-52.426	-9.2963e-02	5.6770e-01	6.3052e-01	3.8106e-02	41	1.4
0669	2455182.37235249	945032186	280.887	-0.198	-9.2963e-02	5.6770e-01	6.3052e-01	3.8106e-02	46	1.4
0670	2455182.42272247	945036538	180.013	-86.062	-1.3370e-01	8.5313e-01	6.3102e-01	3.7539e-02	21	2.4
0671	2455182.55033348	945047563	359.212	-53.044	-1.1724e-01	4.7983e-01	5.2936e-01	3.8897e-02	53	0.9
0672	2455182.88636941	945076597	20.025	14.276	-1.3370e-01	8.5313e-01	6.3102e-01	3.7539e-02	30	2.4
0673	2455182.91177126	945078792	340.218	-37.075	-9.2963e-02	5.6770e-01	6.3052e-01	3.8106e-02	32	1.4
0674	2455182.92972610	945080343	175.828	-26.912	-9.2963e-02	5.6770e-01	6.3052e-01	3.8106e-02	42	1.4
0675	2455182.95503343	945082529	27.317	28.658	-9.2963e-02	5.6770e-01	6.3052e-01	3.8106e-02	52	1.4
0676	2455182.99577626	945086050	163.523	3.164	-9.2963e-02	5.6770e-01	6.3052e-01	3.8106e-02	46	1.4
0677	2455183.31495369	945113626	107.294	-16.030	-9.2963e-02	5.6770e-01	6.3052e-01	3.8106e-02	27	1.4
0678	2455183.60883661	945139018	198.168	-27.954	-9.2963e-02	5.6770e-01	6.3052e-01	3.8106e-02	46	1.4
0679	2455183.72978068	945149468	293.436	-33.187	-9.2963e-02	5.6770e-01	6.3052e-01	3.8106e-02	39	1.4
0680	2455183.75057692	945151264	295.289	-49.467	-9.2963e-02	5.6770e-01	6.3052e-01	3.8106e-02	35	1.4
0681	2455184.30304891	945198998	131.205	1.572	-5.8944e-02	2.9333e-01	5.7306e-01	3.8834e-02	101	0.6
0682	2455184.30656651	945199302	155.365	-12.477	-1.3370e-01	8.5313e-01	6.3102e-01	3.7539e-02	19	2.4
0683	2455184.44487798	945211252	175.855	-48.298	-9.2963e-02	5.6770e-01	6.3052e-01	3.8106e-02	33	1.4
0684	2455184.47752719	945214073	225.544	35.043	-9.2963e-02	5.6770e-01	6.3052e-01	3.8106e-02	51	1.4
0685	2455184.48765474	945214948	119.704	-52.224	-9.2963e-02	5.6770e-01	6.3052e-01	3.8106e-02	46	1.4
0686	2455184.53726252	945219234	323.409	-52.930	-1.2873e-01	4.3155e-01	4.6595e-01	3.9162e-02	54	0.7
0687	2455184.69114048	945232529	333.907	-3.422	-1.1724e-01	4.7983e-01	5.2936e-01	3.8897e-02	50	0.9
0688	2455184.73246867	945236100	307.564	17.928	-9.2963e-02	5.6770e-01	6.3052e-01	3.8106e-02	55	1.4
0689	2455184.99949594	945259171	267.437	-73.667	-9.2963e-02	5.6770e-01	6.3052e-01	3.8106e-02	44	1.4
0690	2455185.01604326	945260601	37.022	6.420	-9.2963e-02	5.6770e-01	6.3052e-01	3.8106e-02	39	1.4
0691	2455185.02234563	945261145	176.017	16.588	-1.3370e-01	8.5313e-01	6.3102e-01	3.7539e-02	22	2.4
0692	2455185.05988826	945264389	130.558	33.827	-1.3370e-01	8.5313e-01	6.3102e-01	3.7539e-02	31	2.4
0693	2455185.07594380	945265776	212.062	-44.087	-9.2963e-02	5.6770e-01	6.3052e-01	3.8106e-02	37	1.4
0694	2455185.16263358	945273266	334.567	-52.112	-9.2963e-02	5.6770e-01	6.3052e-01	3.8106e-02	54	1.4
0695	2455185.19185599	945275791	357.646	-51.206	-1.3370e-01	8.5313e-01	6.3102e-01	3.7539e-02	29	2.4
0696	2455185.19297753	945275888	92.645	-35.479	-9.2963e-02	5.6770e-01	6.3052e-01	3.8106e-02	33	1.4
0697	2455185.25821923	945281525	215.916	-2.103	-9.2963e-02	5.6770e-01	6.3052e-01	3.8106e-02	31	1.4
0698	2455185.31207878	945286178	218.766	11.076	-1.1724e-01	4.7983e-01	5.2936e-01	3.8897e-02	97	0.9
0699	2455185.32505852	945287300	307.682	-27.176	-9.2963e-02	5.6770e-01	6.3052e-01	3.8106e-02	35	1.4
0700	2455185.70732004	945320327	302.210	-34.967	-9.2963e-02	5.6770e-01	6.3052e-01	3.8106e-02	40	1.4
0701	2455185.77454881	945326136	281.345	-11.892	-9.2963e-02	5.6770e-01	6.3052e-01	3.8106e-02	43	1.4
0702	2455185.92937998	945339513	332.200	-25.898	-9.2963e-02	5.6770e-01	6.3052e-01	3.8106e-02	34	1.4
0703	2455186.02294166	945347597	85.141	10.661	-1.2873e-01	4.3155e-01	4.6595e-01	3.9162e-02	65	0.7
0704	2455186.02409992	945347697	174.475	-21.966	-1.3370e-01	8.5313e-01	6.3102e-01	3.7539e-02	31	2.4
0705	2455186.05520124	945350384	216.031	-58.688	-9.2963e-02	5.6770e-01	6.3052e-01	3.8106e-02	49	1.4
0706	2455186.22819540	945365331	193.511	-23.269	-1.1724e-01	4.7983e-01	5.2936e-01	3.8897e-02	56	0.9
0707	2455186.30411782	945371890	225.989	13.623	-1.1724e-01	4.7983e-01	5.2936e-01	3.8897e-02	48	0.9
0708	2455186.30578811	945372035	55.800	-61.690	-9.2963e-02	5.6770e-01	6.3052e-01	3.8106e-02	38	1.4

0709 2455186.31640317 945372952 232.495 3.022 -9.2963e-02 5.6770e-01 6.3052e-01 3.8106e-02 48 1.4
0710 2455186.31770412 945373064 111.159 -45.507 -9.2963e-02 5.6770e-01 6.3052e-01 3.8106e-02 51 1.4
0711 2455186.41036246 945381070 269.648 -24.735 -9.2963e-02 5.6770e-01 6.3052e-01 3.8106e-02 42 1.4
0712 2455186.45940630 945385307 209.129 -64.340 -9.2963e-02 5.6770e-01 6.3052e-01 3.8106e-02 35 1.4
0713 2455186.49715197 945388568 264.619 3.712 -1.1724e-01 4.7983e-01 5.2936e-01 3.8897e-02 68 0.9
0714 2455186.56137737 945394118 157.661 -49.228 -9.2963e-02 5.6770e-01 6.3052e-01 3.8106e-02 39 1.4
0715 2455186.57689280 945395458 117.489 -49.812 -9.2963e-02 5.6770e-01 6.3052e-01 3.8106e-02 54 1.4
0716 2455186.59625851 945397131 55.495 -22.319 -9.2963e-02 5.6770e-01 6.3052e-01 3.8106e-02 41 1.4
0717 2455186.66107419 945402731 51.556 -41.455 -1.1909e-01 7.2127e-01 6.0423e-01 3.7507e-02 27 1.8
0718 2455186.69145344 945405356 86.896 -59.383 -1.3370e-01 8.5313e-01 6.3102e-01 3.7539e-02 24 2.4
0719 2455186.69459665 945405628 75.712 -43.954 -1.2873e-01 4.3155e-01 4.6595e-01 3.9162e-02 34 0.7
0720 2455186.75393546 945410755 297.910 15.664 -1.3370e-01 8.5313e-01 6.3102e-01 3.7539e-02 26 2.4
0721 2455186.78126233 945413116 313.747 -52.164 -1.3370e-01 8.5313e-01 6.3102e-01 3.7539e-02 31 2.4
0722 2455186.81286299 945415846 150.491 -45.271 -1.1724e-01 4.7983e-01 5.2936e-01 3.8897e-02 40 0.9
0723 2455186.81826188 945416312 358.520 12.668 -1.1724e-01 4.7983e-01 5.2936e-01 3.8897e-02 49 0.9
0724 2455186.86866401 945420667 75.767 -57.310 -9.2963e-02 5.6770e-01 6.3052e-01 3.8106e-02 39 1.4
0725 2455188.19673582 945535412 89.244 -42.022 -1.1909e-01 7.2127e-01 6.0423e-01 3.7507e-02 29 1.8
0726 2455188.22021508 945537441 245.781 -69.885 -9.2963e-02 5.6770e-01 6.3052e-01 3.8106e-02 37 1.4
0727 2455188.23699775 945538891 110.626 -36.628 -1.3370e-01 8.5313e-01 6.3102e-01 3.7539e-02 18 2.4
0728 2455188.26880437 945541639 163.605 -65.409 -1.1724e-01 4.7983e-01 5.2936e-01 3.8897e-02 66 0.9
0729 2455188.31900133 945545976 186.434 37.369 -1.3370e-01 8.5313e-01 6.3102e-01 3.7539e-02 18 2.4
0730 2455188.43355275 945555873 216.759 20.508 -1.3370e-01 8.5313e-01 6.3102e-01 3.7539e-02 53 2.4
0731 2455188.60491998 945570680 313.066 -6.654 -9.2963e-02 5.6770e-01 6.3052e-01 3.8106e-02 58 1.4
0732 2455188.62120062 945572086 293.448 -2.703 -9.2963e-02 5.6770e-01 6.3052e-01 3.8106e-02 43 1.4
0733 2455188.71726245 945580386 295.426 -16.357 -1.1909e-01 7.2127e-01 6.0423e-01 3.7507e-02 23 1.8
0734 2455189.17977206 945620347 135.221 8.397 -1.3370e-01 8.5313e-01 6.3102e-01 3.7539e-02 27 2.4
0735 2455189.19309817 945621498 154.937 4.552 -9.2963e-02 5.6770e-01 6.3052e-01 3.8106e-02 58 1.4
0736 2455189.21772394 945623626 240.573 -12.974 -9.2963e-02 5.6770e-01 6.3052e-01 3.8106e-02 71 1.4
0737 2455189.30541555 945631202 109.819 -50.505 -9.2963e-02 5.6770e-01 6.3052e-01 3.8106e-02 52 1.4
0738 2455189.33156785 945633462 98.313 -55.134 -9.2963e-02 5.6770e-01 6.3052e-01 3.8106e-02 41 1.4
0739 2455189.34552145 945634668 291.811 -13.060 -9.2963e-02 5.6770e-01 6.3052e-01 3.8106e-02 58 1.4
0740 2455189.43989452 945642821 261.356 4.773 -9.2963e-02 5.6770e-01 6.3052e-01 3.8106e-02 75 1.4
0741 2455189.50517487 945648462 318.110 0.333 -1.1909e-01 7.2127e-01 6.0423e-01 3.7507e-02 22 1.8
0742 2455189.53259519 945650831 292.638 -28.398 -1.1724e-01 4.7983e-01 5.2936e-01 3.8897e-02 56 0.9
0743 2455189.54650895 945652033 227.451 18.216 -1.3370e-01 8.5313e-01 6.3102e-01 3.7539e-02 28 2.4
0744 2455189.56117206 945653300 241.954 -34.181 -9.2963e-02 5.6770e-01 6.3052e-01 3.8106e-02 33 1.4
0745 2455189.56900697 945653977 12.139 -26.821 -9.2963e-02 5.6770e-01 6.3052e-01 3.8106e-02 38 1.4
0746 2455189.58712903 945655542 84.859 -41.621 -9.2963e-02 5.6770e-01 6.3052e-01 3.8106e-02 41 1.4
0747 2455189.61079032 945657587 23.576 11.120 -9.2963e-02 5.6770e-01 6.3052e-01 3.8106e-02 32 1.4
0748 2455189.67531367 945663162 260.686 3.375 -9.2963e-02 5.6770e-01 6.3052e-01 3.8106e-02 40 1.4
0749 2455189.76234013 945670681 333.358 24.397 -9.2963e-02 5.6770e-01 6.3052e-01 3.8106e-02 62 1.4
0750 2455189.84112265 945677487 295.226 -24.967 -9.2963e-02 5.6770e-01 6.3052e-01 3.8106e-02 48 1.4
0751 2455189.86724503 945679744 28.891 3.611 -1.2873e-01 4.3155e-01 4.6595e-01 3.9162e-02 43 0.7
0752 2455189.88137404 945680965 30.357 -60.141 -1.1724e-01 4.7983e-01 5.2936e-01 3.8897e-02 32 0.9
0753 2455190.06489370 945696821 105.702 4.303 -9.2963e-02 5.6770e-01 6.3052e-01 3.8106e-02 41 1.4
0754 2455190.23295942 945711342 271.920 -16.015 -9.2963e-02 5.6770e-01 6.3052e-01 3.8106e-02 86 1.4
0755 2455190.26165361 945713821 113.719 -33.912 -1.3370e-01 8.5313e-01 6.3102e-01 3.7539e-02 24 2.4
0756 2455190.30101956 945717223 253.703 -20.745 -9.2963e-02 5.6770e-01 6.3052e-01 3.8106e-02 57 1.4
0757 2455190.36577198 945722817 280.345 14.397 -1.1909e-01 7.2127e-01 6.0423e-01 3.7507e-02 27 1.8
0758 2455190.43494695 945728794 173.296 3.863 -1.1909e-01 7.2127e-01 6.0423e-01 3.7507e-02 50 1.8
0759 2455190.43802490 945729060 15.382 -37.340 -1.3370e-01 8.5313e-01 6.3102e-01 3.7539e-02 28 2.4
0760 2455190.58809914 945742026 230.744 -67.190 -9.2963e-02 5.6770e-01 6.3052e-01 3.8106e-02 44 1.4

LIST OF HIGH ENERGY NEUTRINO CANDIDATES FOR THE 2009-2010 DATA

0761 2455190.64852638 945747247 257.281 -43.345 -1.1724e-01 4.7983e-01 5.2936e-01 3.8897e-02 35 0.9
0762 2455190.75656885 945756582 26.679 39.333 -9.2963e-02 5.6770e-01 6.3052e-01 3.8106e-02 41 1.4
0763 2455190.77666783 945758319 346.528 -55.446 -1.3370e-01 8.5313e-01 6.3102e-01 3.7539e-02 31 2.4
0764 2455190.90073477 945769038 353.761 -10.056 -1.3370e-01 8.5313e-01 6.3102e-01 3.7539e-02 22 2.4
0765 2455191.07954270 945784487 94.727 -59.338 -9.2963e-02 5.6770e-01 6.3052e-01 3.8106e-02 47 1.4
0766 2455191.09109280 945785485 169.178 -26.613 -1.1724e-01 4.7983e-01 5.2936e-01 3.8897e-02 45 0.9
0767 2455191.13633636 945789394 239.339 -47.795 -9.2963e-02 5.6770e-01 6.3052e-01 3.8106e-02 33 1.4
0768 2455191.15140879 945790696 228.930 15.437 -1.3370e-01 8.5313e-01 6.3102e-01 3.7539e-02 30 2.4
0769 2455191.20783708 945795572 138.246 -37.687 -1.1724e-01 4.7983e-01 5.2936e-01 3.8897e-02 80 0.9
0770 2455191.21603047 945796280 285.247 -19.755 -1.3370e-01 8.5313e-01 6.3102e-01 3.7539e-02 30 2.4
0771 2455191.24990460 945799206 85.087 -27.823 -9.2963e-02 5.6770e-01 6.3052e-01 3.8106e-02 59 1.4
0772 2455191.27287725 945801191 132.431 16.119 -9.2963e-02 5.6770e-01 6.3052e-01 3.8106e-02 38 1.4
0773 2455191.43364389 945815081 301.206 -3.407 -1.3370e-01 8.5313e-01 6.3102e-01 3.7539e-02 31 2.4
0774 2455191.49072895 945820013 241.216 -50.228 -9.2963e-02 5.6770e-01 6.3052e-01 3.8106e-02 36 1.4
0775 2455191.52547335 945823015 217.600 -3.941 -9.2963e-02 5.6770e-01 6.3052e-01 3.8106e-02 42 1.4
0776 2455191.53177773 945823560 330.378 27.810 -9.2963e-02 5.6770e-01 6.3052e-01 3.8106e-02 39 1.4
0777 2455192.15463775 945877375 289.784 -45.262 -1.1724e-01 4.7983e-01 5.2936e-01 3.8897e-02 42 0.9
0778 2455192.24410402 945885105 105.900 -41.732 -1.1724e-01 4.7983e-01 5.2936e-01 3.8897e-02 45 0.9
0779 2455192.26786255 945887158 121.622 -0.163 -9.2963e-02 5.6770e-01 6.3052e-01 3.8106e-02 60 1.4
0780 2455192.38032764 945896875 42.982 -52.148 -9.2963e-02 5.6770e-01 6.3052e-01 3.8106e-02 37 1.4
0781 2455192.49069143 945906410 210.878 -11.458 -1.1909e-01 7.2127e-01 6.0423e-01 3.7507e-02 22 1.8
0782 2455192.55556949 945912016 209.560 -39.589 -9.2963e-02 5.6770e-01 6.3052e-01 3.8106e-02 42 1.4
0783 2455192.61748737 945917365 339.288 -0.221 -9.2963e-02 5.6770e-01 6.3052e-01 3.8106e-02 47 1.4
0784 2455192.74176696 945928103 120.755 -39.027 -1.3370e-01 8.5313e-01 6.3102e-01 3.7539e-02 29 2.4
0785 2455192.77533777 945931004 22.964 6.706 -9.2963e-02 5.6770e-01 6.3052e-01 3.8106e-02 46 1.4
0786 2455192.79055565 945932319 214.877 -62.088 -9.2963e-02 5.6770e-01 6.3052e-01 3.8106e-02 34 1.4
0787 2455192.85197386 945937625 45.151 -14.234 -9.2963e-02 5.6770e-01 6.3052e-01 3.8106e-02 50 1.4
0788 2455192.86945414 945939135 217.271 -71.745 -9.2963e-02 5.6770e-01 6.3052e-01 3.8106e-02 41 1.4
0789 2455192.93074785 945944431 18.933 28.914 -5.8944e-02 2.9333e-01 5.7306e-01 3.8834e-02 214 0.6
0790 2455193.12625274 945961323 117.358 42.733 -9.2963e-02 5.6770e-01 6.3052e-01 3.8106e-02 32 1.4
0791 2455193.23920794 945971082 157.049 -11.993 -1.3370e-01 8.5313e-01 6.3102e-01 3.7539e-02 30 2.4
0792 2455193.25177703 945972168 177.245 -38.820 -9.2963e-02 5.6770e-01 6.3052e-01 3.8106e-02 49 1.4
0793 2455193.49933465 945993557 169.553 -26.928 -9.2963e-02 5.6770e-01 6.3052e-01 3.8106e-02 66 1.4
0794 2455193.76033573 946016108 299.098 7.281 -9.2963e-02 5.6770e-01 6.3052e-01 3.8106e-02 56 1.4
0795 2455193.77183890 946017101 175.039 -73.664 -1.3370e-01 8.5313e-01 6.3102e-01 3.7539e-02 27 2.4
0796 2455193.88955972 946027272 2.766 -58.139 -9.2963e-02 5.6770e-01 6.3052e-01 3.8106e-02 61 1.4
0797 2455194.21847979 946055691 154.212 24.974 -9.2963e-02 5.6770e-01 6.3052e-01 3.8106e-02 40 1.4
0798 2455194.24334194 946057839 207.659 -3.927 -9.2963e-02 5.6770e-01 6.3052e-01 3.8106e-02 38 1.4
0799 2455194.34810904 946066891 224.203 9.163 -9.2963e-02 5.6770e-01 6.3052e-01 3.8106e-02 44 1.4
0800 2455194.43836779 946074689 253.304 -36.764 -1.2873e-01 4.3155e-01 4.6595e-01 3.9162e-02 48 0.7
0801 2455194.68717315 946096186 42.081 28.673 -9.2963e-02 5.6770e-01 6.3052e-01 3.8106e-02 45 1.4
0802 2455194.68736318 946096203 250.934 -16.820 -9.2963e-02 5.6770e-01 6.3052e-01 3.8106e-02 51 1.4
0803 2455194.83326808 946108809 81.804 7.745 -9.2963e-02 5.6770e-01 6.3052e-01 3.8106e-02 85 1.4
0804 2455194.94157086 946118166 342.996 -41.451 -1.3370e-01 8.5313e-01 6.3102e-01 3.7539e-02 31 2.4
0805 2455195.04014714 946126683 11.335 -32.386 -9.2963e-02 5.6770e-01 6.3052e-01 3.8106e-02 42 1.4
0806 2455195.05106900 946127627 81.040 28.972 -1.3370e-01 8.5313e-01 6.3102e-01 3.7539e-02 26 2.4
0807 2455195.33607486 946152251 205.709 -74.502 -5.3660e-02 3.7117e-01 6.4893e-01 3.6677e-02 72 1.2
0808 2455195.49918680 946166344 60.392 -84.483 -1.1724e-01 4.7983e-01 5.2936e-01 3.8897e-02 71 0.9
0809 2455195.65716034 946179993 233.724 -33.022 -9.2963e-02 5.6770e-01 6.3052e-01 3.8106e-02 42 1.4
0810 2455195.86609631 946198045 195.789 -87.647 -1.2873e-01 4.3155e-01 4.6595e-01 3.9162e-02 60 0.7
0811 2455195.87305563 946198647 359.106 7.661 -1.1724e-01 4.7983e-01 5.2936e-01 3.8897e-02 64 0.9
0812 2455196.03698362 946212810 36.351 7.189 -9.2963e-02 5.6770e-01 6.3052e-01 3.8106e-02 36 1.4

```
0813 2455196.09357134 946217699 128.368 1.391 -9.2963e-02 5.6770e-01 6.3052e-01 3.8106e-02 35 1.4
0814 2455196.10573781 946218750 133.970 36.838 -1.1909e-01 7.2127e-01 6.0423e-01 3.7507e-02 27 1.8
0815 2455196.20104784 946226985 112.585 21.455 -9.2963e-02 5.6770e-01 6.3052e-01 3.8106e-02 76 1.4
0816 2455196.20195120 946227063 229.146 -35.530 -9.2963e-02 5.6770e-01 6.3052e-01 3.8106e-02 34 1.4
0817 2455196.32910411 946238049 270.230 -1.033 -1.1724e-01 4.7983e-01 5.2936e-01 3.8897e-02 34 0.9
0818 2455196.34582890 946239494 355.325 -42.724 -1.3370e-01 8.5313e-01 6.3102e-01 3.7539e-02 27 2.4
0819 2455196.51730728 946254310 347.485 31.268 -9.2963e-02 5.6770e-01 6.3052e-01 3.8106e-02 49 1.4
0820 2455196.68476378 946268778 276.091 12.169 -9.2963e-02 5.6770e-01 6.3052e-01 3.8106e-02 45 1.4
0821 2455196.77623850 946276682 153.640 -70.377 -9.2963e-02 5.6770e-01 6.3052e-01 3.8106e-02 34 1.4
0822 2455196.81660113 946280169 310.156 -69.503 -9.2963e-02 5.6770e-01 6.3052e-01 3.8106e-02 47 1.4
0823 2455197.01356936 946297187 14.566 -9.847 -9.2963e-02 5.6770e-01 6.3052e-01 3.8106e-02 68 1.4
0824 2455197.11318555 946305794 66.453 -0.840 -1.3370e-01 8.5313e-01 6.3102e-01 3.7539e-02 27 2.4
0825 2455197.22022673 946315042 139.423 -23.609 -1.3370e-01 8.5313e-01 6.3102e-01 3.7539e-02 21 2.4
0826 2455197.22654436 946315588 160.856 -0.828 -1.1724e-01 4.7983e-01 5.2936e-01 3.8897e-02 50 0.9
0827 2455197.62020656 946349600 54.788 -44.624 -1.1724e-01 4.7983e-01 5.2936e-01 3.8897e-02 37 0.9
0828 2455197.72030308 946358249 213.686 -52.286 -9.2963e-02 5.6770e-01 6.3052e-01 3.8106e-02 39 1.4
0829 2455197.73813817 946359790 51.332 25.007 -9.2963e-02 5.6770e-01 6.3052e-01 3.8106e-02 45 1.4
0830 2455197.90974396 946374616 90.680 -0.331 -9.2963e-02 5.6770e-01 6.3052e-01 3.8106e-02 43 1.4
0831 2455198.20461957 946400094 115.214 6.246 -9.2963e-02 5.6770e-01 6.3052e-01 3.8106e-02 47 1.4
0832 2455198.48822306 946424597 299.902 18.907 -9.2963e-02 5.6770e-01 6.3052e-01 3.8106e-02 40 1.4
0833 2455198.49936446 946425560 214.464 -38.282 -9.2963e-02 5.6770e-01 6.3052e-01 3.8106e-02 45 1.4
0834 2455198.75505946 946447652 20.804 3.496 -1.1724e-01 4.7983e-01 5.2936e-01 3.8897e-02 39 0.9
0835 2455198.80386155 946451868 29.893 36.624 -9.2963e-02 5.6770e-01 6.3052e-01 3.8106e-02 42 1.4
0836 2455198.84553438 946455469 325.184 -17.620 -9.2963e-02 5.6770e-01 6.3052e-01 3.8106e-02 35 1.4
0837 2455199.11695812 946478920 60.294 -46.073 -9.2963e-02 5.6770e-01 6.3052e-01 3.8106e-02 35 1.4
0838 2455199.32165197 946496605 177.612 -43.608 -1.1724e-01 4.7983e-01 5.2936e-01 3.8897e-02 61 0.9
0839 2455199.50425473 946512382 174.596 -26.646 -1.3370e-01 8.5313e-01 6.3102e-01 3.7539e-02 29 2.4
0840 2455199.65344042 946525272 315.545 -14.142 -1.1909e-01 7.2127e-01 6.0423e-01 3.7507e-02 30 1.8
0841 2455199.67326995 946526985 342.880 11.294 -1.3370e-01 8.5313e-01 6.3102e-01 3.7539e-02 22 2.4
0842 2455199.73837464 946532610 300.436 -17.084 -1.3370e-01 8.5313e-01 6.3102e-01 3.7539e-02 22 2.4
0843 2455199.80482370 946538351 346.532 -9.574 -1.3370e-01 8.5313e-01 6.3102e-01 3.7539e-02 23 2.4
0844 2455199.97867064 946553372 118.522 5.126 -9.2963e-02 5.6770e-01 6.3052e-01 3.8106e-02 43 1.4
0845 2455200.19836435 946572353 156.136 17.143 -1.1724e-01 4.7983e-01 5.2936e-01 3.8897e-02 41 0.9
0846 2455200.21128236 946573469 281.206 -27.685 -5.8944e-02 2.9333e-01 5.7306e-01 3.8834e-02 111 0.6
0847 2455200.24253147 946576169 158.037 -30.857 -9.2963e-02 5.6770e-01 6.3052e-01 3.8106e-02 34 1.4
0848 2455200.39128406 946589021 233.851 -18.053 -9.2963e-02 5.6770e-01 6.3052e-01 3.8106e-02 40 1.4
0849 2455200.40955362 946590600 333.699 -33.135 -9.2963e-02 5.6770e-01 6.3052e-01 3.8106e-02 42 1.4
0850 2455200.49801000 946598243 115.394 -61.523 -1.3370e-01 8.5313e-01 6.3102e-01 3.7539e-02 29 2.4
0851 2455200.50295737 946598670 118.432 -73.416 -1.1909e-01 7.2127e-01 6.0423e-01 3.7507e-02 24 1.8
0852 2455200.63914878 946610437 257.750 -18.706 -1.1724e-01 4.7983e-01 5.2936e-01 3.8897e-02 36 0.9
0853 2455200.73664624 946618861 68.630 -46.294 -5.8944e-02 2.9333e-01 5.7306e-01 3.8834e-02 114 0.6
0854 2455200.82720896 946626685 43.219 -18.838 -1.1724e-01 4.7983e-01 5.2936e-01 3.8897e-02 52 0.9
0855 2455200.85383520 946628986 4.746 -61.413 -1.1724e-01 4.7983e-01 5.2936e-01 3.8897e-02 42 0.9
0856 2455200.86111443 946629615 351.922 -8.619 -9.2963e-02 5.6770e-01 6.3052e-01 3.8106e-02 53 1.4
0857 2455200.91682470 946634428 155.629 2.871 -9.2963e-02 5.6770e-01 6.3052e-01 3.8106e-02 39 1.4
0858 2455201.27852597 946665679 135.621 15.304 -9.2963e-02 5.6770e-01 6.3052e-01 3.8106e-02 52 1.4
0859 2455201.50119943 946684918 272.419 -5.337 -9.2963e-02 5.6770e-01 6.3052e-01 3.8106e-02 46 1.4
0860 2455201.51964677 946686512 182.276 -25.628 -1.3370e-01 8.5313e-01 6.3102e-01 3.7539e-02 25 2.4
0861 2455201.57071479 946690924 118.513 -77.902 -1.3370e-01 8.5313e-01 6.3102e-01 3.7539e-02 53 2.4
0862 2455201.62218506 946695371 300.067 18.551 -1.1724e-01 4.7983e-01 5.2936e-01 3.8897e-02 32 0.9
0863 2455201.71330061 946703244 310.037 -9.823 -1.1724e-01 4.7983e-01 5.2936e-01 3.8897e-02 46 0.9
0864 2455201.90501365 946719808 56.506 15.541 -1.1909e-01 7.2127e-01 6.0423e-01 3.7507e-02 31 1.8
```

```
0865 2455202.56619047 946776933 226.425 -26.198 -9.2963e-02 5.6770e-01 6.3052e-01 3.8106e-02 43 1.4
0866 2455202.57824478 946777975 48.026 -3.908 -9.2963e-02 5.6770e-01 6.3052e-01 3.8106e-02 48 1.4
0867 2455202.89990655 946805766 32.564 -22.498 -9.2963e-02 5.6770e-01 6.3052e-01 3.8106e-02 54 1.4
0868 2455203.00614741 946814946 9.277 -20.964 -1.3370e-01 8.5313e-01 6.3102e-01 3.7539e-02 25 2.4
0869 2455203.13391412 946825985 89.082 -11.646 -1.1724e-01 4.7983e-01 5.2936e-01 3.8897e-02 52 0.9
0870 2455203.28664686 946839181 214.259 -0.251 -1.1724e-01 4.7983e-01 5.2936e-01 3.8897e-02 44 0.9
0871 2455203.64317126 946869984 311.290 -22.788 -1.1724e-01 4.7983e-01 5.2936e-01 3.8897e-02 63 0.9
0872 2455203.79039468 946882705 76.056 12.364 -9.2963e-02 5.6770e-01 6.3052e-01 3.8106e-02 32 1.4
0873 2455203.95790065 946897177 186.720 -16.253 -1.3370e-01 8.5313e-01 6.3102e-01 3.7539e-02 24 2.4
0874 2455204.07717164 946907482 44.618 -23.035 -9.2963e-02 5.6770e-01 6.3052e-01 3.8106e-02 49 1.4
0875 2455204.08132679 946907841 167.712 33.081 -1.1724e-01 4.7983e-01 5.2936e-01 3.8897e-02 34 0.9
0876 2455204.16160983 946914778 177.142 -20.882 -1.1210e-01 3.5816e-01 4.5437e-01 4.0298e-02 130 0.5
0877 2455204.24444168 946921934 73.211 -55.726 -9.2963e-02 5.6770e-01 6.3052e-01 3.8106e-02 54 1.4
0878 2455204.91856534 946980179 101.313 27.139 -9.2963e-02 5.6770e-01 6.3052e-01 3.8106e-02 42 1.4
0879 2455205.34927857 947017392 334.347 -45.866 -9.2963e-02 5.6770e-01 6.3052e-01 3.8106e-02 63 1.4
0880 2455205.37763531 947019842 103.421 -58.168 -8.8598e-02 3.3283e-01 5.3278e-01 3.9884e-02 126 0.6
## stop S6B -- start
0881 2455205.59201854 947038365 267.264 -51.054 -1.1724e-01 4.7983e-01 5.2936e-01 3.8897e-02 48 0.9
0882 2455205.75899046 947052791 118.043 -18.373 -1.1909e-01 7.2127e-01 6.0423e-01 3.7507e-02 30 1.8
0883 2455205.97940864 947071835 115.109 16.753 -1.1724e-01 4.7983e-01 5.2936e-01 3.8897e-02 37 0.9
0884 2455206.00180145 947073770 130.615 -21.946 -9.2963e-02 5.6770e-01 6.3052e-01 3.8106e-02 51 1.4
0885 2455206.26931457 947096883 332.136 -37.905 -1.3370e-01 8.5313e-01 6.3102e-01 3.7539e-02 27 2.4
0886 2455206.36533759 947105180 237.271 -52.013 -9.2963e-02 5.6770e-01 6.3052e-01 3.8106e-02 56 1.4
0887 2455206.40668835 947108752 345.728 -52.192 -1.3370e-01 8.5313e-01 6.3102e-01 3.7539e-02 29 2.4
0888 2455206.52609776 947119069 80.905 -44.259 -1.3370e-01 8.5313e-01 6.3102e-01 3.7539e-02 23 2.4
0889 2455206.63121873 947128152 325.758 -9.835 -1.1724e-01 4.7983e-01 5.2936e-01 3.8897e-02 41 0.9
0890 2455206.66747144 947131284 1.693 19.163 -1.1724e-01 4.7983e-01 5.2936e-01 3.8897e-02 41 0.9
0891 2455206.67259082 947131726 329.613 -44.847 -1.1724e-01 4.7983e-01 5.2936e-01 3.8897e-02 33 0.9
0892 2455206.73749282 947137334 67.664 7.449 -1.1724e-01 4.7983e-01 5.2936e-01 3.8897e-02 55 0.9
0893 2455206.74643766 947138107 203.141 -64.683 -1.1724e-01 4.7983e-01 5.2936e-01 3.8897e-02 56 0.9
0894 2455206.74980613 947138398 87.173 26.354 -9.2963e-02 5.6770e-01 6.3052e-01 3.8106e-02 50 1.4
0895 2455206.75151176 947138545 26.082 -22.605 -1.1724e-01 4.7983e-01 5.2936e-01 3.8897e-02 56 0.9
0896 2455206.87608301 947149308 7.058 -47.541 -9.2963e-02 5.6770e-01 6.3052e-01 3.8106e-02 32 1.4
0897 2455206.91583704 947152743 212.966 -38.042 -9.2963e-02 5.6770e-01 6.3052e-01 3.8106e-02 48 1.4
0898 2455207.01591151 947161389 152.202 15.928 -1.1724e-01 4.7983e-01 5.2936e-01 3.8897e-02 58 0.9
0899 2455207.08166584 947167070 86.772 14.539 -1.1724e-01 4.7983e-01 5.2936e-01 3.8897e-02 32 0.9
0900 2455207.20778341 947177967 117.999 14.092 -1.1724e-01 4.7983e-01 5.2936e-01 3.8897e-02 37 0.9
0901 2455207.22579561 947179523 129.025 19.866 -1.1909e-01 7.2127e-01 6.0423e-01 3.7507e-02 31 1.8
0902 2455207.33615105 947189058 139.241 -22.835 -1.3370e-01 8.5313e-01 6.3102e-01 3.7539e-02 26 2.4
0903 2455207.47513383 947201066 227.609 -3.938 -1.3370e-01 8.5313e-01 6.3102e-01 3.7539e-02 28 2.4
0904 2455207.64567817 947215801 4.079 4.212 -9.2963e-02 5.6770e-01 6.3052e-01 3.8106e-02 42 1.4
0905 2455207.79742100 947228912 81.020 17.226 -1.2873e-01 4.3155e-01 4.6595e-01 3.9162e-02 42 0.7
0906 2455208.19976877 947263675 241.253 -47.750 -1.2873e-01 4.3155e-01 4.6595e-01 3.9162e-02 48 0.7
0907 2455208.24828695 947267866 94.459 -22.668 -1.2873e-01 4.3155e-01 4.6595e-01 3.9162e-02 73 0.7
0908 2455208.27795336 947270430 183.964 31.182 -1.1724e-01 4.7983e-01 5.2936e-01 3.8897e-02 46 0.9
0909 2455208.46690315 947286755 11.208 -2.795 -9.2963e-02 5.6770e-01 6.3052e-01 3.8106e-02 43 1.4
0910 2455208.65447656 947302961 240.837 -83.941 -9.2963e-02 5.6770e-01 6.3052e-01 3.8106e-02 38 1.4
0911 2455208.82690760 947317859 45.053 -35.434 -1.1724e-01 4.7983e-01 5.2936e-01 3.8897e-02 58 0.9
0912 2455208.94043913 947327668 74.696 1.665 -1.3370e-01 8.5313e-01 6.3102e-01 3.7539e-02 21 2.4
0913 2455208.95740231 947329134 33.176 7.278 -9.2963e-02 5.6770e-01 6.3052e-01 3.8106e-02 43 1.4
0914 2455208.95959556 947329324 310.556 -56.006 -1.3370e-01 8.5313e-01 6.3102e-01 3.7539e-02 26 2.4
0915 2455209.13629385 947344590 230.622 -33.109 -1.3370e-01 8.5313e-01 6.3102e-01 3.7539e-02 23 2.4
```

```
0916 2455209.22185271 947351983 277.762 -52.548 -9.2963e-02 5.6770e-01 6.3052e-01 3.8106e-02 39 1.4
0917 2455209.30528449 947359191 14.398 -54.989 -9.2963e-02 5.6770e-01 6.3052e-01 3.8106e-02 56 1.4
0918 2455209.33191709 947361492 149.062 -29.658 -1.3370e-01 8.5313e-01 6.3102e-01 3.7539e-02 25 2.4
0919 2455209.35135004 947363171 253.749 -52.798 -1.1724e-01 4.7983e-01 5.2936e-01 3.8897e-02 50 0.9
0920 2455209.38793623 947366332 311.044 32.084 -9.2963e-02 5.6770e-01 6.3052e-01 3.8106e-02 56 1.4
0921 2455209.44853596 947371568 339.721 -27.964 -1.1724e-01 4.7983e-01 5.2936e-01 3.8897e-02 37 0.9
0922 2455209.47386163 947373756 263.659 13.193 -9.2963e-02 5.6770e-01 6.3052e-01 3.8106e-02 52 1.4
0923 2455209.77249363 947399558 131.683 -28.552 -1.1724e-01 4.7983e-01 5.2936e-01 3.8897e-02 76 0.9
0924 2455209.79083373 947401143 44.297 27.973 -1.1724e-01 4.7983e-01 5.2936e-01 3.8897e-02 80 0.9
0925 2455209.83807158 947405224 28.661 -36.461 -1.3370e-01 8.5313e-01 6.3102e-01 3.7539e-02 23 2.4
0926 2455209.86684556 947407710 205.102 -56.088 -9.2963e-02 5.6770e-01 6.3052e-01 3.8106e-02 81 1.4
0927 2455209.96111612 947415855 108.564 -16.082 -9.2963e-02 5.6770e-01 6.3052e-01 3.8106e-02 43 1.4
0928 2455210.05777507 947424206 23.435 -36.751 -1.3370e-01 8.5313e-01 6.3102e-01 3.7539e-02 31 2.4
0929 2455210.16938478 947433849 219.044 34.427 -1.3370e-01 8.5313e-01 6.3102e-01 3.7539e-02 26 2.4
0930 2455210.18549947 947435242 173.028 36.944 -9.2963e-02 5.6770e-01 6.3052e-01 3.8106e-02 37 1.4
0931 2455210.21484370 947437777 123.166 -37.100 -9.2963e-02 5.6770e-01 6.3052e-01 3.8106e-02 59 1.4
0932 2455210.21804241 947438053 264.968 -49.697 -1.2873e-01 4.3155e-01 4.6595e-01 3.9162e-02 50 0.7
0933 2455210.43937220 947457176 270.955 -6.792 -1.3370e-01 8.5313e-01 6.3102e-01 3.7539e-02 29 2.4
0934 2455210.50426152 947462783 228.357 7.854 -9.2963e-02 5.6770e-01 6.3052e-01 3.8106e-02 45 1.4
0935 2455210.58498972 947469758 267.813 22.353 -9.2963e-02 5.6770e-01 6.3052e-01 3.8106e-02 32 1.4
0936 2455210.63097229 947473731 305.927 26.076 -9.2963e-02 5.6770e-01 6.3052e-01 3.8106e-02 19 1.4
0937 2455210.67885656 947477868 6.182 -25.268 -1.1724e-01 4.7983e-01 5.2936e-01 3.8897e-02 36 0.9
0938 2455210.75309901 947484282 336.174 -26.774 -1.7861e+00 6.7827e+00 8.6368e-01 3.8440e-01 28 1.4
0939 2455210.78665557 947487182 32.647 -50.787 -1.3370e-01 8.5313e-01 6.3102e-01 3.7539e-02 14 2.4
0940 2455210.81492192 947489624 53.093 6.017 -1.1724e-01 4.7983e-01 5.2936e-01 3.8897e-02 36 0.9
0941 2455210.88302667 947495508 159.777 -43.026 -1.3370e-01 8.5313e-01 6.3102e-01 3.7539e-02 21 2.4
0942 2455210.95532939 947501755 121.446 21.508 -1.3370e-01 8.5313e-01 6.3102e-01 3.7539e-02 47 2.4
0943 2455210.96064258 947502214 17.852 -5.590 -9.2963e-02 5.6770e-01 6.3052e-01 3.8106e-02 59 1.4
0944 2455211.02021087 947507361 117.161 -30.028 -1.7861e+00 6.7827e+00 8.6368e-01 3.8440e-01 31 1.4
0945 2455211.17875483 947521059 152.515 23.840 -1.7861e+00 6.7827e+00 8.6368e-01 3.8440e-01 37 1.4
0946 2455211.19979930 947522877 263.441 -47.207 -1.7861e+00 6.7827e+00 8.6368e-01 3.8440e-01 50 1.4
0947 2455211.23356536 947525795 177.446 -20.883 -1.1724e-01 4.7983e-01 5.2936e-01 3.8897e-02 49 0.9
0948 2455211.23625788 947526027 179.400 -5.439 -1.3370e-01 8.5313e-01 6.3102e-01 3.7539e-02 30 2.4
0949 2455211.35794080 947536541 225.210 -32.172 -1.3370e-01 8.5313e-01 6.3102e-01 3.7539e-02 30 2.4
0950 2455211.39414760 947539669 158.473 -15.134 -9.2963e-02 5.6770e-01 6.3052e-01 3.8106e-02 75 1.4
0951 2455211.49668203 947548528 62.133 -47.866 -9.2963e-02 5.6770e-01 6.3052e-01 3.8106e-02 33 1.4
0952 2455211.53471177 947551814 292.684 34.166 -9.2963e-02 5.6770e-01 6.3052e-01 3.8106e-02 61 1.4
0953 2455211.55099228 947553220 353.837 14.121 -9.2963e-02 5.6770e-01 6.3052e-01 3.8106e-02 39 1.4
0954 2455211.57554351 947555341 32.428 -57.857 -1.1724e-01 4.7983e-01 5.2936e-01 3.8897e-02 37 0.9
0955 2455211.59760908 947557248 197.748 -54.015 -1.1724e-01 4.7983e-01 5.2936e-01 3.8897e-02 39 0.9
0956 2455211.65511459 947562216 100.629 -24.442 -9.2963e-02 5.6770e-01 6.3052e-01 3.8106e-02 57 1.4
0957 2455211.76506830 947571716 32.353 40.097 -1.1724e-01 4.7983e-01 5.2936e-01 3.8897e-02 40 0.9
0958 2455212.20425262 947609662 183.042 45.535 -9.2963e-02 5.6770e-01 6.3052e-01 3.8106e-02 41 1.4
0959 2455212.27313993 947615614 49.168 -51.723 -1.1724e-01 4.7983e-01 5.2936e-01 3.8897e-02 93 0.9
0960 2455212.28904463 947616988 148.081 2.273 -1.1724e-01 4.7983e-01 5.2936e-01 3.8897e-02 33 0.9
0961 2455212.37899045 947624759 350.098 -69.949 -9.2963e-02 5.6770e-01 6.3052e-01 3.8106e-02 63 1.4
0962 2455212.41061837 947627492 298.791 -28.302 -9.2963e-02 5.6770e-01 6.3052e-01 3.8106e-02 42 1.4
0963 2455212.46859616 947632501 36.526 -67.883 -1.1724e-01 4.7983e-01 5.2936e-01 3.8897e-02 32 0.9
0964 2455212.56806648 947641095 359.404 -60.557 -1.2873e-01 4.3155e-01 4.6595e-01 3.9162e-02 53 0.7
0965 2455212.58355032 947642433 32.563 3.851 -1.1909e-01 7.2127e-01 6.0423e-01 3.7507e-02 30 1.8
0966 2455212.59013134 947643002 203.433 -45.794 -9.2963e-02 5.6770e-01 6.3052e-01 3.8106e-02 58 1.4
0967 2455212.77125714 947658651 50.658 -59.275 -1.1724e-01 4.7983e-01 5.2936e-01 3.8897e-02 49 0.9
```

LIST OF HIGH ENERGY NEUTRINO CANDIDATES FOR THE 2009-2010 DATA

0968	2455212.79352479	947660575	69.802	-16.268	-1.1724e-01	4.7983e-01	5.2936e-01	3.8897e-02	50	0.9
0969	2455212.81448302	947662386	124.386	17.047	-9.2963e-02	5.6770e-01	6.3052e-01	3.8106e-02	34	1.4
0970	2455212.88081398	947668117	166.762	-22.996	-1.3370e-01	8.5313e-01	6.3102e-01	3.7539e-02	23	2.4
0971	2455212.88892148	947668817	166.939	-31.081	-1.1909e-01	7.2127e-01	6.0423e-01	3.7507e-02	28	1.8
0972	2455212.92046770	947671543	122.686	4.647	-1.3370e-01	8.5313e-01	6.3102e-01	3.7539e-02	19	2.4
0973	2455212.92471797	947671910	74.808	-75.830	-9.2963e-02	5.6770e-01	6.3052e-01	3.8106e-02	61	1.4
0974	2455213.15414407	947691733	238.454	25.548	-1.3370e-01	8.5313e-01	6.3102e-01	3.7539e-02	14	2.4
0975	2455213.19806784	947695528	160.430	-1.371	-9.2963e-02	5.6770e-01	6.3052e-01	3.8106e-02	32	1.4
0976	2455213.21381213	947696888	200.820	-38.225	-1.2873e-01	4.3155e-01	4.6595e-01	3.9162e-02	77	0.7
0977	2455213.35664608	947709229	276.946	-23.016	-9.2963e-02	5.6770e-01	6.3052e-01	3.8106e-02	34	1.4
0978	2455213.39821696	947712820	234.501	34.173	-9.2963e-02	5.6770e-01	6.3052e-01	3.8106e-02	36	1.4
0979	2455213.40174958	947713126	67.726	-53.436	-1.3370e-01	8.5313e-01	6.3102e-01	3.7539e-02	24	2.4
0980	2455213.43431247	947715939	211.552	13.112	-9.2963e-02	5.6770e-01	6.3052e-01	3.8106e-02	56	1.4
0981	2455213.48770472	947720552	250.051	-5.168	-1.1724e-01	4.7983e-01	5.2936e-01	3.8897e-02	64	0.9
0982	2455213.49114798	947720850	261.905	-20.117	-1.3370e-01	8.5313e-01	6.3102e-01	3.7539e-02	20	2.4
0983	2455213.50139438	947721735	299.654	33.847	-9.2963e-02	5.6770e-01	6.3052e-01	3.8106e-02	46	1.4
0984	2455213.51991054	947723335	209.996	-14.521	-1.1724e-01	4.7983e-01	5.2936e-01	3.8897e-02	39	0.9
0985	2455213.53946560	947725024	200.485	-29.139	-1.1724e-01	4.7983e-01	5.2936e-01	3.8897e-02	27	0.9
0986	2455213.53971454	947725046	109.252	-46.437	-9.2963e-02	5.6770e-01	6.3052e-01	3.8106e-02	37	1.4
0987	2455213.54156747	947725206	320.335	-68.918	-9.2963e-02	5.6770e-01	6.3052e-01	3.8106e-02	55	1.4
0988	2455214.01182564	947765836	175.032	-4.417	-9.2963e-02	5.6770e-01	6.3052e-01	3.8106e-02	34	1.4
0989	2455214.11136989	947774437	114.048	-11.184	-1.3370e-01	8.5313e-01	6.3102e-01	3.7539e-02	29	2.4
0990	2455214.28131093	947789120	223.097	-28.813	-9.2963e-02	5.6770e-01	6.3052e-01	3.8106e-02	40	1.4
0991	2455214.30593188	947791247	277.461	-9.760	-9.2963e-02	5.6770e-01	6.3052e-01	3.8106e-02	61	1.4
0992	2455214.36089245	947795996	178.073	-27.653	-1.3370e-01	8.5313e-01	6.3102e-01	3.7539e-02	30	2.4
0993	2455214.42798763	947801793	301.777	24.406	-1.1909e-01	7.2127e-01	6.0423e-01	3.7507e-02	30	1.8
0994	2455214.87267737	947840214	299.101	-41.611	-9.2963e-02	5.6770e-01	6.3052e-01	3.8106e-02	51	1.4
0995	2455214.89370262	947842030	35.968	5.427	-9.2963e-02	5.6770e-01	6.3052e-01	3.8106e-02	69	1.4
0996	2455215.50331896	947894701	283.750	-77.656	-1.3370e-01	8.5313e-01	6.3102e-01	3.7539e-02	25	2.4
0997	2455215.56109982	947899694	276.305	-55.215	-1.1724e-01	4.7983e-01	5.2936e-01	3.8897e-02	35	0.9
0998	2455215.65139634	947907495	357.315	13.840	-1.3370e-01	8.5313e-01	6.3102e-01	3.7539e-02	28	2.4
0999	2455215.78045199	947918646	349.378	16.011	-1.2873e-01	4.3155e-01	4.6595e-01	3.9162e-02	47	0.7
1000	2455215.90226208	947929170	8.882	-52.036	-1.3370e-01	8.5313e-01	6.3102e-01	3.7539e-02	29	2.4
1001	2455216.01085793	947938553	41.373	-84.886	-1.3370e-01	8.5313e-01	6.3102e-01	3.7539e-02	27	2.4
1002	2455216.34873897	947967746	203.507	30.062	-9.2963e-02	5.6770e-01	6.3052e-01	3.8106e-02	47	1.4
1003	2455216.36133052	947968833	201.399	-26.520	-1.3370e-01	8.5313e-01	6.3102e-01	3.7539e-02	31	2.4
1004	2455216.45310313	947976763	249.040	10.568	-9.2963e-02	5.6770e-01	6.3052e-01	3.8106e-02	32	1.4
1005	2455216.59292969	947988844	98.494	-30.628	-1.3370e-01	8.5313e-01	6.3102e-01	3.7539e-02	30	2.4
1006	2455216.72955620	948000648	333.831	7.730	-9.2963e-02	5.6770e-01	6.3052e-01	3.8106e-02	32	1.4
1007	2455216.86105434	948012010	341.944	-11.576	-9.2963e-02	5.6770e-01	6.3052e-01	3.8106e-02	47	1.4
1008	2455216.88993180	948014505	26.279	-39.408	-9.2963e-02	5.6770e-01	6.3052e-01	3.8106e-02	42	1.4
1009	2455216.89107169	948014603	31.229	-15.565	-9.2963e-02	5.6770e-01	6.3052e-01	3.8106e-02	62	1.4
1010	2455216.89991008	948015367	208.509	-31.749	-9.2963e-02	5.6770e-01	6.3052e-01	3.8106e-02	20	1.4
1011	2455216.91641982	948016793	76.145	-33.772	-9.2963e-02	5.6770e-01	6.3052e-01	3.8106e-02	41	1.4
1012	2455217.20964166	948042128	197.893	16.200	-9.2963e-02	5.6770e-01	6.3052e-01	3.8106e-02	26	1.4
1013	2455217.30659437	948050504	140.939	-33.050	-9.2963e-02	5.6770e-01	6.3052e-01	3.8106e-02	78	1.4
1014	2455217.37064803	948056038	153.145	-27.790	-9.2963e-02	5.6770e-01	6.3052e-01	3.8106e-02	79	1.4
1015	2455217.38352752	948057151	267.267	-3.638	-1.1724e-01	4.7983e-01	5.2936e-01	3.8897e-02	53	0.9
1016	2455217.43662342	948061739	70.824	-44.897	-9.2963e-02	5.6770e-01	6.3052e-01	3.8106e-02	44	1.4
1017	2455217.48114018	948065585	35.632	-14.867	-9.2963e-02	5.6770e-01	6.3052e-01	3.8106e-02	44	1.4
1018	2455217.63457306	948078842	318.290	1.948	-1.3370e-01	8.5313e-01	6.3102e-01	3.7539e-02	28	2.4
1019	2455217.68534775	948083229	73.186	-66.497	-9.2963e-02	5.6770e-01	6.3052e-01	3.8106e-02	45	1.4

```
1020 2455217.69372588 948083952 76.056 -24.998 -9.2963e-02 5.6770e-01 6.3052e-01 3.8106e-02 37 1.4
1021 2455217.72233598 948086424 22.124 -41.139 -9.2963e-02 5.6770e-01 6.3052e-01 3.8106e-02 58 1.4
1022 2455217.77375757 948090867 258.509 -50.920 -9.2963e-02 5.6770e-01 6.3052e-01 3.8106e-02 34 1.4
1023 2455217.79942390 948093085 79.440 -10.827 -9.2963e-02 5.6770e-01 6.3052e-01 3.8106e-02 40 1.4
1024 2455217.93751951 948105016 209.026 -29.980 -1.1724e-01 4.7983e-01 5.2936e-01 3.8897e-02 32 0.9
1025 2455217.96018590 948106975 158.933 -9.470 -9.2963e-02 5.6770e-01 6.3052e-01 3.8106e-02 37 1.4
1026 2455218.00320179 948110691 297.851 -71.415 -9.2963e-02 5.6770e-01 6.3052e-01 3.8106e-02 36 1.4
1027 2455218.04921834 948114667 66.443 -9.481 -9.2963e-02 5.6770e-01 6.3052e-01 3.8106e-02 33 1.4
1028 2455218.06026285 948115621 136.881 -48.062 -9.2963e-02 5.6770e-01 6.3052e-01 3.8106e-02 45 1.4
1029 2455218.12468535 948121187 212.250 -21.730 -1.3370e-01 8.5313e-01 6.3102e-01 3.7539e-02 30 2.4
1030 2455218.14745146 948123154 207.128 3.288 -9.2963e-02 5.6770e-01 6.3052e-01 3.8106e-02 52 1.4
1031 2455218.16159433 948124376 306.424 -76.348 -1.1724e-01 4.7983e-01 5.2936e-01 3.8897e-02 40 0.9
1032 2455218.23743555 948130929 203.209 4.090 -1.1724e-01 4.7983e-01 5.2936e-01 3.8897e-02 37 0.9
1033 2455218.28351038 948134910 146.554 6.006 -9.2963e-02 5.6770e-01 6.3052e-01 3.8106e-02 36 1.4
1034 2455218.37466473 948142786 246.216 -25.287 -9.2963e-02 5.6770e-01 6.3052e-01 3.8106e-02 53 1.4
1035 2455218.52024679 948155364 263.409 0.566 -1.3370e-01 8.5313e-01 6.3102e-01 3.7539e-02 26 2.4
1036 2455218.71965313 948172593 54.200 -18.294 -1.1909e-01 7.2127e-01 6.0423e-01 3.7507e-02 28 1.8
1037 2455218.80594342 948180048 113.978 -7.262 -1.3370e-01 8.5313e-01 6.3102e-01 3.7539e-02 21 2.4
1038 2455219.09213103 948204775 244.287 5.275 -1.3370e-01 8.5313e-01 6.3102e-01 3.7539e-02 23 2.4
1039 2455219.14023248 948208931 246.829 -84.491 -1.3370e-01 8.5313e-01 6.3102e-01 3.7539e-02 22 2.4
1040 2455219.15124774 948209882 122.980 23.331 -9.2963e-02 5.6770e-01 6.3052e-01 3.8106e-02 51 1.4
1041 2455219.18000458 948212367 117.554 -7.495 -9.2963e-02 5.6770e-01 6.3052e-01 3.8106e-02 74 1.4
1042 2455219.22247143 948216036 186.590 -6.019 -1.2873e-01 4.3155e-01 4.6595e-01 3.9162e-02 50 0.7
1043 2455219.23366936 948217004 223.687 -36.116 -9.2963e-02 5.6770e-01 6.3052e-01 3.8106e-02 38 1.4
1044 2455219.25388962 948218751 255.211 -29.602 -1.3370e-01 8.5313e-01 6.3102e-01 3.7539e-02 28 2.4
1045 2455219.33250068 948225543 306.654 -6.792 -9.2963e-02 5.6770e-01 6.3052e-01 3.8106e-02 41 1.4
1046 2455219.33472768 948225735 350.803 -62.116 -9.2963e-02 5.6770e-01 6.3052e-01 3.8106e-02 41 1.4
1047 2455219.48966383 948239121 250.112 -13.580 -1.3370e-01 8.5313e-01 6.3102e-01 3.7539e-02 21 2.4
1048 2455219.63133488 948251362 286.211 10.829 -9.2963e-02 5.6770e-01 6.3052e-01 3.8106e-02 36 1.4
1049 2455219.75108672 948261708 324.316 -55.637 -1.1724e-01 4.7983e-01 5.2936e-01 3.8897e-02 36 0.9
1050 2455219.75716941 948262234 4.511 9.788 -1.3370e-01 8.5313e-01 6.3102e-01 3.7539e-02 31 2.4
1051 2455219.78046755 948264247 85.081 24.757 -1.3370e-01 8.5313e-01 6.3102e-01 3.7539e-02 95 2.4
1052 2455219.80331319 948266221 72.520 -3.493 -1.1210e-01 3.5816e-01 4.5437e-01 4.0298e-02 108 0.5
1053 2455219.96904028 948280540 194.174 -73.655 -1.3370e-01 8.5313e-01 6.3102e-01 3.7539e-02 24 2.4
1054 2455220.04206527 948286849 162.689 -53.608 -8.8598e-02 3.3283e-01 5.3278e-01 3.9884e-02 150 0.6
1055 2455220.36821775 948315029 335.818 12.849 -9.2963e-02 5.6770e-01 6.3052e-01 3.8106e-02 37 1.4
1056 2455220.44918721 948322024 305.047 22.556 -1.3370e-01 8.5313e-01 6.3102e-01 3.7539e-02 23 2.4
1057 2455220.49848040 948326283 289.880 32.873 -1.3370e-01 8.5313e-01 6.3102e-01 3.7539e-02 55 2.4
1058 2455220.57302099 948332724 246.263 -8.464 -9.2963e-02 5.6770e-01 6.3052e-01 3.8106e-02 56 1.4
1059 2455220.66813892 948340942 39.348 38.839 -9.2963e-02 5.6770e-01 6.3052e-01 3.8106e-02 44 1.4
1060 2455220.74677507 948347736 107.446 -65.438 -1.1724e-01 4.7983e-01 5.2936e-01 3.8897e-02 61 0.9
1061 2455220.77984676 948350593 183.238 -45.749 -1.3370e-01 8.5313e-01 6.3102e-01 3.7539e-02 28 2.4
1062 2455220.81694154 948353798 99.911 -60.413 -1.1724e-01 4.7983e-01 5.2936e-01 3.8897e-02 42 0.9
1063 2455220.99541059 948369218 51.487 13.658 -1.3370e-01 8.5313e-01 6.3102e-01 3.7539e-02 24 2.4
1064 2455221.06080764 948374868 38.067 -24.461 -1.3370e-01 8.5313e-01 6.3102e-01 3.7539e-02 39 2.4
1065 2455221.13791954 948381531 294.711 -29.451 -5.8944e-02 2.9333e-01 5.7306e-01 3.8834e-02 119 0.6
1066 2455221.27910554 948393729 158.171 -2.711 -9.2963e-02 5.6770e-01 6.3052e-01 3.8106e-02 36 1.4
1067 2455221.30351473 948395838 129.469 -24.215 -1.3370e-01 8.5313e-01 6.3102e-01 3.7539e-02 23 2.4
1068 2455221.33926419 948398927 124.093 -72.093 -9.2963e-02 5.6770e-01 6.3052e-01 3.8106e-02 35 1.4
1069 2455221.50481393 948413230 347.248 37.295 -1.3370e-01 8.5313e-01 6.3102e-01 3.7539e-02 27 2.4
1070 2455221.54215549 948416457 52.033 -5.111 -9.2963e-02 5.6770e-01 6.3052e-01 3.8106e-02 63 1.4
1071 2455221.57922778 948419660 137.678 -78.180 -1.1724e-01 4.7983e-01 5.2936e-01 3.8897e-02 33 0.9
```

LIST OF HIGH ENERGY NEUTRINO CANDIDATES FOR THE 2009-2010 DATA

1072 2455221.64028048 948424935 357.852 47.000 -1.1724e-01 4.7983e-01 5.2936e-01 3.8897e-02 41 0.9
1073 2455221.75557236 948434896 279.748 -56.149 -9.2963e-02 5.6770e-01 6.3052e-01 3.8106e-02 42 1.4
1074 2455222.32131253 948483776 165.999 5.048 -9.2963e-02 5.6770e-01 6.3052e-01 3.8106e-02 37 1.4
1075 2455222.62123264 948509689 286.165 18.345 -9.2963e-02 5.6770e-01 6.3052e-01 3.8106e-02 33 1.4
1076 2455222.69290437 948515881 118.419 -13.132 -9.2963e-02 5.6770e-01 6.3052e-01 3.8106e-02 48 1.4
1077 2455222.74576054 948520448 266.505 -62.370 -1.1724e-01 4.7983e-01 5.2936e-01 3.8897e-02 84 0.9
1078 2455222.75772050 948521482 112.018 1.505 -1.1724e-01 4.7983e-01 5.2936e-01 3.8897e-02 32 0.9
1079 2455222.91335717 948534929 270.682 -56.529 -1.1724e-01 4.7983e-01 5.2936e-01 3.8897e-02 33 0.9
1080 2455223.16058157 948556289 148.651 -61.979 -1.3370e-01 8.5313e-01 6.3102e-01 3.7539e-02 25 2.4
1081 2455223.29012699 948567481 234.251 -28.644 -1.1724e-01 4.7983e-01 5.2936e-01 3.8897e-02 58 0.9
1082 2455223.31370597 948569519 207.332 -25.654 -9.2963e-02 5.6770e-01 6.3052e-01 3.8106e-02 39 1.4
1083 2455223.34636204 948572340 204.991 -24.691 -9.2963e-02 5.6770e-01 6.3052e-01 3.8106e-02 33 1.4
1084 2455223.62032678 948596011 322.678 -0.872 -9.2963e-02 5.6770e-01 6.3052e-01 3.8106e-02 47 1.4
1085 2455223.95972438 948625335 65.928 3.770 -1.1724e-01 4.7983e-01 5.2936e-01 3.8897e-02 33 0.9
1086 2455224.01295691 948629934 137.206 -14.028 -9.2963e-02 5.6770e-01 6.3052e-01 3.8106e-02 32 1.4
1087 2455224.05723229 948633759 243.915 -18.892 -1.3370e-01 8.5313e-01 6.3102e-01 3.7539e-02 27 2.4
1088 2455224.37403218 948661131 196.278 -23.099 -9.2963e-02 5.6770e-01 6.3052e-01 3.8106e-02 74 1.4
1089 2455224.46085038 948668632 235.820 19.710 -9.2963e-02 5.6770e-01 6.3052e-01 3.8106e-02 34 1.4
1090 2455224.66861514 948686583 346.007 -26.315 -9.2963e-02 5.6770e-01 6.3052e-01 3.8106e-02 28 1.4
1091 2455224.79992182 948697928 156.004 -64.575 -9.2963e-02 5.6770e-01 6.3052e-01 3.8106e-02 89 1.4
1092 2455224.89850966 948706446 21.848 5.295 -9.2963e-02 5.6770e-01 6.3052e-01 3.8106e-02 38 1.4
1093 2455225.09116564 948723091 251.221 -41.631 -1.3370e-01 8.5313e-01 6.3102e-01 3.7539e-02 23 2.4
1094 2455225.11815454 948725423 190.873 -1.819 -1.3370e-01 8.5313e-01 6.3102e-01 3.7539e-02 92 2.4
1095 2455225.19082410 948731702 192.131 11.316 -9.2963e-02 5.6770e-01 6.3052e-01 3.8106e-02 34 1.4
1096 2455225.30049046 948741177 91.608 -48.254 -1.1724e-01 4.7983e-01 5.2936e-01 3.8897e-02 84 0.9
1097 2455225.33291445 948743978 229.733 -75.828 -1.1724e-01 4.7983e-01 5.2936e-01 3.8897e-02 60 0.9
1098 2455225.55116786 948762835 342.094 35.552 -9.2963e-02 5.6770e-01 6.3052e-01 3.8106e-02 43 1.4
1099 2455225.55806497 948763431 262.072 11.086 -9.2963e-02 5.6770e-01 6.3052e-01 3.8106e-02 32 1.4
1100 2455225.65571585 948771868 37.747 18.739 -9.2963e-02 5.6770e-01 6.3052e-01 3.8106e-02 33 1.4
1101 2455225.78345525 948782905 77.575 -0.047 -9.2963e-02 5.6770e-01 6.3052e-01 3.8106e-02 36 1.4
1102 2455225.86544796 948789989 162.560 -38.927 -9.2963e-02 5.6770e-01 6.3052e-01 3.8106e-02 35 1.4
1103 2455225.98945937 948800704 208.863 -42.351 -1.3370e-01 8.5313e-01 6.3102e-01 3.7539e-02 23 2.4
1104 2455226.49592804 948844463 12.922 -67.977 -1.1724e-01 4.7983e-01 5.2936e-01 3.8897e-02 52 0.9
1105 2455226.62185065 948855342 244.096 -32.250 -9.2963e-02 5.6770e-01 6.3052e-01 3.8106e-02 48 1.4
1106 2455226.62876391 948855940 30.090 -24.777 -9.2963e-02 5.6770e-01 6.3052e-01 3.8106e-02 57 1.4
1107 2455226.63261844 948856273 326.561 -9.564 -1.3370e-01 8.5313e-01 6.3102e-01 3.7539e-02 29 2.4
1108 2455226.69199090 948861403 317.119 -29.785 -9.2963e-02 5.6770e-01 6.3052e-01 3.8106e-02 32 1.4
1109 2455227.38304052 948921109 274.256 -10.089 -9.2963e-02 5.6770e-01 6.3052e-01 3.8106e-02 43 1.4
1110 2455227.58180827 948938283 88.182 -36.395 -9.2963e-02 5.6770e-01 6.3052e-01 3.8106e-02 33 1.4
1111 2455227.71621039 948949895 65.838 -38.510 -9.2963e-02 5.6770e-01 6.3052e-01 3.8106e-02 39 1.4
1112 2455228.22342598 948993719 230.812 27.397 -9.2963e-02 5.6770e-01 6.3052e-01 3.8106e-02 32 1.4
1113 2455228.55535479 949022397 136.282 -49.505 -9.2963e-02 5.6770e-01 6.3052e-01 3.8106e-02 63 1.4
1114 2455231.82649058 949305023 44.587 -9.319 -9.2963e-02 5.6770e-01 6.3052e-01 3.8106e-02 32 1.4
1115 2455231.96039399 949316593 89.812 -31.333 -1.3370e-01 8.5313e-01 6.3102e-01 3.7539e-02 29 2.4
1116 2455232.01008270 949320886 208.901 6.636 -9.2963e-02 5.6770e-01 6.3052e-01 3.8106e-02 40 1.4
1117 2455232.04375434 949323795 187.660 -66.270 -9.2963e-02 5.6770e-01 6.3052e-01 3.8106e-02 52 1.4
1118 2455232.15063248 949333029 180.283 15.690 -1.2873e-01 4.3155e-01 4.6595e-01 3.9162e-02 59 0.7
1119 2455232.20247236 949337508 1.888 -46.375 -1.3370e-01 8.5313e-01 6.3102e-01 3.7539e-02 26 2.4
1120 2455232.23740823 949340527 221.282 -35.734 -1.1724e-01 4.7983e-01 5.2936e-01 3.8897e-02 80 0.9
1121 2455232.36926152 949351919 195.137 -1.809 -9.2963e-02 5.6770e-01 6.3052e-01 3.8106e-02 43 1.4
1122 2455232.38524317 949353300 167.865 -28.090 -1.3370e-01 8.5313e-01 6.3102e-01 3.7539e-02 24 2.4
1123 2455232.40058797 949354625 9.860 -56.106 -9.2963e-02 5.6770e-01 6.3052e-01 3.8106e-02 40 1.4

```
1124 2455232.59851963 949371727 0.104 -46.954 -1.1724e-01 4.7983e-01 5.2936e-01 3.8897e-02 40 0.9
1125 2455232.60584214 949372359 65.585 -33.839 -1.2873e-01 4.3155e-01 4.6595e-01 3.9162e-02 34 0.7
1126 2455232.63352183 949374751 345.528 17.806 -9.2963e-02 5.6770e-01 6.3052e-01 3.8106e-02 68 1.4
1127 2455232.77243470 949386753 89.698 37.040 -9.2963e-02 5.6770e-01 6.3052e-01 3.8106e-02 72 1.4
1128 2455232.79390368 949388608 125.976 22.166 -9.2963e-02 5.6770e-01 6.3052e-01 3.8106e-02 35 1.4
1129 2455232.89347699 949397211 82.098 -83.428 -9.2963e-02 5.6770e-01 6.3052e-01 3.8106e-02 33 1.4
1130 2455232.96587954 949403466 102.746 1.604 -9.2963e-02 5.6770e-01 6.3052e-01 3.8106e-02 42 1.4
1131 2455233.27333710 949430031 294.057 -0.258 -9.2963e-02 5.6770e-01 6.3052e-01 3.8106e-02 88 1.4
1132 2455233.37104961 949438473 294.315 -12.876 -9.2963e-02 5.6770e-01 6.3052e-01 3.8106e-02 57 1.4
1133 2455233.38794543 949439933 38.527 -41.127 -1.1724e-01 4.7983e-01 5.2936e-01 3.8897e-02 38 0.9
1134 2455233.49782838 949449427 358.312 31.742 -1.1724e-01 4.7983e-01 5.2936e-01 3.8897e-02 34 0.9
1135 2455233.60557642 949458736 116.915 -41.156 -9.2963e-02 5.6770e-01 6.3052e-01 3.8106e-02 64 1.4
1136 2455233.78372019 949474128 264.184 -56.082 -9.2963e-02 5.6770e-01 6.3052e-01 3.8106e-02 31 1.4
1137 2455233.79082307 949474742 81.396 -8.198 -1.2873e-01 4.3155e-01 4.6595e-01 3.9162e-02 60 0.7
1138 2455233.99792775 949492635 178.429 -8.704 -1.2873e-01 4.3155e-01 4.6595e-01 3.9162e-02 47 0.7
1139 2455234.05581226 949497637 304.342 -55.041 -1.1724e-01 4.7983e-01 5.2936e-01 3.8897e-02 32 0.9
1140 2455234.06206055 949498177 203.235 -24.044 -1.1724e-01 4.7983e-01 5.2936e-01 3.8897e-02 50 0.9
1141 2455234.10329669 949501739 203.033 42.253 -1.1724e-01 4.7983e-01 5.2936e-01 3.8897e-02 88 0.9
1142 2455234.11349118 949502620 144.672 -25.741 -9.2963e-02 5.6770e-01 6.3052e-01 3.8106e-02 37 1.4
1143 2455234.17226805 949507698 116.168 -36.173 -1.1909e-01 7.2127e-01 6.0423e-01 3.7507e-02 31 1.8
1144 2455234.17458007 949507898 232.149 -73.066 -9.2963e-02 5.6770e-01 6.3052e-01 3.8106e-02 32 1.4
1145 2455234.20308039 949510361 288.287 17.564 -9.2963e-02 5.6770e-01 6.3052e-01 3.8106e-02 44 1.4
1146 2455234.23349760 949512989 274.625 -85.271 -9.2963e-02 5.6770e-01 6.3052e-01 3.8106e-02 62 1.4
1147 2455234.27105166 949516233 338.716 -11.411 -9.2963e-02 5.6770e-01 6.3052e-01 3.8106e-02 35 1.4
1148 2455234.28405659 949517357 206.358 5.535 -1.3370e-01 8.5313e-01 6.3102e-01 3.7539e-02 22 2.4
1149 2455234.35606033 949523578 291.066 32.423 -1.3370e-01 8.5313e-01 6.3102e-01 3.7539e-02 41 2.4
1150 2455234.43237098 949530171 255.404 -22.884 -9.2963e-02 5.6770e-01 6.3052e-01 3.8106e-02 38 1.4
1151 2455234.43997151 949530828 250.749 -82.903 -9.2963e-02 5.6770e-01 6.3052e-01 3.8106e-02 46 1.4
1152 2455234.46632278 949533105 161.252 -56.190 -9.2963e-02 5.6770e-01 6.3052e-01 3.8106e-02 34 1.4
1153 2455234.50218369 949536203 178.883 -51.967 -9.2963e-02 5.6770e-01 6.3052e-01 3.8106e-02 36 1.4
1154 2455235.00724824 949579841 101.607 -74.960 -9.2963e-02 5.6770e-01 6.3052e-01 3.8106e-02 30 1.4
1155 2455235.48053110 949620732 255.276 21.010 -1.3370e-01 8.5313e-01 6.3102e-01 3.7539e-02 31 2.4
1156 2455235.60015703 949631068 344.160 35.564 -1.3370e-01 8.5313e-01 6.3102e-01 3.7539e-02 54 2.4
1157 2455235.66886048 949637004 91.296 14.301 -1.3370e-01 8.5313e-01 6.3102e-01 3.7539e-02 45 2.4
1158 2455235.90736161 949657611 346.345 -35.238 -9.2963e-02 5.6770e-01 6.3052e-01 3.8106e-02 41 1.4
1159 2455236.09782212 949674066 216.286 -28.671 -1.1724e-01 4.7983e-01 5.2936e-01 3.8897e-02 43 0.9
1160 2455236.51118661 949709781 21.396 -58.381 -1.3370e-01 8.5313e-01 6.3102e-01 3.7539e-02 22 2.4
1161 2455236.65832392 949722494 311.032 -37.363 -1.1909e-01 7.2127e-01 6.0423e-01 3.7507e-02 29 1.8
1162 2455236.69194154 949725398 151.987 -57.454 -1.1724e-01 4.7983e-01 5.2936e-01 3.8897e-02 38 0.9
1163 2455236.79559207 949734354 0.681 -37.195 -1.1909e-01 7.2127e-01 6.0423e-01 3.7507e-02 29 1.8
1164 2455237.05170999 949756482 330.298 -50.913 -1.1724e-01 4.7983e-01 5.2936e-01 3.8897e-02 37 0.9
1165 2455237.05319009 949756610 278.469 -23.573 -1.3370e-01 8.5313e-01 6.3102e-01 3.7539e-02 31 2.4
1166 2455237.05822559 949757045 54.677 -31.165 -9.2963e-02 5.6770e-01 6.3052e-01 3.8106e-02 63 1.4
1167 2455237.27419539 949775705 250.101 1.844 -9.2963e-02 5.6770e-01 6.3052e-01 3.8106e-02 37 1.4
1168 2455237.67022373 949809922 87.573 27.633 -9.2963e-02 5.6770e-01 6.3052e-01 3.8106e-02 37 1.4
1169 2455237.90749359 949830422 194.588 -80.618 -9.2963e-02 5.6770e-01 6.3052e-01 3.8106e-02 40 1.4
1170 2455238.04709435 949842483 129.891 -10.447 -1.2873e-01 4.3155e-01 4.6595e-01 3.9162e-02 41 0.7
1171 2455238.29850840 949864206 268.915 -41.544 -1.1724e-01 4.7983e-01 5.2936e-01 3.8897e-02 48 0.9
1172 2455238.54279775 949885312 233.262 -22.124 -1.3370e-01 8.5313e-01 6.3102e-01 3.7539e-02 22 2.4
1173 2455238.80680592 949908123 318.764 -52.914 -1.3370e-01 8.5313e-01 6.3102e-01 3.7539e-02 30 2.4
1174 2455238.83067321 949910185 16.152 8.161 -9.2963e-02 5.6770e-01 6.3052e-01 3.8106e-02 49 1.4
1175 2455238.84593511 949911503 35.966 17.808 -9.2963e-02 5.6770e-01 6.3052e-01 3.8106e-02 51 1.4
```

LIST OF HIGH ENERGY NEUTRINO CANDIDATES FOR THE 2009-2010 DATA

1176 2455238.86708216 949913330 308.956 -60.607 -9.2963e-02 5.6770e-01 6.3052e-01 3.8106e-02 42 1.4
1177 2455239.15188527 949937937 133.415 2.981 -9.2963e-02 5.6770e-01 6.3052e-01 3.8106e-02 59 1.4
1178 2455239.42988479 949961957 338.995 5.574 -9.2963e-02 5.6770e-01 6.3052e-01 3.8106e-02 44 1.4
1179 2455239.67181225 949982859 67.722 -54.693 -9.2963e-02 5.6770e-01 6.3052e-01 3.8106e-02 56 1.4
1180 2455239.96451713 950008149 172.860 -14.823 -9.2963e-02 5.6770e-01 6.3052e-01 3.8106e-02 52 1.4
1181 2455240.18513263 950027210 284.347 -23.086 -9.2963e-02 5.6770e-01 6.3052e-01 3.8106e-02 49 1.4
1182 2455240.21007501 950029365 242.480 -3.892 -9.2963e-02 5.6770e-01 6.3052e-01 3.8106e-02 34 1.4
1183 2455240.21160765 950029497 211.312 -45.305 -9.2963e-02 5.6770e-01 6.3052e-01 3.8106e-02 36 1.4
1184 2455240.23034532 950031116 185.137 -73.085 -1.1724e-01 4.7983e-01 5.2936e-01 3.8897e-02 58 0.9
1185 2455240.34505034 950041027 272.662 -37.470 -1.1724e-01 4.7983e-01 5.2936e-01 3.8897e-02 63 0.9
1186 2455240.41802997 950047332 351.348 -19.590 -9.2963e-02 5.6770e-01 6.3052e-01 3.8106e-02 55 1.4
1187 2455240.66495751 950068667 21.024 -3.372 -9.2963e-02 5.6770e-01 6.3052e-01 3.8106e-02 35 1.4
1188 2455240.80404601 950080684 130.577 -17.357 -9.2963e-02 5.6770e-01 6.3052e-01 3.8106e-02 43 1.4
1189 2455240.91853798 950090576 91.702 -67.632 -1.1724e-01 4.7983e-01 5.2936e-01 3.8897e-02 39 0.9
1190 2455240.93571007 950092060 44.912 -12.529 -1.3370e-01 8.5313e-01 6.3102e-01 3.7539e-02 29 2.4
1191 2455241.09773842 950106059 266.207 -53.110 -1.3370e-01 8.5313e-01 6.3102e-01 3.7539e-02 34 2.4
1192 2455241.13957804 950109674 196.043 -4.553 -1.1724e-01 4.7983e-01 5.2936e-01 3.8897e-02 50 0.9
1193 2455241.65199051 950153946 69.486 30.920 -9.2963e-02 5.6770e-01 6.3052e-01 3.8106e-02 32 1.4
1194 2455241.72682003 950160412 212.961 -69.030 -1.1724e-01 4.7983e-01 5.2936e-01 3.8897e-02 36 0.9
1195 2455241.96851666 950181294 58.341 8.207 -1.3370e-01 8.5313e-01 6.3102e-01 3.7539e-02 22 2.4
1196 2455242.14205350 950196288 159.121 -46.988 -1.1724e-01 4.7983e-01 5.2936e-01 3.8897e-02 54 0.9
1197 2455242.21229851 950202357 331.966 -59.103 -1.1909e-01 7.2127e-01 6.0423e-01 3.7507e-02 30 1.8
1198 2455242.39309355 950217978 232.213 0.320 -1.3370e-01 8.5313e-01 6.3102e-01 3.7539e-02 27 2.4
1199 2455242.50935854 950228023 216.341 -30.679 -9.2963e-02 5.6770e-01 6.3052e-01 3.8106e-02 58 1.4
1200 2455242.53919763 950230601 248.625 -35.295 -1.3370e-01 8.5313e-01 6.3102e-01 3.7539e-02 29 2.4
1201 2455242.62830058 950238300 267.614 -27.172 -1.3370e-01 8.5313e-01 6.3102e-01 3.7539e-02 50 2.4
1202 2455242.64813353 950240013 304.941 5.364 -9.2963e-02 5.6770e-01 6.3052e-01 3.8106e-02 46 1.4
1203 2455242.69406945 950243982 101.511 -44.945 -9.2963e-02 5.6770e-01 6.3052e-01 3.8106e-02 41 1.4
1204 2455242.74461460 950248349 331.102 -37.505 -9.2963e-02 5.6770e-01 6.3052e-01 3.8106e-02 54 1.4
1205 2455242.98259308 950268911 166.229 9.696 -9.2963e-02 5.6770e-01 6.3052e-01 3.8106e-02 38 1.4
1206 2455242.98397481 950269030 266.530 -63.085 -1.1724e-01 4.7983e-01 5.2936e-01 3.8897e-02 43 0.9
1207 2455243.02402614 950272490 153.353 17.113 -9.2963e-02 5.6770e-01 6.3052e-01 3.8106e-02 44 1.4
1208 2455243.26316068 950293152 273.627 13.975 -1.3370e-01 8.5313e-01 6.3102e-01 3.7539e-02 31 2.4
1209 2455244.04238785 950360477 105.430 -19.063 -1.3370e-01 8.5313e-01 6.3102e-01 3.7539e-02 25 2.4
1210 2455244.11037502 950366351 309.510 -35.744 -1.1724e-01 4.7983e-01 5.2936e-01 3.8897e-02 57 0.9
1211 2455244.18681015 950372955 110.253 -58.106 -1.1724e-01 4.7983e-01 5.2936e-01 3.8897e-02 42 0.9
1212 2455244.34751617 950386840 49.400 -46.820 -9.2963e-02 5.6770e-01 6.3052e-01 3.8106e-02 65 1.4
1213 2455244.70301797 950417555 49.645 -6.026 -9.2963e-02 5.6770e-01 6.3052e-01 3.8106e-02 56 1.4
1214 2455245.06326866 950448681 206.368 -49.273 -9.2963e-02 5.6770e-01 6.3052e-01 3.8106e-02 46 1.4
1215 2455245.08729539 950450757 144.462 -25.738 -1.3370e-01 8.5313e-01 6.3102e-01 3.7539e-02 21 2.4
1216 2455245.11403893 950453067 159.365 32.917 -1.1724e-01 4.7983e-01 5.2936e-01 3.8897e-02 52 0.9
1217 2455245.27470075 950466949 164.540 -60.394 -1.1724e-01 4.7983e-01 5.2936e-01 3.8897e-02 59 0.9
1218 2455245.44499140 950481662 231.172 -85.484 -1.3370e-01 8.5313e-01 6.3102e-01 3.7539e-02 24 2.4
1219 2455245.44966551 950482066 244.638 -4.769 -9.2963e-02 5.6770e-01 6.3052e-01 3.8106e-02 83 1.4
1220 2455245.45975074 950482937 300.302 14.171 -9.2963e-02 5.6770e-01 6.3052e-01 3.8106e-02 33 1.4
1221 2455245.60601843 950495574 106.127 -65.269 -9.2963e-02 5.6770e-01 6.3052e-01 3.8106e-02 38 1.4
1222 2455245.71563288 950505045 53.773 13.446 -9.2963e-02 5.6770e-01 6.3052e-01 3.8106e-02 54 1.4
1223 2455246.02217481 950531530 97.378 -16.582 -9.2963e-02 5.6770e-01 6.3052e-01 3.8106e-02 57 1.4
1224 2455246.03158917 950532344 233.263 -46.073 -9.2963e-02 5.6770e-01 6.3052e-01 3.8106e-02 35 1.4
1225 2455246.09805670 950538087 174.332 -1.822 -1.3370e-01 8.5313e-01 6.3102e-01 3.7539e-02 25 2.4
1226 2455246.11528234 950539575 214.466 17.640 -9.2963e-02 5.6770e-01 6.3052e-01 3.8106e-02 70 1.4
1227 2455246.28998500 950554669 197.475 9.682 -9.2963e-02 5.6770e-01 6.3052e-01 3.8106e-02 64 1.4

```
1228 2455246.33228058 950558324 312.487 -16.123 -9.2963e-02 5.6770e-01 6.3052e-01 3.8106e-02 50 1.4
1229 2455246.42955897 950566728 165.777 -50.785 -9.2963e-02 5.6770e-01 6.3052e-01 3.8106e-02 33 1.4
1230 2455246.75944578 950595231 25.761 15.246 -9.2963e-02 5.6770e-01 6.3052e-01 3.8106e-02 99 1.4
1231 2455246.88573043 950606142 159.477 36.232 -9.2963e-02 5.6770e-01 6.3052e-01 3.8106e-02 65 1.4
1232 2455246.91716358 950608857 111.797 21.931 -9.2963e-02 5.6770e-01 6.3052e-01 3.8106e-02 58 1.4
1233 2455247.21308151 950634425 209.838 -49.177 -1.1724e-01 4.7983e-01 5.2936e-01 3.8897e-02 50 0.9
1234 2455247.24815218 950637455 349.328 -72.661 -1.3370e-01 8.5313e-01 6.3102e-01 3.7539e-02 24 2.4
1235 2455247.38435043 950649222 300.730 -81.634 -1.1724e-01 4.7983e-01 5.2936e-01 3.8897e-02 58 0.9
1236 2455247.64487348 950671732 333.654 -35.879 -1.1724e-01 4.7983e-01 5.2936e-01 3.8897e-02 38 0.9
1237 2455248.12800971 950713475 244.347 6.203 -1.3370e-01 8.5313e-01 6.3102e-01 3.7539e-02 30 2.4
1238 2455248.15882571 950716137 189.658 -63.631 -1.2873e-01 4.3155e-01 4.6595e-01 3.9162e-02 83 0.7
1239 2455248.37754314 950735034 216.336 5.409 -1.2873e-01 4.3155e-01 4.6595e-01 3.9162e-02 53 0.7
1240 2455248.70727778 950763523 298.895 -33.968 -9.2963e-02 5.6770e-01 6.3052e-01 3.8106e-02 52 1.4
1241 2455248.87771300 950778249 99.719 -15.781 -1.1724e-01 4.7983e-01 5.2936e-01 3.8897e-02 51 0.9
1242 2455248.91453510 950781430 239.154 -23.460 -1.1724e-01 4.7983e-01 5.2936e-01 3.8897e-02 32 0.9
1243 2455249.05170480 950793282 109.860 -2.231 -1.3370e-01 8.5313e-01 6.3102e-01 3.7539e-02 31 2.4
1244 2455249.07433209 950795237 288.527 -70.925 -9.2963e-02 5.6770e-01 6.3052e-01 3.8106e-02 65 1.4
1245 2455249.32470947 950816869 352.745 -11.411 -9.2963e-02 5.6770e-01 6.3052e-01 3.8106e-02 50 1.4
1246 2455249.48498370 950830717 331.292 -45.173 -9.2963e-02 5.6770e-01 6.3052e-01 3.8106e-02 48 1.4
1247 2455249.53726233 950835234 104.269 -29.206 -9.2963e-02 5.6770e-01 6.3052e-01 3.8106e-02 36 1.4
1248 2455249.90214154 950866760 88.128 -32.685 -1.1724e-01 4.7983e-01 5.2936e-01 3.8897e-02 61 0.9
1249 2455249.94436753 950870408 133.525 39.457 -1.1909e-01 7.2127e-01 6.0423e-01 3.7507e-02 31 1.8
1250 2455250.04090446 950878749 147.859 -28.125 -1.1909e-01 7.2127e-01 6.0423e-01 3.7507e-02 28 1.8
1251 2455250.04838391 950879395 147.227 22.454 -9.2963e-02 5.6770e-01 6.3052e-01 3.8106e-02 39 1.4
1252 2455250.47216235 950916009 223.921 -39.904 -9.2963e-02 5.6770e-01 6.3052e-01 3.8106e-02 54 1.4
1253 2455250.50063640 950918469 316.257 -3.098 -1.3370e-01 8.5313e-01 6.3102e-01 3.7539e-02 28 2.4
1254 2455250.54714032 950922487 246.636 -32.686 -1.1724e-01 4.7983e-01 5.2936e-01 3.8897e-02 35 0.9
1255 2455250.70674558 950936277 25.209 21.320 -9.2963e-02 5.6770e-01 6.3052e-01 3.8106e-02 36 1.4
1256 2455251.06517422 950967246 171.914 42.818 -9.2963e-02 5.6770e-01 6.3052e-01 3.8106e-02 60 1.4
1257 2455251.11415422 950971477 183.872 -24.055 -9.2963e-02 5.6770e-01 6.3052e-01 3.8106e-02 55 1.4
1258 2455251.13918401 950973640 354.176 -81.250 -1.1724e-01 4.7983e-01 5.2936e-01 3.8897e-02 43 0.9
1259 2455251.19776064 950978701 280.767 -6.270 -1.1724e-01 4.7983e-01 5.2936e-01 3.8897e-02 58 0.9
1260 2455251.28195543 950985975 355.240 -7.914 -9.2963e-02 5.6770e-01 6.3052e-01 3.8106e-02 33 1.4
1261 2455251.37408099 950993935 257.172 25.183 -9.2963e-02 5.6770e-01 6.3052e-01 3.8106e-02 44 1.4
1262 2455251.43607378 950999291 273.004 -26.267 -1.1724e-01 4.7983e-01 5.2936e-01 3.8897e-02 44 0.9
1263 2455251.45271221 951000729 242.559 -48.993 -1.3370e-01 8.5313e-01 6.3102e-01 3.7539e-02 27 2.4
1264 2455251.53134595 951007523 120.158 -52.530 -1.3370e-01 8.5313e-01 6.3102e-01 3.7539e-02 31 2.4
1265 2455254.56912428 951269987 300.560 -22.486 -1.1724e-01 4.7983e-01 5.2936e-01 3.8897e-02 38 0.9
1266 2455254.83440150 951292907 113.376 -39.305 -9.2963e-02 5.6770e-01 6.3052e-01 3.8106e-02 50 1.4
1267 2455255.15049270 951320217 334.300 -27.545 -1.3370e-01 8.5313e-01 6.3102e-01 3.7539e-02 30 2.4
1268 2455255.19945811 951324448 305.669 8.883 -9.2963e-02 5.6770e-01 6.3052e-01 3.8106e-02 54 1.4
1269 2455255.21161200 951325498 299.542 -66.919 -1.1724e-01 4.7983e-01 5.2936e-01 3.8897e-02 52 0.9
1270 2455255.27759747 951331199 239.712 -50.950 -1.1724e-01 4.7983e-01 5.2936e-01 3.8897e-02 76 0.9
1271 2455255.28326351 951331688 341.809 -38.533 -1.3370e-01 8.5313e-01 6.3102e-01 3.7539e-02 29 2.4
1272 2455255.43858706 951345108 104.708 -49.112 -1.3370e-01 8.5313e-01 6.3102e-01 3.7539e-02 34 2.4
1273 2455255.75018716 951372031 32.381 -24.453 -1.3370e-01 8.5313e-01 6.3102e-01 3.7539e-02 27 2.4
1274 2455255.83863293 951379672 198.367 -22.289 -9.2963e-02 5.6770e-01 6.3052e-01 3.8106e-02 45 1.4
1275 2455255.90554189 951385453 95.598 -57.626 -1.3370e-01 8.5313e-01 6.3102e-01 3.7539e-02 30 2.4
1276 2455256.15353235 951406880 265.867 -14.570 -1.1724e-01 4.7983e-01 5.2936e-01 3.8897e-02 33 0.9
1277 2455256.29602770 951419191 153.135 -27.213 -9.2963e-02 5.6770e-01 6.3052e-01 3.8106e-02 62 1.4
1278 2455256.40462749 951428574 272.305 34.817 -1.1724e-01 4.7983e-01 5.2936e-01 3.8897e-02 47 0.9
1279 2455256.60036258 951445486 113.578 -58.128 -1.3370e-01 8.5313e-01 6.3102e-01 3.7539e-02 27 2.4
```

LIST OF HIGH ENERGY NEUTRINO CANDIDATES FOR THE 2009-2010 DATA

1280 2455256.60499258 951445886 40.650 28.305 -9.2963e-02 5.6770e-01 6.3052e-01 3.8106e-02 50 1.4
1281 2455256.71003407 951454961 68.124 16.054 -9.2963e-02 5.6770e-01 6.3052e-01 3.8106e-02 47 1.4
1282 2455256.79754508 951462522 122.853 -74.560 -1.1724e-01 4.7983e-01 5.2936e-01 3.8897e-02 42 0.9
1283 2455256.89157759 951470647 137.086 37.464 -1.1724e-01 4.7983e-01 5.2936e-01 3.8897e-02 47 0.9
1284 2455256.91242316 951472448 92.657 -35.438 -1.1909e-01 7.2127e-01 6.0423e-01 3.7507e-02 31 1.8
1285 2455256.93188579 951474129 186.059 -27.492 -1.1909e-01 7.2127e-01 6.0423e-01 3.7507e-02 29 1.8
1286 2455257.31602508 951507319 247.774 28.999 -9.2963e-02 5.6770e-01 6.3052e-01 3.8106e-02 57 1.4
1287 2455257.47023293 951520643 251.381 -6.165 -9.2963e-02 5.6770e-01 6.3052e-01 3.8106e-02 66 1.4
1288 2455257.66049793 951537082 152.998 -27.867 -1.2873e-01 4.3155e-01 4.6595e-01 3.9162e-02 58 0.7
1289 2455257.70898795 951541271 137.758 -63.620 -1.2873e-01 4.3155e-01 4.6595e-01 3.9162e-02 59 0.7
1290 2455257.73587488 951543594 29.546 27.063 -1.3370e-01 8.5313e-01 6.3102e-01 3.7539e-02 31 2.4
1291 2455257.79489538 951548693 61.982 2.317 -1.3370e-01 8.5313e-01 6.3102e-01 3.7539e-02 88 2.4
1292 2455258.03068668 951569066 244.968 -5.899 -1.1909e-01 7.2127e-01 6.0423e-01 3.7507e-02 30 1.8
1293 2455258.06352406 951571903 252.012 -74.408 -1.1909e-01 7.2127e-01 6.0423e-01 3.7507e-02 32 1.8
1294 2455258.08327040 951573609 224.081 -12.926 -1.1724e-01 4.7983e-01 5.2936e-01 3.8897e-02 80 0.9
1295 2455258.10306321 951575319 112.776 -2.369 -9.2963e-02 5.6770e-01 6.3052e-01 3.8106e-02 97 1.4
1296 2455258.16277478 951580478 311.195 -16.847 -9.2963e-02 5.6770e-01 6.3052e-01 3.8106e-02 43 1.4
1297 2455258.25098552 951588100 199.424 -68.796 -9.2963e-02 5.6770e-01 6.3052e-01 3.8106e-02 45 1.4
1298 2455259.94614591 951734562 147.978 14.078 -9.2963e-02 5.6770e-01 6.3052e-01 3.8106e-02 52 1.4
1299 2455259.96364018 951736073 32.567 -41.438 -1.3370e-01 8.5313e-01 6.3102e-01 3.7539e-02 28 2.4
1300 2455260.02215769 951741129 189.316 -66.285 -9.2963e-02 5.6770e-01 6.3052e-01 3.8106e-02 35 1.4
1301 2455260.12224479 951749776 157.221 30.385 -9.2963e-02 5.6770e-01 6.3052e-01 3.8106e-02 46 1.4
1302 2455260.18633076 951755313 232.560 18.338 -1.3370e-01 8.5313e-01 6.3102e-01 3.7539e-02 30 2.4
1303 2455260.32220811 951767053 288.229 -11.089 -1.3370e-01 8.5313e-01 6.3102e-01 3.7539e-02 30 2.4
1304 2455260.43713780 951776983 38.091 14.978 -9.2963e-02 5.6770e-01 6.3052e-01 3.8106e-02 71 1.4
1305 2455260.44574146 951777727 252.298 5.147 -9.2963e-02 5.6770e-01 6.3052e-01 3.8106e-02 46 1.4
1306 2455260.53491109 951785431 322.231 -40.597 -1.1909e-01 7.2127e-01 6.0423e-01 3.7507e-02 31 1.8
1307 2455260.60643335 951791610 137.134 -63.994 -1.3370e-01 8.5313e-01 6.3102e-01 3.7539e-02 31 2.4
1308 2455260.75423916 951804381 38.562 -31.526 -9.2963e-02 5.6770e-01 6.3052e-01 3.8106e-02 40 1.4
1309 2455261.19588286 951842539 315.265 -7.455 -9.2963e-02 5.6770e-01 6.3052e-01 3.8106e-02 35 1.4
1310 2455261.31298374 951852656 230.839 16.296 -9.2963e-02 5.6770e-01 6.3052e-01 3.8106e-02 35 1.4
1311 2455261.34274907 951855228 286.390 -75.079 -9.2963e-02 5.6770e-01 6.3052e-01 3.8106e-02 35 1.4
1312 2455261.76379208 951891606 339.817 -33.331 -9.2963e-02 5.6770e-01 6.3052e-01 3.8106e-02 60 1.4
1313 2455261.78229491 951893205 154.027 10.076 -1.3370e-01 8.5313e-01 6.3102e-01 3.7539e-02 30 2.4
1314 2455261.80862669 951895480 138.568 -13.318 -1.3370e-01 8.5313e-01 6.3102e-01 3.7539e-02 31 2.4
1315 2455261.89353787 951902816 33.102 -15.791 -1.3370e-01 8.5313e-01 6.3102e-01 3.7539e-02 35 2.4
1316 2455261.93239698 951906174 95.193 11.129 -9.2963e-02 5.6770e-01 6.3052e-01 3.8106e-02 35 1.4
1317 2455263.29721293 952024094 210.043 3.714 -9.2963e-02 5.6770e-01 6.3052e-01 3.8106e-02 82 1.4
1318 2455267.62379628 952397910 83.137 -15.107 -1.1724e-01 4.7983e-01 5.2936e-01 3.8897e-02 40 0.9
1319 2455267.67307166 952402168 132.980 -18.113 -9.2963e-02 5.6770e-01 6.3052e-01 3.8106e-02 33 1.4
1320 2455267.67338965 952402195 3.705 -35.560 -1.3370e-01 8.5313e-01 6.3102e-01 3.7539e-02 28 2.4
1321 2455267.67367323 952402220 100.637 37.467 -1.3370e-01 8.5313e-01 6.3102e-01 3.7539e-02 60 2.4
1322 2455267.81031033 952414025 159.353 32.380 -1.3370e-01 8.5313e-01 6.3102e-01 3.7539e-02 30 2.4
1323 2455267.84146818 952416717 233.180 -26.350 -1.3370e-01 8.5313e-01 6.3102e-01 3.7539e-02 29 2.4
1324 2455268.35150423 952460784 189.398 -60.340 -1.3370e-01 8.5313e-01 6.3102e-01 3.7539e-02 24 2.4
1325 2455268.35481495 952461071 214.756 -29.087 -1.3370e-01 8.5313e-01 6.3102e-01 3.7539e-02 30 2.4
1326 2455268.40013440 952464986 301.321 -50.569 -1.1724e-01 4.7983e-01 5.2936e-01 3.8897e-02 49 0.9
1327 2455280.29903374 953493051 274.970 -70.396 -9.2963e-02 5.6770e-01 6.3052e-01 3.8106e-02 37 1.4
1328 2455283.30609960 953752862 198.173 -42.956 -9.2963e-02 5.6770e-01 6.3052e-01 3.8106e-02 38 1.4
1329 2455283.43377335 953763893 18.049 -35.932 -9.2963e-02 5.6770e-01 6.3052e-01 3.8106e-02 33 1.4
1330 2455283.47959317 953767851 66.466 -22.341 -9.2963e-02 5.6770e-01 6.3052e-01 3.8106e-02 52 1.4
1331 2455283.77032782 953792971 131.524 -17.652 -1.1724e-01 4.7983e-01 5.2936e-01 3.8897e-02 52 0.9

1332 2455284.90541283 953891042 71.241 -33.435 -9.2963e-02 5.6770e-01 6.3052e-01 3.8106e-02 37 1.4
1333 2455284.91821652 953892148 227.039 -65.340 -9.2963e-02 5.6770e-01 6.3052e-01 3.8106e-02 31 1.4
1334 2455285.01907694 953900863 155.875 -29.601 -9.2963e-02 5.6770e-01 6.3052e-01 3.8106e-02 61 1.4
1335 2455285.22608287 953918748 316.749 -64.999 -9.2963e-02 5.6770e-01 6.3052e-01 3.8106e-02 61 1.4
1336 2455285.32338085 953927155 232.948 -29.647 -9.2963e-02 5.6770e-01 6.3052e-01 3.8106e-02 54 1.4
1337 2455285.45588485 953938603 111.069 -50.826 -9.2963e-02 5.6770e-01 6.3052e-01 3.8106e-02 47 1.4
1338 2455285.50638051 953942966 43.810 0.722 -9.2963e-02 5.6770e-01 6.3052e-01 3.8106e-02 35 1.4
1339 2455285.63365691 953953962 342.064 -46.721 -9.2963e-02 5.6770e-01 6.3052e-01 3.8106e-02 42 1.4
1340 2455285.78249703 953966822 78.165 30.326 -9.2963e-02 5.6770e-01 6.3052e-01 3.8106e-02 37 1.4
1341 2455285.84646996 953972350 166.717 23.895 -1.1724e-01 4.7983e-01 5.2936e-01 3.8897e-02 52 0.9
1342 2455286.05485091 953990354 76.126 -71.186 -5.8944e-02 2.9333e-01 5.7306e-01 3.8834e-02 106 0.6
1343 2455286.12994036 953996841 272.941 33.026 -9.2963e-02 5.6770e-01 6.3052e-01 3.8106e-02 42 1.4
1344 2455286.19644749 954002588 333.943 -54.377 -9.2963e-02 5.6770e-01 6.3052e-01 3.8106e-02 94 1.4
1345 2455286.45788897 954025176 265.583 -7.233 -9.2963e-02 5.6770e-01 6.3052e-01 3.8106e-02 36 1.4
1346 2455286.65496167 954042203 117.467 -31.204 -1.1724e-01 4.7983e-01 5.2936e-01 3.8897e-02 46 0.9
1347 2455286.68027402 954044390 34.538 -83.079 -9.2963e-02 5.6770e-01 6.3052e-01 3.8106e-02 43 1.4
1348 2455286.69960489 954046060 60.444 -40.071 -1.1724e-01 4.7983e-01 5.2936e-01 3.8897e-02 83 0.9
1349 2455286.70877901 954046853 347.634 -31.890 -1.1724e-01 4.7983e-01 5.2936e-01 3.8897e-02 43 0.9
1350 2455286.83997087 954058188 124.098 -20.895 -9.2963e-02 5.6770e-01 6.3052e-01 3.8106e-02 38 1.4
1351 2455287.02338135 954074035 163.752 -62.606 -1.3370e-01 8.5313e-01 6.3102e-01 3.7539e-02 23 2.4
1352 2455287.08176524 954079079 277.041 -13.477 -1.3370e-01 8.5313e-01 6.3102e-01 3.7539e-02 28 2.4
1353 2455287.61673736 954125301 83.916 32.279 -1.1909e-01 7.2127e-01 6.0423e-01 3.7507e-02 31 1.8
1354 2455287.86721703 954146942 104.179 -35.902 -5.8944e-02 2.9333e-01 5.7306e-01 3.8834e-02 107 0.6
1355 2455287.88643340 954148602 105.853 32.275 -1.3370e-01 8.5313e-01 6.3102e-01 3.7539e-02 27 2.4
1356 2455288.20731313 954176326 242.669 -7.154 -1.3370e-01 8.5313e-01 6.3102e-01 3.7539e-02 25 2.4
1357 2455288.21580076 954177060 164.575 -21.435 -9.2963e-02 5.6770e-01 6.3052e-01 3.8106e-02 35 1.4
1358 2455288.42881651 954195464 335.653 -1.559 -9.2963e-02 5.6770e-01 6.3052e-01 3.8106e-02 44 1.4
1359 2455288.59563127 954209877 95.769 -49.679 -9.2963e-02 5.6770e-01 6.3052e-01 3.8106e-02 42 1.4
1360 2455288.62424942 954212350 108.890 23.990 -9.2963e-02 5.6770e-01 6.3052e-01 3.8106e-02 36 1.4
1361 2455288.68381763 954217496 165.791 -20.770 -1.1724e-01 4.7983e-01 5.2936e-01 3.8897e-02 65 0.9
1362 2455289.15006982 954257781 270.689 -28.074 -9.2963e-02 5.6770e-01 6.3052e-01 3.8106e-02 36 1.4
1363 2455291.12335500 954428272 262.101 20.130 -1.1724e-01 4.7983e-01 5.2936e-01 3.8897e-02 47 0.9
1364 2455291.46249512 954457574 343.776 -15.150 -1.1724e-01 4.7983e-01 5.2936e-01 3.8897e-02 48 0.9
1365 2455291.69763300 954477890 54.094 19.770 -9.2963e-02 5.6770e-01 6.3052e-01 3.8106e-02 37 1.4
1366 2455292.22765110 954523684 247.471 -29.202 -1.3370e-01 8.5313e-01 6.3102e-01 3.7539e-02 31 2.4
1367 2455292.24820815 954525460 234.509 21.605 -1.1724e-01 4.7983e-01 5.2936e-01 3.8897e-02 94 0.9
1368 2455292.29463392 954529471 270.203 8.486 -9.2963e-02 5.6770e-01 6.3052e-01 3.8106e-02 39 1.4
1369 2455292.49014666 954546363 359.652 -10.742 -1.3370e-01 8.5313e-01 6.3102e-01 3.7539e-02 29 2.4
1370 2455292.52128847 954549054 33.260 14.021 -9.2963e-02 5.6770e-01 6.3052e-01 3.8106e-02 36 1.4
1371 2455292.57108652 954553356 51.280 -35.735 -9.2963e-02 5.6770e-01 6.3052e-01 3.8106e-02 66 1.4
1372 2455292.68902117 954563546 96.097 -32.419 -8.8598e-02 3.3283e-01 5.3278e-01 3.9884e-02 111 0.6
1373 2455292.73629607 954567630 91.906 10.251 -1.3370e-01 8.5313e-01 6.3102e-01 3.7539e-02 30 2.4
1374 2455292.75246910 954569028 203.231 -3.709 -9.2963e-02 5.6770e-01 6.3052e-01 3.8106e-02 36 1.4
1375 2455292.81947784 954574817 127.065 12.601 -1.3370e-01 8.5313e-01 6.3102e-01 3.7539e-02 31 2.4
1376 2455292.89357225 954581219 44.004 -29.827 -1.3370e-01 8.5313e-01 6.3102e-01 3.7539e-02 31 2.4
1377 2455293.11053481 954599965 2.780 -40.146 -9.2963e-02 5.6770e-01 6.3052e-01 3.8106e-02 35 1.4
1378 2455293.11912271 954600707 292.842 17.945 -9.2963e-02 5.6770e-01 6.3052e-01 3.8106e-02 43 1.4
1379 2455293.17125132 954605211 262.566 -41.919 -9.2963e-02 5.6770e-01 6.3052e-01 3.8106e-02 41 1.4
1380 2455293.27960597 954614572 256.933 0.180 -1.3370e-01 8.5313e-01 6.3102e-01 3.7539e-02 30 2.4
1381 2455293.28418842 954614968 91.264 -78.875 -9.2963e-02 5.6770e-01 6.3052e-01 3.8106e-02 45 1.4
1382 2455293.30188583 954616497 18.778 -34.856 -1.3370e-01 8.5313e-01 6.3102e-01 3.7539e-02 28 2.4
1383 2455293.41606072 954626362 6.602 2.667 -1.1724e-01 4.7983e-01 5.2936e-01 3.8897e-02 32 0.9

LIST OF HIGH ENERGY NEUTRINO CANDIDATES FOR THE 2009-2010 DATA

1384 2455293.41668533 954626416 325.188 37.603 -9.2963e-02 5.6770e-01 6.3052e-01 3.8106e-02 61 1.4
1385 2455293.44424809 954628798 77.478 11.282 -9.2963e-02 5.6770e-01 6.3052e-01 3.8106e-02 43 1.4
1386 2455293.45458253 954629690 31.232 -9.580 -1.1724e-01 4.7983e-01 5.2936e-01 3.8897e-02 44 0.9
1387 2455293.49485037 954633170 101.306 -2.677 -1.1724e-01 4.7983e-01 5.2936e-01 3.8897e-02 37 0.9
1388 2455293.57516357 954640109 4.230 -29.401 -9.2963e-02 5.6770e-01 6.3052e-01 3.8106e-02 40 1.4
1389 2455293.60671236 954642834 255.412 -46.157 -9.2963e-02 5.6770e-01 6.3052e-01 3.8106e-02 41 1.4
1390 2455293.63365788 954645163 103.551 19.820 -1.3370e-01 8.5313e-01 6.3102e-01 3.7539e-02 31 2.4
1391 2455293.69882299 954650793 41.047 -30.233 -1.2873e-01 4.3155e-01 4.6595e-01 3.9162e-02 80 0.7
1392 2455293.75432706 954655588 292.463 -47.971 -1.1724e-01 4.7983e-01 5.2936e-01 3.8897e-02 47 0.9
1393 2455293.76192011 954656244 219.685 -27.691 -1.3370e-01 8.5313e-01 6.3102e-01 3.7539e-02 25 2.4
1394 2455293.92012988 954669914 164.733 -37.380 -9.2963e-02 5.6770e-01 6.3052e-01 3.8106e-02 41 1.4
1395 2455294.13527096 954688502 140.999 -32.182 -9.2963e-02 5.6770e-01 6.3052e-01 3.8106e-02 29 1.4
1396 2455294.38711661 954710261 316.658 8.995 -9.2963e-02 5.6770e-01 6.3052e-01 3.8106e-02 33 1.4
1397 2455295.03622396 954766344 25.019 -57.540 -9.2963e-02 5.6770e-01 6.3052e-01 3.8106e-02 41 1.4
1398 2455297.80116550 955005235 232.497 -15.102 -9.2963e-02 5.6770e-01 6.3052e-01 3.8106e-02 48 1.4
1399 2455298.00370654 955022735 31.428 -47.200 -9.2963e-02 5.6770e-01 6.3052e-01 3.8106e-02 68 1.4
1400 2455298.18076100 955038032 300.351 -16.365 -9.2963e-02 5.6770e-01 6.3052e-01 3.8106e-02 81 1.4
1401 2455299.04094349 955112352 209.653 29.951 -9.2963e-02 5.6770e-01 6.3052e-01 3.8106e-02 85 1.4
1402 2455299.89983036 955186560 231.575 -24.476 -9.2963e-02 5.6770e-01 6.3052e-01 3.8106e-02 37 1.4
1403 2455300.09199446 955203163 313.716 -61.118 -1.3370e-01 8.5313e-01 6.3102e-01 3.7539e-02 23 2.4
1404 2455300.10737209 955204491 323.104 -32.401 -1.1909e-01 7.2127e-01 6.0423e-01 3.7507e-02 30 1.8
1405 2455300.11100524 955204805 312.823 -44.083 -9.2963e-02 5.6770e-01 6.3052e-01 3.8106e-02 36 1.4
1406 2455300.13246019 955206659 225.520 -44.910 -1.1724e-01 4.7983e-01 5.2936e-01 3.8897e-02 62 0.9
1407 2455316.80675897 956647318 231.896 -23.457 -9.2963e-02 5.6770e-01 6.3052e-01 3.8106e-02 42 1.4
1408 2455316.85196370 956651224 122.597 15.279 -9.2963e-02 5.6770e-01 6.3052e-01 3.8106e-02 48 1.4
1409 2455316.94276806 956659070 254.038 26.451 -9.2963e-02 5.6770e-01 6.3052e-01 3.8106e-02 67 1.4
1410 2455317.02226984 956665939 232.771 -44.501 -1.2873e-01 4.3155e-01 4.6595e-01 3.9162e-02 50 0.7
1411 2455317.08609056 956671453 352.206 -74.182 -1.1724e-01 4.7983e-01 5.2936e-01 3.8897e-02 51 0.9
1412 2455317.11340286 956673813 1.290 -25.203 -9.2963e-02 5.6770e-01 6.3052e-01 3.8106e-02 36 1.4
1413 2455317.73010541 956727096 280.399 -79.105 -1.1724e-01 4.7983e-01 5.2936e-01 3.8897e-02 34 0.9
1414 2455317.76486827 956730099 152.380 7.549 -9.2963e-02 5.6770e-01 6.3052e-01 3.8106e-02 32 1.4
1415 2455320.27713519 956947159 33.757 -0.495 -9.2963e-02 5.6770e-01 6.3052e-01 3.8106e-02 48 1.4
1416 2455322.80545293 957165606 174.047 -55.550 -9.2963e-02 5.6770e-01 6.3052e-01 3.8106e-02 41 1.4
1417 2455322.84338650 957168883 158.385 -71.000 -9.2963e-02 5.6770e-01 6.3052e-01 3.8106e-02 59 1.4
1418 2455322.91332532 957174926 249.189 -28.790 -9.2963e-02 5.6770e-01 6.3052e-01 3.8106e-02 46 1.4
1419 2455322.91586188 957175145 181.247 5.545 -9.2963e-02 5.6770e-01 6.3052e-01 3.8106e-02 46 1.4
1420 2455344.35894043 959027827 63.679 -65.365 -1.3370e-01 8.5313e-01 6.3102e-01 3.7539e-02 28 2.4
1421 2455344.42181101 959033259 47.194 -38.129 -9.2963e-02 5.6770e-01 6.3052e-01 3.8106e-02 62 1.4
1422 2455345.19932765 959100436 259.712 -78.579 -9.2963e-02 5.6770e-01 6.3052e-01 3.8106e-02 67 1.4
1423 2455358.21125349 960224667 234.974 -37.476 -9.2963e-02 5.6770e-01 6.3052e-01 3.8106e-02 50 1.4
1424 2455358.35228472 960236852 17.868 8.193 -9.2963e-02 5.6770e-01 6.3052e-01 3.8106e-02 42 1.4
1425 2455358.37698580 960238986 120.692 -7.779 -9.2963e-02 5.6770e-01 6.3052e-01 3.8106e-02 60 1.4
1426 2455358.41296782 960242095 73.628 -61.822 -9.2963e-02 5.6770e-01 6.3052e-01 3.8106e-02 48 1.4
1427 2455358.47477294 960247435 109.298 -53.125 -9.2963e-02 5.6770e-01 6.3052e-01 3.8106e-02 42 1.4
1428 2455358.95643379 960289050 202.414 28.594 -9.2963e-02 5.6770e-01 6.3052e-01 3.8106e-02 42 1.4
1429 2455359.00592964 960293327 129.586 -41.588 -9.2963e-02 5.6770e-01 6.3052e-01 3.8106e-02 32 1.4
1430 2455359.19807954 960309929 56.894 -74.614 -9.2963e-02 5.6770e-01 6.3052e-01 3.8106e-02 80 1.4
1431 2455359.26808122 960315977 10.652 -49.793 -9.2963e-02 5.6770e-01 6.3052e-01 3.8106e-02 53 1.4
1432 2455361.23326367 960485768 274.802 -67.332 -1.3370e-01 8.5313e-01 6.3102e-01 3.7539e-02 22 2.4
1433 2455363.94296776 960719887 180.786 -46.451 -1.1724e-01 4.7983e-01 5.2936e-01 3.8897e-02 47 0.9
1434 2455364.48756816 960766940 127.780 -27.446 -1.1724e-01 4.7983e-01 5.2936e-01 3.8897e-02 47 0.9
1435 2455364.82054339 960795709 56.488 -75.717 -9.2963e-02 5.6770e-01 6.3052e-01 3.8106e-02 45 1.4

```
1436 2455364.82141812 960795785 189.450 -24.416 -9.2963e-02 5.6770e-01 6.3052e-01 3.8106e-02 47 1.4
1437 2455365.38584119 960844551 115.391 23.256 -1.3370e-01 8.5313e-01 6.3102e-01 3.7539e-02 28 2.4
1438 2455365.55524306 960859188 219.344 -31.908 -9.2963e-02 5.6770e-01 6.3052e-01 3.8106e-02 42 1.4
1439 2455365.63625495 960866187 74.309 -9.347 -9.2963e-02 5.6770e-01 6.3052e-01 3.8106e-02 53 1.4
1440 2455365.72809334 960874122 118.809 9.255 -9.2963e-02 5.6770e-01 6.3052e-01 3.8106e-02 43 1.4
1441 2455366.08878634 960905286 7.788 25.082 -1.3370e-01 8.5313e-01 6.3102e-01 3.7539e-02 24 2.4
1442 2455366.15344437 960910872 334.794 11.446 -1.3370e-01 8.5313e-01 6.3102e-01 3.7539e-02 43 2.4
1443 2455366.17056137 960912351 118.883 -43.657 -9.2963e-02 5.6770e-01 6.3052e-01 3.8106e-02 71 1.4
1444 2455366.26401931 960920426 137.585 -38.630 -9.2963e-02 5.6770e-01 6.3052e-01 3.8106e-02 33 1.4
1445 2455366.32874271 960926018 63.457 -16.829 -9.2963e-02 5.6770e-01 6.3052e-01 3.8106e-02 54 1.4
1446 2455366.67018804 960955519 221.094 -11.824 -9.2963e-02 5.6770e-01 6.3052e-01 3.8106e-02 48 1.4
1447 2455366.68754250 960957018 242.556 -36.774 -8.8598e-02 3.3283e-01 5.3278e-01 3.9884e-02 148 0.6
1448 2455366.78625159 960965547 29.983 -84.119 -8.8598e-02 3.3283e-01 5.3278e-01 3.9884e-02 29 0.6
1449 2455366.86441567 960972300 341.787 -51.758 -1.1724e-01 4.7983e-01 5.2936e-01 3.8897e-02 65 0.9
1450 2455366.94538879 960979296 334.229 -21.182 -5.8944e-02 2.9333e-01 5.7306e-01 3.8834e-02 115 0.6
1451 2455366.96332096 960980845 55.272 -46.520 -9.2963e-02 5.6770e-01 6.3052e-01 3.8106e-02 41 1.4
1452 2455367.37588935 961016491 71.926 -29.398 -9.2963e-02 5.6770e-01 6.3052e-01 3.8106e-02 48 1.4
1453 2455367.99364515 961069865 284.757 -37.977 -9.2963e-02 5.6770e-01 6.3052e-01 3.8106e-02 41 1.4
1454 2455368.26262811 961093106 38.030 -5.528 -9.2963e-02 5.6770e-01 6.3052e-01 3.8106e-02 48 1.4
1455 2455368.36648407 961102079 6.572 -49.190 -9.2963e-02 5.6770e-01 6.3052e-01 3.8106e-02 60 1.4
1456 2455368.70294318 961131149 113.119 -33.695 -9.2963e-02 5.6770e-01 6.3052e-01 3.8106e-02 44 1.4
1457 2455368.89872659 961148064 248.170 -19.935 -9.2963e-02 5.6770e-01 6.3052e-01 3.8106e-02 43 1.4
1458 2455368.99524298 961156403 291.187 -54.659 -9.2963e-02 5.6770e-01 6.3052e-01 3.8106e-02 56 1.4
1459 2455369.10473938 961165864 300.718 -28.056 -1.2873e-01 4.3155e-01 4.6595e-01 3.9162e-02 60 0.7
1460 2455369.18190296 961172531 59.854 4.334 -1.2873e-01 4.3155e-01 4.6595e-01 3.9162e-02 46 0.7
1461 2455369.98898602 961242263 207.260 -35.786 -1.2873e-01 4.3155e-01 4.6595e-01 3.9162e-02 76 0.7
1462 2455371.69582045 961389733 266.951 -9.712 -1.2873e-01 4.3155e-01 4.6595e-01 3.9162e-02 76 0.7
1463 2455371.91391682 961408577 235.455 40.263 -9.2963e-02 5.6770e-01 6.3052e-01 3.8106e-02 54 1.4
1464 2455371.91509862 961408679 203.451 11.810 -9.2963e-02 5.6770e-01 6.3052e-01 3.8106e-02 38 1.4
1465 2455372.02870194 961418494 354.329 -2.969 -9.2963e-02 5.6770e-01 6.3052e-01 3.8106e-02 61 1.4
1466 2455372.75174290 961480965 184.012 -22.011 -1.1724e-01 4.7983e-01 5.2936e-01 3.8897e-02 55 0.9
1467 2455372.83658108 961488295 176.420 -1.942 -9.2963e-02 5.6770e-01 6.3052e-01 3.8106e-02 39 1.4
# stop S6C -- start
1468 2455373.90313579 961580445 5.989 -70.629 -9.2963e-02 5.6770e-01 6.3052e-01 3.8106e-02 63 1.4
1469 2455374.49172512 961631300 123.617 4.409 -1.1724e-01 4.7983e-01 5.2936e-01 3.8897e-02 66 0.9
1470 2455375.14686582 961687904 44.359 -3.731 -1.1724e-01 4.7983e-01 5.2936e-01 3.8897e-02 86 0.9
1471 2455375.51446072 961719664 67.031 -6.509 -9.2963e-02 5.6770e-01 6.3052e-01 3.8106e-02 56 1.4
1472 2455375.76383908 961741210 175.990 -2.733 -1.1724e-01 4.7983e-01 5.2936e-01 3.8897e-02 53 0.9
1473 2455376.04986419 961765923 358.947 13.176 -9.2963e-02 5.6770e-01 6.3052e-01 3.8106e-02 40 1.4
1474 2455376.07209754 961767844 306.986 -18.809 -9.2963e-02 5.6770e-01 6.3052e-01 3.8106e-02 60 1.4
1475 2455376.60249931 961813670 358.852 -50.026 -9.2963e-02 5.6770e-01 6.3052e-01 3.8106e-02 33 1.4
1476 2455379.12838555 962031907 288.827 35.383 -1.1724e-01 4.7983e-01 5.2936e-01 3.8897e-02 41 0.9
1477 2455379.16635990 962035188 302.257 -19.197 -9.2963e-02 5.6770e-01 6.3052e-01 3.8106e-02 50 1.4
1478 2455379.45978149 962060540 108.331 9.730 -9.2963e-02 5.6770e-01 6.3052e-01 3.8106e-02 35 1.4
1479 2455379.73571086 962084380 281.294 -46.943 -9.2963e-02 5.6770e-01 6.3052e-01 3.8106e-02 51 1.4
1480 2455380.12874386 962118338 265.592 -52.702 -1.1724e-01 4.7983e-01 5.2936e-01 3.8897e-02 34 0.9
1481 2455380.21582264 962125862 41.444 2.236 -9.2963e-02 5.6770e-01 6.3052e-01 3.8106e-02 58 1.4
1482 2455381.26283730 962216324 46.290 -22.895 -9.2963e-02 5.6770e-01 6.3052e-01 3.8106e-02 38 1.4
1483 2455381.32268154 962221494 36.502 4.215 -9.2963e-02 5.6770e-01 6.3052e-01 3.8106e-02 39 1.4
1484 2455381.52888911 962239311 170.937 16.473 -8.8598e-02 3.3283e-01 5.3278e-01 3.9884e-02 121 0.6
1485 2455381.55279714 962241376 210.295 -3.444 -1.3370e-01 8.5313e-01 6.3102e-01 3.7539e-02 31 2.4
1486 2455383.34716509 962396410 41.078 -1.939 -9.2963e-02 5.6770e-01 6.3052e-01 3.8106e-02 56 1.4
```

LIST OF HIGH ENERGY NEUTRINO CANDIDATES FOR THE 2009-2010 DATA

1487 2455384.07014133 962458875 268.290 11.144 -9.2963e-02 5.6770e-01 6.3052e-01 3.8106e-02 44 1.4
1488 2455384.14838615 962465635 280.349 -0.236 -9.2963e-02 5.6770e-01 6.3052e-01 3.8106e-02 43 1.4
1489 2455384.50147035 962496142 141.142 -51.345 -9.2963e-02 5.6770e-01 6.3052e-01 3.8106e-02 39 1.4
1490 2455384.58535537 962503389 34.387 -72.951 -9.2963e-02 5.6770e-01 6.3052e-01 3.8106e-02 50 1.4
1491 2455384.58735360 962503562 82.034 -5.806 -1.1724e-01 4.7983e-01 5.2936e-01 3.8897e-02 51 0.9
1492 2455384.67206094 962510881 211.819 -59.991 -1.1724e-01 4.7983e-01 5.2936e-01 3.8897e-02 53 0.9
1493 2455384.84454509 962525783 340.199 -18.425 -1.3370e-01 8.5313e-01 6.3102e-01 3.7539e-02 27 2.4
1494 2455385.01038952 962540112 255.698 -17.156 -9.2963e-02 5.6770e-01 6.3052e-01 3.8106e-02 39 1.4
1495 2455385.04728529 962543300 226.310 -24.719 -1.1909e-01 7.2127e-01 6.0423e-01 3.7507e-02 31 1.8
1496 2455385.26635610 962562228 136.573 -39.175 -1.1909e-01 7.2127e-01 6.0423e-01 3.7507e-02 94 1.8
1497 2455385.42705640 962576112 84.338 33.769 -1.1724e-01 4.7983e-01 5.2936e-01 3.8897e-02 48 0.9
1498 2455385.84846503 962612522 350.902 -58.961 -9.2963e-02 5.6770e-01 6.3052e-01 3.8106e-02 48 1.4
1499 2455385.87065587 962614439 209.722 -9.175 -1.2873e-01 4.3155e-01 4.6595e-01 3.9162e-02 57 0.7
1500 2455386.64829265 962681627 204.374 38.929 -9.2963e-02 5.6770e-01 6.3052e-01 3.8106e-02 59 1.4
1501 2455386.68276354 962684605 219.334 24.891 -1.3370e-01 8.5313e-01 6.3102e-01 3.7539e-02 26 2.4
1502 2455387.02261932 962713969 246.653 -45.851 -9.2963e-02 5.6770e-01 6.3052e-01 3.8106e-02 34 1.4
1503 2455387.19454592 962728823 318.334 -14.532 -1.7861e+00 6.7827e+00 8.6368e-01 3.8440e-01 26 1.4
1504 2455387.22718896 962731644 217.429 -61.109 -9.2963e-02 5.6770e-01 6.3052e-01 3.8106e-02 41 1.4
1505 2455387.23182377 962732044 309.818 -56.973 -9.2963e-02 5.6770e-01 6.3052e-01 3.8106e-02 32 1.4
1506 2455387.42003623 962748306 122.565 -0.590 -1.3370e-01 8.5313e-01 6.3102e-01 3.7539e-02 31 2.4
1507 2455387.66092453 962769118 109.719 11.035 -9.2963e-02 5.6770e-01 6.3052e-01 3.8106e-02 39 1.4
1508 2455387.79549742 962780745 317.174 -8.815 -9.2963e-02 5.6770e-01 6.3052e-01 3.8106e-02 37 1.4
1509 2455388.25188769 962820178 336.079 -41.845 -1.1724e-01 4.7983e-01 5.2936e-01 3.8897e-02 46 0.9
1510 2455388.27647286 962822302 239.542 -45.034 -9.2963e-02 5.6770e-01 6.3052e-01 3.8106e-02 34 1.4
1511 2455388.45725814 962837922 75.514 -64.535 -9.2963e-02 5.6770e-01 6.3052e-01 3.8106e-02 42 1.4
1512 2455388.49139560 962840871 77.617 -26.651 -1.2873e-01 4.3155e-01 4.6595e-01 3.9162e-02 49 0.7
1513 2455388.64444318 962854094 147.968 14.852 -9.2963e-02 5.6770e-01 6.3052e-01 3.8106e-02 82 1.4
1514 2455388.76476178 962864490 185.579 8.436 -9.2963e-02 5.6770e-01 6.3052e-01 3.8106e-02 41 1.4
1515 2455388.76672677 962864660 94.380 -61.145 -9.2963e-02 5.6770e-01 6.3052e-01 3.8106e-02 53 1.4
1516 2455388.85713631 962872471 208.389 -14.968 -9.2963e-02 5.6770e-01 6.3052e-01 3.8106e-02 40 1.4
1517 2455388.88175389 962874598 305.962 -51.989 -1.1724e-01 4.7983e-01 5.2936e-01 3.8897e-02 38 0.9
1518 2455389.18574832 962900863 286.138 -18.429 -1.1724e-01 4.7983e-01 5.2936e-01 3.8897e-02 48 0.9
1519 2455389.49712053 962927766 130.908 11.714 -9.2963e-02 5.6770e-01 6.3052e-01 3.8106e-02 45 1.4
1520 2455389.52152963 962929875 160.448 -42.283 -1.1724e-01 4.7983e-01 5.2936e-01 3.8897e-02 52 0.9
1521 2455389.53943972 962931422 165.847 29.750 -9.2963e-02 5.6770e-01 6.3052e-01 3.8106e-02 69 1.4
1522 2455389.63683500 962939837 179.316 -20.342 -1.3370e-01 8.5313e-01 6.3102e-01 3.7539e-02 31 2.4
1523 2455389.87726054 962960610 336.881 -38.636 -9.2963e-02 5.6770e-01 6.3052e-01 3.8106e-02 32 1.4
1524 2455390.02402431 962973290 151.515 -62.033 -9.2963e-02 5.6770e-01 6.3052e-01 3.8106e-02 52 1.4
1525 2455390.54528381 963018327 27.766 -41.501 -9.2963e-02 5.6770e-01 6.3052e-01 3.8106e-02 41 1.4
1526 2455390.68555944 963030447 222.228 8.629 -1.3370e-01 8.5313e-01 6.3102e-01 3.7539e-02 28 2.4
1527 2455390.69935538 963031639 254.640 -10.566 -1.3370e-01 8.5313e-01 6.3102e-01 3.7539e-02 29 2.4
1528 2455390.93820683 963052276 210.622 3.885 -9.2963e-02 5.6770e-01 6.3052e-01 3.8106e-02 41 1.4
1529 2455391.26882551 963080841 332.910 -13.269 -9.2963e-02 5.6770e-01 6.3052e-01 3.8106e-02 32 1.4
1530 2455391.29238911 963082877 150.464 -48.353 -1.1724e-01 4.7983e-01 5.2936e-01 3.8897e-02 48 0.9
1531 2455391.29684010 963083261 33.686 -80.121 -9.2963e-02 5.6770e-01 6.3052e-01 3.8106e-02 41 1.4
1532 2455391.44676429 963096215 346.265 -23.497 -9.2963e-02 5.6770e-01 6.3052e-01 3.8106e-02 62 1.4
1533 2455391.51726329 963102306 101.889 -71.360 -9.2963e-02 5.6770e-01 6.3052e-01 3.8106e-02 54 1.4
1534 2455391.98485833 963142706 312.346 7.081 -9.2963e-02 5.6770e-01 6.3052e-01 3.8106e-02 85 1.4
1535 2455392.09837487 963152514 313.628 -65.214 -1.1724e-01 4.7983e-01 5.2936e-01 3.8897e-02 48 0.9
1536 2455392.11320869 963153796 105.445 -41.411 -9.2963e-02 5.6770e-01 6.3052e-01 3.8106e-02 38 1.4
1537 2455392.19615406 963160962 7.207 46.000 -1.3370e-01 8.5313e-01 6.3102e-01 3.7539e-02 19 2.4
1538 2455392.48761505 963186144 93.162 -11.278 -9.2963e-02 5.6770e-01 6.3052e-01 3.8106e-02 88 1.4

1539 2455392.51090710 963188157 96.435 36.323 -9.2963e-02 5.6770e-01 6.3052e-01 3.8106e-02 44 1.4
1540 2455392.68417985 963203128 239.970 -0.784 -1.3370e-01 8.5313e-01 6.3102e-01 3.7539e-02 29 2.4
1541 2455396.07159846 963495801 296.094 17.169 -9.2963e-02 5.6770e-01 6.3052e-01 3.8106e-02 40 1.4
1542 2455396.29105526 963514762 57.010 6.188 -9.2963e-02 5.6770e-01 6.3052e-01 3.8106e-02 54 1.4
1543 2455396.42950057 963526723 133.517 8.850 -1.3370e-01 8.5313e-01 6.3102e-01 3.7539e-02 24 2.4
1544 2455396.44622235 963528168 59.009 -3.628 -5.8944e-02 2.9333e-01 5.7306e-01 3.8834e-02 101 0.6
1545 2455396.53987868 963536260 75.075 3.888 -1.3370e-01 8.5313e-01 6.3102e-01 3.7539e-02 25 2.4
1546 2455396.59061666 963540644 112.253 2.542 -1.3370e-01 8.5313e-01 6.3102e-01 3.7539e-02 38 2.4
1547 2455396.69411137 963549586 256.047 20.499 -1.3370e-01 8.5313e-01 6.3102e-01 3.7539e-02 23 2.4
1548 2455397.05813910 963581038 78.141 -60.199 -1.1724e-01 4.7983e-01 5.2936e-01 3.8897e-02 38 0.9
1549 2455397.06047488 963581240 215.015 -42.034 -1.3370e-01 8.5313e-01 6.3102e-01 3.7539e-02 23 2.4
1550 2455397.19554695 963592910 329.391 -16.566 -1.1724e-01 4.7983e-01 5.2936e-01 3.8897e-02 47 0.9
1551 2455397.64009648 963631319 48.756 -64.158 -9.2963e-02 5.6770e-01 6.3052e-01 3.8106e-02 76 1.4
1552 2455397.69566175 963636120 54.397 -41.147 -9.2963e-02 5.6770e-01 6.3052e-01 3.8106e-02 33 1.4
1553 2455397.95582273 963658598 19.932 -21.140 -1.3370e-01 8.5313e-01 6.3102e-01 3.7539e-02 30 2.4
1554 2455398.07279179 963668704 30.381 15.265 -1.3370e-01 8.5313e-01 6.3102e-01 3.7539e-02 23 2.4
1555 2455398.16670441 963676818 47.179 -59.568 -1.3370e-01 8.5313e-01 6.3102e-01 3.7539e-02 28 2.4
1556 2455398.20316353 963679968 28.490 -4.236 -9.2963e-02 5.6770e-01 6.3052e-01 3.8106e-02 41 1.4
1557 2455398.36393923 963693859 54.360 4.932 -1.1724e-01 4.7983e-01 5.2936e-01 3.8897e-02 48 0.9
1558 2455398.44059353 963700482 77.734 -21.196 -9.2963e-02 5.6770e-01 6.3052e-01 3.8106e-02 44 1.4
1559 2455398.46876191 963702916 63.192 10.778 -1.1724e-01 4.7983e-01 5.2936e-01 3.8897e-02 52 0.9
1560 2455398.54297531 963709328 145.348 -51.806 -9.2963e-02 5.6770e-01 6.3052e-01 3.8106e-02 56 1.4
1561 2455398.73030620 963725513 263.267 0.649 -1.3370e-01 8.5313e-01 6.3102e-01 3.7539e-02 25 2.4
1562 2455398.82056218 963733311 65.161 -49.828 -9.2963e-02 5.6770e-01 6.3052e-01 3.8106e-02 41 1.4
1563 2455398.90865081 963740922 165.275 -61.816 -1.3370e-01 8.5313e-01 6.3102e-01 3.7539e-02 29 2.4
1564 2455399.07744975 963755506 326.980 12.709 -9.2963e-02 5.6770e-01 6.3052e-01 3.8106e-02 49 1.4
1565 2455399.17494927 963763930 277.281 -57.701 -9.2963e-02 5.6770e-01 6.3052e-01 3.8106e-02 35 1.4
1566 2455399.75873374 963814369 157.299 -40.395 -9.2963e-02 5.6770e-01 6.3052e-01 3.8106e-02 33 1.4
1567 2455405.34960546 964297420 50.755 -62.232 -9.2963e-02 5.6770e-01 6.3052e-01 3.8106e-02 92 1.4
1568 2455405.53609605 964313533 97.317 -35.782 -9.2963e-02 5.6770e-01 6.3052e-01 3.8106e-02 37 1.4
1569 2455405.98854355 964352625 328.322 -77.202 -9.2963e-02 5.6770e-01 6.3052e-01 3.8106e-02 42 1.4
1570 2455406.26117066 964376180 89.769 -36.885 -9.2963e-02 5.6770e-01 6.3052e-01 3.8106e-02 34 1.4
1571 2455406.63367816 964408364 187.842 17.240 -9.2963e-02 5.6770e-01 6.3052e-01 3.8106e-02 44 1.4
1572 2455406.79152398 964422002 54.867 -61.780 -9.2963e-02 5.6770e-01 6.3052e-01 3.8106e-02 48 1.4
1573 2455407.00565888 964440503 286.714 -13.592 -1.1724e-01 4.7983e-01 5.2936e-01 3.8897e-02 55 0.9
1574 2455407.11088480 964449595 285.558 -53.702 -9.2963e-02 5.6770e-01 6.3052e-01 3.8106e-02 44 1.4
1575 2455407.25114877 964461714 354.543 -33.245 -9.2963e-02 5.6770e-01 6.3052e-01 3.8106e-02 47 1.4
1576 2455407.40058597 964474625 140.357 -29.592 -9.2963e-02 5.6770e-01 6.3052e-01 3.8106e-02 35 1.4
1577 2455407.58625397 964490667 138.391 -19.949 -9.2963e-02 5.6770e-01 6.3052e-01 3.8106e-02 64 1.4
1578 2455407.79421643 964508635 171.837 7.523 -9.2963e-02 5.6770e-01 6.3052e-01 3.8106e-02 44 1.4
1579 2455407.89173694 964517061 235.571 27.482 -1.3370e-01 8.5313e-01 6.3102e-01 3.7539e-02 24 2.4
1580 2455408.60103370 964578344 165.047 26.423 -9.2963e-02 5.6770e-01 6.3052e-01 3.8106e-02 34 1.4
1581 2455409.54893676 964660243 122.521 -8.117 -9.2963e-02 5.6770e-01 6.3052e-01 3.8106e-02 53 1.4
1582 2455409.71998793 964675021 213.815 -14.903 -9.2963e-02 5.6770e-01 6.3052e-01 3.8106e-02 50 1.4
1583 2455410.34271102 964728825 118.803 -21.503 -9.2963e-02 5.6770e-01 6.3052e-01 3.8106e-02 36 1.4
1584 2455410.65032080 964755402 189.118 27.898 -9.2963e-02 5.6770e-01 6.3052e-01 3.8106e-02 77 1.4
1585 2455410.72016895 964761437 186.235 42.879 -9.2963e-02 5.6770e-01 6.3052e-01 3.8106e-02 47 1.4
1586 2455410.95517517 964781742 278.609 20.398 -9.2963e-02 5.6770e-01 6.3052e-01 3.8106e-02 99 1.4
1587 2455410.98121297 964783991 278.015 -0.243 -9.2963e-02 5.6770e-01 6.3052e-01 3.8106e-02 49 1.4
1588 2455411.20149212 964803023 328.739 22.200 -9.2963e-02 5.6770e-01 6.3052e-01 3.8106e-02 47 1.4
1589 2455411.29430793 964811043 131.155 -41.499 -9.2963e-02 5.6770e-01 6.3052e-01 3.8106e-02 58 1.4
1590 2455411.40650879 964820737 240.098 -49.745 -9.2963e-02 5.6770e-01 6.3052e-01 3.8106e-02 50 1.4

LIST OF HIGH ENERGY NEUTRINO CANDIDATES FOR THE 2009-2010 DATA

1591 2455411.44335445 964823920 150.859 21.608 -9.2963e-02 5.6770e-01 6.3052e-01 3.8106e-02 39 1.4
1592 2455411.68580267 964844868 138.110 -3.563 -1.1724e-01 4.7983e-01 5.2936e-01 3.8897e-02 35 0.9
1593 2455411.72122069 964847928 201.585 43.448 -1.1724e-01 4.7983e-01 5.2936e-01 3.8897e-02 40 0.9
1594 2455411.82257757 964856685 1.722 -59.887 -1.1724e-01 4.7983e-01 5.2936e-01 3.8897e-02 52 0.9
1595 2455411.89406440 964862862 54.756 -49.620 -1.1724e-01 4.7983e-01 5.2936e-01 3.8897e-02 74 0.9
1596 2455411.94043781 964866868 182.167 -30.453 -9.2963e-02 5.6770e-01 6.3052e-01 3.8106e-02 57 1.4
1597 2455412.05739074 964876973 340.269 24.848 -9.2963e-02 5.6770e-01 6.3052e-01 3.8106e-02 44 1.4
1598 2455412.06133395 964877314 231.903 -26.820 -9.2963e-02 5.6770e-01 6.3052e-01 3.8106e-02 40 1.4
1599 2455412.06920058 964877993 25.985 26.147 -9.2963e-02 5.6770e-01 6.3052e-01 3.8106e-02 42 1.4
1600 2455412.09714234 964880408 82.909 -74.640 -9.2963e-02 5.6770e-01 6.3052e-01 3.8106e-02 47 1.4
1601 2455412.23159644 964892024 81.573 -54.420 -1.2873e-01 4.3155e-01 4.6595e-01 3.9162e-02 47 0.7
1602 2455412.31984813 964899649 355.591 5.232 -9.2963e-02 5.6770e-01 6.3052e-01 3.8106e-02 38 1.4
1603 2455412.45190219 964911059 219.013 -20.328 -9.2963e-02 5.6770e-01 6.3052e-01 3.8106e-02 77 1.4
1604 2455412.47150470 964912753 5.474 -43.144 -9.2963e-02 5.6770e-01 6.3052e-01 3.8106e-02 40 1.4
1605 2455412.67484742 964930321 121.704 5.153 -9.2963e-02 5.6770e-01 6.3052e-01 3.8106e-02 49 1.4
1606 2455413.24667944 964979728 126.881 -30.190 -1.3370e-01 8.5313e-01 6.3102e-01 3.7539e-02 23 2.4
1607 2455413.26990541 964981734 100.996 7.694 -9.2963e-02 5.6770e-01 6.3052e-01 3.8106e-02 48 1.4
1608 2455413.62293001 965012236 202.157 9.644 -9.2963e-02 5.6770e-01 6.3052e-01 3.8106e-02 45 1.4
1609 2455413.62309067 965012250 197.447 -53.627 -9.2963e-02 5.6770e-01 6.3052e-01 3.8106e-02 46 1.4
1610 2455413.65482573 965014991 65.591 -47.281 -9.2963e-02 5.6770e-01 6.3052e-01 3.8106e-02 37 1.4
1611 2455413.84677035 965031575 238.036 -8.435 -9.2963e-02 5.6770e-01 6.3052e-01 3.8106e-02 55 1.4
1612 2455413.86081947 965032789 304.777 14.607 -9.2963e-02 5.6770e-01 6.3052e-01 3.8106e-02 45 1.4
1613 2455413.88250034 965034663 2.283 -62.468 -9.2963e-02 5.6770e-01 6.3052e-01 3.8106e-02 43 1.4
1614 2455414.06564428 965050486 34.480 -19.110 -9.2963e-02 5.6770e-01 6.3052e-01 3.8106e-02 54 1.4
1615 2455414.19301958 965061491 51.291 13.925 -1.3370e-01 8.5313e-01 6.3102e-01 3.7539e-02 26 2.4
1616 2455414.20250958 965062311 124.313 -3.286 -9.2963e-02 5.6770e-01 6.3052e-01 3.8106e-02 51 1.4
1617 2455414.81650328 965115360 189.228 5.082 -9.2963e-02 5.6770e-01 6.3052e-01 3.8106e-02 45 1.4
1618 2455414.88050599 965120890 313.700 -33.401 -9.2963e-02 5.6770e-01 6.3052e-01 3.8106e-02 38 1.4
1619 2455415.32265675 965159092 127.642 5.416 -1.3370e-01 8.5313e-01 6.3102e-01 3.7539e-02 28 2.4
1620 2455415.79980090 965200317 230.472 -23.253 -9.2963e-02 5.6770e-01 6.3052e-01 3.8106e-02 55 1.4
1621 2455416.24052251 965238396 32.097 9.841 -9.2963e-02 5.6770e-01 6.3052e-01 3.8106e-02 45 1.4
1622 2455416.39728093 965251940 93.417 -2.898 -9.2963e-02 5.6770e-01 6.3052e-01 3.8106e-02 64 1.4
1623 2455416.41189513 965253202 39.306 -51.194 -9.2963e-02 5.6770e-01 6.3052e-01 3.8106e-02 58 1.4
1624 2455416.85135381 965291171 228.601 27.528 -9.2963e-02 5.6770e-01 6.3052e-01 3.8106e-02 31 1.4
1625 2455416.99133890 965303266 325.211 18.155 -9.2963e-02 5.6770e-01 6.3052e-01 3.8106e-02 48 1.4
1626 2455418.11804856 965400614 51.357 -38.619 -9.2963e-02 5.6770e-01 6.3052e-01 3.8106e-02 65 1.4
1627 2455419.17279374 965491744 334.367 -19.407 -9.2963e-02 5.6770e-01 6.3052e-01 3.8106e-02 47 1.4
1628 2455419.66193775 965534006 274.301 -2.131 -9.2963e-02 5.6770e-01 6.3052e-01 3.8106e-02 40 1.4
1629 2455420.58188819 965613490 134.184 -9.965 -9.2963e-02 5.6770e-01 6.3052e-01 3.8106e-02 50 1.4
1630 2455420.64478845 965618924 140.585 25.252 -9.2963e-02 5.6770e-01 6.3052e-01 3.8106e-02 37 1.4
1631 2455421.01842883 965651207 52.057 -20.234 -1.3370e-01 8.5313e-01 6.3102e-01 3.7539e-02 24 2.4
1632 2455421.13481522 965661263 47.267 -17.304 -9.2963e-02 5.6770e-01 6.3052e-01 3.8106e-02 41 1.4
1633 2455421.17550090 965664778 341.923 -30.664 -1.3370e-01 8.5313e-01 6.3102e-01 3.7539e-02 28 2.4
1634 2455421.18388006 965665502 356.147 -54.737 -9.2963e-02 5.6770e-01 6.3052e-01 3.8106e-02 44 1.4
1635 2455421.20734816 965667529 193.559 -59.953 -9.2963e-02 5.6770e-01 6.3052e-01 3.8106e-02 49 1.4
1636 2455421.26966946 965672914 33.709 -8.258 -1.1724e-01 4.7983e-01 5.2936e-01 3.8897e-02 55 0.9
1637 2455421.31489924 965676822 145.228 -6.521 -9.2963e-02 5.6770e-01 6.3052e-01 3.8106e-02 32 1.4
1638 2455421.50370376 965693135 61.422 -22.894 -9.2963e-02 5.6770e-01 6.3052e-01 3.8106e-02 71 1.4
1639 2455421.64049105 965704953 162.548 38.503 -9.2963e-02 5.6770e-01 6.3052e-01 3.8106e-02 33 1.4
1640 2455421.64943180 965705725 305.359 -28.389 -9.2963e-02 5.6770e-01 6.3052e-01 3.8106e-02 40 1.4
1641 2455421.70295410 965710350 121.166 -24.871 -9.2963e-02 5.6770e-01 6.3052e-01 3.8106e-02 34 1.4
1642 2455421.97428930 965733793 290.181 -41.123 -9.2963e-02 5.6770e-01 6.3052e-01 3.8106e-02 44 1.4

```
1643 2455422.01567384 965737369 285.616 -20.758 -9.2963e-02 5.6770e-01 6.3052e-01 3.8106e-02 65 1.4
1644 2455422.10703200 965745262 325.751 -38.644 -1.3370e-01 8.5313e-01 6.3102e-01 3.7539e-02 28 2.4
1645 2455422.19272734 965752666 322.679 -41.813 -1.3370e-01 8.5313e-01 6.3102e-01 3.7539e-02 38 2.4
1646 2455422.20932694 965754100 63.902 17.355 -1.3370e-01 8.5313e-01 6.3102e-01 3.7539e-02 31 2.4
1647 2455422.34728654 965766020 61.990 -29.209 -1.3370e-01 8.5313e-01 6.3102e-01 3.7539e-02 26 2.4
1648 2455422.37016411 965767997 168.206 -14.173 -1.1724e-01 4.7983e-01 5.2936e-01 3.8897e-02 46 0.9
1649 2455422.54721552 965783294 0.807 -50.504 -1.3370e-01 8.5313e-01 6.3102e-01 3.7539e-02 23 2.4
1650 2455422.70648059 965797054 300.507 7.048 -9.2963e-02 5.6770e-01 6.3052e-01 3.8106e-02 49 1.4
1651 2455422.93377367 965816693 300.421 17.063 -9.2963e-02 5.6770e-01 6.3052e-01 3.8106e-02 35 1.4
1652 2455423.07352596 965828767 320.854 -18.990 -9.2963e-02 5.6770e-01 6.3052e-01 3.8106e-02 34 1.4
1653 2455423.09972906 965831031 294.205 15.139 -1.2873e-01 4.3155e-01 4.6595e-01 3.9162e-02 59 0.7
1654 2455423.10299524 965831313 50.049 -47.905 -1.2873e-01 4.3155e-01 4.6595e-01 3.9162e-02 60 0.7
1655 2455423.61643567 965875675 309.142 -28.397 -9.2963e-02 5.6770e-01 6.3052e-01 3.8106e-02 50 1.4
1656 2455423.80698012 965892138 350.920 -31.017 -9.2963e-02 5.6770e-01 6.3052e-01 3.8106e-02 51 1.4
1657 2455423.83849925 965894861 199.005 -61.231 -1.2873e-01 4.3155e-01 4.6595e-01 3.9162e-02 57 0.7
1658 2455423.84040886 965895026 190.940 -61.557 -9.2963e-02 5.6770e-01 6.3052e-01 3.8106e-02 37 1.4
1659 2455423.87209296 965897763 196.226 -0.480 -9.2963e-02 5.6770e-01 6.3052e-01 3.8106e-02 25 1.4
1660 2455424.21539309 965927424 73.948 -35.590 -1.1724e-01 4.7983e-01 5.2936e-01 3.8897e-02 39 0.9
1661 2455424.23310282 965928955 164.980 -22.524 -9.2963e-02 5.6770e-01 6.3052e-01 3.8106e-02 33 1.4
1662 2455424.52232128 965953943 272.523 -67.829 -9.2963e-02 5.6770e-01 6.3052e-01 3.8106e-02 33 1.4
1663 2455425.06198192 966000570 23.139 -42.407 -1.1909e-01 7.2127e-01 6.0423e-01 3.7507e-02 31 1.8
1664 2455425.56386018 966043932 177.165 -45.668 -1.2873e-01 4.3155e-01 4.6595e-01 3.9162e-02 92 0.7
1665 2455425.95365897 966077611 10.359 24.096 -9.2963e-02 5.6770e-01 6.3052e-01 3.8106e-02 45 1.4
1666 2455426.00529824 966082072 260.094 9.219 -9.2963e-02 5.6770e-01 6.3052e-01 3.8106e-02 32 1.4
1667 2455426.02304114 966083605 267.758 -16.403 -1.3370e-01 8.5313e-01 6.3102e-01 3.7539e-02 30 2.4
1668 2455426.02816909 966084048 2.878 12.071 -1.3370e-01 8.5313e-01 6.3102e-01 3.7539e-02 31 2.4
1669 2455426.18466108 966097569 300.647 -74.729 -1.3370e-01 8.5313e-01 6.3102e-01 3.7539e-02 24 2.4
1670 2455426.27978837 966105788 104.893 -46.328 -9.2963e-02 5.6770e-01 6.3052e-01 3.8106e-02 33 1.4
1671 2455426.68160543 966140505 284.851 -81.391 -9.2963e-02 5.6770e-01 6.3052e-01 3.8106e-02 60 1.4
1672 2455427.03499794 966171038 316.091 22.544 -9.2963e-02 5.6770e-01 6.3052e-01 3.8106e-02 39 1.4
1673 2455427.07843445 966174791 62.896 -45.680 -9.2963e-02 5.6770e-01 6.3052e-01 3.8106e-02 41 1.4
1674 2455427.21933358 966186965 85.067 -51.409 -9.2963e-02 5.6770e-01 6.3052e-01 3.8106e-02 44 1.4
1675 2455427.40387959 966202910 158.621 -34.187 -9.2963e-02 5.6770e-01 6.3052e-01 3.8106e-02 53 1.4
1676 2455427.44496192 966206459 298.221 -50.612 -1.3370e-01 8.5313e-01 6.3102e-01 3.7539e-02 29 2.4
1677 2455427.65459995 966224572 293.625 -51.197 -1.1724e-01 4.7983e-01 5.2936e-01 3.8897e-02 36 0.9
1678 2455427.66846274 966225770 30.561 -59.887 -9.2963e-02 5.6770e-01 6.3052e-01 3.8106e-02 32 1.4
1679 2455428.08346722 966261626 341.423 -26.854 -9.2963e-02 5.6770e-01 6.3052e-01 3.8106e-02 51 1.4
1680 2455428.11037461 966263951 109.837 -10.540 -9.2963e-02 5.6770e-01 6.3052e-01 3.8106e-02 34 1.4
1681 2455428.21922358 966273355 332.675 5.883 -1.3370e-01 8.5313e-01 6.3102e-01 3.7539e-02 27 2.4
1682 2455428.23824451 966274999 122.614 -42.221 -9.2963e-02 5.6770e-01 6.3052e-01 3.8106e-02 34 1.4
1683 2455441.45374207 967416818 94.562 -25.760 -1.1724e-01 4.7983e-01 5.2936e-01 3.8897e-02 41 0.9
1684 2455441.48969199 967419924 67.477 -35.895 -9.2963e-02 5.6770e-01 6.3052e-01 3.8106e-02 58 1.4
1685 2455441.56147618 967426126 104.308 -48.963 -1.3370e-01 8.5313e-01 6.3102e-01 3.7539e-02 27 2.4
1686 2455441.56792120 967426683 158.748 -35.408 -9.2963e-02 5.6770e-01 6.3052e-01 3.8106e-02 54 1.4
1687 2455442.03270271 967466840 295.604 -58.742 -9.2963e-02 5.6770e-01 6.3052e-01 3.8106e-02 50 1.4
1688 2455442.21609640 967482685 9.822 12.791 -1.1724e-01 4.7983e-01 5.2936e-01 3.8897e-02 46 0.9
1689 2455442.31723545 967491424 192.412 -78.016 -1.1909e-01 7.2127e-01 6.0423e-01 3.7507e-02 29 1.8
1690 2455442.36213883 967495303 155.833 17.577 -9.2963e-02 5.6770e-01 6.3052e-01 3.8106e-02 58 1.4
1691 2455442.70921974 967525291 27.780 -81.366 -9.2963e-02 5.6770e-01 6.3052e-01 3.8106e-02 43 1.4
1692 2455442.71087246 967525434 327.359 -45.899 -9.2963e-02 5.6770e-01 6.3052e-01 3.8106e-02 31 1.4
1693 2455442.87448866 967539570 294.521 40.132 -9.2963e-02 5.6770e-01 6.3052e-01 3.8106e-02 64 1.4
1694 2455442.89214633 967541096 230.263 -66.383 -1.1724e-01 4.7983e-01 5.2936e-01 3.8897e-02 54 0.9
```

LIST OF HIGH ENERGY NEUTRINO CANDIDATES FOR THE 2009-2010 DATA

1695 2455443.02464581 967552544 1.238 44.416 -9.2963e-02 5.6770e-01 6.3052e-01 3.8106e-02 35 1.4
1696 2455443.20190358 967567859 191.607 -49.942 -1.1724e-01 4.7983e-01 5.2936e-01 3.8897e-02 61 0.9
1697 2455443.20944823 967568511 28.412 -57.455 -9.2963e-02 5.6770e-01 6.3052e-01 3.8106e-02 52 1.4
1698 2455443.28496185 967575035 22.892 -15.778 -9.2963e-02 5.6770e-01 6.3052e-01 3.8106e-02 36 1.4
1699 2455443.28555079 967575086 89.108 13.049 -1.3370e-01 8.5313e-01 6.3102e-01 3.7539e-02 21 2.4
1700 2455443.78091011 967617885 99.606 -55.991 -1.3370e-01 8.5313e-01 6.3102e-01 3.7539e-02 29 2.4
1701 2455444.11103544 967646408 28.467 8.555 -9.2963e-02 5.6770e-01 6.3052e-01 3.8106e-02 42 1.4
1702 2455444.81675966 967707383 338.543 2.164 -9.2963e-02 5.6770e-01 6.3052e-01 3.8106e-02 34 1.4
1703 2455444.89938478 967714521 17.411 9.451 -1.3370e-01 8.5313e-01 6.3102e-01 3.7539e-02 30 2.4
1704 2455444.98906271 967722270 7.528 -20.007 -9.2963e-02 5.6770e-01 6.3052e-01 3.8106e-02 36 1.4
1705 2455445.24470879 967744357 86.630 33.205 -9.2963e-02 5.6770e-01 6.3052e-01 3.8106e-02 44 1.4
1706 2455445.26592067 967746190 22.609 -71.529 -9.2963e-02 5.6770e-01 6.3052e-01 3.8106e-02 52 1.4
1707 2455445.28335692 967747697 160.296 -69.197 -9.2963e-02 5.6770e-01 6.3052e-01 3.8106e-02 53 1.4
1708 2455445.85291538 967796906 358.180 -31.748 -1.3370e-01 8.5313e-01 6.3102e-01 3.7539e-02 25 2.4
1709 2455445.87460896 967798781 230.756 6.897 -9.2963e-02 5.6770e-01 6.3052e-01 3.8106e-02 44 1.4
1710 2455446.05589751 967814444 314.241 -32.061 -9.2963e-02 5.6770e-01 6.3052e-01 3.8106e-02 40 1.4
1711 2455446.46786945 967850038 117.580 -46.652 -1.1724e-01 4.7983e-01 5.2936e-01 3.8897e-02 70 0.9
1712 2455446.54708421 967856883 279.306 -11.358 -9.2963e-02 5.6770e-01 6.3052e-01 3.8106e-02 35 1.4
1713 2455446.75667797 967874991 140.782 -63.664 -1.1909e-01 7.2127e-01 6.0423e-01 3.7507e-02 30 1.8
1714 2455446.80403547 967879083 1.952 -23.709 -9.2963e-02 5.6770e-01 6.3052e-01 3.8106e-02 63 1.4
1715 2455446.94695755 967891432 59.918 -8.642 -9.2963e-02 5.6770e-01 6.3052e-01 3.8106e-02 49 1.4
1716 2455446.99029482 967895176 59.824 14.294 -9.2963e-02 5.6770e-01 6.3052e-01 3.8106e-02 68 1.4
1717 2455447.03362027 967898919 308.926 -22.196 -9.2963e-02 5.6770e-01 6.3052e-01 3.8106e-02 105 1.4
1718 2455447.26917945 967919272 52.097 -41.938 -9.2963e-02 5.6770e-01 6.3052e-01 3.8106e-02 40 1.4
1719 2455447.27743756 967919985 134.272 2.371 -9.2963e-02 5.6770e-01 6.3052e-01 3.8106e-02 54 1.4
1720 2455447.83084432 967967799 350.188 23.967 -9.2963e-02 5.6770e-01 6.3052e-01 3.8106e-02 51 1.4
1721 2455447.97088409 967979899 61.608 -35.476 -9.2963e-02 5.6770e-01 6.3052e-01 3.8106e-02 40 1.4
1722 2455448.08618777 967989861 49.698 -3.116 -9.2963e-02 5.6770e-01 6.3052e-01 3.8106e-02 35 1.4
1723 2455448.31741339 968009839 179.983 -35.432 -9.2963e-02 5.6770e-01 6.3052e-01 3.8106e-02 30 1.4
1724 2455448.39402879 968016459 200.622 12.571 -9.2963e-02 5.6770e-01 6.3052e-01 3.8106e-02 67 1.4
1725 2455448.42772426 968019370 217.913 2.598 -1.3370e-01 8.5313e-01 6.3102e-01 3.7539e-02 29 2.4
1726 2455448.68787973 968041847 282.067 -29.940 -9.2963e-02 5.6770e-01 6.3052e-01 3.8106e-02 36 1.4
1727 2455448.77399536 968049288 24.896 -48.870 -9.2963e-02 5.6770e-01 6.3052e-01 3.8106e-02 49 1.4
1728 2455448.79541924 968051139 219.211 -0.092 -9.2963e-02 5.6770e-01 6.3052e-01 3.8106e-02 20 1.4
1729 2455448.83752018 968054776 193.173 -35.721 -1.1909e-01 7.2127e-01 6.0423e-01 3.7507e-02 30 1.8
1730 2455448.87335538 968057872 43.387 -84.199 -1.1724e-01 4.7983e-01 5.2936e-01 3.8897e-02 42 0.9
1731 2455449.00031679 968068842 44.362 2.314 -9.2963e-02 5.6770e-01 6.3052e-01 3.8106e-02 39 1.4
1732 2455449.38702265 968102253 98.425 -39.494 -9.2963e-02 5.6770e-01 6.3052e-01 3.8106e-02 46 1.4
1733 2455449.54458668 968115867 117.406 -59.687 -9.2963e-02 5.6770e-01 6.3052e-01 3.8106e-02 34 1.4
1734 2455449.78084109 968136279 252.108 43.031 -9.2963e-02 5.6770e-01 6.3052e-01 3.8106e-02 32 1.4
1735 2455449.78381254 968136536 280.903 -39.117 -1.2873e-01 4.3155e-01 4.6595e-01 3.9162e-02 37 0.7
1736 2455449.84177884 968141544 262.672 -48.550 -9.2963e-02 5.6770e-01 6.3052e-01 3.8106e-02 40 1.4
1737 2455449.98687581 968154081 285.448 -51.109 -9.2963e-02 5.6770e-01 6.3052e-01 3.8106e-02 33 1.4
1738 2455450.08299150 968162385 33.874 6.552 -9.2963e-02 5.6770e-01 6.3052e-01 3.8106e-02 39 1.4
1739 2455450.08345315 968162425 313.492 -21.837 -1.1909e-01 7.2127e-01 6.0423e-01 3.7507e-02 29 1.8
1740 2455450.13989163 968167301 258.531 -67.610 -1.1909e-01 7.2127e-01 6.0423e-01 3.7507e-02 45 1.8
1741 2455450.29677551 968180856 285.437 -87.541 -1.3370e-01 8.5313e-01 6.3102e-01 3.7539e-02 21 2.4
1742 2455450.83399792 968227272 238.619 23.875 -9.2963e-02 5.6770e-01 6.3052e-01 3.8106e-02 94 1.4
1743 2455450.86255113 968229739 266.493 -69.117 -1.1724e-01 4.7983e-01 5.2936e-01 3.8897e-02 75 0.9
1744 2455450.87407838 968230735 67.154 -33.516 -1.1724e-01 4.7983e-01 5.2936e-01 3.8897e-02 43 0.9
1745 2455451.07600479 968248181 339.338 18.516 -9.2963e-02 5.6770e-01 6.3052e-01 3.8106e-02 79 1.4
1746 2455451.23133647 968261602 53.617 -31.862 -1.1909e-01 7.2127e-01 6.0423e-01 3.7507e-02 25 1.8

1747 2455451.28454823 968266199 67.115 33.041 -9.2963e-02 5.6770e-01 6.3052e-01 3.8106e-02 48 1.4
1748 2455451.50674469 968285397 115.947 -2.447 -9.2963e-02 5.6770e-01 6.3052e-01 3.8106e-02 48 1.4
1749 2455451.78208613 968309187 184.436 -52.226 -1.1724e-01 4.7983e-01 5.2936e-01 3.8897e-02 41 0.9
1750 2455451.80424182 968311101 197.555 0.462 -1.3370e-01 8.5313e-01 6.3102e-01 3.7539e-02 27 2.4
1751 2455452.07326191 968334344 65.706 -4.102 -1.1909e-01 7.2127e-01 6.0423e-01 3.7507e-02 29 1.8
1752 2455452.08551482 968335403 28.354 -49.227 -9.2963e-02 5.6770e-01 6.3052e-01 3.8106e-02 52 1.4
1753 2455452.10731938 968337287 343.683 -79.519 -1.3370e-01 8.5313e-01 6.3102e-01 3.7539e-02 24 2.4
1754 2455452.20449255 968345683 57.043 -1.560 -1.1724e-01 4.7983e-01 5.2936e-01 3.8897e-02 38 0.9
1755 2455452.22965164 968347856 250.902 -83.167 -9.2963e-02 5.6770e-01 6.3052e-01 3.8106e-02 42 1.4
1756 2455452.23154252 968348020 151.291 -35.510 -1.3370e-01 8.5313e-01 6.3102e-01 3.7539e-02 30 2.4
1757 2455452.36088703 968359195 162.197 12.472 -1.1724e-01 4.7983e-01 5.2936e-01 3.8897e-02 49 0.9
1758 2455452.36702477 968359725 176.041 29.863 -1.3370e-01 8.5313e-01 6.3102e-01 3.7539e-02 24 2.4
1759 2455452.57756140 968377916 294.351 -54.310 -1.1724e-01 4.7983e-01 5.2936e-01 3.8897e-02 57 0.9
1760 2455453.24560289 968435635 90.253 -58.855 -1.1724e-01 4.7983e-01 5.2936e-01 3.8897e-02 63 0.9
1761 2455453.25190889 968436179 211.328 -67.028 -9.2963e-02 5.6770e-01 6.3052e-01 3.8106e-02 33 1.4
1762 2455453.25259588 968436239 35.524 -70.161 -9.2963e-02 5.6770e-01 6.3052e-01 3.8106e-02 34 1.4
1763 2455453.36087261 968445594 53.510 -16.938 -1.3370e-01 8.5313e-01 6.3102e-01 3.7539e-02 28 2.4
1764 2455453.41293734 968450092 206.813 15.460 -9.2963e-02 5.6770e-01 6.3052e-01 3.8106e-02 45 1.4
1765 2455453.41348776 968450140 162.361 42.798 -1.1210e-01 3.5816e-01 4.5437e-01 4.0298e-02 114 0.5
1766 2455453.42685768 968451295 143.073 25.880 -1.1724e-01 4.7983e-01 5.2936e-01 3.8897e-02 40 0.9
1767 2455453.86968999 968489556 320.407 24.216 -9.2963e-02 5.6770e-01 6.3052e-01 3.8106e-02 34 1.4
1768 2455453.93808666 968495465 265.853 3.678 -9.2963e-02 5.6770e-01 6.3052e-01 3.8106e-02 46 1.4
1769 2455454.30271870 968526969 282.908 -51.377 -1.7861e+00 6.7827e+00 8.6368e-01 3.8440e-01 26 1.4
1770 2455454.37953530 968533606 72.904 -37.762 -1.1724e-01 4.7983e-01 5.2936e-01 3.8897e-02 48 0.9
1771 2455454.43112392 968538064 204.179 -38.790 -1.3370e-01 8.5313e-01 6.3102e-01 3.7539e-02 30 2.4
1772 2455454.46976008 968541402 82.501 -53.496 -9.2963e-02 5.6770e-01 6.3052e-01 3.8106e-02 38 1.4
1773 2455454.48323023 968542566 133.147 -46.521 -1.3370e-01 8.5313e-01 6.3102e-01 3.7539e-02 30 2.4
1774 2455454.50385255 968544347 124.003 -30.084 -1.1724e-01 4.7983e-01 5.2936e-01 3.8897e-02 89 0.9
1775 2455454.77093044 968567423 249.674 -4.856 -9.2963e-02 5.6770e-01 6.3052e-01 3.8106e-02 57 1.4
1776 2455454.91359343 968579749 89.688 -42.864 -9.2963e-02 5.6770e-01 6.3052e-01 3.8106e-02 33 1.4
1777 2455454.96372225 968584080 52.293 4.365 -1.3370e-01 8.5313e-01 6.3102e-01 3.7539e-02 28 2.4
1778 2455454.98309502 968585754 253.150 -27.544 -1.1909e-01 7.2127e-01 6.0423e-01 3.7507e-02 23 1.8
1779 2455455.20882833 968605257 0.276 8.491 -1.3370e-01 8.5313e-01 6.3102e-01 3.7539e-02 28 2.4
1780 2455455.51356785 968631587 102.524 -7.292 -9.2963e-02 5.6770e-01 6.3052e-01 3.8106e-02 51 1.4
1781 2455455.80973056 968657175 20.353 -55.592 -1.7861e+00 6.7827e+00 8.6368e-01 3.8440e-01 29 1.4
1782 2455455.90317996 968665249 225.192 -52.217 -1.1909e-01 7.2127e-01 6.0423e-01 3.7507e-02 28 1.8
1783 2455455.99218813 968672940 77.351 -4.361 -9.2963e-02 5.6770e-01 6.3052e-01 3.8106e-02 45 1.4
1784 2455456.15787180 968687255 129.863 -65.277 -1.1724e-01 4.7983e-01 5.2936e-01 3.8897e-02 34 0.9
1785 2455456.20172689 968691044 44.735 5.830 -1.3370e-01 8.5313e-01 6.3102e-01 3.7539e-02 27 2.4
1786 2455456.20605460 968691418 191.833 -57.155 -9.2963e-02 5.6770e-01 6.3052e-01 3.8106e-02 44 1.4
1787 2455456.59749667 968725238 172.467 9.421 -9.2963e-02 5.6770e-01 6.3052e-01 3.8106e-02 42 1.4
1788 2455456.61395583 968726660 223.122 -33.374 -1.1724e-01 4.7983e-01 5.2936e-01 3.8897e-02 72 0.9
1789 2455457.12617472 968770916 62.516 30.053 -1.1724e-01 4.7983e-01 5.2936e-01 3.8897e-02 46 0.9
1790 2455457.27603636 968783864 149.913 -57.385 -9.2963e-02 5.6770e-01 6.3052e-01 3.8106e-02 44 1.4
1791 2455457.70004021 968820498 311.329 -24.458 -9.2963e-02 5.6770e-01 6.3052e-01 3.8106e-02 30 1.4
1792 2455457.74421786 968824315 315.362 -83.810 -9.2963e-02 5.6770e-01 6.3052e-01 3.8106e-02 34 1.4
1793 2455457.76773135 968826346 261.090 -43.762 -9.2963e-02 5.6770e-01 6.3052e-01 3.8106e-02 47 1.4
1794 2455457.81715868 968830617 216.741 -3.327 -9.2963e-02 5.6770e-01 6.3052e-01 3.8106e-02 44 1.4
1795 2455458.27230883 968869942 13.094 -10.294 -9.2963e-02 5.6770e-01 6.3052e-01 3.8106e-02 69 1.4
1796 2455458.32611694 968874591 7.234 -62.816 -9.2963e-02 5.6770e-01 6.3052e-01 3.8106e-02 32 1.4
1797 2455458.45893698 968886067 182.219 39.801 -1.1724e-01 4.7983e-01 5.2936e-01 3.8897e-02 36 0.9
1798 2455458.61452063 968899509 246.751 12.499 -9.2963e-02 5.6770e-01 6.3052e-01 3.8106e-02 36 1.4

LIST OF HIGH ENERGY NEUTRINO CANDIDATES FOR THE 2009-2010 DATA

1799 2455458.81424959 968916766 118.206 -48.445 -1.3370e-01 8.5313e-01 6.3102e-01 3.7539e-02 31 2.4
1800 2455458.86849402 968921452 189.228 -35.980 -9.2963e-02 5.6770e-01 6.3052e-01 3.8106e-02 40 1.4
1801 2455458.94910179 968928417 264.027 -44.981 -1.3370e-01 8.5313e-01 6.3102e-01 3.7539e-02 30 2.4
1802 2455459.05437309 968937512 42.274 30.380 -9.2963e-02 5.6770e-01 6.3052e-01 3.8106e-02 45 1.4
1803 2455459.13172550 968944196 340.949 13.071 -9.2963e-02 5.6770e-01 6.3052e-01 3.8106e-02 40 1.4
1804 2455459.18837762 968949090 122.851 5.024 -9.2963e-02 5.6770e-01 6.3052e-01 3.8106e-02 48 1.4
1805 2455459.35471725 968963462 124.037 45.249 -1.3370e-01 8.5313e-01 6.3102e-01 3.7539e-02 25 2.4
1806 2455459.52773436 968978411 319.930 -54.225 -9.2963e-02 5.6770e-01 6.3052e-01 3.8106e-02 54 1.4
1807 2455459.70348314 968993595 271.569 44.217 -9.2963e-02 5.6770e-01 6.3052e-01 3.8106e-02 42 1.4
1808 2455459.70862106 968994039 2.090 -36.578 -1.1724e-01 4.7983e-01 5.2936e-01 3.8897e-02 39 0.9
1809 2455459.93289750 969013417 315.066 -64.835 -8.8598e-02 3.3283e-01 5.3278e-01 3.9884e-02 125 0.6
1810 2455460.12238082 969029788 215.906 -49.693 -1.3370e-01 8.5313e-01 6.3102e-01 3.7539e-02 18 2.4
1811 2455460.34336759 969048881 155.483 -5.338 -9.2963e-02 5.6770e-01 6.3052e-01 3.8106e-02 49 1.4
1812 2455460.35634849 969050003 135.241 0.318 -9.2963e-02 5.6770e-01 6.3052e-01 3.8106e-02 44 1.4
1813 2455460.37567663 969051673 101.999 -1.694 -9.2963e-02 5.6770e-01 6.3052e-01 3.8106e-02 58 1.4
1814 2455461.16192720 969119605 152.141 -9.531 -9.2963e-02 5.6770e-01 6.3052e-01 3.8106e-02 57 1.4
1815 2455461.87336644 969181073 287.104 -2.908 -9.2963e-02 5.6770e-01 6.3052e-01 3.8106e-02 40 1.4
1816 2455461.89217576 969182698 43.941 13.215 -1.1724e-01 4.7983e-01 5.2936e-01 3.8897e-02 53 0.9
1817 2455461.98280990 969190529 6.948 34.909 -9.2963e-02 5.6770e-01 6.3052e-01 3.8106e-02 39 1.4
1818 2455462.02469139 969194148 337.255 25.388 -9.2963e-02 5.6770e-01 6.3052e-01 3.8106e-02 36 1.4
1819 2455462.31736533 969219435 105.227 -43.216 -9.2963e-02 5.6770e-01 6.3052e-01 3.8106e-02 40 1.4
1820 2455462.38022886 969224866 35.947 -54.463 -9.2963e-02 5.6770e-01 6.3052e-01 3.8106e-02 42 1.4
1821 2455462.40710516 969227188 152.609 16.647 -1.1724e-01 4.7983e-01 5.2936e-01 3.8897e-02 87 0.9
1822 2455462.52875500 969237699 124.849 -24.464 -9.2963e-02 5.6770e-01 6.3052e-01 3.8106e-02 39 1.4
1823 2455462.58753144 969242777 173.333 -7.415 -9.2963e-02 5.6770e-01 6.3052e-01 3.8106e-02 48 1.4
1824 2455462.65078916 969248243 174.637 -45.211 -9.2963e-02 5.6770e-01 6.3052e-01 3.8106e-02 33 1.4
1825 2455462.91259969 969270863 63.928 2.929 -9.2963e-02 5.6770e-01 6.3052e-01 3.8106e-02 41 1.4
1826 2455462.95610410 969274622 125.749 -65.055 -9.2963e-02 5.6770e-01 6.3052e-01 3.8106e-02 35 1.4
1827 2455463.78877374 969346565 277.962 -0.582 -1.1724e-01 4.7983e-01 5.2936e-01 3.8897e-02 48 0.9
1828 2455463.92620325 969358438 3.320 24.990 -9.2963e-02 5.6770e-01 6.3052e-01 3.8106e-02 36 1.4
1829 2455463.94571679 969360124 355.573 4.437 -1.1724e-01 4.7983e-01 5.2936e-01 3.8897e-02 37 0.9
1830 2455464.18784837 969381045 342.251 -38.295 -1.1724e-01 4.7983e-01 5.2936e-01 3.8897e-02 64 0.9
1831 2455464.24919048 969386345 102.662 -29.369 -1.1724e-01 4.7983e-01 5.2936e-01 3.8897e-02 48 0.9
1832 2455464.25432507 969386788 63.376 -33.042 -1.3370e-01 8.5313e-01 6.3102e-01 3.7539e-02 22 2.4
1833 2455464.47117015 969405524 117.889 -12.746 -1.3370e-01 8.5313e-01 6.3102e-01 3.7539e-02 40 2.4
1834 2455464.52591589 969410254 149.584 29.662 -9.2963e-02 5.6770e-01 6.3052e-01 3.8106e-02 60 1.4
1835 2455464.59014824 969415803 329.730 -41.640 -9.2963e-02 5.6770e-01 6.3052e-01 3.8106e-02 43 1.4
1836 2455464.76883134 969431242 286.862 28.859 -1.3370e-01 8.5313e-01 6.3102e-01 3.7539e-02 31 2.4
1837 2455464.98477664 969449899 336.140 -53.616 -9.2963e-02 5.6770e-01 6.3052e-01 3.8106e-02 68 1.4
1838 2455465.20217247 969468682 300.366 -64.441 -1.3370e-01 8.5313e-01 6.3102e-01 3.7539e-02 24 2.4
1839 2455465.22110820 969470318 9.733 -66.005 -1.2873e-01 4.3155e-01 4.6595e-01 3.9162e-02 45 0.7
1840 2455465.26766302 969474341 3.905 -54.082 -1.2873e-01 4.3155e-01 4.6595e-01 3.9162e-02 50 0.7
1841 2455465.34250419 969480807 61.534 -9.946 -1.3370e-01 8.5313e-01 6.3102e-01 3.7539e-02 23 2.4
1842 2455465.71727566 969513187 163.475 -77.000 -1.3370e-01 8.5313e-01 6.3102e-01 3.7539e-02 25 2.4
1843 2455465.81941184 969522012 336.446 -10.660 -9.2963e-02 5.6770e-01 6.3052e-01 3.8106e-02 41 1.4
1844 2455465.98171801 969536035 264.668 -15.524 -1.3370e-01 8.5313e-01 6.3102e-01 3.7539e-02 21 2.4
1845 2455466.06624986 969543338 15.199 -68.529 -1.1724e-01 4.7983e-01 5.2936e-01 3.8897e-02 44 0.9
1846 2455466.18644652 969553723 16.764 26.422 -9.2963e-02 5.6770e-01 6.3052e-01 3.8106e-02 36 1.4
1847 2455466.21055843 969555807 40.706 -3.228 -9.2963e-02 5.6770e-01 6.3052e-01 3.8106e-02 34 1.4
1848 2455466.42180381 969574058 181.618 15.791 -9.2963e-02 5.6770e-01 6.3052e-01 3.8106e-02 67 1.4
1849 2455466.51320002 969581955 234.615 -47.282 -1.1724e-01 4.7983e-01 5.2936e-01 3.8897e-02 41 0.9
1850 2455466.51323532 969581958 31.811 -47.983 -9.2963e-02 5.6770e-01 6.3052e-01 3.8106e-02 55 1.4

```
1851 2455466.73762422 969601345 295.242 19.950 -9.2963e-02 5.6770e-01 6.3052e-01 3.8106e-02 44 1.4
1852 2455466.76198870 969603450 90.070 -54.647 -9.2963e-02 5.6770e-01 6.3052e-01 3.8106e-02 32 1.4
1853 2455466.78865597 969605754 335.481 17.898 -1.1909e-01 7.2127e-01 6.0423e-01 3.7507e-02 29 1.8
1854 2455466.88795078 969614333 302.620 -83.652 -9.2963e-02 5.6770e-01 6.3052e-01 3.8106e-02 51 1.4
1855 2455466.93633213 969618514 39.241 -67.012 -1.1724e-01 4.7983e-01 5.2936e-01 3.8897e-02 37 0.9
1856 2455466.98716546 969622906 100.356 -3.848 -9.2963e-02 5.6770e-01 6.3052e-01 3.8106e-02 60 1.4
1857 2455467.42747723 969660949 49.092 -81.461 -9.2963e-02 5.6770e-01 6.3052e-01 3.8106e-02 49 1.4
1858 2455467.43249122 969661382 224.770 6.317 -9.2963e-02 5.6770e-01 6.3052e-01 3.8106e-02 75 1.4
1859 2455467.76027688 969689702 299.915 19.464 -9.2963e-02 5.6770e-01 6.3052e-01 3.8106e-02 34 1.4
1860 2455467.80525130 969693588 267.331 -54.250 -1.2873e-01 4.3155e-01 4.6595e-01 3.9162e-02 46 0.7
1861 2455468.01548934 969711753 57.472 -1.745 -9.2963e-02 5.6770e-01 6.3052e-01 3.8106e-02 37 1.4
1862 2455468.12238422 969720988 47.996 -10.893 -1.1909e-01 7.2127e-01 6.0423e-01 3.7507e-02 19 1.8
1863 2455468.40786635 969745654 54.319 -58.179 -1.3370e-01 8.5313e-01 6.3102e-01 3.7539e-02 27 2.4
1864 2455468.51448225 969754866 180.319 -5.392 -1.1724e-01 4.7983e-01 5.2936e-01 3.8897e-02 56 0.9
1865 2455468.52250588 969755559 264.080 20.810 -9.2963e-02 5.6770e-01 6.3052e-01 3.8106e-02 36 1.4
1866 2455468.53763206 969756866 91.030 -50.021 -1.3370e-01 8.5313e-01 6.3102e-01 3.7539e-02 31 2.4
1867 2455468.57377213 969759988 267.644 -10.242 -1.1724e-01 4.7983e-01 5.2936e-01 3.8897e-02 39 0.9
1868 2455468.76184332 969776238 189.447 -36.529 -9.2963e-02 5.6770e-01 6.3052e-01 3.8106e-02 38 1.4
1869 2455468.89205756 969787488 0.389 -16.059 -9.2963e-02 5.6770e-01 6.3052e-01 3.8106e-02 75 1.4
1870 2455470.45784087 969922772 180.031 -11.653 -1.3370e-01 8.5313e-01 6.3102e-01 3.7539e-02 22 2.4
1871 2455470.55339879 969931028 222.317 38.197 -9.2963e-02 5.6770e-01 6.3052e-01 3.8106e-02 44 1.4
1872 2455470.60049885 969935098 144.127 -39.135 -9.2963e-02 5.6770e-01 6.3052e-01 3.8106e-02 37 1.4
1873 2455470.61300779 969936178 54.832 -48.685 -9.2963e-02 5.6770e-01 6.3052e-01 3.8106e-02 68 1.4
1874 2455471.09057801 969977440 301.358 -26.443 -9.2963e-02 5.6770e-01 6.3052e-01 3.8106e-02 26 1.4
1875 2455471.12168407 969980128 21.267 20.121 -1.3370e-01 8.5313e-01 6.3102e-01 3.7539e-02 28 2.4
1876 2455471.19216048 969986217 348.237 -17.299 -1.3370e-01 8.5313e-01 6.3102e-01 3.7539e-02 23 2.4
1877 2455471.27659978 969993513 56.015 -18.756 -1.3370e-01 8.5313e-01 6.3102e-01 3.7539e-02 31 2.4
1878 2455471.44108016 970007724 141.301 27.161 -9.2963e-02 5.6770e-01 6.3052e-01 3.8106e-02 43 1.4
1879 2455471.44284181 970007876 103.697 13.652 -9.2963e-02 5.6770e-01 6.3052e-01 3.8106e-02 38 1.4
1880 2455471.48984280 970011937 75.428 -34.192 -9.2963e-02 5.6770e-01 6.3052e-01 3.8106e-02 35 1.4
1881 2455472.15431079 970069347 47.518 -15.983 -9.2963e-02 5.6770e-01 6.3052e-01 3.8106e-02 37 1.4
1882 2455472.22932264 970075828 108.595 1.605 -9.2963e-02 5.6770e-01 6.3052e-01 3.8106e-02 63 1.4
1883 2455472.29622119 970081608 61.476 -26.025 -1.3370e-01 8.5313e-01 6.3102e-01 3.7539e-02 22 2.4
1884 2455472.32062918 970083717 145.591 -6.634 -9.2963e-02 5.6770e-01 6.3052e-01 3.8106e-02 47 1.4
1885 2455472.41634610 970091987 138.004 11.225 -1.3370e-01 8.5313e-01 6.3102e-01 3.7539e-02 23 2.4
1886 2455472.57447945 970105650 136.947 -81.216 -9.2963e-02 5.6770e-01 6.3052e-01 3.8106e-02 40 1.4
1887 2455472.70844984 970117225 204.603 10.738 -9.2963e-02 5.6770e-01 6.3052e-01 3.8106e-02 66 1.4
1888 2455472.88317258 970132321 248.890 0.717 -9.2963e-02 5.6770e-01 6.3052e-01 3.8106e-02 42 1.4
1889 2455473.04086075 970145945 284.629 -24.863 -1.3370e-01 8.5313e-01 6.3102e-01 3.7539e-02 27 2.4
1890 2455473.30473971 970168744 106.459 -24.086 -1.3370e-01 8.5313e-01 6.3102e-01 3.7539e-02 24 2.4
1891 2455474.02785861 970231221 10.296 6.186 -1.3370e-01 8.5313e-01 6.3102e-01 3.7539e-02 28 2.4
1892 2455474.41903012 970265019 114.811 23.813 -9.2963e-02 5.6770e-01 6.3052e-01 3.8106e-02 71 1.4
1893 2455474.46438909 970268938 130.208 13.199 -1.3370e-01 8.5313e-01 6.3102e-01 3.7539e-02 28 2.4
1894 2455474.52924379 970274541 209.702 -19.198 -1.3370e-01 8.5313e-01 6.3102e-01 3.7539e-02 22 2.4
1895 2455474.85116494 970302355 2.157 20.246 -9.2963e-02 5.6770e-01 6.3052e-01 3.8106e-02 57 1.4
1896 2455474.95486273 970311315 41.393 6.314 -9.2963e-02 5.6770e-01 6.3052e-01 3.8106e-02 41 1.4
1897 2455475.03581629 970318309 48.341 25.042 -9.2963e-02 5.6770e-01 6.3052e-01 3.8106e-02 81 1.4
1898 2455475.05119788 970319638 303.291 -10.743 -9.2963e-02 5.6770e-01 6.3052e-01 3.8106e-02 41 1.4
1899 2455475.25459109 970337211 103.881 18.048 -9.2963e-02 5.6770e-01 6.3052e-01 3.8106e-02 41 1.4
1900 2455475.33083298 970343798 95.339 -23.100 -9.2963e-02 5.6770e-01 6.3052e-01 3.8106e-02 64 1.4
1901 2455475.69275791 970375069 357.122 -22.579 -9.2963e-02 5.6770e-01 6.3052e-01 3.8106e-02 48 1.4
1902 2455475.83398988 970387271 330.954 -55.084 -1.1724e-01 4.7983e-01 5.2936e-01 3.8897e-02 46 0.9
```

LIST OF HIGH ENERGY NEUTRINO CANDIDATES FOR THE 2009-2010 DATA

1903	2455476.17378727	970416630	90.707	19.135	-1.3370e-01	8.5313e-01	6.3102e-01	3.7539e-02	25	2.4
1904	2455476.61735227	970454954	311.182	-11.663	-1.1909e-01	7.2127e-01	6.0423e-01	3.7507e-02	26	1.8
1905	2455476.69835011	970461952	324.323	-55.779	-1.1724e-01	4.7983e-01	5.2936e-01	3.8897e-02	47	0.9
1906	2455476.84185180	970474350	169.516	-51.599	-1.1724e-01	4.7983e-01	5.2936e-01	3.8897e-02	42	0.9
1907	2455476.86915061	970476709	67.844	-9.655	-1.3370e-01	8.5313e-01	6.3102e-01	3.7539e-02	26	2.4
1908	2455476.87110898	970476878	114.738	-54.099	-9.2963e-02	5.6770e-01	6.3052e-01	3.8106e-02	33	1.4
1909	2455477.13119858	970499350	107.767	-5.724	-9.2963e-02	5.6770e-01	6.3052e-01	3.8106e-02	77	1.4
1910	2455477.26743633	970511121	269.986	-48.508	-9.2963e-02	5.6770e-01	6.3052e-01	3.8106e-02	49	1.4
1911	2455478.54320654	970621348	339.811	-49.212	-9.2963e-02	5.6770e-01	6.3052e-01	3.8106e-02	33	1.4
1912	2455478.66409797	970631793	276.690	-0.243	-1.1724e-01	4.7983e-01	5.2936e-01	3.8897e-02	52	0.9
1913	2455478.69726989	970634659	13.426	-79.916	-1.3370e-01	8.5313e-01	6.3102e-01	3.7539e-02	27	2.4
1914	2455478.95793565	970657180	271.367	-68.747	-9.2963e-02	5.6770e-01	6.3052e-01	3.8106e-02	34	1.4
1915	2455478.98190327	970659251	332.564	2.512	-9.2963e-02	5.6770e-01	6.3052e-01	3.8106e-02	46	1.4
1916	2455479.00982090	970661663	263.958	-46.564	-9.2963e-02	5.6770e-01	6.3052e-01	3.8106e-02	38	1.4
1917	2455479.02115066	970662642	44.158	-9.799	-1.2873e-01	4.3155e-01	4.6595e-01	3.9162e-02	59	0.7
1918	2455479.03418574	970663768	10.564	-15.409	-9.2963e-02	5.6770e-01	6.3052e-01	3.8106e-02	44	1.4
1919	2455479.03642127	970663961	110.156	-44.611	-9.2963e-02	5.6770e-01	6.3052e-01	3.8106e-02	25	1.4
1920	2455479.06134852	970666115	311.090	-26.609	-1.3370e-01	8.5313e-01	6.3102e-01	3.7539e-02	29	2.4
1921	2455479.10224807	970669649	345.468	-10.674	-9.2963e-02	5.6770e-01	6.3052e-01	3.8106e-02	75	1.4
1922	2455479.34993596	970691049	65.110	-22.549	-1.3370e-01	8.5313e-01	6.3102e-01	3.7539e-02	23	2.4
1923	2455479.95994526	970743754	6.694	-59.147	-1.1724e-01	4.7983e-01	5.2936e-01	3.8897e-02	33	0.9
1924	2455479.97126507	970744732	18.951	18.034	-9.2963e-02	5.6770e-01	6.3052e-01	3.8106e-02	33	1.4
1925	2455480.00556085	970747695	129.718	-33.692	-9.2963e-02	5.6770e-01	6.3052e-01	3.8106e-02	26	1.4
1926	2455480.04324654	970750951	145.303	-17.009	-9.2963e-02	5.6770e-01	6.3052e-01	3.8106e-02	75	1.4
1927	2455480.08674619	970754709	181.854	-49.848	-1.1724e-01	4.7983e-01	5.2936e-01	3.8897e-02	43	0.9
1928	2455480.12686491	970758176	158.766	-22.579	-1.1724e-01	4.7983e-01	5.2936e-01	3.8897e-02	25	0.9
1929	2455480.19020144	970763648	258.119	-61.760	-9.2963e-02	5.6770e-01	6.3052e-01	3.8106e-02	62	1.4
1930	2455480.31483632	970774416	215.226	-53.528	-1.3370e-01	8.5313e-01	6.3102e-01	3.7539e-02	29	2.4
1931	2455480.38875956	970780803	119.721	-24.317	-9.2963e-02	5.6770e-01	6.3052e-01	3.8106e-02	38	1.4
1932	2455480.43083866	970784439	119.501	-71.390	-9.2963e-02	5.6770e-01	6.3052e-01	3.8106e-02	36	1.4
1933	2455480.49024313	970789572	96.431	-37.780	-9.2963e-02	5.6770e-01	6.3052e-01	3.8106e-02	38	1.4
1934	2455480.52861682	970792887	228.597	27.745	-9.2963e-02	5.6770e-01	6.3052e-01	3.8106e-02	56	1.4
1935	2455480.53011919	970793017	120.579	-18.015	-9.2963e-02	5.6770e-01	6.3052e-01	3.8106e-02	38	1.4
1936	2455480.75810719	970812715	222.309	6.494	-9.2963e-02	5.6770e-01	6.3052e-01	3.8106e-02	43	1.4
1937	2455481.15369736	970846894	36.564	26.380	-9.2963e-02	5.6770e-01	6.3052e-01	3.8106e-02	58	1.4
1938	2455481.49201310	970876124	223.065	7.969	-9.2963e-02	5.6770e-01	6.3052e-01	3.8106e-02	35	1.4
1939	2455481.49501402	970876384	216.875	-33.004	-9.2963e-02	5.6770e-01	6.3052e-01	3.8106e-02	32	1.4
1940	2455481.69228371	970893428	341.109	-71.517	-1.2873e-01	4.3155e-01	4.6595e-01	3.9162e-02	65	0.7
1941	2455481.76719164	970899900	244.308	10.344	-1.3370e-01	8.5313e-01	6.3102e-01	3.7539e-02	30	2.4
1942	2455481.90847431	970912107	64.283	18.936	-1.3370e-01	8.5313e-01	6.3102e-01	3.7539e-02	49	2.4
1943	2455482.06437262	970925576	79.706	-31.700	-9.2963e-02	5.6770e-01	6.3052e-01	3.8106e-02	35	1.4
1944	2455482.06639273	970925751	19.136	-66.978	-9.2963e-02	5.6770e-01	6.3052e-01	3.8106e-02	57	1.4
1945	2455482.36233079	970951320	190.485	26.391	-1.1909e-01	7.2127e-01	6.0423e-01	3.7507e-02	26	1.8
1946	2455482.38583820	970953351	172.135	-6.447	-9.2963e-02	5.6770e-01	6.3052e-01	3.8106e-02	47	1.4
1947	2455482.55774061	970968203	160.126	-41.528	-9.2963e-02	5.6770e-01	6.3052e-01	3.8106e-02	37	1.4
1948	2455482.62741040	970974223	150.044	-38.405	-9.2963e-02	5.6770e-01	6.3052e-01	3.8106e-02	34	1.4
1949	2455483.09039424	971014225	274.654	-44.501	-9.2963e-02	5.6770e-01	6.3052e-01	3.8106e-02	93	1.4
1950	2455483.11543480	971016388	308.764	-47.814	-9.2963e-02	5.6770e-01	6.3052e-01	3.8106e-02	47	1.4
1951	2455483.16705295	971020848	135.085	-17.001	-9.2963e-02	5.6770e-01	6.3052e-01	3.8106e-02	44	1.4
1952	2455483.55215420	971054121	189.108	-29.403	-1.3370e-01	8.5313e-01	6.3102e-01	3.7539e-02	29	2.4
1953	2455483.58125118	971056635	252.514	-8.394	-9.2963e-02	5.6770e-01	6.3052e-01	3.8106e-02	43	1.4
1954	2455483.75950707	971072036	171.680	-44.441	-9.2963e-02	5.6770e-01	6.3052e-01	3.8106e-02	38	1.4

```
1955 2455483.76670481 971072658 75.469 -40.554 -1.1724e-01 4.7983e-01 5.2936e-01 3.8897e-02 35 0.9
1956 2455484.10195056 971101623 43.278 -74.754 -9.2963e-02 5.6770e-01 6.3052e-01 3.8106e-02 42 1.4
1957 2455484.13545589 971104518 38.247 -41.413 -9.2963e-02 5.6770e-01 6.3052e-01 3.8106e-02 38 1.4
1958 2455484.14975944 971105754 2.375 -8.639 -1.1724e-01 4.7983e-01 5.2936e-01 3.8897e-02 43 0.9
1959 2455484.41203071 971128414 280.092 -62.120 -1.3370e-01 8.5313e-01 6.3102e-01 3.7539e-02 17 2.4
1960 2455484.48576566 971134785 334.616 -50.421 -1.3370e-01 8.5313e-01 6.3102e-01 3.7539e-02 29 2.4
1961 2455485.04007020 971182677 343.340 -6.544 -9.2963e-02 5.6770e-01 6.3052e-01 3.8106e-02 35 1.4
1962 2455485.51717531 971223898 190.861 12.885 -9.2963e-02 5.6770e-01 6.3052e-01 3.8106e-02 44 1.4
1963 2455485.73196050 971242456 298.942 18.580 -1.3370e-01 8.5313e-01 6.3102e-01 3.7539e-02 27 2.4
1964 2455485.75650172 971244576 221.307 -5.957 -9.2963e-02 5.6770e-01 6.3052e-01 3.8106e-02 38 1.4
1965 2455485.99184515 971264910 25.740 -3.819 -1.3370e-01 8.5313e-01 6.3102e-01 3.7539e-02 31 2.4
1966 2455486.09282488 971273635 135.081 -32.208 -1.1724e-01 4.7983e-01 5.2936e-01 3.8897e-02 35 0.9
1967 2455486.17871571 971281056 111.959 22.295 -9.2963e-02 5.6770e-01 6.3052e-01 3.8106e-02 38 1.4
1968 2455486.33948603 971294946 130.302 10.915 -9.2963e-02 5.6770e-01 6.3052e-01 3.8106e-02 44 1.4
1969 2455486.55353586 971313440 227.097 -18.404 -9.2963e-02 5.6770e-01 6.3052e-01 3.8106e-02 33 1.4
1970 2455486.80741430 971335375 271.299 -36.165 -9.2963e-02 5.6770e-01 6.3052e-01 3.8106e-02 46 1.4
1971 2455487.20057691 971369344 193.583 -24.483 -9.2963e-02 5.6770e-01 6.3052e-01 3.8106e-02 50 1.4
1972 2455487.50511508 971395656 143.687 -13.520 -1.3370e-01 8.5313e-01 6.3102e-01 3.7539e-02 26 2.4
1973 2455487.55444858 971399919 28.339 -47.858 -1.1724e-01 4.7983e-01 5.2936e-01 3.8897e-02 46 0.9
1974 2455487.66057022 971409088 163.845 -20.206 -1.1724e-01 4.7983e-01 5.2936e-01 3.8897e-02 46 0.9
1975 2455487.69682804 971412220 5.155 -25.859 -1.1724e-01 4.7983e-01 5.2936e-01 3.8897e-02 41 0.9
1976 2455487.79404768 971420620 19.083 -11.251 -9.2963e-02 5.6770e-01 6.3052e-01 3.8106e-02 51 1.4
1977 2455487.83337128 971424018 333.221 -85.966 -1.1724e-01 4.7983e-01 5.2936e-01 3.8897e-02 49 0.9
1978 2455488.50990453 971482470 182.515 -31.720 -9.2963e-02 5.6770e-01 6.3052e-01 3.8106e-02 43 1.4
1979 2455488.91902069 971517818 279.349 -8.999 -9.2963e-02 5.6770e-01 6.3052e-01 3.8106e-02 37 1.4
1980 2455489.35628250 971555597 83.036 -56.437 -9.2963e-02 5.6770e-01 6.3052e-01 3.8106e-02 43 1.4
1981 2455489.37466819 971557186 277.268 -62.564 -9.2963e-02 5.6770e-01 6.3052e-01 3.8106e-02 75 1.4
1982 2455489.50905998 971568797 263.016 -6.010 -1.3370e-01 8.5313e-01 6.3102e-01 3.7539e-02 25 2.4
1983 2455489.62683338 971578973 190.642 7.864 -1.3370e-01 8.5313e-01 6.3102e-01 3.7539e-02 26 2.4
1984 2455489.72343844 971587320 248.142 -20.239 -1.3370e-01 8.5313e-01 6.3102e-01 3.7539e-02 17 2.4
1985 2455489.72775112 971587692 216.433 -0.482 -9.2963e-02 5.6770e-01 6.3052e-01 3.8106e-02 37 1.4
1986 2455489.87829766 971600699 26.194 -11.058 -1.2873e-01 4.3155e-01 4.6595e-01 3.9162e-02 58 0.7
## stop S6D
```

LIST OF HIGH ENERGY NEUTRINO CANDIDATES FOR THE 2009-2010 DATA

Résumé: L'objectif de ce travail est la détection conjointe d'ondes gravitationnelles et de neutrinos cosmique de haute énergie à travers une approche multi-messagers. Les astronomies neutrinos et ondes gravitationnelles sont encore en phase de développement, mais elles sont appelées à jouer un rôle fondamental dans le futur. En effet, ces messagers peuvent parcourir de grandes distances grâce à leur faible interaction avec la matière (contrairement aux photons qui, à haute énergie, sont rapidement absorbés), sans être affectés par les champs magnétiques (contrairement aux rayons cosmiques chargés). Ils peuvent également s'échapper de milieux denses et fournir des informations sur les processus qui ont lieu au coeur des sources astrophysique (les photons s'échappent des couches périphériques des objets célestes). En un mot, ces astronomies sont susceptibles d'ouvrir une nouvelle fenêtre d'observation sur le cosmos.
La collaboration ANTARES a construit en Méditerranée un télescope sous-marin de neutrino de haute énergie d'une surface de détection proche de 0.1 km^2. C'est le télescope le plus sensible pour la partie du ciel observée. Les interféromètres Virgo et LIGO sont des détecteur terrestres pour l'observation directe d'ondes gravitationnelles, instalés en Europe et aux États-Unis d'Amérique respectivement. Les instruments ANTARES, Virgo et LIGO offrent une sensibilité inégalée dans la zone de recherche commune.
Le premier chapitre de cette thèse introduit les motivations théoriques pour une recherche jointe d'ondes gravitationnelles et de neutrinos de haute énergies en développant les différents scénarios d'émission. Le deuxième et troisième chapitres sont consacrés à l'étude des techniques de détection avec les interféromètres Virgo-LIGO et le télescope à neutrinos ANTARES. Les quatriéme et cinquième chapitres de ce travail présentent les résultats d'analyses de données combinées d'ANTARES, Virgo et LIGO prises séparement pendant les années 2007 et 2009-2010.

Mots clés : Neutrinos de haute énergie, ondes gravitationnelles, sursauts gamma, astronomie multi-messager, ANTARES, Virgo, LIGO.

Abstract: The aim of this work is the joint detection of gravitational waves and high energy neutrinos in a multi-messengers context. The neutrino and gravitational waves astronomies are still in the phase of development, but they are expected to play a fundamental role in the future. In fact, these messengers can travel big distances because of their weak interaction with matter (contrary to photons that at high energy are rapidly absorbed) without being affected by magnetic fields (contrary to charged cosmic rays). They can also escape dense media and provide informations on the processes taking place in the heart of astrophysics sources. Particularly, GW+HEN multi-messenger astronomy may open a new observational window on the Universe. ANTARES collaboration has built a telescope of area 0.1 km^2 in the Mediterranean Sea for the detection of high energy neutrinos. This is the most sensitive telescope for the observed part of the sky. LIGO and Virgo interferometers are ground-based detectors for direct observation of gravitational waves, instaled in Europe and the USA respectively. Instruments ANTARES, Virgo and LIGO offer unrivaled sensitivity in the area of joint observation. The first chapter of this thesis introduces the theoretical motivations for GW+HEN search by developing different emission scenarios. The second and third chapters give an overview of the experiments and review the data analysis tools. The fourth and fifth chapters of this work present the results of the analysis of the combined data from ANTARES, Virgo and LIGO taken separately in 2007 and 2009-2010.

Keywords: High-energy neutrino, Gravitational waves, Gamma-ray Burst, multimessenger astronomy, ANTARES, Virgo, LIGO.